Inaugural dissertation

for

obtaining the doctoral degree

of the

Combined Faculty of Mathematics, Engineering and Natural Sciences

of the

Ruprecht – Karls – University

Heidelberg

Presented by

M.Sc. Annkathrin Chiara Teschner

born in: Tübingen

Oral examination: 20.12.2022

Use of TCR antibody fusion proteins as bispecific agents for NK and T cell-mediated immunotherapy

Referees: Prof. Dr. Viktor Umansky

PD Dr. Frank Momburg

Inhaltsverzeichnis

Zusammenfassung

Bispezifische T-Zell-aktivierende Reagenzien sind von großem Interesse in der Tumorimmuntherapie, da sie einerseits Antigene auf der Tumorzelloberfläche binden und andererseits zytotoxische Lymphozyten über die Bindung an aktivierende Rezeptoren zu Tumorzellen rekrutieren. Dabei erkannte Tumorantigene lassen sich in zwei Gruppen unterteilen: Haupthistokompatibilitätskomplex-Klasse-I-Molekül (MHC-I)-gebundene Peptide, die von antigenspezifischen T-Zell-Rezeptoren (TCR) erkannt werden, und Zelloberflächenantigene, die von Antikörpern erkannt werden. MHC-I-gebundene Peptide stammen ursprünglich von intrazellulären Proteinen, welche den Großteil des Proteoms ausmachen. Das macht von TCR erkannte MHC-I-gebundene Peptide zu therapeutisch sehr attraktiven Antigenen. Im Gegensatz zu TCR-transgenen T-Zellen, die neue TCR-Spezifitäten im natürlichen Kontext exprimieren, ist die Entwicklung von Therapeutika, welche auf löslichen TCR basieren, durch eine geringe Stabilität rekombinanter TCR und die zumeist deutlich niedrigere Affinität im Vergleich zu Antikörpern eingeschränkt. In den letzten Jahren wurden jedoch Wege erforscht, welche eine höhere Stabilität sowie Affinitätsreifung des löslichen TCR ermöglichen. So wurden inzwischen erste rekombinante bispezifische TCR-basierte Fusionsproteine für die klinische Anwendung entwickelt, die T-Zellen an Tumorzellen rekrutieren und durch intrazelluläre Tumorantigene aktivieren.

Ziel dieser Studie war die Entwicklung neuartiger bispezifischer NK- und T-Zell-bindender TCR-Fusionsproteine. Um möglichst effektive bispezifische Moleküle zu generieren, wurde ein Immunoglobulin-G (IgG)-ähnliches Format genutzt. Dabei wurde die Ektodomäne von TCR Vα/Cα mit der Hinge und Fc eines humanen IgG1 fusioniert, während die Ektodomäne von TCR Vβ/Cβ als separates Protein in *cis* über eine ribosomale „skipping“ Sequenz exprimiert wurde. Für eine effizientere Zusammenlagerung der TCRα- und TCRβ-Ketten wurde eine zusätzliche intermolekulare Disulfidbrücke in die TCR-Cα/Cβ-Domänen integriert. Homodimerisierung des TCR-Fc-Fusionsproteins wurde wiederum über die natürlichen intermolekularen Disulfidbrücken in der humanen IgG1-*Hinge*-Region vermittelt. Die antikörperähnlichen Konstrukte wurden schließlich erfolgreich durch transiente Transfektion von CHO-S Zellen produziert und aufgereinigt.

Um NK-Zell-Bindung zu ermöglichen, wurden in das Fc-Fragment spezifische Mutationen eingeführt, welche die Bindung an den FcγRIIIa verstärken. Des Weiteren wurden Fusionsproteine getestet, in welchen scFvs (*single chain variable fragments*) C-terminal von TCR-Cα oder -Cβ integriert wurden. Dabei wurde die T-Zellbindung und Aktivierung über CD3ε-spezifische scFvs vermittelt und die NK-Zellbindung und Aktivierung über CD16- bzw. NKp46-spezifische scFvs. Als Modell wurde ein Cytomegalovirus (CMV) pp65-Peptid/ HLA-A*02:01-spezifischer TCR genutzt. Um die Rolle der TCR-Affinität zu analysieren, wurde der

Wildtyp-TCR mit einer affinitätsgereiften Variante verglichen. Die löslichen IgG1-ähnlichen TCR-Konstrukte zeigten dabei eine spezifische, affinitäts- und konzentrationsabhängige Antigenbindung sowie NK- und T-Zell-vermittelte Immunantworten in der Kokultur mit peptidbeladenen oder transfizierten Zellen. Dabei stellten sich TCR-αNKp46-Fc^{enh} und TCRβ-αCD3(OKT3$_{HGL}$)-Fc^{enh} als besonders effektiv für die NK- beziehungsweise T-Zell-vermittelte Immunantworten heraus. Diese TCR-scFv-Ig Fusionsproteine lösten eine antigenspezifische Aktivierung aufgereinigter NK- und T-Zellen aus und induzierten Zytotoxizität gegenüber verschiedenen Tumorzellen.

Diese Ergebnisse wurden durch die Verwendung von niedrig- und hochaffinen Varianten von drei verschiedenen TCR, die HLA-A*02:01-restringierte Peptide aus den Tumorantigenen gp100, MART-1 und NY-ESO-1 erkennen, weiter verifiziert. Allerdings konnte ein TCR$^{high\ aff.}$-αNKp46-Fc^{enh}-Konstrukt gegenüber den HLA-A2^{+} und antigenexprimierenden Melanomzellen keine NK-Zell-vermittelte Antwort oder Zytotoxizität vermitteln, außer diese wurden zusätzlich mit hohen Mengen des spezifischen HLA-A2-bindenden Antigenpeptids beladen. Somit scheinen die NK-Zell-spezifischen TCR-Konstrukte nicht ausreichend sensitiv gegenüber Melanomzellen zu sein, welche infolge der natürlichen Antigenprozessierung nur geringe Mengen an spezifischen Peptid/MHC-Komplexen präsentieren.

Zusammenfassend lässt sich feststellen, dass in dieser Arbeit eine Reihe an neuartigen, rekombinanten bispezifischen TCR-Fc und TCR-scFv-Fc Fusionsproteinen kloniert und produziert wurden, welche eine NK- und T-Zellaktivierung sowie Zytotoxizität gegenüber Tumorzellen vermitteln, die einen Modell-Peptid-MHC-I-Komplex in ausreichenden Mengen exprimieren. Weitere Untersuchungen sind notwendig um herauszufinden, ob die Avidität von löslichen TCR-Fc Konstrukten durch Multimerisierung ausreichend erhöht werden kann, um das Sensitivitätsproblem zu überwinden, welches sich aus der geringen Dichte an Peptid-MHC-I-Komplexen und TCR mit geringer Affinität ergibt.

Summary

Bispecific agents are a promising approach for cancer immunotherapy as they enable the redirection of cytotoxic lymphocytes towards tumor cells by targeting different structures on the tumor cell surface and triggering cytotoxic lymphocytes through agonistic binding to activating receptors. Targeted tumor antigens can be roughly divided into peptide antigens presented by major histocompatibility complex (MHC) class I molecules to antigen-specific T cell receptors and cell surface antigens recognized by antibodies. Peptides presented in the context of an MHC-I molecule mostly result from intracellular proteins, which make up the majority of the proteome, and thus serve as an highly attractive target for immunotherapeutic strategies. In contrast to TCR-transgenic T cells that express novel TCR specificities in the natural cellular context, the development of soluble TCR-based therapies is hampered due to the poor stability of recombinant TCRs and a generally significantly lower affinity in comparison to therapeutic antibodies. In the past years progress has been made to address these problems, which include different modifications improving construct stability and methods for TCR affinity maturation enabling the development and clinical application of first TCR-based bispecific recombinant fusion proteins that retarget T cells to tumors displaying intracellular antigens through MHC molecules.

This study aimed to develop novel soluble bispecific TCR-based agents for the redirection of NK and T cells. To achieve potent bispecific mediators a bivalent immunoglobulin G (IgG)-like TCR-Fc fusion format was adapted. The ectodomain of the TCR Vα/Cα chain was fused to the hinge/Fc part of human IgG1 and the ectodomain of the TCR Vβ/Cβ chain was expressed as a second soluble protein in *cis* using a ribosomal skipping sequence. Efficient assembly of TCR α and β chains was facilitated by an additional artificial intermolecular disulfide bridge in the TCR constant domains. The natural intermolecular disulfide bonds of the human IgG1 hinge region enabled assembly of TCR-Fc fusion proteins to stable homodimers which could be successfully expressed by transient transfection of CHO-S producer cells.

To enable NK cell redirection, specific mutations known to enhance FcγRIIIa binding were introduced in the Fc fragment. Other investigated formats made use of single chain variable fragments (scFv) recognizing CD16 or NKp46 for NK cell redirection or binding CD3ε for the redirection and activation of T cells. NK- and T-cell-binding scFv antibodies were analyzed after insertion at C-terminal end of TCR Cα or Cβ, respectively. A cytomegalovirus (CMV) pp65 peptide/HLA-A*02:01-specific TCR sequence was used as a model system. To analyze the influence of TCR affinity, the wildtype TCR was compared to an affinity-maturated variant. The soluble IgG1-like TCRs showed a target-specific, affinity- and concentration-dependent binding as well as NK and T cell redirection and activation upon co-culture with peptide-pulsed or transfected cells. In particular, the TCRα-αNKp46-Fc^{enhanced} and TCRα-

αCD3ε-Fc^{aglycan} constructs were found to be highly potent in redirecting NK and T cells, respectively. TCR-scFv-Ig fusion proteins efficiently elicited peptide antigen-specific activation of purified NK cells and T cells and induced cytotoxicity against different tumor targets.

These results were further confirmed using low- and and high-affinity variants of three TCRs recognizing HLA-A*02:01-restricted gp100, MART-1 and NY-ESO-1 peptides, respectively, for the redirection of NK cells. TCR$^{high\ aff.}$-αNKp46-Fc^{enh} constructs, however, failed to facilitate NK cytotoxicity against HLA-A2^{+} melanoma cell lines expressing the antigens of choice unless the cell lines were incubated with an excess of the cognate HLA-A2-binding peptide. Thus, the NK cell-engaging TCR-Fc fusion proteins constructs apparently were not sensitive enough to redirect and activate NK cells against melanoma cells presenting low quantities of naturally processed specific peptide/MHC-I complexes.

In sum, in this work a panel of novel recombinant bispecific TCR-Fc and TCR-scFv-Fc fusion proteins were genetically engineered, produced and demonstrated to facilitate the activation and cytotoxicity of NK and T cells towards tumor cells expressing a model peptide-MHC-I complex in sufficient quantities. Further investigations are required to investigate if the avidity of soluble TCR-Fc constructs can be sufficiently increased by multimerization approaches in order to overcome the sensitivity issues resulting from low abundance of peptide-MHC-I complexes and low-affinity TCRs.

Abbreviations

aa	Amino acids
ACT	Adoptive cell transfer
ADCC	Antibody-dependent cellular cytotoxicity
ADCP	Antibody-dependent cellular phagocytosis
BCMA	B-cell maturation antigen
BiMAb	Bispecific monoclonal antibody
BSA	Bovine serum albumin
CDC	Complement-dependent cytotoxicity
CEA	Carcinoembryonic antigen
CFSE	Carboxyfluorescein diacetate succinimidyl ester
CHO	Chinese hamster ovarian
CMV	Cytomegalovirus
DPBS	Dulbecco’s phosphate-buffered saline
EGFR	Epidermal growth factor receptor
ELISA	Enzyme-linked immunosorbent assay
EpCAM	Epithelial cell adhesion molecule
ER	Endoplasmic reticulum
Fab	Fragment antigen binding
FACS	Fluorescence activated cell sorting
Fc	Fragment crystallizable
FcR	Fragment crystallisable receptor
FCS	Fetal calf serum
GM-CSF	Granulocyte-macrophage colony-stimulating factor
HEK	Human embryonic kidney
HER	Human epidermal receptor

HLA	Human leukocyte antigen
IgG/ Ig-κ	Immunoglobulin G/ kappa
IgSF	Immunoglobulin superfamily
ImmTAC	Immune mobilising monoclonal T-cell receptor against cancer
ITAM	Immunoreceptor tyrosine-based activation motif
ITIM	Immunoreceptor tyrosine-based inhibitory motif
MAPK	Mitogen-activated protein kinase
MFI	Median fluorescence intensity
MHC	Major histocompatibility complex
ND	Not detected
NF-κB	Nuclear factor-κB
NK	Natural killer
PEI	Polyethyleneimine
PI	Propidium iodide
PMA	Phorbol-12-myristate-13-acetate
PSCA	Prostate stem cell antigen
PSMA	Prostate-specific membrane antigen
scFv	Single-chain variable fragment
SDS-PAGE	Sodium dodecyl sulfate–polyacrylamide gel electrophoresis
TAA	Tumor-associated antigen
TAP	Transporter associated with antigen processing
TCR	T cell receptor
TIL	Tumor-infiltrating lymphocytes
TIM-3	T cell immunoglobulin and mucin domain-containing molecule 3
TNF	Tumor necrosis factor
VEGF	Vascular endothelial growth factor

VPA	Valproic acid sodium salt

List of figures

List of tables

1 Introduction

Cancer is globally ranked as one of the leading causes of death. Together with our aging population, the cancer incidence is rising worldwide. In 2020 ca. 19 million new cases have been diagnosed and an 1.5 fold increase is expected till 2040 demonstrating the need for potent treatment options (Bray et al., 2021; Sung et al., 2021). The contribution of the immune system to tumor growth and elimination is described as a dynamic process called immunoediting, which consist of three phases (Pandya et al., 2016; Vesely et al., 2011): In the elimination phase, the active immune response enables an efficient recognition and elimination of the malignant cells, a mechanism also called immune surveillance. However, a complete eradication is not always reached. Thus, in the equilibrium phase, few tumor cells remain in body tissues and the immune system only inhibits their further outgrowth. In the escape phase, the malignant cells acquire different immune-evasive characteristics such as loss of target antigen expression or immunosuppressive features. This change is also driven by the selective pressure mediated by the immune system itself and finally enables the tumor cells to grow out immunologically unrestricted. In addition to the classical treatment options consisting of chemotherapy, radiotherapy and surgery, cancer immunotherapy aims to support tumor eradication by specifically supporting the immune system. In the past decades various immunotherapeutic approaches have been investigated including vaccination, oncolytic viruses, adoptive cellular therapy using cells that can be genetically engineered to express a tumor-specific receptor, small molecules, checkpoint inhibitors and other antibody-based therapies (Farkona et al., 2016; Pandya et al., 2016; Tan et al., 2020). Meanwhile, there are several immunotherapeutic approaches that have been clinically approved and are currently used for the treatment of various cancer types. However, there is still a need for research as their use and outcome depends on various immunological and clinical factors and thus yet not all patients can benefit from these options.

1.1 Key players in the antitumor immune response

The immune system can roughly be subdivided in the branches “innate” and “adaptive” immune system, which both play important roles not only in the elimination of external pathogens such as bacteria and viruses but also in the elimination of malignant cells (Gonzalez et al., 2018; Pandya et al., 2016).

The innate immune system usually mediates a fast and initial response using different receptors that enable the recognition of “non-self” or damage-related patterns (Liu & Zeng, 2012; Pandya et al., 2016). The cellular anti-tumor response within the innate immune system is mostly mediated by NK (natural killer) cells and different phagocytes. NK cells carry a range

of stimulatory and inhibitory receptors that enable the recognition of stressed and altered cells based on their ligand “profile”. The major histocompatibility complex class I (MHC-I) molecules for example are recognized by different types of inhibitory NK cell receptors including the killer immunoglobulin like receptor (KIR) family (Chester et al., 2015; Pegram et al., 2011). MHC-I molecules are expressed by all nucleated cells throughout the body, albeit at greatly varying levels, and typically loaded with short peptides resulting from degraded intracellular proteins (Pishesha et al., 2022). Tumor cells however often downregulate expression of MHC-I molecules, thus promoting NK cell activation (Liu & Zeng, 2012; Pandya et al., 2016). Upon sufficient activation, NK cells release cytolytic granules resulting in tumor cell apoptosis. Additionally, NK cells possess another way of tumor cell recognition that involves the action of tumor-specific antibodies produced by the adaptive immune system: a process called antibody-dependent cell-mediated cytotoxicity (ADCC) (described in more detail in 1.1.3). Phagocytes of the innate immune system such as macrophages and dendritic cells can finally engulf and digest the apoptotic tumor cells, a process that results in the presentation of tumor-derived peptides on MHC class II molecules. The MHC-II complex is predominantly expressed by so-called professional antigen-presenting cells and loaded with peptides resulting from extracellular proteins or endocytosed cell surface proteins that are degraded in the endolysosomal compartment (Pishesha et al., 2022). Peptides presented in the context of MHC-I and MHC-II can then be recognized by $CD8^+$ and $CD4^+$ T cell subsets, respectively, belonging to the adaptive immune system.

The main feature of the adaptive immune system is the immense repertoire of antigen-specific receptors expressed by B and T cells that arise through somatic recombination during their maturation in the bone marrow and thymus, respectively (De Villartay et al., 2003; Market & Papavasiliou, 2003). Thus, the variable part of the B and T cell receptor (BCR/ TCR) sequence is generated by recombination of different gene segment sets: V – variable, D – diversity, J – joining, which generates a diversity of ca. 10^{14} and 10^{18} combinations, respectively. Additionally, both receptors are heterodimeric proteins consisting of two polypeptide chains, one generated by VDJ and one by VJ recombination, which further increases the number of possible combinations and thus receptor specificities. However, not all specificities are present in the periphery as autoreactive clones are usually removed during B and T development. Using the antigen-specific BCR, B cells can recognize and endocytose extracellular antigens. Following activation, they can differentiate into plasma cells secreting immunoglobulins (Ig, antibodies) of the same specificity as the BCR. Upon antigen binding, the Fc part of these immunoglobulins can induce different effector functions. Thus, antibody-bound tumor cells can be recognized by the complement system, which is composed of different serum factors, inducing complement-dependent cytotoxicity (CDC). Furthermore, they can activate Fc receptor expressing immune cells, such as NK cells and macrophages leading to ADCC or

antibody-dependent cell-mediated phagocytosis (ADCP), respectively (Graziano & Engelhardt, 2019; Van Erp et al., 2019). Besides antibody production, B cells the function as professional APC through MHC class II expression (Pandya et al., 2016). As mentioned above, T cells are able to bind peptides in context of the MHC complex using the T cell receptor (Gonzalez et al., 2018). Depending on the expression of the CD4 or CD8 co-receptor, which stabilize TCR-MHC interaction through additional binding of the MHC molecule, they can be further divided in two subsets: $CD4^+$ T helper cells and $CD8^+$ cytotoxic T cells, which recognize MHC-II- and MHC-I-restricted peptides, respectively. Following antigen-specific stimulation, $CD4^+$ T helper cells mainly function in promoting the immune response, for example by expressing B cell stimulating ligands or secreting proinflammatory cytokines, which promote the activation of several immune cells including $CD8^+$ T cells, NK cells and macrophages for example (Borst et al., 2018; Luckheeram et al., 2012). However, there are also regulatory $CD4^+$ T cells (T_{reg}) that serve to dampen the immune response following antigen clearance. Similar to NK cells $CD8^+$ T cells contain cytolytic granules. Thus, recognition of “non-self” or mutated peptides presented by MHC-I of infected or malignant cells results in $CD8^+$ T cell-mediated target cell destruction (Zhang & Bevan, 2011).

In addition to NK cells, macrophages and dendritic cells, other cells have been described to serve as bridge linking innate and adaptive immune response, which include the less frequent NKT cells and $\gamma\delta$ T cells recognizing non-peptide antigens (Pellicci et al., 2020).

1.1.1 MHCs and antigen presentation

1.1.1.1 MHC structure

The classical major histocompatibility complex is a highly polymorphic membrane protein complex consisting of two peptide chains that bind short peptide fragments serving as a T cell epitope (Pishesha et al., 2022; Wieczorek et al., 2017) (Figure 1). MHC-I is expressed by all healthy nucleated cells throughout the body and consists of a membrane-anchored MHC-I heavy α-chain (divided in 3 domains: $\alpha1$, $\alpha2$, $\alpha3$) and a non-covalently associated beta-2 microglobulin (β_2m). MHC-II, which is usually only found on professional APCs, consists of two membrane-anchored polypeptide chains – named alpha and beta (each with two domains: $\alpha1$ and $\alpha2$, $\beta1$ and $\beta2$). In both MHC complexes, the elongated peptide binding groove consists of two α-helices forming the walls and β-sheets forming its floor. Depending on the precise structure, MHC-I typically binds peptides of 8-10 amino acids (aa) length as the peptide groove has closed ends and MHC-II binds longer peptides of in average 10-15 aa length as the peptide groove has open ends. Peptide binding is furthermore influenced by charge and hydrophobicity of the binding groove. In humans, the MHC proteins are encoded by three different highly

polymorphic genes: Human leukocyte antigen (HLA)-A, -B and -C in case of MHC-I, and HLA-DR, -DP, -DQ in case of MHC-II. The generated variety enables to bind a huge repertoire of peptides – also termed immunopeptidome – that in case of MHC-I usually result from degraded intracellular proteins and in case of MHC-II from extracellularly acquired proteins. One exception, however, is peptide cross-presentation, which is a phenomenon unique to professional APCs resulting in loading of MHC-I with peptides from extracellularly acquired proteins as decribed in more detail later (1.1.1.2).

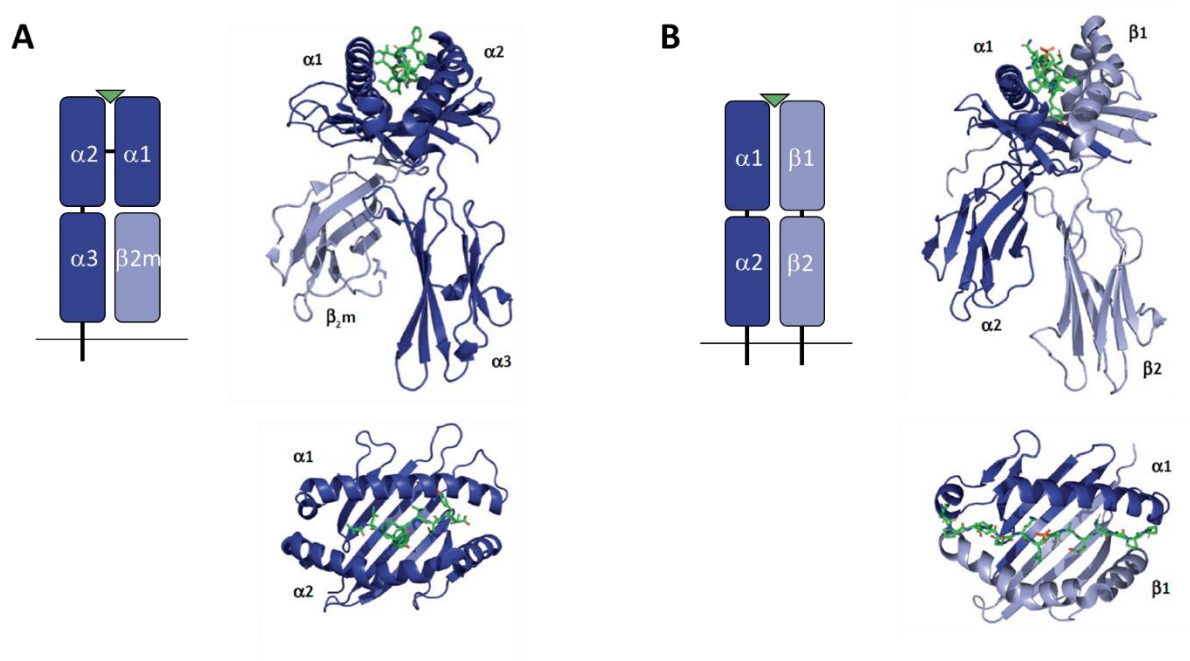

Figure 1: Structure of major histocompatibility protein complex class I and II
Shown is the architecture and crystal structure of a peptide-bound MHC class I (A) and class II (B) complex. MHC-I consists of a membrane-bound alpha chain and the non-covalently associated β_2-microglobulin. MHC-II consists of membrane-bound alpha and beta chains. The crystal structure is shown from a side and top view for HLA-A2 bound by a HuD peptide and (A) and HLA-DR1 bound by a Mart-1 peptide (B). Adapted from Pishesha et al., 2022.

1.1.1.2 Antigen processing and presentation

In case of MHC-I (Figure 2A), antigens are mostly sampled from the cytosol and processed via the ubiquitin-proteasome pathway (Pishesha et al., 2022; Wieczorek et al., 2017). The proteasome is a complex multiprotein machinery that degrades ubiquitin-tagged proteins (Leone et al., 2013). Many proteins are regularly tagged for degradation in this way such as regulatory, damaged, misfolded, mutated or upon infection also virus-derived proteins. The cylindrical shaped proteasome consists of three components: a catalytic core responsible for protein proteolysis and two regulators attached at both ends that mediate protein entry, deubiquitination, unfolding and translocation. The exact proteasome composition however can vary. The catalytical core also called 20S proteasome is formed by 4 rings: the two outer rings each consist of 7 α subunits interacting with the regulators and the two rings in the center

usually each contain seven β subunits with different proteolytic activity. In case of the so-called immunoproteasome that is typically found in professional APCs, three of the β subunits get replaced by IFN-γ inducible subunits with slightly different peptide cleavage properties. Furthermore, most proteasomes use the ATP-dependent 19S regulators, however there are also ATP-independent regulator complexes. In any case, for MHC-I loading, the resulting cytosolic peptides need to access the endoplasmic reticulum (ER). This transport is mediated by the dimeric transmembrane TAP1-TAP2 (transporter associated with antigen processing) transporter, which operates most efficiently for peptides of 8-12 aa length (Leone et al., 2013; Pishesha et al., 2022). Inside the ER, the peptides get loaded onto the MHC-I with the help of following chaperones: tapasin, ERp57, calreticulin and calnexin – also called the peptide-loading complex. Afterwards, the peptide-bound MHC-I complex gets translocated to the cell surface membrane.

As already mentioned, it is furthermore possible that proteins from the endolysosomal pathway get sampled for MHC-I presentation – a process in professional APCs commonly referred to as cross-presentation (Joffre et al., 2012). How exactly this happens is not entirely clear yet. However, it has been reported to occur via two different pathways. In the cytosolic pathway extracellular proteins enter the cytosol and get degraded by the proteasome. In the vacuolar pathway, MHC-I loading is believed to occur in the endolysosomal compartment.

In case of MHC-II (Figure 2B), antigens are sampled from the endolysosomal compartment (Pishesha et al., 2022; Wieczorek et al., 2017). Following internalization, the proteins get exposed to decreasing pH levels, reducing conditions and endolysosomal proteases resulting in protein destabilization and degradation. The resulting peptides can then bind to MHC-II molecules which have been translocated to the endolysosomal compartment due to a signal peptide contained within the associated invariant chain (Ii) that assembles with MHC-II molecules in the ER preventing the binding of TAP-translocated peptides. In late endosomes, this invariant chain gets cleaved leaving an MHC-II-bound CLIP peptide behind. This peptide functions as a placeholder and can be exchanged by a suitable MHC-II ligand with help of HLA-DM, which displaces low affinity ligands and thus promotes a stable peptide MHC complex with a high affinity ligand. For antigen presentation, the complex is transported in vesicles to the plasma membrane.

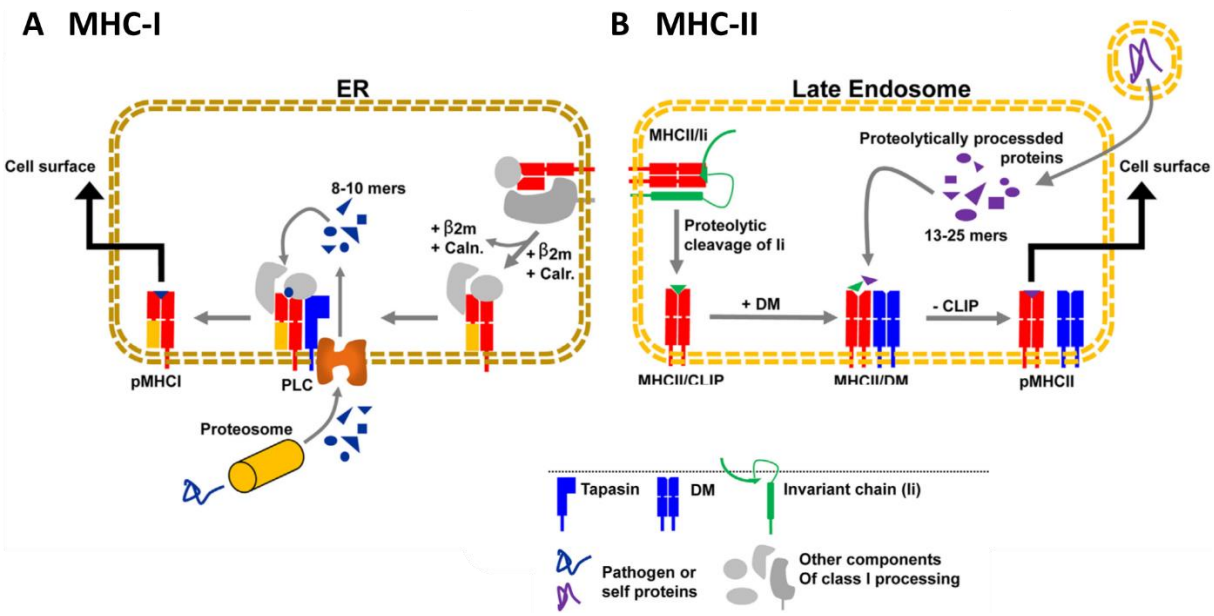

Figure 2: MHC class I and II antigen processing
Shown is an illustration of MHC-I (A) and MHC-II (II) antigen processing. MHC-I is typically loaded with peptides from degraded intracellular proteins, which get transported into the ER and loaded on the empty MHC-I with the help of a peptide loading complex (consisting of TAP, tapasin and chaperones). MHC-II is loaded in endosomes with peptides from endocytosed degraded proteins. In endosomes, the MHC-II-associated li chain gets cleaved leaving a short placeholder peptide behind (CLIP). CLIP is then exchanged with matching high affinity MHC-II ligands with the help of HLA-DM. Adapted from Wieczorek et al., 2017.

1.1.2 T cells

1.1.2.1 TCR and antigen recognition

The T cell receptor (Figure 3) is a heterodimeric disulfide-linked membrane protein that consists of an alpha and beta chain (Dong et al., 2019; Krogsgaard & Davis, 2005; Mariuzza et al., 2020). Each chain comprises an extracellular immunoglobulin-like variable region, followed by a constant domain, a connecting peptide (CP) including the cysteine for disulfide bridge formation, a transmembrane domain and a short cytoplasmic tail. In the membrane the TCR forms an 1:1:1:1 ice-cream cone-shaped multiprotein complex together with three different CD3 dimers: CD3εδ, CD3εγ, CD3ζζ (Dong et al., 2019; Mariuzza et al., 2020). Similar to the TCR, all CD3 molecules contain an immunoglobulin-like domain followed by a CP, a transmembrane and cytoplasmic domain. In contrast to the TCR however, the cytoplasmic domain of the CD3 molecules include one (CD3ε/γ/δ) to three (CD3ζ) immunoreceptor tyrosine-based activation motifs (ITAM), which mediate TCR signaling.

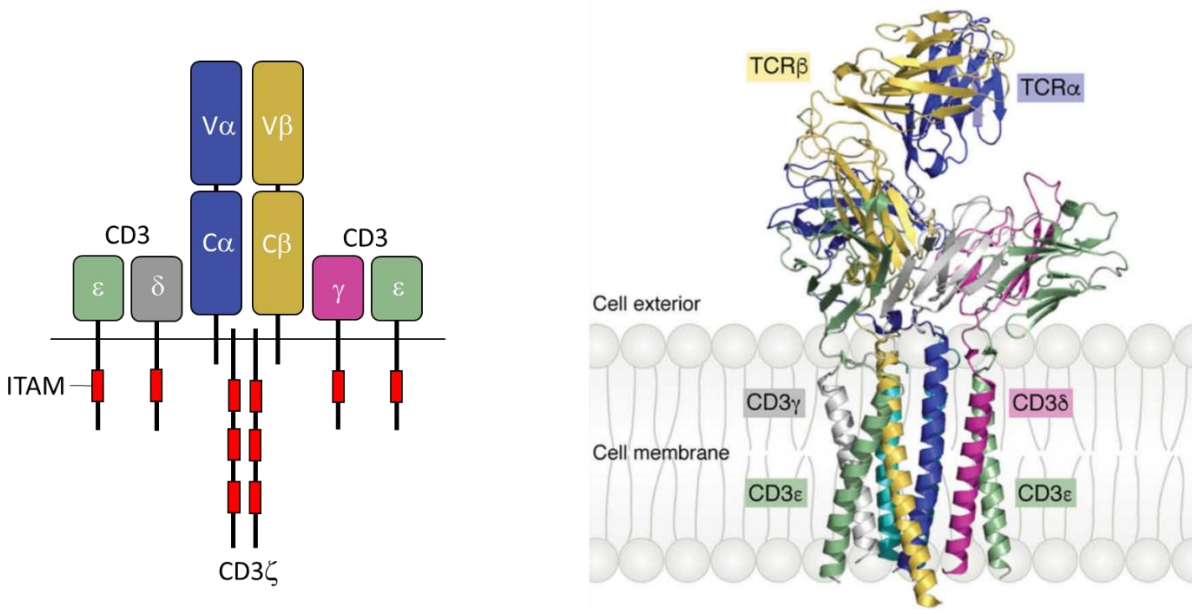

Figure 3: Structure of the TCR complex
Shown is the general architecture (left) and crystal structure (right) of a TCR complex. The TCR complex includes the T cell receptor, which consists of alpha and beta chain, associated with six CD3 molecules of which CD3 ε, δ and γ contain each one ITAM in the cytoplasmic tail and CD3 ζ contains three ITAMs. The cytoplasmic tails are not visible in the crystal structure. Adapted from Mariuzza et al., 2020.

As already mentioned above, the TCR's variable domain is generated by recombination of the gene segments VDJ, in case of TCRα, and VJ, in case of TCRβ (Dong et al., 2019; Krogsgaard & Davis, 2005; Mariuzza et al., 2020). Similar to the variable region of an immunoglobulin it contains three complimentary-determining regions (CDR) that mediate antigen contact. From these three regions CDR3 is the most variable one as it arises from the gene junction site, whereas CDR1 and 2 are encoded within the V gene segment. Thus, interaction with the peptide is mostly mediated by CDR3α and CDR3β, while CDR1 and CDR2 are more relevant for MHC binding (Krogsgaard & Davis, 2005). Furthermore during the interaction with pMHC-I, TCRVα is usually in contact with the MHC-I α2 helix and TCRVβ with the MHC-I α1 helix; and during the interaction with pMHC-II, TCRVα is in contact with the MHC-II β chain and TCRVβ with MHC-IIα generating a relatively conserved and diagonal TCR binding mode (Rossjohn et al., 2015; Szeto et al., 2021). Overall, binding to the pMHC complex is typically characterized by a very low affinity of 1-50 µM, which is around 1:1000-10000 lower compared to the affinity of an antibody (Krogsgaard & Davis, 2005). However, since TCRs are membrane bound this low affinity functions to enable detachment of the T cell following APC contact. Consistently, the half-life of the TCR–pMHC interaction itself is only seconds, a stable interaction between a T cell and an APC however can persist for several hours (Fooksman et al., 2010; Krogsgaard & Davis, 2005). How exactly TCR signaling is induced following pMHC binding is still unclear and different mechanisms have been suggested that include clustering,

mechanosensing, steric segregation of inhibitory molecules and allosteric effects (Mariuzza et al., 2020).

1.1.2.2 T cell activation

T cell activation is a process that commonly occurs in lymphoid organs induced by an antigen-specific interaction with an activated mature professional APC (Curtsinger & Mescher, 2010; Halle et al., 2017; Kedzierska & Koutsakos, 2020; Tai et al., 2018). More precisely, this interaction includes three signals that together induce T cell activation: antigen-recognition via the T cell receptor (1), delivery of co-stimulatory signals by the antigen presenting cell expressing co-stimulatory ligands (2) and secretion of cytokines (3). This initial antigen contact – also called T cell priming – typically occurs in secondary lymphoid organs and induces T cell activation, proliferation and differentiation into different effector and memory subsets. Following T cell priming, the activated cells egress from the lymph node and migrate towards their effector site. In contrast, TCR triggering in absence of sufficient co-stimulatory signals is not able to induce T cell activation and results in anergy, which is characterized by a tolerant unresponsive phenotype (Schwartz, 2003).

TCR signaling: T cells are constantly exposed to some degree of TCR triggering as all TCRs recognize a small spectrum of peptides and are thus slightly auto-reactive (Malissen & Bongrand, 2015). The induced response, however, depends on TCR affinity towards the pMHC complex which is typically higher towards non-self peptides. This constant TCR "tickling" is believed to induce a state of increased reactivity and there are several models that suggest different initiating events for a full T cell activation. In general, TCR signaling results in phosphorylation of the cytoplasmic CD3 ITAM domains as the cytoplasmic tails of the TCR α and β chains exert no function (Malissen & Bongrand, 2015; Mørch et al., 2020). This phosphorylation is mediated by the protein kinase LCK, which exists freely diffusing as well as associated to the cytoplasmic tail of the $CD4^+$ and $CD8^+$ co-receptors, and leads to recruitment and phosphorylation of another protein kinase called ZAP-70 (Figure 4). Upon TCR "tickling", ZAP-70 is believed to be partially phosphorylated and thus not catalytically active and only a strong non-self-pMHC agonist induces complete phosphorylation. Active ZAP-70 in turn facilitates the phosphorylation of LAT and SLP-76, which form a signaling scaffold initiating downstream signaling for example via activation of phospholipase C-γ.

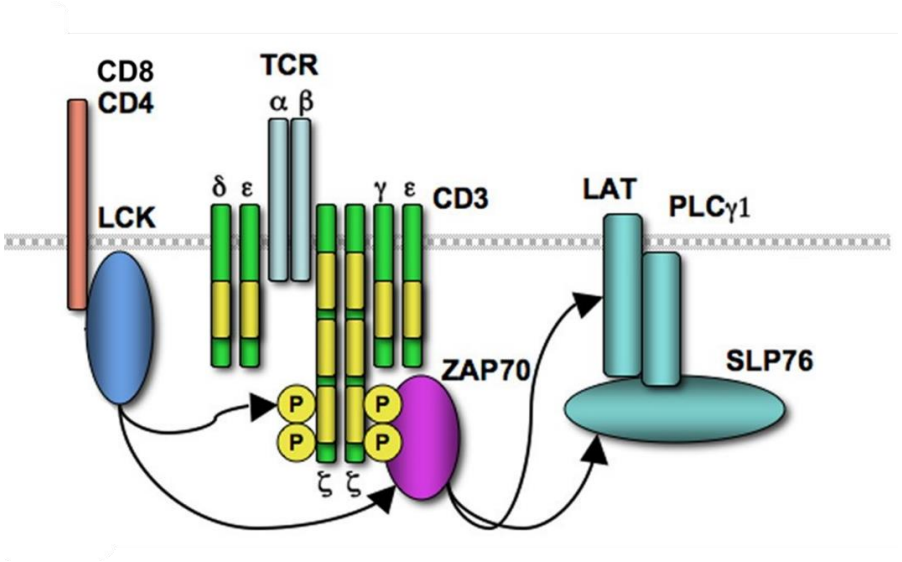

Figure 4: Initial events in TCR signaling
Following pMHC engagement, TCR signaling events are initiated via LCK-mediated phosphorylation of the immunoreceptor tyrosine-based activation motifs (ITAM) of CD3 co-receptors and the thereby recruited ZAP-70 kinase. ZAP-70 results in phosphorylation of LAT and SLP76, which build a signaling scaffold enabling further downstream signaling for example by activation of phospholipase C-γ (PLCγ) and other proteins not shown here. Adapted from Zikherman & Weiss, 2009.

Immunological synapse: Upon a strong cognate pMHC-TCR interaction, the downstream signaling also induces the formation of a so-called immunological synapse (IS) at the cell contact site (Cassioli & Baldari, 2019; Fooksman et al., 2010; Malissen & Bongrand, 2015) (Figure 5). In a bull's eyes view this synapse can be divided into 3 regions as first described by Kupfer and colleagues (Monks et al., 1998). The center called central supramolecular activation complex (cSMAC) is characterized by a high density of microclusters containing engaged TCRs and co-stimulatory receptors (Cassioli & Baldari, 2019; Fooksman et al., 2010; Monks et al., 1998). This region is surrounded by a "ring" called peripheral SMAC (pSMAC), which is characterized by the adhesion molecule lymphocyte function-associated antigen 1 (LFA-1) that binds to the intracellular adhesion molecule 1 (ICAM-1) on the APC. The third region following pSMAC is called distal SMAC (dSMAC) and contains a high density of glycoproteins on the "outside" and actin filaments inside the cell. Beyond this general structure, however, the IS formed between professional APCs and target cells differ considering function and precise organization. For example, cytolytic $CD8^+$ T cells form an asymmetric IS in contact with the target cell that includes a secretory cleft for the secretion of apoptosis inducing effector molecules as described in more detail later (1.1.2.4) (De La Roche et al., 2016; Dustin & Long, 2010).

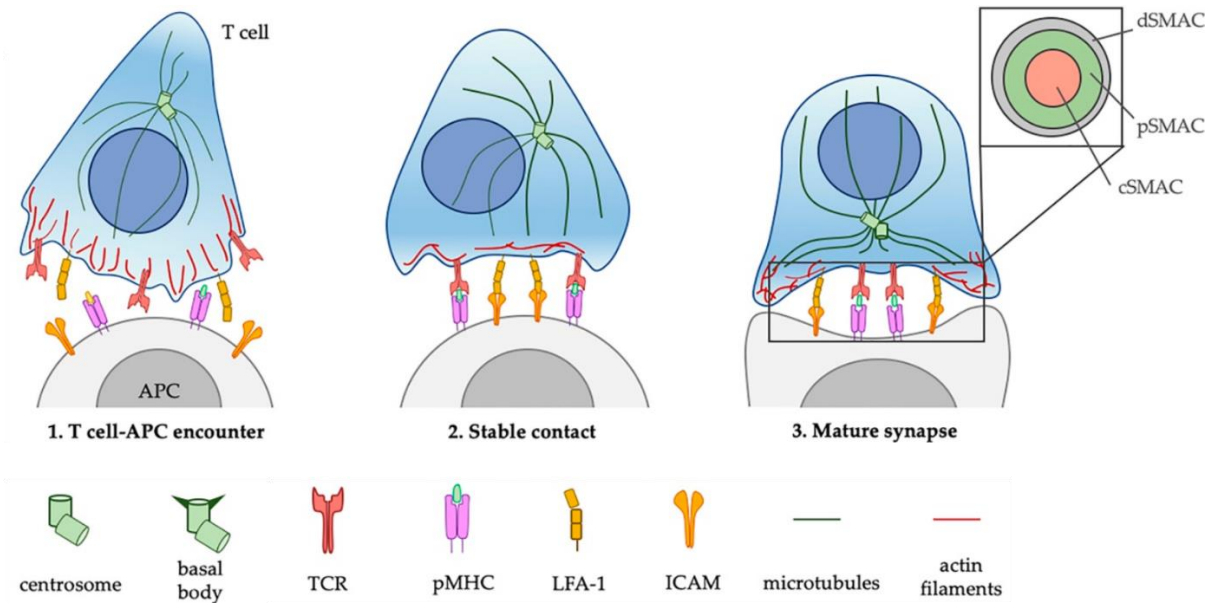

Figure 5: Immunological synapse between T cell and APC
Shown is the formation of an immunological synapse between T cell and APC. This interaction can be divided into different zones, called SMACs. The central zone (cSMAC) is characterized by a high density of engaged TCR-pMHC complexes. The peripheral (p)SMAC forms cell-cell interaction via LFA-1 and ICAM-1 and the distal (d)SMAC is characterized by rearranged actin filaments. Adapted from Cassioli & Baldari, 2019.

Co-signaling receptors: Dependent on their activation state, T cells express different co-stimulatory as well as co-inhibitory receptors (Chen & Flies, 2013). As mentioned above, co-stimulatory signals promote T cell activation and proliferation. In contrast, co-inhibitory receptors function to downmodulate the T cell response and are also often expressed in exhausted T cells that arise through chronic antigen stimulation and are characterized by an hyporesponsive phenotype. The best described co-stimulatory receptor is CD28, which belongs to the immunoglobulin superfamily (IgSF) (Chen & Flies, 2013). CD28 is constitutively expressed on naïve T cells and binds to CD80 and CD86 (B7 family). Its supports activation and proliferation via activation of the phosphatidylinositol 3-kinase, which activates different factors such as NF-κB (nuclear factor-κB) or mTOR (mammalian target of rapamycin). The same ligands can also induce inhibition when binding to the co-inhibitory receptor CTLA-4 (cytotoxic T lymphocyte antigen 4), which is only expressed following T cell activation while CD28 expression gets downregulated. In contrast to CD28, CTLA-4 recruits protein phosphatases that prohibit TCR signaling for example through of CD3 ITAM dephosphorylation. Other well characterized co-stimulatory receptor – ligand pairs are CD27 – CD70, 4-1BB – 4-1BBL and OX40 – OX40L belonging to the tumor necrosis factor (TNF) receptor superfamily. All TNF receptors recognize trimerized ligands and thus build trimeric complexes upon recognition. TNF receptor signaling results in the recruitment of TNF receptor-associated factors, which in turn activate different molecules including NF-κB or the mitogen-activated protein kinase (MAPK). Whereas CD27 is also important upon T cell priming, 4-1BB

and OX40 get upregulated following T cell activation and thus support already activated T cells. Other well characterized co-inhibitory receptors that are induced following T cell activation include the IgSF receptors PD1 binding PD-L1 and PD-L2, TIM-3 (T cell immunoglobulin and mucin domain-containing molecule 3) binding galectin 9, and LAG-3 (lymphocyte activation gene 3 protein) binding MHC-II (Chen & Flies, 2013; De Sousa Linhares et al., 2018).

1.1.2.3 $CD4^+$ T cells

$CD4^+$ T cells, also called T helper cells, get activated upon recognition of the matching antigen-MHC-II complex expressed on mature professional APCs that themselves have been activated through recognition of “non-self” or damage-associated patterns. Following activation, $CD4^+$ T cells can differentiate into long-lived memory cells as well as different types of short-lived effector cells that each mediate distinct functions in orchestrating the immune response (Luckheeram et al., 2012; Zhu & Paul, 2008). These effector cell subsets include T helper cell 1 (Th1), Th2, Th9, Th17, follicular T helper cells (Tfh) and Tregs - including naturally Tregs (nTregs) and induced Tregs (iTregs). Except for nTregs, which arise as a distinct $CD4^+$ T cell subset directly from the thymus, all other T cell subsets develop through differentiation following T cell activation induced by the presence of different fate-inducing cytokines.

Th1 develop in the presence of interferon γ (IFNγ) and interleukin 12 (IL-12) and are part of the immune response towards intracellular pathogens. Following differentiation, they secrete mainly IFNγ – supporting the activation of macrophages; IL-2 – supporting $CD8^+$ T cell proliferation and T cell memory formation; and lymphotoxin α, which was shown to be involved in the development of autoimmune diseases.

Th2 cells differentiate in the presence of IL-4 and IL-2, are part of the immune response towards extracellular pathogens and secrete following effector-cytokines: amphiregulin – an epidermal growth factor; IL-4 – important for IgE isotype switch and further promoting Th2 differentiation; IL-5 – leading to the recruitment of eosinophils; IL-9 – leading to increased mucus production by epithelial cells; IL-10 – acting anti-inflammatory; IL-13 – important upon helminth infection; and IL-25 – promoting the IgE isotype switch and IL-4, IL-5 and IL-13 production.

Th9 differentiate in the presence of transforming growth factor β (TGF-β) and IL-4, were shown to be involved in allergic conditions and are characterized by IL-9 production.

Th17 cells are also important to eliminate extracellular pathogens and develop in the presence of IL-6, IL-21, IL-23 and TGF-β. The main effector cytokines are IL-17A, IL-17F, IL-21 and IL-22. IL-17A and IL-17F both bind to the IL-17RA receptor and lead to increased production of

IL-6, IL-1 and TNFα; IL-21 further supports Th17 differentiation, T and NK cell activation and B cell differentiation; IL-22 can act pro- as well as anti-inflammatory.

Regulatory T cells, including nTregs and iTregs, are characterized by expression of the transcription factor FOXP3. iTregs develop in the presence of high concentrations of TGF-β (compared to Th17) and IL-2. The main effector cytokines of both Treg subsets include the anti-inflammatory IL-10 and IL-35; and TGF-β, which further promotes iTreg development.

1.1.2.4 $CD8^+$ T cells

Similar to the activation of $CD4^+$ T cells, $CD8^+$ T cell activation requires antigen-specific stimulation by mature professional APCs (Figure 6). $CD8^+$ T cells, however, only recognize peptides in context of MHC-I. Thus, a special process called antigen cross-presentation is required. As described above, this process is limited to APCs and enables them to present extracellularly acquired (tumor-derived) peptides on MHC-I instead of MHC-II (Borst et al., 2018). Furthermore, a previous or simultaneous activation of the APC not only by innate receptor signaling but also by antigen-specific interaction with a $CD4^+$ T cell accompanied by CD40-CD40L engagement, was shown to be required to induce sufficient $CD8^+$ T cell activation and differentiation (Borst et al., 2018). In DCs for example, this interaction leads to upregulation of CD80 and CD86, which bind to the co-stimulatory receptor CD28 on T cells; upregulation of CD70, which binds to the costimulatory receptor CD27; and secretion of IL-12 and IL-15, which promote $CD8^+$ T cell differentiation. Additional to TCR signaling and co-stimulation by the APC, $CD8^+$ T cells also require the presence of the inflammatory cytokines IL-12 and/ or type I interferons to generate a productive immune response (Borst et al., 2018; Cox et al., 2011; Curtsinger & Mescher, 2010).

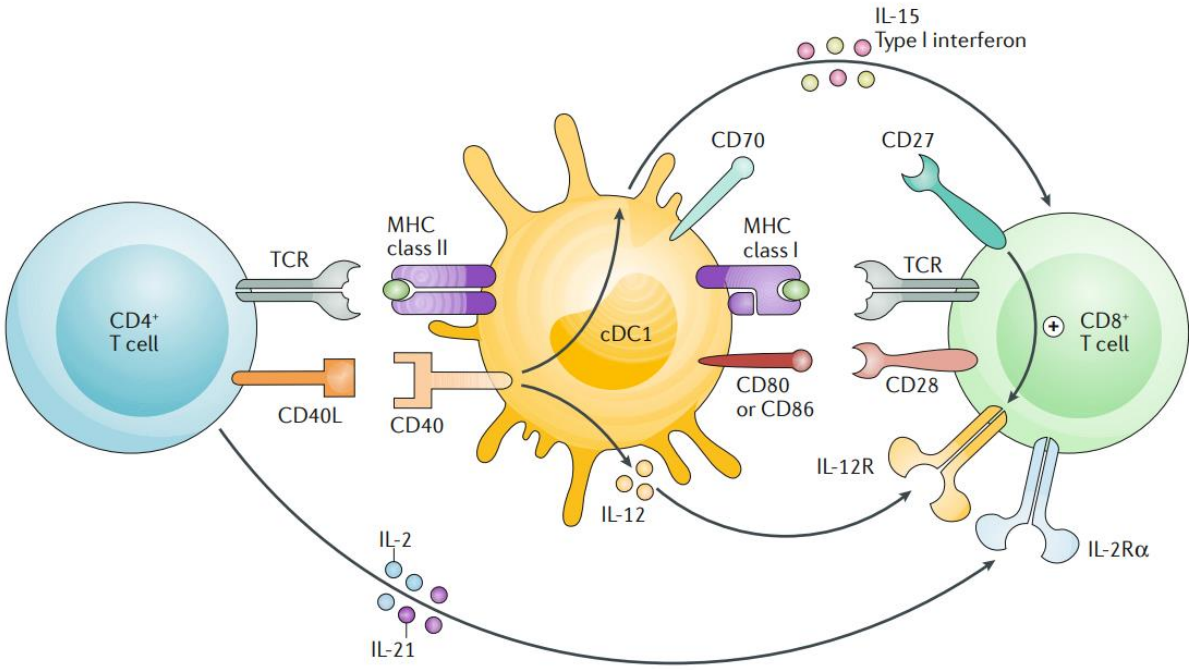

Figure 6: Activation of CD8⁺ T cells
CD8⁺ T cells get activated by professional antigen-presenting cells (e.g., conventional DCs - cDC). This interaction requires three signals: TCR triggering by recognition of MHC-I-restricted peptides, engagement of co-stimulatory ligands expressed by the dendritic cells (e.g., via CD28-CD80/86 or CD27-CD70 pairing) and cytokines secreted by dendritic cell as well as by CD4⁺ T cells that got activated following recognition of MHC-II-restricted peptides presented by professional APCs. A previous or simultaneous antigen-specific interaction of the professional APC with CD4⁺ T cells results in CD40-CD40L engagement that was shown to increase the APCs co-stimulatory functions and thus T cell activation. Adapted from Borst et al., 2018.

Similar to CD4⁺ T cells, activated CD8⁺ T cells give rise to a heterogeneous population consisting of effector and memory cells. Upon activation, most cells terminally differentiate into short-lived effector cells, which are characterized by their ability to induce target cell apoptosis through different mechanisms (Kedzierska & Koutsakos, 2020; Trapani & Smyth, 2002; Voskoboinik et al., 2015). These include the release of granules containing perforin and granzyme into the immunological synapse formed following antigen recognition (De La Roche et al., 2016; Trapani & Smyth, 2002; Voskoboinik et al., 2015). In this process, the granules are transported to the membrane via microtubule-organizing centers and released by exocytosis. The released perforins form a pore in the target cell membrane, which enables the granzymes to enter the cell. Inside the target cell, these serine proteases induce apoptosis via activation of the caspase pathway or caspase-independent targeting mitochondrial pathways. Another cell-death mechanism is the expression of FasL and TRAIL, which binds to the cell death receptors FasR and TRAILR on the target cell inducing caspase-dependent apoptosis. Following clearance of pathogens or tumor cells, the effector cell subset contracts and only few cells remain to form the memory population (Cox et al., 2011; Cui & Kaech, 2010; Kedzierska & Koutsakos, 2020). In contrast to the nomenclature, effector and memory cells do

not form two completely distinct subsets but rather exist as a continuum with many intermediate phenotypes and different factors influencing their differentiation. Thus, for example, it was shown that a high IL-2 concentration – produced by activated $CD8^+$ and $CD4^+$ T cells – promotes an effector cell phenotype. To date there are different models that try to explain how $CD8^+$ T cell differentiation is regulated (Joshi & Kaech, 2008; Kedzierska & Koutsakos, 2020). The exact mechanisms however still remain elusive.

1.1.3 NK cells

NK cells belong to the innate immune system and show similar functions to $CD8^+$ and Th1 T cells due to their cytotoxic properties and effector cytokine profile (Abel et al., 2018; Paul & Lal, 2017). In contrast to $CD8^+$ T cells however, they naturally mediate cytotoxicity without the need of antigen priming or clonotypic receptors. Instead, NK cells express various germline-encoded activating and inhibitory receptors that together control target recognition and NK cell activation. Human NK cells are defined as $CD3^-CD56^+$ cells that arise from hematopoietic progenitor cells through IL-15 stimulation. Well-known NK cell subsets include $CD56^{bright}CD16^-$, $CD56^{dim}CD16^+$ and the more recently discovered adaptive/memory-like NK cells $CD56^{dim}CD16^+CD57^+NKG2C^+$ (Abel et al., 2018; Paul & Lal, 2017; Pierce et al., 2020). According to the linear development model, $CD56^{bright}CD16^-$ are believed to be a more immature precursor of $CD56^{dim}CD16^+$, which are characterized by production of inflammatory cytokines such as IL-10, IL-13, GM-CSF (granulocyte-macrophage colony-stimulating factor), IFNγ and TNFα (Abel et al., 2018; Cichocki et al., 2019; Cooper et al., 2001; Di Vito et al., 2019). $CD56^{dim}CD16^+$ are the predominant population in the blood and show reduced cytokine production but strong cytotoxic properties. Likewise, adaptive NK cells should display a further matured development state that arises during viral infections or through cytokine stimulation (e.g., IL-12, IL-15 and IL-18) (Gang et al., 2020; Mujal et al., 2021). These cells have been most intensely studied upon CMV (cytomegalovirus) infection and show memory-like features similar to that of the adaptive immune system as well as increased effector functions including cytotoxicity and IFNγ secretion. The enhanced cytotoxicity is probably caused by a loss of FcRγ expression, which is the commonly used signaling adaptor to induce antibody-dependent cytotoxicity (Liu et al., 2020; Mujal et al., 2021; Zhang et al., 2013). However, as this results in FcRγ being replaced by the even more potent signaling adaptor CD3ζ, the loss actually leads to increased effector functions.

As mentioned above, NK cell activity is regulated by a broad range of germline-encoded receptors (Myers & Miller, 2021; Paul & Lal, 2017). Whether NK cells get activated or not depends on the balance of activating and inhibitory signals received. Thus, two common mechanisms for NK cell activation include “induced self”, which means the upregulation of

activating ligands; and “missing self”, which means the downregulation of inhibitory ligands such as MHC-I. Activating receptors typically signal through ITAMs, which get phosphorylated following ligand engagement. This results in activation of the kinases Syk and ZAP70, which initiate downstream signaling inducing the NK cell response. In contrast, signaling of inhibitory receptors is mediated through phosphorylation of so-called ITIMs (Immunoreceptor tyrosine-based inhibitory motifs), which leads to the recruitment of different phosphatases that counteract the activating signaling. One important receptor family, the killer immunoglobulin-like receptor (KIR) family, contains both inhibitory receptors with a long ITIM containing cytoplasmic tail and activating receptors with a short cytoplasmic tail that associates with an ITAM containing signaling adaptor (Blunt & Khakoo, 2020; Pende et al., 2019). These receptors bind to classical MHC-I molecules (HLA-A/B/C) mostly in a peptide-dependent manner. Thus, upon MHC-I downregulation, a common mechanism used by tumor cells to evade T cell recognition, missing stimulation of inhibitory KIRs can promote NK cell activation according to the “missing self” principle. Activating KIRs also recognize MHC-I molecules however with a lower affinity.

Other important activating receptors include:

- FcγRIIIa (also CD16a), which mediates the so-called antibody-dependent cell-mediated cytotoxicity and is the only one whose signaling is able to induce an NK cell response on its own. CD16a binds to the Fc part of IgGs (immunoglobulin G) and thus enables recognition and lysis of IgG-opsonized tumor cells. The affinity of CD16a varies and depends on a polymorphism at position 158 (V/F), whereby $CD16a_{158V}$ showed stronger binding and better clinical results upon antibody-based therapies (Coënon & Villalba, 2022; Paul & Lal, 2017).
- Natural cytotoxicity receptors NKp30, NKp44, NKp46 each binding to different (pathogen- and) host-derived ligands such as heparan sulfate glycosaminoglycans, which is part of cell surface and extracellular matrix and important for tumor progression; B7-H6 upregulated on different tumor cells; nuclear proteins that usually reside inside the cell but become exposed to the cell surface in tumor cells; galectin-3, which is important for the tumor microenvironment; nidogen-1, which is part of the basement membrane; and platelet-derived growth factor-DD, which supports tumor growth (Barrow et al., 2019).
- NKG2D binding to MHC-I polypeptide-related sequence A and B (MICA & MICB) and the MHC-I related UL16 binding protein (ULBP) family upregulated in tumor cells (Xuan et al., 2015).
- CD94-NKG2C and CD94-NKG2E dimers binding to HLA-E, a non-classical MHC-I protein that binds peptides resulting from the leader sequence of different MHC-I molecules as well as viral sources. Interestingly, a peptide resulting from HLA-G,

whose expression is upregulated upon CMV infection, was furthermore shown to promote adaptive NK cell development (Orbelyan et al., 2014; Rölle et al., 2018).

Other important inhibitory receptors include:

- CD94-NKG2A that recognizes HLA-E equally to the other CD94 dimers, however with 6 times higher affinity and less peptide restriction in comparison to NKG2C (Myers & Miller, 2021; Rölle et al., 2018).

Similar to $CD8^+$ T cells NK cells possess two mechanism to induce cytotoxicity, namely the expression of cell death receptor ligands (FasL, TNF, TRAIL) and the release of granzyme and perforin containing granules (Dustin & Long, 2010; Paul & Lal, 2017). Likewise, this requires the formation of an immunological synapse, which is structurally similar to that of T cells (1.1.2.2) as it can be divided in the above-mentioned SMAC compartments using the adhesion protein LFA-1 for cell-cell contact. Further, it also induces the reorganization of the actin cytoskeleton and polarization of the microtubule-organizing centers for granule transport. Depending on the signals received, the cSMAC can contain different ratios of tyrosine kinases (promoting activation by phosphorylation) and tyrosine phosphatases (inhibiting activation by dephosphorylation).

1.2 Antibody-based therapies

The field of antibody-based therapies is highly manifold as it comprises many different therapeutic strategies that make use of different targets, molecule formats and mechanisms of action (Jin et al., 2022; Shah et al., 2021; Suurs et al., 2019). Thus for example, antibody-based reagents can be used to neutralize or block specific receptor-ligand interactions important for tumor physiology, they can promote immune cell activation by activating or inhibiting specific receptor pathways, they can promote tumor cell recognition and killing by bridging immune and tumor cell using multispecific molecules with multiple binding sites, they can directly induce cytotoxicity when conjugated to a toxic payload or they can stimulate the immune response when fused to cytokines. Furthermore, due to advances in the generation of recombinant proteins, antibody-based molecules can be designed that serve several of these purposes at once.

1.2.1 Formats

Today there are numerous formats of antibody-based proteins that differ depending on their intended mode of action (Chiu et al., 2019; Suurs et al., 2019).

Basic structure of a full-length IgG: Immunoglobulin G antibodies are Y-shaped proteins consisting of four polypeptide chains (Figure 7) including each two identical heavy and light chains connected by disulfide bridges (Chiu et al., 2019). Similar to the TCR (1.1.2.1) heavy and light chain each consist of a variable and constant domain, of which the variable is mediating antigen contact. Structurally both variable domains are characterized by tightly packed β-strands, that expose important connecting loops at the "tip" of the arm. These finger-like loops contain the highly variable complementarity determining regions that arise through VDJ (heavy chain) and VJ (light chain) gene rearrangement, and that contact the surface of the recognized antigen. The variable domain of the light chain is followed by the constant domain of the light chain (C_L), and the variable heavy chain domain is followed by a constant domain (C_H1), a hinge region and two more constant domains (hinge-C_H2-C_H3). For protein assembly a disulfide bridge is formed between C_L and C_H1 and two disulfide bridges between the hinge of both heavy chains. Overall, an antibody can be divided in two fragment antigen binding (Fab) regions (N-terminal of the hinge domain) fused to the Fc part (fragment crystallizable, C-terminal of the hinge domain). In unmodified human isotype G immunoglobulins, the asparagine 297 within the Fc part is typically glycosylated. This N-linked glycan is highly important for different effector functions, such as FcγR binding important for NK-cell mediated ADCC and antibody-dependent cell-mediated phagocytosis by macrophages and dendritic cells. In addition to the cell-mediated effects, another function of the Fc part is to mediate complement-dependent cytotoxicity (CDC) as Fc binding by C1q results in a cascade that leads to formation of a lytic membrane attack complex in the antibody-bound target cell membrane. Other immunoglobulin isotypes include additional constant domains or domains to enable multimerization. However, these isotypes are less often used for therapeutic antibodies.

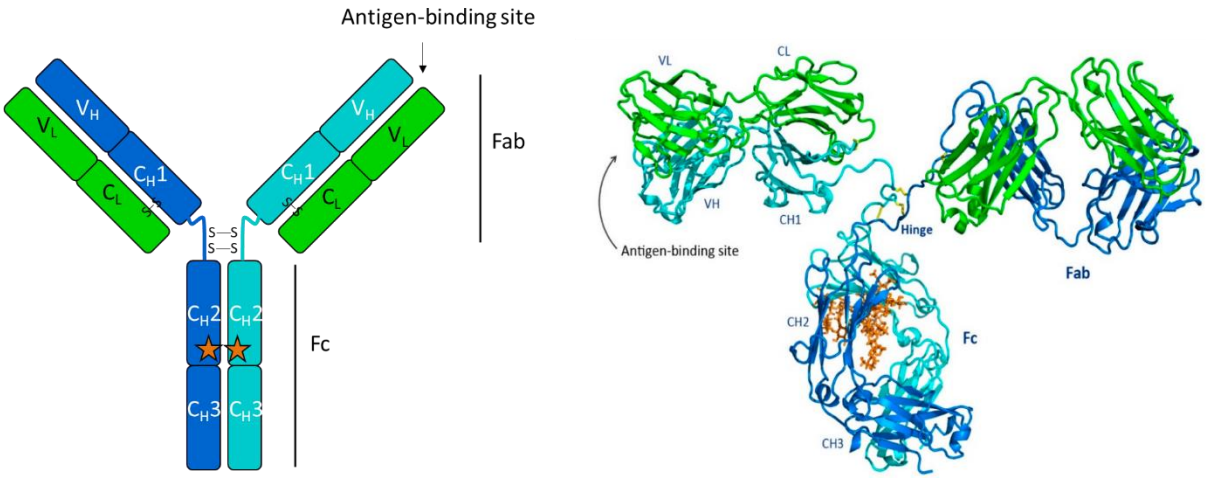

Figure 7: Structure of an immunoglobulin G
Immunoglobulins of the isotype G are Y-shaped proteins composed of four disulfide-linked peptide chains: two identical heavy chains composed of a variable domain (V_H), followed by a constant heavy domain (C_H) 1, the hinge domain and constant heavy domains 2 and 3; and two identical light chains composed of a variable and constant domain (V_L-C_L). The antigen-binding site is jointly formed by V_L and V_H at the top of the Y arms. The part that is N-terminal of the hinge domain is also referred to as Fab fragment and the C-terminal site as Fc fragment. The Fc part is typically glycosylated (shown in orange). On the left side the general architecture is illustrated. The right side shows the crystal structure of a glycosylated IgG adapted from (Chiu et al., 2019).

Antibody fragments compared to IgGs: Besides full-length IgGs other Fc-lacking antibody fragments have been investigated for target binding (Jin et al., 2022). These include a single Fab-arm fragment, a F(ab')2 fragment that contains two Fab-arms connected by the hinge domain, scFvs (single-chain variable fragments) that consist of V_H and V_L connected via a flexible glycine-serine linker, and a special camelid-derived 15 kDa antigen-binding VHH domain. Upon *in vivo* administration the molecular weight plays an important role for the half-life as proteins below 60 kDa are usually cleared via the kidney and those above 60 kDa are excreted in a slower process *via* the liver. Thus, bigger constructs offer an increased serum half-life but proteins of lower molecular weight on the other hand enable easier tissue penetration and thus might be especially interesting for the treatment of solid tumors. In addition to a higher molecular weight, Fc-bearing proteins retain a longer half-life by binding to neonatal Fc receptors that regulate IgG blood levels.

Multispecific IgG-like and non-IgG-like proteins: In the last two decades multispecific agents evolved to an exciting research topic after their development was dampened for a long time due to the lack of necessary technologies (Jin et al., 2022; Ma et al., 2021; Suurs et al., 2019). Thus, in the beginning bispecific antibodies were generated by fusion of two different antibody-producing hybridoma cell clones. However, upon random association of light and heavy chains, there are 16 combinations possible of which only two would have the desired

specificity. Meanwhile advanced DNA technologies enable to engineer recombinant proteins of any desired constellation each offering different properties, which drove development of many different multispecific Fc-bearing and Fc-lacking formats.

Strategies used to generate a bispecific full-length IgG-like protein include (Figure 8A):

- Fc portions with knob-in-hole mutations, where one heavy chain incorporates large knob-forming amino acids and the other is engineered to form a matching pocket favouring heterodimerization
- the SEED platform, which also generates asymmetric but complementary C_H3 domains by using alternating IgA and IgG sequences
- the DEKK and ART-Ig platform, which introduce different amino acid exchanges in both heavy chains that mediate a stable non-covalent interaction
- Orthogonal Fab, which generates a special interface in the variable region to favour correct light chain association
- DuoBody, which enables a controlled exchange of the heavy-light chain pair between two antibodies
- Fit- and DVD-Ig, which use a format with extended Fab-arms that each incorporate both antigen-binding domains
- DAF, which uses phage display to generate an antigen-binding domain specific for two different epitopes
- CrossMab, which favours correct light chain association by exchanging C_H1 and C_L within one arm
- Wuxibody, which favours correct light chain association by exchanging C_H1 and C_L of one arm with the constant domains of a TCR

On the other hand, multispecific non-IgG-like proteins can be generated by connection of different antibody fragments (Figure 8B). Thus, for example two scFvs can be connected simply via another glycine-serine linker. A similar approach are DART proteins, which consist of two V_H-V_L polypeptide chains connected via a disulfide bridge. TandAbs consist of two peptide chains (e.g. V_H1-V_L2-V_H2-V_L1) that form a tetravalent homodimeric protein upon reverse pairing and bi-nanobodies use only V_H domains connected in a single protein chain. However, possible combinations of Fc-bearing and Fc-lacking constructs are diverse and many more formats have been used that are not described here.

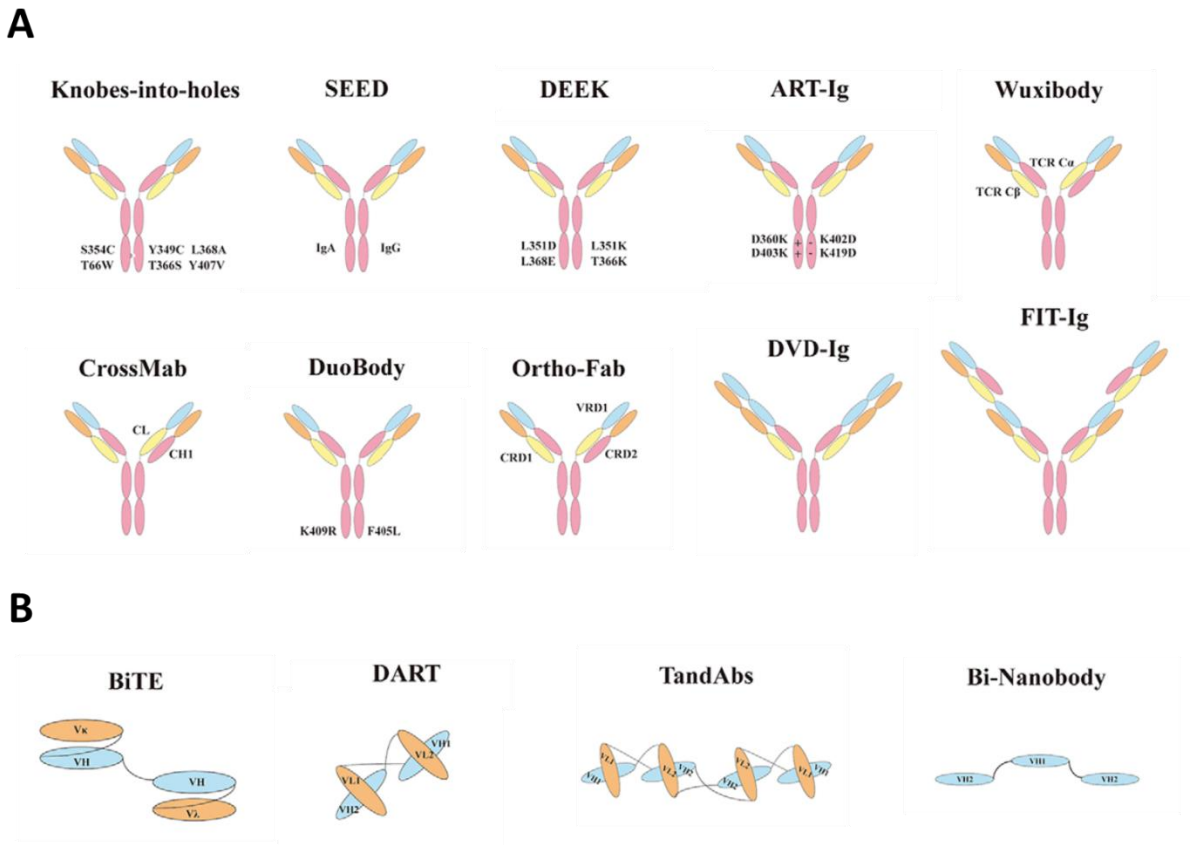

Figure 8: Different formats of multispecific antibody-based proteins
Shown are some strategies for generating bi- and multispecific antibody-based proteins using IgG-like Fc-bearing (A) and non-IgG-like Fc-lacking formats (B). Adapted from (Ma et al., 2021).

1.2.2 Mode of action

As mentioned above antibody-based agents can serve many different purposes, which will be discussed in the following section with the main focus placed on immune cell engagers.

Blocking receptor signaling: Antibodies and antibody-based proteins that block receptor engagement and signalling have been developed for different tumor-growth promoting and immune cell-inhibiting receptors, which either bind the relevant receptor, its ligand or both (Shah et al., 2021; Suurs et al., 2019). Well-known examples that have been targeted using therapeutic antibodies or antibody-based reagents include the tumor-associated receptors EGFR (epidermal growth factor receptor), HER2 (human epidermal receptor 2), HER3 and c-met; the soluble ligand VEGF (vascular endothelial growth factor) and its receptor VEGF-R, which support angiogenesis important for tumor growth; and the “don’t eat me signal” CD47 upregulated on tumor cells, which protects from macrophage-mediated phagocytosis. Furthermore, blocking of inhibitory immune cell receptors and their ligands is commonly referred to as checkpoint blockade and aims to neutralize or counteract immunosuppressive signals from the tumor. FDA approved checkpoint inhibitors include pembrolizumab, nivolumab and cemiplimab that block PD-1 on T cells; atezolizumab, durvalumab and avelumab targeting

PD-Ligand 1 on the tumor cell; ipilimumab that blocks CTLA-4 on T cells; and relatlimab, which targets LAG-3 (Naimi et al., 2022; Sidaway, 2022).

Activating receptor signaling: In contrast to blocking the engagement of disadvantageous receptors, another immunotherapeutic strategy on the other hand can be to activate specific receptor pathways that promote the anti-tumor immune response (Heckel et al., 2022; Mascarelli et al., 2021; Warwas et al., 2021). Thus, in addition to checkpoint inhibitors, antibody-based proteins have been developed that stimulate activating co-signaling receptors on T cells and serve to deliver important co-stimulating signals that are often scarce in the tumor microenvironment. Some co-stimulatory receptors that have been investigated as target include CD27, CD28, 4-1BB and OX40. If antibody binding is able to trigger receptor signaling or not depends on the targeted epitope and the degree of receptor clustering induced. Besides using antibody-derived antigen binding domains for receptor targeting, some fusion proteins incorporate the ligand itself. Furthermore, the use of multispecific tumor-directed formats enables a more tumor site-restricted delivery limiting systemic toxicities observed for monoclonal antibody formats.

Immune cell engagers: A mechanism that gains increasing interest is the redirection of immune cells using multispecific formats that serve as a bridge between tumor and immune cell and thereby mediate tumor cell recognition and killing independent of the immune cells' specificity (Fucà et al., 2021; Labrijn et al., 2019; Suurs et al., 2019). These molecules are also commonly referred to as immune cell engagers, more specifically "BiTe" for bispecific T cell engagers and "NKCE" for all general NK cell engagers or "BiKe" and "TriKe" for bispecific and trispecific NK cell engagers, respectively.

For T cell redirection most engagers target CD3ε within the TCR complex triggering its signalling independent of TCR specificity and without any pMHC engagement. Upon crosslinking of cytotoxic $CD8^+$ T cells, this results in tumor killing. The CD3 engagement however does not differentiate between T cell subsets and high numbers of immunosuppressive regulatory T cells can dampen their effect. Nevertheless, great clinical results have already been achieved using different CD3-directed T cell engagers. The first CD3ε targeting T cell engager that received FDA approval in 2009 was the bispecific full-length antibody catumaxomab with one arm targeting CD3 and one arm targeting the epithelial cell adhesion molecule (EpCAM). Additionally to the induction of T cell-mediated cytotoxicity, the functionally active Fc part induced ADCC and ADCP by binding to the Fcγ receptors of NK cells, macrophages and dendritic cells (Moon et al., 2022). However, intravenous administration of catumaxomab led to partially fatal hepatotoxicity due to binding of $Fc\gamma R^+$ Kupffer cells as their activation led to strong T cell infiltration in the liver and activation in absence of any $EpCAM^+$ target cells (Borlak et al., 2016). Thus, most of the subsequently

developed engagers were designed without an Fc or with an engineered Fc part showing reduced FcγR binding (Labrijn et al., 2019). For example, blinatumomab, which was approved by the FDA for certain acute lymphatic leukaemias (ALL) in 2014, is a small bispecific Fc-lacking tandem-scFv targeting CD19 and CD3 that achieved impressive responses upon intravenous administration (Brown, 2018; Labrijn et al., 2019). Since then, many CD3-targeting BiTes of different formats have been developed especially for hematological malignancies for example by targeting BCMA (B-cell maturation antigen), CD123, CD20, CD33 or CD38; but also for solid cancers expressing CEA (carcinoembryonic antigen), EGFR, EpCAM, HER2, PSMA (prostate-specific membrane antigen) etc. In addition to CD3-directed engagers, other T cell engagers investigated target the CD8 co-receptor expressed by cytotoxic T cells and should thus prohibit an unwanted activation of regulatory T cells lacking CD8 expression and avoid the potential risk of a cytokine release syndrome posed by massive CD4 T helper cell activation (Suurs et al., 2019). However, upon direct comparison of a CD8- and CD3-directed PSCA (prostate stem cell antigen)-specific engager, the CD8-directed engager was found to be less effective in vitro and also required T cell pre-activation to mediate tumor cell killing (Michalk et al., 2014).

For NK cell redirection most engagers target the FcγRIII (CD16). This can be done using any IgG-based agents bearing a functional glycosylated Fc part inducing antibody-dependent cellular cytotoxicity (1.1.3) as well as with CD16-specific antigen-binding domains (Demaria et al., 2021; Fucà et al., 2021; Shah et al., 2021). The first NK-cell engaging, Fc-bearing monoclonal antibody reached the market already over two decades ago in 1997. The CD20-specific antibody called rituximab was approved for non-Hodgkin lymphoma patients and is still regularly prescribed today. Since then, many more monoclonal antibodies have been developed such as cetuximab targeting EGFR, trastuzumab targeting HER2, Ofatumumab targeting CD20, Avelumab targeting PD-L1, Nivolumab targeting PD-1 to only mention some examples (Seidel et al., 2013; Zahavi & Weiner, 2020). While monoclonal antibodies can also function by blocking receptor signaling as mentioned above, ADCC is thought to be the most important therapeutic mechanism and one important factor influencing this effector function is a polymorphism of the FcγR (Mellor et al., 2013; Zahavi & Weiner, 2020). Thus, the FcγRIIIa F185V isoform mediates stronger IgG binding in vitro and was furthermore shown to correlate with a better outcome upon rituximab administration in diffuse large B cell lymphoma patients. Based on these observations, researchers also tried to boost ADCC by engineering monoclonal antibodies to gain increased FcγRIIIa binding (Seidel et al., 2013; van der Horst et al., 2020). Effective modifications include changes in the Fc-glycan composition and different amino acid exchanges such as S239D in combination with I332E or the combination of S298A, E333A and K334A. In addition to Fc-bearing antibodies, NK cell targeting can be enabled via antibody derived antigen-binding domains. The bispecific NK cell engagers AFM13 and

AFM24 for example are tetravalent Fc-lacking tandem antibodies targeting CD16 and CD30 or EGFR respectively (Demaria et al., 2021; Wu et al., 2015). In a clinical phase I trial AFM13 already demonstrated great potency for Hodgkin lymphoma patients. Another NK cell engager that reached clinical stage is the αCD16-IL-15-αCD33 TriKe that includes an IL-15 moiety shown to support NK cell proliferation, activation and survival *in vivo* (Demaria et al., 2021; Vallera et al., 2016). In addition to CD16, other NK cell receptors have been targeted with promising results such as NKG2D, NKp30 or NKp46 (Demaria et al., 2021). Even though, stimulation of one of these receptors was enough to induce cytotoxicity the combination with a CD16-engaging component was shown to yield better effects. Thus, an αNKp46-Fc-αCD20 TriKe incorporating an engineered Fc part mediating enhanced FcγRIIIa binding was more effective in mediated NK-cell dependent tumor-cell lysis than the BiKe variant incorporating a silent Fc part incapable of FcγRIIIa binding and also more potent compared to the CD20-specific monoclonal antibody rituximab (Gauthier et al., 2019). This demonstrates that co-engagement of several NK cell activating receptors can further boost their effector function.

Cytotoxic conjugates: Antibody-drug conjugates can directly induce tumor cell lysis without contribution of the cytotoxic immune cells. Thus, upon tumor cell binding the antibody-drug conjugates get internalized and degraded in the endolysosomal compartment, which results in release of the conjugated cytotoxic payload (Jin et al., 2022; Shah et al., 2021). These payloads typically induce toxic DNA damage or interfere with tubulin polymerization during cell division. Currently there are 10 antibody-drug conjugates available approved for cancer treatment.

Cytokine fusions: Antibody-cytokine fusion proteins also referred to as immunocytokines can be used for target-specific delivery of pro-inflammatory cytokines (Jin et al., 2022; Runbeck et al., 2021). This enables locally restricted high cytokine concentrations, which can support the activation of T and NK cells avoiding dose-limiting toxicities of systemic cytokine administrations. Most immunocytokines comprise IL-2, however others cytokines are being investigated as well.

1.3 Targeting MHC-restricted peptides using TCR-based therapies

Protein-derived antigens can result from membrane-associated proteins as well as from intracellular proteins, which become surface-exposed on MHC-I complexes upon antigen-presentation. Targeting of membrane-associated antigens requires antibody-based agents, whereas MHC-restricted peptides require TCR-based therapies for targeting (Chandran & Klebanoff, 2019; Lowe et al., 2019). Within the proteome intracellular proteins were predicted to make up the largest part with about 73% in contrast to 27% membrane-associated proteins.

Thus, targeting of MHC-I-restricted peptides is highly attractive as it offers the access to many more possible antigens than most antibody-based strategies. Additionally, oncogenic driver mutations, which are less likely to form escape variants due to their important role in tumor physiology, usually only occur in intracellular proteins such as TP53 or PIK3CA. The following section describes different TCR-based therapies with a special focus on soluble TCR-based agents.

Expansion of tumor-specific T cells: As the TCR is a naturally membrane-bound receptor, one way to target MHC-restricted peptides is using T cells endogenously expressing a matching TCR and different approaches aim to expand such tumor-reactive T cells *ex vivo* or *in vivo* (Jones et al., 2021). For example, vaccination with the respective peptide, whole proteins, antigen-encoding nucleic acids or viruses, or administration of *ex vivo* antigen-loaded dendritic cells enables *in vivo* T cell priming (Connerotte et al., 2008; Sahin et al., 2017; Saxena et al., 2021). Sipuleucel-T, a DC-focused vaccine, was already approved 10 years ago and several other cancer vaccines are currently under clinical investigation, most of them as combination therapy. Usually, tumor-reactive T cells can be found within the patients tumor-infiltrating lymphocytes (TILs) or circulating in the blood (Chandran & Klebanoff, 2019; Jones et al., 2021; Morotti et al., 2021). Thus, another commonly used approach is to enrich and expand these cells *ex vivo* outside of a potentially immunosuppressive tumor environment to generate high numbers of tumor-reactive T cells for an adoptive cell transfer (ACT) back into the patient. The first clinical study exploiting the use of TILs for an adoptive cell transfer was conducted 1994 for melanoma patients and gained an objective response rate of 34% (Rosenberg et al., 1994). A later study with melanoma patients even reached an objective response rate of 72% (Rosenberg et al., 2011). However, not all patients can benefit from an adoptive transfer of *ex vivo* expanded TILs and outcome can be dampened by different factors such as T cell exhaustion, amount of antigen-specific T cells or tumor immunosuppression (Morotti et al., 2021).

Engineered TCR-cells: Instead of using unmodified TILs for adoptive cell transfer, another possibility is the use of engineered T cells that have been equipped with a receptor of desired specificity. This can be done either using a chimeric antigen receptors (CAR) that makes use of an membrane-bound scFv connected to intracellular T cell signaling domains recognizing membrane-associated proteins or for targeting of MHC-restricted peptides using another TCR then also referred to as CAR-T and TCR-T cells respectively (Jones et al., 2021; Wei et al., 2022). CAR-T cells have already shown great success in hematological malignancies. The FDA-approved CD19-CAR-T for example reached up to 90% complete response in B cell leukemia (Davila et al., 2014; Maude et al., 2014; Turtle et al., 2016). The TCR gene therapy on the other hand faces some practical challenges due to co-expression with the endogenous TCRs (Jones et al., 2021; Wei et al., 2022). Thus, mis-pairing with the endogenous TCR

peptide chains can occur, which might result in auto-reactivity. To overcome this problem, different strategies have been deployed to favour correct dimer formation including the knob-in-hole approach as already described in the antibody section (1.2.1), introduction of additional cysteines to form a second inter-chain disulfide bond, exchange of the TCR Cα and Cβ with constant domains of a human γδ TCR or a murine αβ TCR, or the formation of a single-chain T cell receptor similar to the chimeric antigen receptor format. In contrast to CAR-T cells, TCR-T cells show a higher sensitivity towards lower antigen levels as they can recognize and react to a single target molecule. While CAR-T cells were less effective in solid tumors, TCR-T cells gained promising results for different tumor entities (Tsimberidou et al., 2021). Common targets that have been investigated in clinical trials include gp100, Mart-1, MAGE-A3 and NY-ESO-1. Using NY-ESO-1 specific TCR-T cells for example, a complete response rate of 70% was obtained in myeloma patients (Rapoport et al., 2015). Besides T cells, also NK cells have been exploited as effector cells for engineered TCR therapies (Morton et al., 2022; Tsimberidou et al., 2021). Since they naturally do not express an endogenous TCR, they do not require any special strategies to avoid TCR mismatches, but on the other hand additionally need to be equipped with the CD3 co-receptor signaling domains to enable TCR signaling. As TCR-T cells, TCR-NK cells are able to mediate a potent anti-tumor response.

The use of engineered TCR-T or TCR-NK cells also offers the possibility of TCR affinity maturation through mutation of the CDR regions in the variable domains (Campillo-Davo et al., 2020; Jones et al., 2021). This can be done by introducing structurally guided mutations, by artificially inducing somatic hypermutation as observed for B cells upon antibody maturation, by T cell differentiation or by random mutagenesis using mammalian, phage or yeast display that enable selection of high affinity binders. Many affinity-enhanced TCRs have been generated using these protocols and were shown to mediate increased anti-tumor responses (Bassan et al., 2019; Rapoport et al., 2015; Robbins et al., 2008). Unfortunately, some cases of severe and fatal toxicity were observed, too, indicating that affinity maturation also increases the risk of cross-reactivity (Campillo-Davo et al., 2020; Jones et al., 2021). Thus, for example MAGE-A3-specific HLA-A*01-restricted TCR-T cells developed for the treatment of myeloma and melanoma patients were found to mediate fatal off-target reactivity as they recognized the structurally similar peptide Titin expressed in the cardiac muscle cells (Linette et al., 2013). Initial preclinical investigations did not show any cross-reactivity and this was only found upon a more detailed follow-up investigation using an alanine and glycine scan, which analyses recognition of peptides that each have one amino acid position exchanged with an alanine or glycine in this case (Cameron et al., 2013). The thereby determined binding motif was then used to identify potentially cross-reactive peptides in silico. Other cases of severe toxicity have been observed using affinity-enhanced TCR-T cells targeting another HLA-A*02 bound MAGE-A3 peptide and HLA-A*02 bound CEA peptide highlighting the importance of efficient pre-

clinical safety screens (Campillo-Davo et al., 2020; Oates et al., 2015). Predicted cross-reactivity, however, does not necessarily preclude the application of TCR-T cells as actual expression of the antigen needs to be confirmed.

Soluble TCR and TCRm: In addition to cell-based therapies, there are also non-cellular TCR-based formats, that can be used to target MHC-restricted peptides (He et al., 2019; Jones et al., 2021; Robinson et al., 2021). When targeting shared antigens, this can be a fast off-the-shelf approach avoiding time-consuming and expensive protocols required for adoptive cell transfer of TCR-T cells. Non-cellular TCR-based agents include two entities: a soluble version of the TCR itself without the transmembrane domains and TCR-mimetic (TCRm) antibodies that are designed to recognize peptide-MHC complexes in a TCR-like manner. The generation and application of soluble TCRs, however, faced some challenges. One such challenge is the comparatively very low affinity of native TCRs, which is thought to be important in the cellular context to enable serial target recognition and killing as well as to avoid T cell exhaustion, in the soluble context however, higher affinities are required. Another challenge is the poor stability of soluble TCRs that led to overall poor production yields, protein misfolding and aggregation in initial investigations. Thus, to circumvent these obstacles, initial studies focused on TCR-mimetic antibodies (Dahan & Reiter, 2012; He et al., 2019). As mentioned above (1.1.2.1), antibodies usually have a 1:1000-10000 higher affinity than native TCRs ranging between pico- and nanomolar values in contrast to micromolar affinities observed for native TCRs. Currently, there are more than 40 TCRm antibodies under pre-clinical investigation targeting different MHC-restricted antigens including peptides derived from gp100, NY-ESO-1, MAGE-A3, HER2, Mart-1, p53 and WT1 (Bernardeau et al., 2005; Dao et al., 2013; Denkberg et al., 2002, 2003; Held et al., 2004; Klechevsky et al., 2008; D. Li et al., 2017; Q. Zhao et al., 2015). Most of them are generated by phage display and some by hybridoma cells. The phage display technology enables a fast screening of large antibody libraries. Hybridoma cells in turn are generated following immunization and usually produce antibodies of slightly higher affinities. Immunotherapeutic formats that have been investigated include the classical full-length monoclonal antibody that induces ADCC, ADCP and CDC; antibody-drug conjugates; bispecific engagers; and a membrane-bound TCRm CAR constructs. In contrast to the TCRs, which are characterized by a conserved binding mode with the TCR diagonally sitting on top of the MHC's peptide binding groove, TCR-mimetics show different binding modes. For example, it was found for some TCR-mimetic antibodies that they did not bind the whole peptide and close contact was only generated with the HLA molecule and the peptide's N- or C-terminal end (Ataie et al., 2016; Hülsmeyer et al., 2005). A study by Cole in 2020 also compared binding mode and peptide specificity of different TCR and TCRm antibodies and found that a non-native binding mode did correlate with lower specificity (Holland et al., 2020). Ataie et al. however suggested that a non-conserved binding mode could also broaden their

application by generating TCR mimetics that mediate peptide recognition in the context of several HLA subtypes as demonstrated using an antibody that recognized the same WT1 peptide in context of different HLA-A*02 variants containing similar binding motifs (Ataie et al., 2016). However, since the antibody primarily interacted with the peptide's N-terminus, they also predicted and confirmed cross-reactivity towards peptides with several amino acids difference in the C-terminus. Thus, the generation of truly peptide-specific TCR mimetic antibodies seems equally challenging.

Considering the initial challenges encountered for the development of soluble TCR-based agents, technical advances have been made that meanwhile enable production of functional TCR constructs in sufficient amounts as well as high affinity (Oates et al., 2015; Robinson et al., 2021). Since the production of native TCRs as soluble molecule resulted in low yields, protein aggregation and misfolding, different strategies have been investigated to improve soluble TCR production. Initial approaches used a format similar to scFv antibody fragments (1.2.1) by linking both variable domains (Gunnarsen et al., 2018; Novotny et al., 1991; Hoo et al., 1992). However, since many single-chain TCRs were poorly soluble, potentially through the exposure of naturally buried hydrophobic regions, individual mutagenesis was required to improve solubility. Other attempts focused on a rather universal TCR dimer stabilizations, for example using leucine zippers fused to the C-terminus (Chang et al., 1994; Willcoj et al., 1999) or by incorporation of a non-native disulfide bridge between the constant domains (Boulter et al., 2003; Sádio et al., 2020; van Boxel et al., 2009). To date, most soluble TCRs use the disulfide bridged format, although this approach does not necessarily work for all clones as a gluten-specific TCR for example was only stable using a scTCR upon comparison with two different disulfide bridged formats (Gunnarsen et al., 2018). In addition to the disulfide bridge, Wagner et al. generated an immunoglobulin-like format by fusing two disulfide bridged TCRs to an IgG-derived hinge and Fc part, which enabled easy purification and gained high yields comparable to antibody productions (Wagner et al., 2019). Considering the naturally low TCR affinity, different protocols have been used to increase TCR affinity by mutating the CDR regions in the variable segment (Jones et al., 2021; Oates et al., 2015; Robinson et al., 2021). Using these methods, many TCRs have been generated with up to picomolar affinities that are sensitive enough to recognize tumor cells with very low antigen-presentation of only 10 molecules per cell (Y. Li et al., 2005; Liddy et al., 2012; Wagner et al., 2019). However, as described above, TCR affinity maturation was also shown to increase the risk of cross-reactivity. Thus, careful safety evaluations are necessary, although the cross-reactivity observed in the TCR-T cell setting does not necessarily transfer to soluble TCRs. In contrast to TCR-T cells, an important benefit of soluble TCRs is that their concentration is easily adjustable and lower concentration might still enable a good response to the intended target

while cross-reactive peptides with lower expression levels or lower affinity are spared due to insufficient binding.

The most advanced therapeutic soluble TCRs stem from the so-called ImmTAC (immune mobilising monoclonal T-cell receptor against cancer) design developed by Immunocore (Lowe et al., 2019; Oates et al., 2015). This bispecific T cell engager is composed of a single affinity-enhanced disulfide bridged TCR generated by phage display and a single CD3ε-specific scFv linked to the TCRβ chain (Y. Li et al., 2005; Liddy et al., 2012). Production was carried out in *Escherichia coli* requiring subsequent *in vitro* refolding. ImmTACs have been developed against multiple targets including gp100, NY-ESO-1, MAGE-A3, MAGE-A4 and MART-1 and were shown to induce potent target-specific immune responses even towards cells with very low antigen levels with preferential activation of $CD8^+$ T cells (Harper et al., 2018; Liddy et al., 2012; Lowe et al., 2019; McCormack et al., 2013; Sato et al., 2018). The gp100-specific TCR construct Kimmtrak® just recently gained FDA approval for the treatment of uveal melanoma and a clinical trial is running for its application in cutaneous melanoma (Dolgin, 2022). Besides Kimmtrak®, several other ImmTACs reached clinical stage as well as a structurally different soluble TCR developed by Immatics targeting MAGE-A4. The TCER® format used by Immatics is based on an asymmetric immunoglobulin-like format incorporating the knob-in-hole mutations to favour correct assembly (Dilchert et al., 2022). One site contains an affinity-enhanced scTCR generated by yeast and mammalian cell display and one site an αCD3 scFv each fused to IgG1-derived C_H2-C_H3 domains with abrogated FcR binding. Production was carried out using mammalian cells and thus no refolding was required. Another investigated therapeutic soluble TCR includes a TCR-Fc fusion protein in which a single affinity-enhanced NY-ESO-1-specific TCR was fused to an Fc with knob-in-hole mutations (W. Bin Zhao et al., 2021). Following production using mammalian cells, an αCD3 scFv was chemically linked to the Fc part. However, although they used the same TCR sequence, the efficiency was lower compared to the ImmTAC format potentially due to the larger molecule creating a bigger distance between both cells. Another recent study tested different bispecific formats using published high affinity NY-ESO-1 and MAGE-A3 TCR clones (Froning et al., 2022). The investigated formats included an TCR-scFv fusion protein similar to the ImmTAC design, a TCR-Fab that fuses a disulfide bridged TCR to a single αCD3 Fab fragment and an asymmetric IgG-like format in which one arm is composed of a disulfide bridged TCR and the other arm of an αCD3 Fab fragment. Upon direct comparison, they found the greatest potency for the TCR-Fab format, while the ImmTAC-like TCR-scFv was less potent and the IgG-like TCR was least effective potentially due to less flexible orientation of the antigen-binding domains. Besides bispecific engagers, soluble TCRs also have been used for targeted delivery of toxic docetaxel-loaded nanoparticles (McDaid et al., 2021).

1.4 Aim of this study

MHC-I restricted peptides are highly attractive targets for cancer immunotherapy, as they generate access to the universe of intracellular tumor antigens. However, current TCR-based therapies that are mostly based on expansion of endogenous tumor-specific T cells and adoptive cell transfer of expanded unmodified or TCR engineered T cells that face different challenges and are not always applicable for every patient. Thus, this study aimed to further investigate the immunotherapeutic potential of soluble TCRs, which offer an off-the-shelf approach that is applicable rather independently of the endogenous T cell repertoire and avoids the requirement of time-consuming and expensive protocols for adoptive cell transfer or TCR engineering. To offer a broad applicability in terms of immune effector cells, I tested soluble TCRs for the redirection of NK cells as well as T cells using a new construct format.

In this study, the soluble TCR constructs were based on a bivalent immunoglobulin G-format, in which the two Fab fragments were each replaced by a disulfide bridged TCR monomer. Since, a high TCR affinity seemed important in previous studies, the increased avidity resulting from the bivalent format should thus help to improve their performance. To enable NK cell redirection, specific mutations known to enhance FcγRIIIA binding were introduced in the Fc fragment of the IgG-like TCR constructs. Other investigated formats made use of single chain variable fragments (scFv) directed against CD3ε for the redirection of T cells and against CD16a and NKp46 for the redirection of NK cells, respectively.

Recombinant fusion proteins containing published TCR sequences targeting HLA-A*02:01-restricted peptides of the cytomegalovirus pp65, gp100, NY-ESO-1 and MART-1 proteins and incorporating anti-NKp46, anti-CD16a or anti-CD3ε scFv were cloned, produced and carefully investigated in functional assays.

2 Materials and methods

2.1 Materials

Table 1: Devices used in this thesis

Devise	Designation	Manufacturer
Beaker	500 ml, 1 l	Fisherbrand
Cassette for peristaltic pump	Cassettes with occlusion lever	Ismatec
Centrifuge	ROTANTA 460 RC	Hettich
Centrifuge	Multifuge X3 FR	Thermo Scientific
Centrifuge	Megafuge 2.0R	Heraeus
Counting chamber	Brand® counting chamber Blaubrand ® Neubauer improved	Sigma-Aldrich
Electrophoresis chamber	XCell SureLock™ mini cell	Thermo Scientific
Electrophoresis power supply	EV231	CONSORT
Erlenmeyer flask	500 ml	VWR
Flow cytometer	BD FACS Canto™ II	BD Biosciences
Freezing container	Nalgene™ Mr. Frosty™	Thermo Scientific
Incubator	Heracell™240i CO_2	Thermo Scientific
Incubator	INFORS HT Minitron with integrated orbital shaker (50 mm shaking diameter)	INFORS HT
Incubator shaker	Eppendorf™ Innova™ 44	Eppendorf
Laminar flow hood	HERAsafe® HS/HSP	Heraeus
Liquid chromatography column	Low-pressure liquid chromatography column with luer lock, non-jacketed (0.7x10cm)	Sigma-Aldrich
MACS magnet	QuadroMACS™ Seperator	Miltenyi Biotec
MACS magnet stand	MACS® MultiStand	Miltenyi Biotec
Magnetic stirrer	MR 2002	Heidolph Instruments
Microcentrifuge	Fresco 17	Thermo Scientific
Microscope	DM IL LED	LEICA
Nano Drop	ONE^C	Thermo Scientific
Peristaltic Pump	REGLO digital MS-4/6-100	Ismatec
pH-Meter	766	Knick
Pipetboy	Pipetboy acu 2	INTEGRA
Pipette	Xplorer plus	Eppendorf
Pipette	Research plus	Eppendorf
Plate reader	Multiskan EX	Thermo Scientific
Scale	AE 163	Mettler Toledo
Scale	HF3000G	A&D WEIGHING
Scanner	Perfection V500 Photo	Epson
Schott bottle	500 ml, 1 l	Fisherbrand

Shaker	KS 250	IKA
Tube roller	RS-TR 5	Phoenix Instrument
Tubing	Saint-Gobain TygonTM LMT-55 Tubing - 3.17 mm inner diameter x 38.1 mm length - Three stop configuration - Tygon R3607 material	Fisher Scientific
Vortex	Reax 2000	Heidolph Instruments
Water bath	-	Köttermann

Table 2: Consumables used in this thesis

Product	Manufacturer
Biosphere® plus screw cap micro tube (2 ml)	SARSTEDT
Costar® 50 ml reagent reservoir	Corning Incorporated
Eppendorf safe-lock tubes (1.5, 2ml)	Eppendorf
FACS tubes	BD Biosciences
Falcon™ conical (15, 50 ml)	BD Biosciences
Graduated TipONE® tips (10, 200, 1000 µl)	Starlab
Graduates TipONE® Filter tip (10, 200, 1000 µl)	Starlab
Greiner multiwell plate sealers	Sigma-Aldrich
Greiner-Cellstar® 96 well tissue culture plate (round bottom)	TPP
LS columns	Miltenyi Biotec
MEDOJECT® Hypodermic needles (0.6 x 25 mm 2 3G x 1'')	CHIRANA T. Injecta
Millex-GV, 0.22 µM PVDF 4 and 13 mm syringe-driven filter unit	Merck
Nunc-Immuno™ 96-well MaxiSorp™ plate	Sigma-Aldrich
Nunclon™ Sphera™ 96-Well, Nunclon Sphera-Treated, U-Shaped-Bottom Microplate	Thermo Fisher Scientific
Nunc™ 96-well Microwell™ Maxisorp™ flat-bottom plate	Thermo Scientific
Nunc™ 96-well polypropylene V-bottom plate	Thermo Scientific
Serological pipettes	Falcon
Slide-A-Lyzer™ dialysis cassettes, 20 kDa mwco, 3 ml	Thermo Scientific
Terumo® Syringes (2.5, 5, 20, 50 ml)	Terumo Europe
Tissue culture dish 60 mm	TPP
Tissue culture flasks (25, 75, 150 mm; with filter screw cap)	TPP
Tissue culture plates (96, 48, 24, 12, 6 well; flat bottom)	TPP
Vacuum filtration system „rapid"-FilterMax	TPP
VWR® Weighing Boat	VWR

Table 3: Media, Supplements, reagents used for general cell culture and *in vitro* assays

Product	Manufacturer	Catalog number
Antibiotic Antimycotic Solution for Cell Culture (100x)	Sigma-Aldrich	A5955-100ML
B-27™ Plus Supplement 50x	Thermo Fisher Scientific	A3582801
BD GolgiPlug™ (contains brefeldin A)	BD Biosciences	51-2301KZ
BD GolgiStop™ (contains monensin)	BD Biosciences	51-2092KZ
Benzonase® Nuclease HC	Merck Millipore	71205
Biocoll® Separating Solution (1.077 g/ml isotonic)	Biochrom	L 6115
Blasticidin	Thermo Fisher Scientific	R21001
CellTrace™ Violet Cell Proliferation Kit	Thermo Fisher Scientific	C34557
CFSE (Carboxyfluorescein diacetate succinimidyl ester) Cell Division Tracker Kit	Biolegend	423801
CMV pp65 peptide (50 mM in DMSO)	DKFZ, in house production	-
CyQUANT™ LDH Cytotoxicity Assay kit	Thermo Fisher Scientific	C20301
DMEM, high glucose, GlutaMAX™ Supplement, pyruvate	Thermo Fisher Scientific	31966047
DMEM/F-12, HEPES, no phenol red	Thermo Fisher Scientific	11039021
FCS (Fetal calf serum)	Biochrom	S 0615
G418	Meck Millipore	A2912
GelTrex™ LDEV-Free Reduced Growth Factor Basement Membrane Matrix	Thermo Fisher Scientific	A1413201
GlutaMax™ Supplement	Thermo Fisher Scientific	35050061
GP100 peptide 280-288 (50 mM in DMSO)	Genaxxon bioscience	P2757.9501
HT Media Supplement (50x) Hybri-Max™	Sigma-Aldrich	H0137-10VL
Ionomycin • 1 mg/ml in Ethanol	Merck	I0634
Lipofectamine™ 3000 Transfection Reagent	Thermo Fisher Scientific	L3000150
MART-1 peptide 26-35 (A27L) (50 mM in DMSO)	DKFZ, in house production	-
NY-ESO-1 peptide 157-165* (C165V) (50 mM in DMSO)	DKFZ, in house production	-
Opti-MEM™ Reduced Serum Media	Thermo Fisher Scientific	31985062
OptiPro™ SFM	Thermo Fisher Scientific	12309-050
Penicillin-Streptomycin (Pen/Strep)	Sigma-Aldrich	P4333
PMA (Phorbol-12-myristate-13-acetate) • 1 mg/ml in DMSO	Merck	P8139
Polyethyleneimine (PEI), linear, MW 25000, transfection grade • 1 mg/ml in ddH_2O (stirred at pH 2.0 for 3 h, followed by neutralization to pH 7.0) • 0.22 µm sterile filtered	Polysciences	23966-2
PowerCHO™ 2 Serum-free Medium – Chemically Defined	Lonza	BELN12-771Q
ProCHO™ 4 Protein-free CHO Medium	Lonza	BEBP12-029Q

RPMI Medium 1640 no glutamine	Thermo Fisher Scientific	31870025
Survivin peptide 96-104 (50 mM in DMSO)	DKFZ, in house production	-
VPA (Valproic acid sodium salt) • 500 mM in ddH_2O • 0.22 µm sterile filtered	Sigma-Aldrich	P4543-25G

Table 4: Buffers and reagents used for flow cytometry

Product	Manufacturer	Catalog number
"FACS Buffer"		
DPBS without calcium chloride and magnesium chloride (1x) supplemented with	Sigma-Aldrich	D8537-500ML
• 1% FCS	Biochrom	S 0615
• 2 mM EDTA (Ethylenediamine tetraacetic acid)	Sigma-Aldrich	03690-100ML
AbC™ Total Antibody Compensation Bead Kit	Thermo Fisher Scientific	A10497
ArC™ Amine Reactive Compensation Bead Kit	Thermo Fisher Scientific	A10346
Fixation solution		
DPBS without calcium chloride and magnesium chloride (1x) supplemented with	Sigma-Aldrich	D8537-500ML
• 2.5% paraformaldehyde	Thermo Fisher Scientific	28908
• 1% FCS	Biochrom	S 0615
Fixation/ Permeabilization Kit	BD Biosciences	554714
Human TruStain FcX™ (Fc Receptor Blocking Solution)	Biolegend	422302
Propidium iodide (PI), 1mg/ml in H_2O	Merck	P4864
RBC (Red Blood Cell) Lysis Buffer (10x)	Biolegend	420302
Streptavidin-PE	Biolegend	405203
Zombie Aqua™ Fixable Viability Kit	Biolegend	423102

Table 5: Antibodies used for flow cytometry

Specificity [clone]	Isotype	Conjugate	Manufacturer	Catalog number
Human CD107a (LAMP-1) [H4A3]	Mouse IgG1, κ	Alexa Fluor® 647	Biolegend	328612
Human CD134 (OX40) [Ber-ACT45]	Mouse IgG1, κ	PE/Cyanine7	Biolegend	350012
Human CD137 (4-1BB) [4B4-1]	Mouse IgG1, κ	PE/Cyanine7	Biolegend	309818
Human CD137 (4-1BB) [4B4-1]	Mouse IgG1, κ	PE	Biolegend	309804

Human CD14 [M5E2]	Mouse IgG2a, κ	Brilliant Violet 510™	Biolegend	301842
Human CD16 [3G8]	Mouse IgG1, κ	APC	Biolegend	302012
Human CD19 [HIB19]	Mouse IgG1, κ	Brilliant Violet 510™	Biolegend	302242
Human CD25 [BC96]	Mouse IgG1, κ	Alexa Fluor® 647	Biolegend	302618
Human CD25 [BC96]	Mouse IgG1, κ	PE/Cyanine7	Biolegend	302612
Human CD3 [HIT3a]	Mouse IgG2a, κ	APC/Cyanine7	Biolegend	300318
Human CD3 [HIT3a]	Mouse IgG2a, κ	PerCP/ Cyanine5.5	Biolegend	300328
Human CD3 [UCHT1]	Mouse IgG1, κ	Brilliant Violet 510™	Biolegend	300448
Human CD335 (NKp46) [9E2]	Mouse IgG1, κ	APC	Biolegend	331918
Human CD4 [RPA-T4]	Mouse IgG1, κ	Alexa Fluor® 488	Biolegend	300519
Human CD4 [RPA-T4]	Mouse IgG1, κ	Alexa Fluor® 488	Biolegend	300519
Human CD4 [RPA-T4]	Mouse IgG1, κ	PE	Biolegend	300508
Human CD45RA [HI100]	Mouse IgG2b, κ	Alexa Fluor® 488	Biolegend	304114
Human CD56 (NCAM) [5.1H11]	Mouse IgG1, κ	APC/Fire™ 750	Biolegend	362554
Human CD56 (NCAM) [HCD56]	Mouse IgG1, κ	FITC	Biolegend	318304
Human CD56 (NCAM) [HCD56]	Mouse IgG1, κ	Brilliant Violet 510™	Biolegend	318340
Human CD62L [DREG-56]	Mouse IgG1, κ	PerCP/ Cyanine5.5	Biolegend	304824
Human CD69 [FN50]	Mouse IgG1, κ	Alexa Fluor® 647	Biolegend	310918
Human CD69 [FN50]	Mouse IgG1, κ	Brilliant Violet 421™	Biolegend	310930
Human CD8 [RPA-T8]	Mouse IgG1, κ	APC	Biolegend	301049
Human CD8 [SK1]	Mouse IgG1, κ	Pacific Blue™	Biolegend	344718
Human CD80 [2D10]	Mouse IgG1, κ	APC	Biolegend	305220
Human CD8a [RPA-T8]	Mouse IgG1, κ	PerCP/ Cyanine5.5	Biolegend	301032
Human HLA-A2 [BB7.2]	Mouse IgG2b, κ	APC	Biolegend	343308
Human IFN-γ [4S.B3]	Mouse IgG1, κ	PE	Biolegend	502509
Human IgG, Fcγ fragment specific [polyclonal]	Goat IgG	PE	Jackson Immuno Research	109-115-098
Human TNF-α [Mab11]	Mouse IgG1, κ	PE/Cyanine7	Biolegend	502930
Isotype control	Mouse IgG1, κ	APC	Biolegend	400120

Table 6: Buffers and reagents used for MACS isolation

Product	Manufacturer	Catalog number
"MACS Buffer" DPBS without calcium chloride and magnesium chloride (1x) supplemented with • 1% FCS • 2 mM EDTA (Ethylenediamine tetraacetic acid)	Sigma-Aldrich Biochrom Sigma-Aldrich	D8537-500ML S 0615 03690-100ML
Anti-APC MicroBeads	Miltenyi Biotec	130-090-855
Anti-PE MicroBeads	Miltenyi Biotec	130-048-801
NK cell Isolation Kit, human	Miltenyi Biotec	130-092-657
Pan T cell Isolation Kit, human	Miltenyi Biotec	130-096-535

Table 7: Buffers and reagents used for ELISA

Product	Manufacturer	Catalog Number
1 M H_2SO_4	Carl Roth	9316.1
Anti-human IgG (Fc specific)	Sigma-Aldrich	I2136-1ML
Anti-human IgG (Fc specific)	Sigma-Aldrich	M2650-1ML
Anti-human IgG (Fc specific)-HRP (horse radish peroxidase)	Sigma-Aldrich	A0170-1ML
Anti-mouse IgG (Fc specific)-HRP	Sigma-Aldrich	A0168-1ML
Blocking Buffer DPBS without calcium chloride and magnesium chloride (1x) supplemented with • 2.5% BSA (bovine serum albumin)	Sigma-Aldrich PAA	D8537-500ML K45-001
Carbonate-bicarbonate coating buffer (0.05 M, pH 9.6)	Sigma-Aldrich	C3041-50CAP
Sample Buffer DPBS without calcium chloride and magnesium chloride (1x) supplemented with • 0.5% BSA (Bovine Serum Albumin)	Sigma-Aldrich PAA	D8537-500ML D8537-500ML
TMB Substrate Set (HRP substrate)	Biolegend	421101
Washing Buffer: PBS-T DPBS without calcium chloride and magnesium chloride (1x) supplemented with • 0,05% Tween-20	Sigma-Aldrich Sigma-Aldrich	D8537-500ML P1379-100ML

Table 8: Buffers and reagents used for protein purification and SDS-page analysis

Product	Manufacturer	Catalog number
10x PBS (pH 7.4)		
• 80 mM NaH_2PO_4	Sigma-Aldrich	715071KG
• 15 mM KH_2PO_4	Carl Roth	T878.2

• 27 mM KCl	Carl Roth	6781.1
• 1.45 M NaCl	Carl Roth	9265.1
Dithiothreitol (DTT)	Sigma-Aldrich	D0632-1G
InstantBlue™ Coomassie protein staining solution	Expedeon	NXB50500
RunBlue™ LDS Sample Buffer 4x	Expedeon	NXB31010
RunBlue™ SDS Running Buffer 20x	Expedeon	NXB50500
RunBlue™ TEO-Tricine SDS-Precast Gels	Expedeon	NXG01012
Strep-Tactin® elution buffer Self-prepared 1x PBS, pH 7.4 supplemented with • 5 mM desthiobiotin	IBA Lifesciences	2-1000-002
Strep-Tactin® Superflow® high capacity resin (50% suspension)	IBA Lifesciences	2-1208-010

Table 9: Cells used in this thesis.

Cell type	Description	Culture medium	Source
FreeStyle™ CHO-S	Chinese hamster ovarian cells (CHO)	<u>Maintenance:</u> PowerCHO™ 2 Serum-free Medium – Chemically Defined supplemented with • 8 mM GlutaMax™ • 1x HT Media Supplement (13.6 mg/l hypoxanthine, 3.9 mg/l thymidine) • 0.5x Antibiotic Antimycotic solution (50 Units/ml penicillin, 0.05 mg/ml streptomycin, 0.1 µg/ml amphotericin B) <u>Production:</u> ProCHO-4™ Protein-free medium supplemented with • 4 mM GlutaMax™ • 1x HT Media Supplement (13.6 mg/l hypoxanthine, 3.9 mg/l thymidine) • 0.5x Antibiotic Antimycotic solution (50 Units/ml penicillin, 0.05 mg/ml streptomycin, 0.1 µg/ml amphotericin B)	Thermo Fisher Scientific (R80007)
MCF-7	Human breast adenocarcinoma cell line	RPMI supplemented with • 10% FCS • 1% GlutaMax (2 mM) • 1% Pen/Strep (100 Units/ml penicillin, 0,1 mg/ml streptomycin)	DKFZ, Heidelberg

MeWo	Human malignant melanoma	DMEM (with GlutaMax) supplemented with • 10% FCS • 1% Pen/Strep (100 Units/ml penicillin, 0,1 mg/ml streptomycin)	DKFZ, Heidelberg
PBMC	Human peripheral blood mononuclear cells	RPMI supplemented with • 10% FCS • 1% GlutaMax (2 mM) • 1% Pen/Strep (100 Units/ml penicillin, 0,1 mg/ml streptomycin)	Blut Bank, Deutsches Rotes Kreuz (Heidelberg/ Mannheim)
SK-Mel-37	Human malignant melanoma	DMEM (with GlutaMax) supplemented with • 10% FCS • 1% Pen/Strep (100 Units/ml penicillin, 0,1 mg/ml streptomycin)	DKFZ, Heidelberg
SK-Mel-5	Human malignant melanoma	DMEM (with GlutaMax) supplemented with • 10% FCS • 1% Pen/Strep (100 Units/ml penicillin, 0,1 mg/ml streptomycin)	CLS Cell Lines Service
T2	Human TxB hybrid lymphoblastoid cell line	RPMI supplemented with • 10% FCS • 1% GlutaMax (2 mM) • 1% Pen/Strep (100 Units/ml penicillin, 0,1 mg/ml streptomycin)	ATCC (CRL-1992)
A375	Human malignant melanoma	DMEM (with GlutaMax) supplemented with • 10% FCS • 1% Pen/Strep (100 Units/ml penicillin, 0,1 mg/ml streptomycin)	CLS Cell Lines Service

2.2 Methods

2.2.1 Soluble antibody fusion proteins

2.2.1.1 Design and cloning of soluble TCR-Fc fusion proteins

The TCR-Fc fusion protein design was adapted from Wagner and colleagues (Wagner et al., 2019) and was further engineered for optimal NK or T cell binding together with PD Dr. Frank Momburg. The cloning was performed by PD Dr. Frank Momburg with the help of Nadja Bulbuc. The basic construct format was designed in a bivalent IgG-like manner in which the two Fab fragments of the IgG have each been replaced by a TCR monomer. More precisely, V_L/C_L of an human IgG1 was replaced by TCR Vβ/Cβ and V_H/C_H1 was replaced by TCR Vα/Cα, which was further connected to the Fc fragment (hinge-C_H2-C_H3). For an equimolar expression of the TCRα-hinge-C_H2-C_H3 and TCRβ peptide chains, they were combined in one open reading frame connected by a T2A sequence inducing ribosomal skipping during mRNA translation. To promote TCRα and TCRβ pairing following translation, artificial cysteines were introduced to form two inter-polypeptide disulfide bonds in the constant domain (Cα: T48C and Cβ:S57C). In contrast to Wagner et al., 2019, who fused the TCR-Cα stalk region at an undisclosed residue with the IgG1 hinge to use Cys220 of the hIgG1 hinge region for disulfide bridge formation with a Cys at the C-terminal end of TCR-Cβ, these constructs made use of the natural disulfide bridge formed between Cys95 and Cys131 in the stalk domains of TCR-Cα and -Cβ, respectively, and introduced the mutation C220S in the hIgG1 hinge region instead. Additionally, cysteines within the hinge domain of the Fc fragment form two intermolecular disulfide bonds resulting in the formation of a bivalent TCR-Fc homodimer. Finally, an N-terminal hIg-κ endoplasmic reticulum (ER) signal peptide induces secretion of the refolded TCRα-Fc protein complex and a C-terminal Strep-Tag II was included to enable a Strep-Tactin®-based purification (2.2.1.4). For secretion of the TCRβ chain, the IL-2 ER leader sequence was used. For expression in mammalian cells, all constructs were cloned in the expression vector pcDNA3.1(–).

To generate fusion proteins that are able to bind NK or T cells, different mutations and construct modifications were adapted (Table 10). For NK cell binding and activation, the activating NK cell receptors FcγRIII (also named CD16) and NKp46 were targeted. For T cell binding, the TCR co-receptor CD3 was targeted. In first line, targeting of the FcγRIII was enabled by introducing specific mutations in the Fc part for enhanced FcγRIII receptor binding (S239D, A330L, I332E) – later abbreviated as Fc^{enh} (Lazar et al., 2006). To generate a negative control that is not able to bind NK or T cells, the *N*-glycosylation site in the Fc part was mutated (N297Q), which abolishes binding to FcγRIII – later abbreviated as Fc^{aglyc} (Tao & Morrison, 1989; Wang et al., 2018). Other constructs contain single-chain variable fragments (scFvs)

directed against CD16A (FcγRIIIa) or NKp46 – for NK cell targeting – or scFvs directed against CD3ε – for T cell targeting. These were either incorporated at the C-terminus of TCRβ (TCRβ-scFv-Fc) or the TCRα (TCRα-scFv-Fc) chain. For T cell binding, the TCR-scFv-Fc constructs were combined with the aglycan Fc part, for NK cell binding, with the aglycan as well as with the enhanced Fc part.

For scFv the following sequences were used: Anti-NKp46, clone NKp46-1 (V_H, PDB:6IAP_H; V_L, PDB:6IAP_L), anti-CD16A, clone 4-LS21 (V_H, GenBank:AME94873.1; V_L, GenBank:AME94866.1), anti-CD3ε, clone OKT3 (V_H, GenBank:A22261.1; V_L, GenBank:A22259.1), anti-CD3, clone r3M (V_L-linker-V_H scFv, GenBank:AJ853735). V_H and V_L sequences were joined using a flexible $(Gly_4Ser)_3$ linker. The OKT3 scFv was engineered in V_H-linker-V_L ("HGL") and V_L-linker-V_H ("LGH") orientation.

Table 10: TCR-antibody fusion formats used in this thesis
TCRs fused to the hinge and Fc part of an human IgG1. Details about the Fc part and variants containing an scFv (LGH = N-terminal V_L, glycine-serine linker, C-terminal V_H. HGL = N-terminal V_H, glycine-serine linker, C-terminal V_L) are indicated.

Abbreviation	Immune cell targeting	Fc modification	scFv clone, position
TCR-Fc^{aglyc}	None	Aglycan (N297Q)	None
TCR-Fc^{enh}	NK cells	Enhanced FcγR binding (S239D, A330L, I332E)	None
TCRα-αCD16-Fc^{aglyc}	NK cells	Aglycan (N297Q)	αCD16a, C-terminal of TCRα
TCRβ-αCD16-Fc^{aglyc}	NK cells	Aglycan (N297Q)	αCD16a, C-terminal of TCRβ
TCRα-αNKp46-Fc^{aglyc}	NK cells	Aglycan (N297Q)	αNKp46, C-terminal of TCRα
TCRβ-αNKp46-Fc^{aglyc}	NK cells	Aglycan (N297Q)	αNKp46, C-terminal of TCRβ
TCRα-αCD16-Fc^{enh}	NK cells	Enhanced FcγR binding (S239D, A330L, I332E)	αCD16a, C-terminal of TCRα
TCRβ-αCD16- Fc^{enh}	NK cells	Enhanced FcγR binding (S239D, A330L, I332E)	αCD16a, C-terminal of TCRβ
TCRα-αNKp46- Fc^{enh}	NK cells	Enhanced FcγR binding (S239D, A330L, I332E)	αNKp46, C-terminal of TCRα
TCRβ-αNKp46-Fc^{enh}	NK cells	Enhanced FcγR binding (S239D, A330L, I332E)	αNKp46, C-terminal of TCRβ

TCRα-αCD3-Fc^{aglyc}	T cells	Aglycan (N297Q)	αCD3ε OKT3 LGH, C-terminal of TCRα
TCRβ-αCD3-Fc^{aglyc}	T cells	Aglycan (N297Q)	αCD3ε OKT3 LGH, C-terminal of TCRβ
TCRα-αCD3-Fc^{aglyc}	T cells	Aglycan (N297Q)	αCD3ε OKT3 HGL, C-terminal of TCRα
TCRβ-αCD3-Fc^{aglyc}	T cells	Aglycan (N297Q)	αCD3ε OKT3 HGL, C-terminal of TCRβ
TCRα-αCD3-Fc^{aglyc}	T cells	Aglycan (N297Q)	αCD3ε r3M humanized UCHT1, C-terminal of TCRα
TCRβ-αCD3-Fc^{aglyc}	T cells	Aglycan (N297Q)	αCD3ε r3M humanized UCHT1, C-terminal of TCRβ

The TCRs investigated include several published HLA-A*02:01-restricted TCR clones, which were previously also affinity maturated or mutated (Table 11). TCR Ra14 (PDB: 3GSN_A, PDB:3GSN_B) recognizes the human CMV peptide pp65$_{495-503}$ (Wagner et al., 2019), clone 1G4 is directed against NY-ESO-1$_{157-165}$ (Robbins et al., 2008), clone IMCgp100 against the gp100$_{280-288}$ peptide (Boudousquie et al., 2017; Li et al., 2005) and clone DMF5 against the MART-1$_{26-35}$ peptide (Johnson et al., 2006; Robbins et al., 2008).

Table 11: TCR clones used in this thesis

TCR clone	Target	Mutation/ WT
Ra14	HLA-A*02:01 bound Human CMV pp65$_{495-503}$ (NLVPMVATV)	WT
		CDR3 TCRα: T108Y, Q115H
		CDR3 TCRβ: P108L, I113V, G115L
		CDR3 TCRα: T108Y, Q115H CDR3 TCRβ: P108L, I113V, G115L
1G4	HLA-A*02:01 bound NY-ESO-1$_{157-165}$ (SLLMWITQC)	WT
		TCRα: T95L, S96Y
IMCgp100	HLA-A*02:01 bound gp100$_{280-288}$ (YLEPGPVTA)	WT
		TCRα: D93S, L96M, V97Q TCRβ: Q50W, I51A, V52Q, N53G, I95W, G97A

DMF5	HLA-A*02:01 bound MART-1_{26-35} (EAAGIGILTV)	WT
		TCRβ: T54A

2.2.1.2 Design and cloning of soluble pMHC-SCT-Fc fusion proteins

To generate stable soluble peptide-MHC complexes (Table 12), PD Dr. Frank Momburg and Dr. Marten Meyer designed single chain trimers (SCT) consisting out of the peptide ligand, followed by the human β_2-microglobulin (β_2m) and the matching human MHC-I ectodomain (Greten et al., 2002; Truscott et al., 2008). Cloning of these constructs was jointly performed by PD Dr. Frank Momburg and Nadja Bulbuc. For a covalent binding of the peptide to the MHC-I binding groove, two artificial cysteines were introduced to build a stabilizing disulfide bond - one in the MHC-I alpha 1 domain (Y84C) and one C-terminal of the peptide sequence (2^{nd} amino acid of a glycine-serine linker). Some peptide ligands were furthermore mutated at the anchor positions (2^{nd}, 9^{th} amino acid) to increase peptide binding without affecting its recognition by the T cell receptor. To increase production yields, a pMHC-I SCT-Fc fusion protein was generated by incorporating the hinge-C_H2-C_H3 of a murine IgG2a at the C-terminus of the MHC-I ectodomain. In this thesis, two different pMHC-I SCT-Fc designs were used: pMHC-I (SCT)-mIgG2a-Fc-Strep-Tag-II and pMHC-I (SCT)-*mIgG2a-Fc-Strep-Tag-II. In both variants a Strep-Tag II peptide was included at the C-terminus of the construct enabling a Strep-Tactin®-based purification. In the second format the linker between the SCT and Fc part was extended (-*mIgG2a) with an His_8-Tag for His Mag Sepharose-based purification, an AviTag for a site-specific *in vivo* biotinylation (BirA ligase recognition site) and a thrombin site to enable an enzymatic separation of the monomeric (potentially biotinylated) pMHC-I SCTs. For both formats, an N-terminal hIg-κ endoplasmic reticulum (ER) signal peptide was used to induce secretion of the pMHC-I SCT-Fc fusion protein. For expression in mammalian cells, all constructs were cloned in the expression vector pcDNA3.1(-).

Table 12: pMHC-I SCT-Fc constructs used in this thesis
pMHC-I SCT fused to the hinge and Fc part of an mouse IgG2a. Details about structure, MHC allele, Antigen and peptide sequence are given. Some peptides were mutated at the anchor positions (2^{nd}, 9^{th} amino acid) as indicated with a star.

Structure	MHC Allele	Antigen	Peptide Sequence
Disulfide-trapped pMHC-I (SCT)-mIgG2a-Fc-Strep-Tag II	HLA-A*02:01	HCMV $pp65_{495-503}$	NLVPMVATV
Disulfide-trapped pMHC-I (SCT)-mIgG2a-Fc-Strep-Tag II	HLA-A*02:01	$Survivin_{96-104*(T97M)}$	LM*LGEFLKL
Disulfide-trapped pMHC-I (SCT)-*mIgG2a-Fc-Strep-Tag II	HLA-A*02:01	$gp100_{280-288*(A288V)}$	YLEPGPVTV*

Disulfide-trapped pMHC-I (SCT)-*mIgG2a-Fc-Strep-Tag II	HLA-A*02:01	MART-$1_{26-35*(A27L)}$	EL*AGIGILTV
Disulfide-trapped pMHC-I (SCT)-*mIgG2a-Fc-Strep-Tag II	HLA-A*02:01	NY-ESO-$1_{157-165*}$ (C165V)	SLLMWITQV*

2.2.1.3 Design and cloning of BiMAbs

Bispecific monoclonal antibodies (BiMAbs) were designed by PD Dr. Frank Momburg. Cloning was jointly performed by PD Dr. Frank Momburg and Nadja Bulbuc. The tetravalent BiMAb design combined an scFv against a tumor-associated antigen (TAA) with an scFv against CD3ε for T cell redirection or against CD28 for T cell co-stimulation (Table 13). To this end, the αTAA scFv was connected via an expanded glycine-serine linker ($GNS(G_4S)_3AS$) to the hinge-C_H2-C_H3 of an human IgG1, which is followed by a Strep-Tag II sequence, another $(Gly)_4$ linker and the αCD3ε/αCD28 scFv (Warwas et al., 2021). The Fc part contains several specific mutations, which serve to increase stability as well as to avoid binding to Fc receptors or to complement components (C220S, E233P, L234A, L235A, ΔG236, N297Q, K322A, A327G, P329A, A330S, P331S) (Boesch et al., 2017; Brinkhaus et al., 2020; Dumet et al., 2019; Schlothauer et al., 2016; Shields et al., 2001; Tao & Morrison, 1989; Wang et al., 2018; Xu et al., 2000). Cysteines within the hinge domain form two inter-peptide disulfide bonds resulting in the formation of a tetravalent homodimer. On the N-terminus an hIg-HC ER signal peptide was included to enable secretion of the construct. Additionally, a C-terminal Strep-Tag II was included to enable a Strep-Tactin®-based purification (2.2.1.4). For expression in mammalian cells, all constructs were cloned in the expression vector pcDNA3.1(-).

Table 13: BiMAbs used in this thesis

αTAA scFv	**αCD3/ αCD28 scFv**
αCD19 (clone BCE19)	αCD3 (clone OKT3)
αCD19 (clone BCE19)	αCD28 (clone 9.3)
αEpCAM (clone HEA125)	αCD3 (clone OKT3)
αEpCAM (clone HEA125)	αCD28 (clone 9.3)

BiMAb sequences are described in Warwas et al., 2021.

2.2.1.4 Protein production

Production of the antibody fusion proteins was carried out by Selina Börsig and Susanne Knabe. The protocols used for production were previously set up by Dr. Marten Meyer. For the protein production using Chinese hamster ovary cells (CHO-S), the cells were transfected as previously described resulting in a transient gene expression (Rajendra et al., 2011a, 2011b; Wulhfard et al., 2008, 2010). For maintenance, the cells were cultivated shaking (50 mm

diameter, 100 rpm) at 37°C and 8% CO_2 in 100 ml complete PowerCHO-2CD medium (+ 8mM GlutaMax™ + 1x HT Supplement + 0.5x Antibiotic Antimycotic) in 500 ml glass bottles (round bottom) till they reached $4*10_6$ cells/ ml. For further subcultivation, the cells were diluted 1:10. For transfection, the cells were resuspended in complete PowerCHO-2CD medium at a concentration of $2*10^6$ cells/ ml. After one day, the cells were collected by centrifugation (1500 rpm, 5min) and $300*10^6$ cells were resuspended in 100ml complete ProCHO-4 (+ 4mM GlutaMax™ + 1x HT Supplement + 0.5x Antibiotic Antimycotic). For each production batch, 2 bottles with each 100 ml culture volume were prepared and 2.5 µg PEI and 0.625 µg plasmid DNA were added per $1*10^6$ cells. Following 6 h shaking (50 mm diameter, 100 rpm) at 37°C and 8% CO_2, the culture was supplemented with 1 mM valproic acid. The protein rich cell culture supernatant was finally collected after 6 days shaking (50 mm, 100 rpm) at 32°C and 5% CO_2.

2.2.1.5 Protein quantification

Quantification of the antibody fusion proteins was carried out by Selina Börsig and Susanne Knabe. The protocols used for quantification were previously set up by Dr. Marten Meyer. To confirm a successful protein production, the protein titer in the cell supernatant was quantified using an enzyme-linked immunosorbent assay (ELISA). To this end, the cell suspension resulting from transfection (2.2.1.4) was centrifuged at 1500 rpm and 4°C for 10 min. To ensure a completely cell-free supernatant, the supernatant was centrifuged again at 4000 rpm and 4°C for 30 min and the resulting cell-free supernatant was processed for ELISA. For detection of human or mouse Fc fusion proteins, a MaxiSorb ELISA plate was coated with 5 µg/ml anti-human or anti-mouse IgG-Fc antibody in carbonate-bicarbonate coating buffer (Table 7) at 37°C for 45 min. Afterwards, the plate was washed three times using washing buffer (Table 7, 200 µl/ well). To block unspecific protein binding, 100 µl blocking buffer (Table 7) supplemented with 0.05% Tween were added per well and incubated at 37°C for 45 min. Before adding the sample, the plate was washed one time using washing buffer (200 µl/ well). The cleared cell culture supernatant was then added in different dilutions ranging from 1:100-1:900 (100 µl/ well, diluted in washing buffer supplemented with 0.5% BSA). To generate a standard curve for quantification, pMHC-I SCT-mIgG2a-Fc or pMHC-I SCT-hIgG1-Fc proteins of known concentration were simultaneously applied in different concentrations (100 µl/ well, diluted in washing buffer supplemented with 0.5% BSA). Following 45 min incubation at 37°C, the plate was washed three times using washing buffer (200 µl/ well). For detection of the bound Fc fusion proteins, a peroxidase conjugated anti-human or anti-mouse IgG-Fc antibody was applied (Table 7, 100 µl/ well, diluted 1:10.000 in washing buffer supplemented with 0.5% BSA). Following 45 min incubation at room temperature, the plate was washed three times as described before and 100 µl TMB substrate solution (Table 7) were added per well and

incubated for 5-15 min. To stop the enzymatic reaction, 100 µl of 1M H_2SO_4 were added per well. Absorbance of the reaction product was measured at 420 nM and 540 nm was used as reference.

2.2.1.6 Protein purification

Following a successful protein production as determined by ELISA (2.2.1.5), the protein of interest was purified from the cell-free cell culture supernatant by Selina Börsig and Susanne Knabe using protocols previously set up by Dr. Marten Meyer. For purification via the Strep-Tag II the Strep-Tactin® Superflow® system was used. To this end, a low-pressure liquid chromatography (LPLC) with 0.7 cm diameter was filled with 1.5 ml Strep-Tactin® Superflow® high capacity resin (for 200 ml cell-free supernatant). Before purification, the supernatant was supplemented with 1x PBS (10x PBS, diluted 1:10). To equilibrate the resin, the column was washed two times with 5 ml 1x PBS. Afterwards, the PBS supplemented supernatant was loaded on the column using a peristaltic pump and a flow rate of 1.5-2.5 ml/min. To remove any unbound proteins, the column was washed twice using 2.5 ml 1x PBS. Elution of the bound protein of interest was then enabled by addition of 2.5 ml of a 5 mM desthiobiotin solution (diluted in PBS). 0.25 ml fractions were collected at a flowrate of 1.5 ml/min and protein concentration was measured using a Nanodrop (280 nm). The fractions with the highest protein concentration were pooled and dialyzed over night at 4°C to remove excess desthiobiotin using dialysis cassettes with a 20 kDa cutoff.

To confirm that the purified proteins showed the expected molecular weight, a sodium dodecyl sulfate–polyacrylamide gel electrophoresis (SDS-PAGE) was performed. To this end, 2.5 µg of the dialyzed protein was supplemented with 1x RunBlue™ LDS Sample Buffer. For reducing conditions, the sample was supplemented with 10 mM DTT and denatured by incubation at 70°C for 10 min. To run the SDS-PAGE, the XCell SureLock™ mini cell system and 1x RunBlue™ SDS running buffer were used, the proteins were loaded on the RunBlue™ TEO-Tricine SDS-Precast gel and the proteins were separated at 140 V for 90 min. Proteins were visualized by incubating the gel was in InstantBlue™ Coomassie staining solution on an orbital shaker for 3-4 h. Afterwards, the gel was destained by incubation in ddH_2O overnight and scanned using a Perfection V500 Photo Scanner.

2.2.2 Isolation of peripheral blood mononuclear cells (PBMCs)

For the isolation of human peripheral blood mononuclear cells (PBMCs), fresh blood from healthy donors was received from the DRK (Deutsches Rotes Kreuz) in Heidelberg/ Mannheim. The blood was diluted 1:3 with PBS, carefully layered on top of Biocoll and

centrifuged at 1800 rpm for 25 minutes without break. Using this protocol, the cells were separated according to differences in density, which lead to an accumulation of red blood and granulocytes at the bottom and of PBMCs in a white layer at the interphase. To remove remaining platelets from the PBMCs, the collected PBMC layer was washed three times with PBS at low centrifugation speed (800 rpm, 20/15/5 min, with break). Afterwards, the cells were resuspended at 5-10*10^6 cells per ml in complete RPMI medium (with 10% FCS, 2 mM GlutaMax™ Supplement, 1% Penicillin/ Streptomycin) with 2.5 units/ml nuclease and incubated at 37°C and 5% CO_2 until further use.

2.2.3 T & NK cell isolation

The isolation of human T and NK cells from PBMCs was conducted using MACS isolation. A negative selection was performed according to the manufacturer's protocol using the human pan T cell and NK cell isolation kit from Miltenyi Biotec (Table 6). If not used directly, the cells were resuspended in complete RPMI (with 10% FCS, 2 mM GlutaMax™ Supplement, 1% Penicillin/ Streptomycin) and incubated at 37°C and 5% CO_2.

2.2.4 Flow cytometry

To analyze cells using flow cytometry, around 0.2-1*10^6 cells were used per sample. All the following staining steps were incubated under protection from light. Washing steps were performed using a final volume of 200 µl/ sample and 3 min centrifugation at 1500 rpm and 4°C. For discrimination of living and dead cells, the sample was stained with the Zombie Aqua™ Fixable Viability Kit as instructed in the manufacturer's protocol and incubated at room temperature for 10 min. If required, an FcR blocking solution was applied afterwards (Human TruStain FcX™ resuspended in FACS buffer, Table 4) and incubated at room temperature for additional 10 min. Afterwards, the cells were centrifuged at 1500 rpm for 3 min and the supernatant was discarded.

- To stain markers expressed on the cell surface, the cells were resuspended in 50 µl antibody solution (diluted in FACS buffer) and incubated at 4 °C for at least 15 min. Afterwards, the cells were washed twice with FACS buffer.
- To analyze the TCR-Fc fusion proteins for a functional TCR target binding, the target cells were incubated with 1 µg/ml fusion protein (if not stated otherwise) diluted in 50 µl FACS buffer for 1 h at 4°C. Afterwards, the cells were washed twice with FACS buffer. For detection of the TCR-Fc fusion protein, the cells were incubated with a goat-anti-human-IgG1 PE secondary antibody (50 µl/ sample diluted 1:200 in FACS buffer) for 15 min at 4°C. Afterwards the cells were washed twice with FACS buffer.

- To analyze the binding of the CMV pp65-specific TCR-Fc and TCR-scFv-Fc fusion proteins to NK or T cells, the cells were incubated in 2-5 µg/ml TCR diluted in 50 µl FACS buffer for 1 h at 4°C. Afterwards, the cells were washed twice with FACS buffer. Detection was enabled using a goat-anti-human-IgG1 PE secondary antibody (50 µl/ sample diluted 1:200 in FACS buffer) or a fluorochrome-conjugated pCMV-MHC-I SCT streptavidin multimer (in house production, 0.5 µl multimer diluted in 50 µl FACS buffer per sample). Following 15 min incubation at 4°C, the cells were washed twice with FACS buffer.
- To stain intracellular markers, the BD Cytofix/Cytoperm™ Fixation/Permeabilization Kit was used. The staining of intracellular markers was always performed following other extracellular staining steps. At first the cells were fixed by resuspension in fixation/ permeabilization solution (100 µl/ sample). Following 10 min incubation, the cells were washed twice with 1x Perm/Wash solution (diluted in water). Afterwards, the cells were resuspended in the antibody solution diluted in 100µl 1x Perm/Wash solution per sample. Following 30 min incubation at 4°C, the cells were washed once with 1x Perm/Wash solution and once with PBS.

For acquisition, the cells were resuspended in FACS buffer or in fixation solution (Table 4). Acquisition was done using a BD FACS Canto II and analysis using FlowJo.

2.2.5 Enzyme-linked Immunosorbent Assay (ELISA) to assess TCR binding

To analyze the target binding properties of the soluble TCR-Fc fusion proteins an ELISA was performed. First, 5 µg/ml pMHC-I SCT-Fc fusion protein were used for coating (100 µl/ well diluted in PBS) of a 96-well MaxiSorb ELISA plate. Following incubation overnight at 4°C, the plate was washed three times. For the washing steps, 200 µl washing buffer were used per well (Table 7). To block unspecific protein binding, 100 µl blocking buffer (Table 7) were added per well. Following 45 min incubation at 37°C, the plate was washed three times. The TCR-Fc fusion proteins were diluted in sample buffer (Table 7) as indicated. 100 µl sample was applied per well and incubated for 1.5 hours at 37°C. Afterwards, the plate was washed three times. For the detection of bound TCR-Fc, the peroxidase conjugated anti-human Fc antibody was diluted 1:10.000 in sample buffer and added to the wells (100 µl/ well). Following 30 min incubation at 37°C, the plate was washed three times and 100 µl TMB peroxidase substrate solution (Table 7) were applied per well. Following 5 to 15 min incubation, 100 µl 1 M H_2SO_4 were added to stop the enzymatic reaction. Absorbance of the reaction product was measured using 420 nM and 540 nm was used as reference.

2.2.6 Tumor cell lines and culture conditions

Except for CHO-S (2.2.1.4), all cell lines and primary cells were cultivated at 37°C and 5% CO_2 (Table 9). For passaging of adherent cells, the culture supernatant was removed and the adherent cell layer was carefully rinsed with PBS. Detachment of the cells was enabled by addition of a trypsin-EDTA solution and incubation at 37 °C for 3 min. The cell solution obtained was collected using fresh medium and centrifuged at 1500 rpm for 5 min. For further cultivation, the cells were resuspended in fresh medium as required. For passaging of suspension cells, the required number of cells was directly diluted in fresh medium. For MCF-7, MeWo, SK-Mel-5 and SK-Mel-37 cells a division time of 24 h was assumed, for T2 cells a division time of 48 h was assumed. The cells were passaged once or twice a week.

For conservation, the cells were resuspended in FCS containing 10% DMSO and transferred to -80°C using a Mr. Frosty™ freezing container for a slow cooling of -1 °C/ min. For long-term storage, the cells were transferred to liquid nitrogen.

2.2.6.1 Generation of pMHC-mSCT transfectants

To generate an ideal target cell that offers a high peptide presentation without the need for an endogenous protein expression or an exogenous peptide pulse, the indicated cell lines were transfected with membrane-bound peptide-tethered MHC-I single chain trimers (mSCT) (Table 14) using lipofectamine™ 3000. The constructs used for transfection were designed and cloned by PD Dr. Frank Momburg. The SCTs are expressed as a single polypeptide chain that consists of a influenvirus HA ER signal sequence, a peptide ligand, followed by the human β_2-microglobulin (β_2m) sequence and the matching human MHC-I allele including its transmembrane domain and cytoplasmic tail. As for the pMHC-I SCT-Fc fusion proteins (2.2.1.2), an artificially introduced cysteine in the MHC-I allele (Y84C) enables the formation of a disulfide bond with another cysteine introduced C-terminal of the peptide ligand (2^{nd} amino acid in the first glycine-serine-rich flexible linker), which enables irreversible peptide binding to the binding groove of the MHC-I molecule. Some peptide ligands were furthermore mutated at the anchor positions (2^{nd}, 9^{th} amino acid) to increase peptide binding without affecting its recognition by the T cell receptor. Additionally, an AviTag in the flexible linker between the β_2m and MHC-I alpha1 domain enables an intracellular site-specific biotinylation by co-transfected ER-resident BirA ligase and thus an easy detection using a fluorochrome-conjugated Streptavidin protein. To ensure a simultaneous expression of the SCT and *E. coli* BirA ligase introduced into the secretory pathway by an Ig-κ ER signal sequence and tagged with the C-terminal ER retention motif KDEL, the Igκ-$BirA_{KDEL}$ sequence was included downstream in the same open reading frame separated through a T2A sequence. This sequence induces ribosomal skipping upon translation, which leads to the synthesis of two separate polypeptide

chains. For expression in mammalian cells, all constructs were cloned in the expression vector pcDNA3.1(+).

In case of pCMV-A*0201-mSCT and pSur-A*0201-mSCT transfected MCF-7, the cells were cultivated in presence of 600 µg/ml G418 for two weeks to generate a stably transfected cell line. To enhance the co-stimulatory properties, the pCMV- and pSur-A*0201-mSCT transfected MCF-7 were furthermore super-transfected with CD80 (cloned in the vector pcDNA6-V5/HisA) using lipofectamine™ 3000. To select for stable transfectants, the cells were cultivated in the presence of 8 µg/ml blasticidin for two weeks. To enrich for pMHC-mSCT and CD80 expressing cells following each transfection and selection process, the cells were stained with CD80-APC (2 µl/ $0.5*10^6$ cells/ 100µl) or streptavidin-PE (1 µl/ $0.5*10^6$ cells/ 100µl) in MACS Buffer (Table 6) for 15 min at 4°C and isolated with anti-APC and anti-PE microbeads according to the manufacturer's protocol.

Table 14: pMHC-I mSCT constructs used for transfection in this thesis
Details about MHC allele, Antigen and peptide sequence are given. Some peptides were mutated at the anchor positions (2^{nd}, 9^{th} amino acid) as indicated with a star.

Allele	Antigen	Peptide Sequence
HLA-A*02:01	HCMV $pp65_{495-503}$	NLVPMVATV
HLA-A*02:01	$Survivin_{96-104\ (T97M)}$	LM*LGEFLKL
HLA-A*02:01	$gp100_{280-288\ (A288V)}$	YLEPGPVTV*
HLA-A*02:01	$MART\text{-}1_{26-35\ (A27L)}$	EL*AGIGILTV
HLA-A*02:01	$NY\text{-}ESO\text{-}1_{157-165\ (C165V)}$	SLLMWITQV*

2.2.7 *In vitro* co-culture of tumor cells with T/NK cells

To analyze if the soluble TCR-Fc and TCR-scFv-Fc fusion proteins are able to induce T and NK cell redirection and target-directed cytotoxicity, an *in vitro* co-culture assay was used. Target cells were seeded one day before co-culture in a 96 well plate (flat bottom for adherent cells, round bottom for suspension cells) to reach 50.000 cells/100 µl/well at the day of co-culture in complete culture medium (Table 9). If required, soluble synthetic peptide was added to the cell suspension during seeding to reach 100 µM in 100 µl/well if not stated otherwise. This enables a peptide exchange on surface-expressed MHC-I molecules and peptide presentation independent of endogenous protein expression. Following incubation overnight at 37°C and 5% CO_2, the effector cells and the soluble TCR-Fc and TCR-scFv-Fc fusion proteins as well as other monoclonal antibodies and BiMAbs were added (diluted in complete culture medium) resulting in a final volume of 200 µl/ well. T or NK cells were added using an effector-to-target ratio (E:T) of an 5:1 or 2.5:1 respectively. For setting up the co-culture with NK cells, the peptide solution was removed, the target cells were washed once and fresh medium was added (100 µl/well). This prohibits that the peptide might bind to HLA-$A2^+$ NK

cells, as the PBMC donor was chosen according to the largest NK cell population (analyzed by flow cytometry) independent of the HLA type. The co-culture was then incubated at 37°C and 5% CO_2. The co-culture with NK cells was analyzed after 4 h considering target-directed cytotoxicity (2.2.7.1), NK cell degranulation and intracellular cytokines levels (2.2.7.2) and after 24 h considering activation markers expressed on the cell surface (2.2.7.3). For the co-culture of T cells, an HLA-A2$^-$ PBMC donor was chosen (analyzed by flow cytometry). In this case, the peptide solution was not washed away, to avoid unnecessary decrease in peptide presentation over time. The co-culture with T cells was analyzed after 24 h incubation considering target-directed cytotoxicity (2.2.7.1), expression of a panel of different activation markers (2.2.7.3) as well as T cell degranulation and intracellular cytokine levels (2.2.7.2) and after 5 days considering T cell proliferation (2.2.7.4). As a high control for degranulation, intracellular cytokine production, activation and proliferation, 50 ng/ml phorbol-12-myristate-13-acetate (PMA) and 1 µg/ml ionomycin were added to a sample containing only effector cells when setting up the co-culture.

2.2.7.1 Cytotoxicity assay

To determine the relative cytotoxicity in the co-culture setup, the enzyme lactate dehydrogenase (LDH) released by dying cells was detected using the CyQUANT™ LDH Cytotoxicity Assay kit from Roche. Each condition was setup in triplicates. As a high control, 10 µl lysis buffer/well were added to the tumor cells when setting up the co-culture. To determine the basal LDH level resulting from spontaneous lysis, controls with only tumor cells or effector cells were included. Following incubation, the co-culture containing 96-well plate was centrifuged at 1500 rpm for 3 min, 100 µl supernatant were transferred to a fresh flat bottom 96-well plate and 100 µl of the reaction mixture were added that contains the substrate sodium lactate, iodotetrazolium chloride and diaphorase. Upon the LDH-catalyzed substrate conversion nicotinamide adenine dinucleotide hydrogen (NADH)/H^+ is generated, which is used for the diaphorase-catalyzed reduction of the iodotetrazolium chloride to red formazan salt. After around 10 min incubation at room temperature in the dark, the absorbance of the formazan salt was measured. To correct for optical artefacts, the values measured at 620nM (reference wavelength) were subtracted from the values measured at 492 nm (absorbance maximum). To account for any background signal resulting from the medium color, the mean value obtained from medium only was subtracted. To calculate the relative cytotoxicity, the sample value (subtracted with the spontaneous release of effector and target cells) was divided by the maximum release detected in the high control (subtracted with the spontaneous release of target cells) and multiplied by 100 to yield percent of cytotoxicity.

$$\%\ \text{Cytotoxicity} = \frac{\text{sample release} - \text{effector cell spontaneous release} - \text{target cell spontaneous release}}{\text{target cell maximum release} - \text{target cell spontaneous release}} \text{x } 100$$

2.2.7.2 Degranulation and intracellular cytokines

To measure effector cell degranulation and intracellular cytokine levels, the co-culture was setup in presence of monensin and brefeldin A (each diluted 1:1000), which prohibits protein transport and secretion. Additionally, 0.5 µl of the fluorochrome-conjugated αCD107a antibody were added per well when setting up the co-culture. Following 4 or 24 h incubation using NK or T cells respectively, the samples were processed for acquisition using flow cytometry (2.2.4). To this end, the samples were stained with different surface markers to enable a clear identification of the effector cell population (NK cells: Table 15, T cells: Table 16) and fluorochrome-conjugated antibodies against interferon(IFN)-γ and tumor necrosis factor(TNF)-α (Table 17).

Table 15: NK cell surface marker panel for degranulation and intracellular cytokine detection

Antibody	µl/ test
CD56-FITC	1
CD3/CD14/CD19-BV510™	0.5

Table 16: T cell surface marker panel for degranulation and intracellular cytokine detection

Antibody	µl/ test
CD3-APC/Cy7	1
CD4-Alexa Fluor® 488	1
CD8-Pacific Blue™	1
CD14/19/56-BV510™	0.5

Table 17: Intracellular cytokine staining panel for NK and T cells

Antibody	µl/ test
IFNγ-PE	2.5
TNFα-PE	1.5

2.2.7.3 Activation marker profiling

To measure NK cell activation in the co-culture setup, the cells were stained for the expression of the activation markers CD69 and CD137 (4-1BB) (Table 18). To measure T cell activation in the co-culture setup, the cells were stained for the expression of the activation markers CD25, CD69, CD134 (OX40) and CD137 (Table 19). The staining was measured using flow cytometry (2.2.4).

Table 18: Activation marker panel for NK cells

Antibody	µl/ test
CD56-FITC	1

CD69-Alexa Fluor® 647	2
CD137-PE	1
CD3/14/19-BV510™	0.5

Table 19: Activation marker panel for T cells

Antibody	µl/ test
CD3-APC/Cy7	1
CD4-Alexa Fluor® 488	1
CD8-PerCP/Cyanine5.5	1
CD25-Alexa Fluor® 647	0.5
CD69-BV421™	1
CD134-PE/Cyanine7	0.5
CD137-PE	0.5
CD14/19/56-BV510™	0.5

2.2.7.4 T cell proliferation assay

To measure T cell proliferation, the T cells were labeled with CellTrace™ Violet shortly before setting up the co-culture. To prevent loss in fluorescence, all the following incubation steps were performed in the dark. The required amount of cells was collected and washed (centrifugation at 1500 rpm, 5 min) with PBS to remove remaining serum. For labeling, the cells were resuspended at a concentration of $1*10^6$ cells/ ml in a 1 µM CellTrace™ Violet solution (diluted in PBS) and incubated for 20 min at 37°C. To remove excessive free dye, one volume of cold FCS was added. Following 5 min incubation at room temperature, one volume of complete RPMI (with 10% FCS, 1% GlutaMax™ Supplement, 1% penicillin/streptomycin) was added and the cells were collected by centrifugation at 1500 rpm for 5 min. Afterwards, the cells were resuspended in complete RPMI. Following another 15 min incubation at 37°C, the cells were centrifuged (1500 rpm, 5 min) and resuspended as required for the co-culture. After 5 days co-culture, the cells were stained and processed for flow cytometry (Table 20).

Table 20: Surface marker panel for analysis of T cell proliferation

Antibody	µl/ test
CD3-APC/Cy7	1
CD4-PE	1
CD8-APC	1

2.2.7.5 3D spheroid model

Tumor cell spheroids resemble some features of solid tumors and were generated as a 3D culture model for the *in vitro* co-culture with T/ NK cells (2.2.7). For the generation of tumor

spheroids, 50.000 cells were seeded per well of a Nunclon™ Sphera™ 96 well plate in ice-cold spheroid medium (100 µl/ well, DMEM/F-12 + 10% FCS + 2% Geltrex™ + 2% B-27) two days before co-culture. To enable spheroid formation, the cells were centrifuged at 120 rpm and 4°C for 5 min, before incubation at 37°C. The *in vitro* co-culture was then setup as described (2.2.7) using DMEM/F-12 + 10% FCS + 2% B-27 as culture medium. In case of NK cells, the co-culture was extended to 24 h for all readouts including cytotoxicity (2.2.7.1), degranulation and intracellular cytokines (2.2.7.2) as well as the activation marker profiling (2.2.7.3). In case of T cells, the co-culture was incubated as described before (2.2.7).

3 Results

3.1 Soluble TCR-Fc fusion protein design

To produce TCR-based bispecific agents for the redirection of NK and T cells, a recently described bivalent immunoglobulin-like format was adapted (Wagner et al., 2019) (Figure 9). In this format two disulfide bridged TCR monomers are fused to the Fc part of an human IgG1. Using this format Wagner et al. (2019) were able to achieve high protein yields upon production in Chinese ovarian hamster (CHO) cells. Thus, the immunoglobulin's V_L/C_L domains are replaced by TCR Vβ/Cβ and V_H/C_H1 are replaced by TCR Vα/Cα, which are further connected to the hinge and Fc fragment (C_H2-C_H3) giving rise to two different polypeptide chains - TCRα-hinge-C_H2-C_H3 and TCRβ (Figure 9A). To enable an equimolar expression, both peptide chains are combined in one open reading frame connected by a T2A sequence inducing ribosomal skipping during mRNA translation (Liu et al., 2017). To promote full assembly of the TCR-Fc homodimer following translation, the constructs make use of native and artificial inter-polypeptide disulfide bonds. Thus, TCRα and TCRβ association is promoted by the introduction of an artificial disulfide bridge in the constant domain (Cα:T48C and Cβ:S57C), a disulfide bridge originally described by Boulter and colleagues (Boulter et al., 2003) and by using the natural disulfide bridge formed between Cys95 and Cys131 in the stalk domains of TCR-Cα and -Cβ, respectively. As common for immunoglobulins, homodimer association is mediated through two natural intermolecular disulfide bonds within the hinge domain of the Fc fragment. The hIg-κ endoplasmic reticulum (ER) signal peptide N-terminal of TCRα and the IL-2 ER signal peptide N-terminal of TCRβ together enable full assembly within the ER and secretion via ER and golgi apparatus. A C-terminal Strep-Tag II was included to enable a Strep-Tactin®-based purification (2.2.1.4).

To enable NK and T cell redirection, different construct modifications have been investigated (Figure 9B). As a negative control that does not bind NK nor T cells, a TCR-Fc^{aglyc} construct was designed that uses an aglycan Fc part with a mutated *N*-glycosylation site (N297Q). NK cell redirection was enabled either by using a glycosylated Fc part with few additional mutations that were shown to further enhance binding to the ADCC-inducing FcγRIIIa (S239D, A330L, I332E) – as from now abbreviated as Fc^{enh} (Lazar et al., 2006); or by incorporation of scFvs targeting FcγRIIIa (in context of the scFv also referred to as αCD16a) or by targeting the natural cytotoxicity receptor NKp46; or by the combination of both, an scFv and the "enhanced" Fc. For the redirection of T cells on the other hand, the TCR-Fc^{aglyc} was extended by different scFv constructs targeting CD3ε within the TCR complex: the humanized UCHT1 clone r3M (V_L-linker-V_H orientation) and OKT3 in two different orientations, V_L-linker-V_H ($OKT3_{LGH}$) and V_H-linker-V_L ($OKT3_{HGL}$). To investigate the optimal scFv positioning, two different TCR-scFv-Fc designs were tested in each case, in which the scFv was incorporated either at the C-terminus

of TCRα (referred to as TCRα-scFv-Fc) or TCRβ (referred to as TCRβ-scFv-Fc) using a short flexible linker (G_3S or SG_4S). (Figure 9A). As demonstrated in Figure 32 (appendix), all recombinant proteins could be produced and showed high purity when analysed by SDS-PAGE.

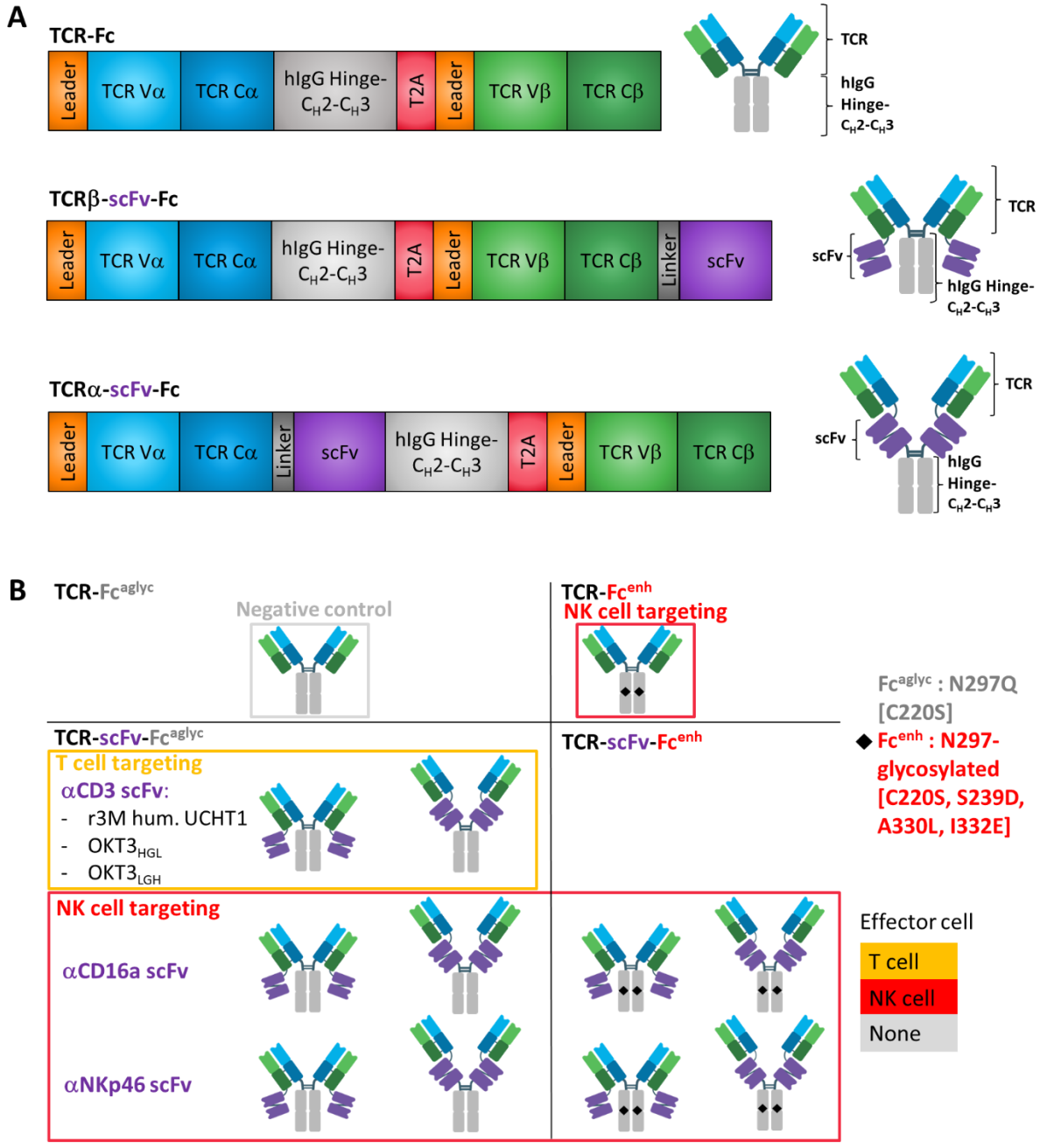

Figure 9: Architecture of TCR-Fc fusion proteins used in this thesis
The soluble TCR constructs are designed in an IgG-like format as two TCR monomers that are fused to the hinge-C_H2-C_H3 domain of a human IgG1 molecule including a C220S mutation. A) For equal expression of both polypeptide chains a T2A sequence inducing ribosomal skipping upon mRNA translation was used. An ER leader sequence enables secretion of each construct. In addition to the TCR-Fc format, the TCR-scFv-Fc constructs are equipped with an scFv incorporated either at the C-terminus of the TCRα (TCRα-scFv-Fc) or TCRβ (TCRβ-scFv-Fc) chain. B) NK cell redirection is enabled using an engineered Fc part with enhanced binding to the FcγRIIIa (CD16a) (abbreviated as Fc^{enh}) expressed on NK cells, and/or scFvs against CD16a or NKp46. To prohibit Fc binding to the FcγRIIIa,

an aglycan Fc part was used (mutation N297Q) abbreviated as Fc^{aglyc}. For T cell redirection the TCR-scFv-Fc^{aglyc} format was equipped with scFvs against CD3ε (clone r3M [humanized UCHT1], clone OKT3 with two different orientations of variable light and heavy chain: LGH = N-terminal V_L, glycine-serine linker, C-terminal V_H. HGL = N-terminal V_H, glycine-serine linker, C-terminal V_L).

3.2 Evaluation of soluble TCR-Fc fusion proteins using a CMV pp65-specific TCR

3.2.1 Target binding

As a proof-of-concept initial experiments were performed with the same cytomegalovirus (CMV) tegument $pp65_{495-503}$ peptide-specific TCR clone Ra14 as used by Wagner et al. (Wagner et al., 2019). To investigate the influence and importance of TCR affinity, the wildtype TCR and an affinity-maturated variant were compared, which were shown to have an affinity of 3 µM and 50 nM in the bivalent IgG-like format respectively (Wagner et al., 2019). To confirm a functional TCR, the CMV pp65-specific TCR-Fc constructs were analyzed for their target binding using ELISA (Figure 10A, 2.2.5) and flow cytometry (Figure 10B, 2.2.4). For the ELISA, 5 µg/ml CMV pp65 peptide-tethered HLA-A*02:01 SCT-Fc fusion protein (pCMV-MHC) were coated and different concentrations of the TCR-Fc fusion protein were added. This construct comprises the peptide MHC-ligand linked to β2-microglobulin using a glycine-serine linker followed by the HLA-A*02:01 allele without the transmembrane domain and a hinge-C_H1-C_H2 of a murine IgG2a (2.2.1.2). A so-called disulfide trap was included, which builds a stabilizing disulphide bridge between an artificially introduced cysteine (Y84C) in the HLA allele and a cysteine included in the linker between peptide and β2m (2^{nd} aa). As a negative control a survivin peptide-tethered HLA-A*02:01 SCT-Fc (pSur-MHC) was included. For analysis using flow cytometry, TAP-deficient HLA-A*02:01$^+$ T2 cells were pulsed with the indicated HLA-A*02:01-restricted peptides. This human hybrid lymphoblastoid cell line is generated by an artificial fusion of B and T cell lymphoblasts and offers a high peptide presentation following peptide pulse due to their TAP-deficiency. They were either pulsed with 100 µM CMV pp65 peptide and different concentrations of TCR-Fc were added or pulsed with different concentration of peptide and 6 nM TCR-Fc were added. 100 µM survivin peptide were included as negative control. Bound TCR-Fc protein was detected using a secondary human Fc-specific fluorophore-conjugated antibody. ELISA and flow cytometry showed a CMV pp65-specific target binding as no binding was detected towards the survivin peptide-tethered MHC or peptide-pulsed T2 cells. Furthermore, the binding was dependent on TCR concentration and TCR affinity, as the TCR-Fc constructs incorporating the maturated high-affinity TCR variant showed a stronger binding upon lower TCR or peptide concentrations compared to the wildtype variant. In case of the ELISA, an EC_{50} of 19 nM was determined for the low-affinity TCR and 0.17 nM for the high-affinity variant. Using flow cytometry, EC_{50} of the low-affinity variant was not within the tested range (estimated >100nM) and 0.25 nM for the high-affinity variant. Similar

was observed for the peptide titration with an EC_{50} above 100 µM for the low-affinity variant and 98 µM for the high-affinity TCR.

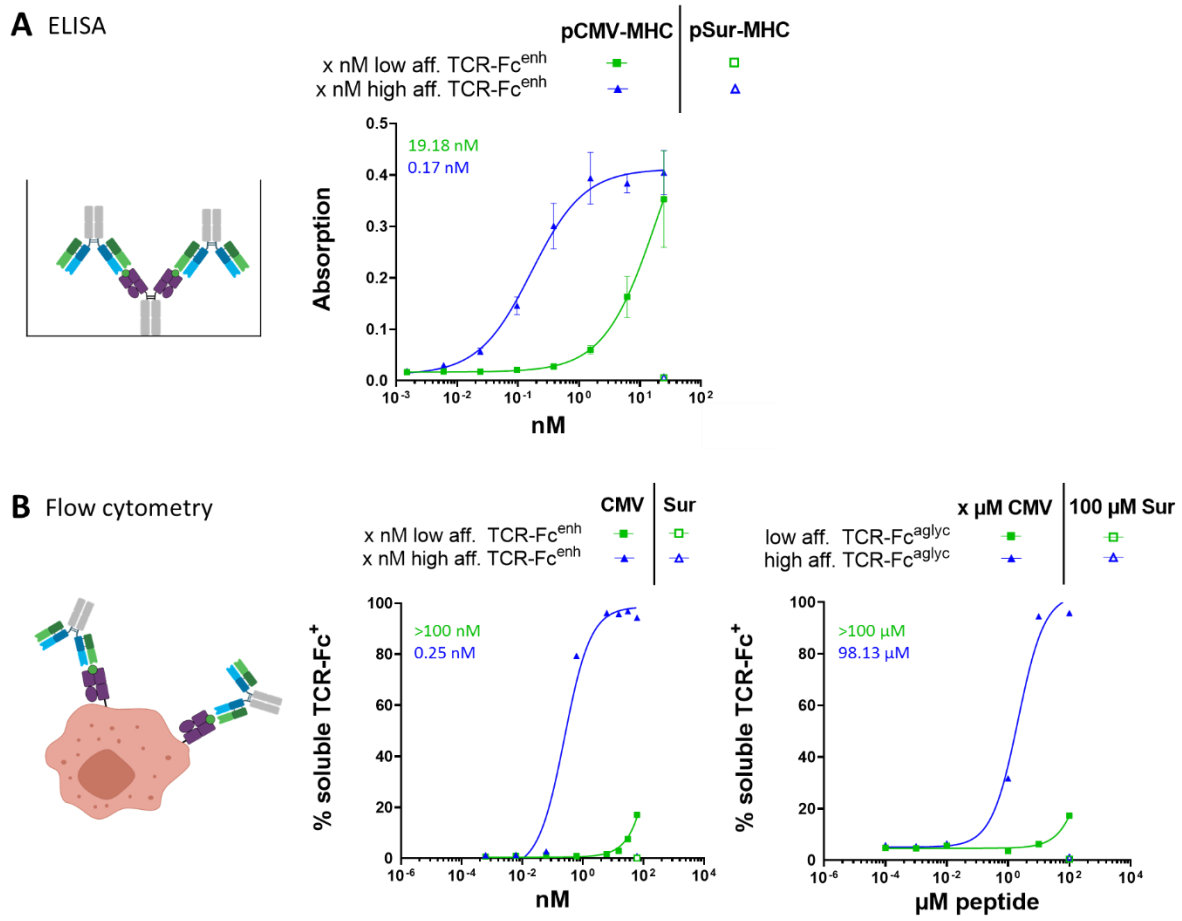

Figure 10: Target binding of the low- and high-affinity CMV pp65-specific TCR-Fc fusion proteins
Target binding was analyzed for the low (wild-type) and high (maturated) affinity CMV pp65-specific TCR-Fc fusion proteins using ELISA and flow cytometry. A) In the ELISA, binding was analyzed towards CMV pp65 (pCMV-MHC) and survivin (pSur-MHC) peptide-tethered MHC-Fc fusion proteins. Concentration of the soluble TCR-Fc protein was titrated. Shown are the results of three independent experiments. B) Using flow cytometry, binding was analyzed towards CMV pp65 (CMV) and survivin (Sur) peptide-pulsed HLA-A*02:01$^+$ T2 cells. TCR-Fc (left) and peptide concentrations (right) were titrated. Computed EC_{50} values are indicated in the matching color in the upper left corner.

3.2.2 NK cell redirection

To analyze NK cell redirection of the TCR-Fc format, a co-culture was set up using peptide pulsed T2 cells as artificial target cells (Figure 11A). NK cell-mediated cytotoxicity was then analyzed following 4 h co-culture by measuring the release of the intracellular enzyme lactate dehydrogenase (LDH) upon cell lysis compared to that induced by the addition of lysis buffer, which was defined as 100% cytotoxicity (2.2.7.1). Cytotoxic NK cell degranulation was analyzed by cell surface staining of the degranulation marker CD107a using flow cytometry (Figure 11B, 2.2.7.2). NK cell activation was analyzed using flow cytometry by staining for intracellular cytokines IFNγ and TNFα (2.2.7.2) and the surface markers CD69 and CD137 (4-

1BB) (Figure 11B, 2.2.7.3). NK cell degranulation and intracellular cytokines were measured after 4 h co-culture in presence of Golgi transport inhibitors and CD69 and CD137 were assessed after 24 h co-culture (without supplement). In the presence of the high-affinity TCR-Fc^{enh} fusion protein, the co-culture with CMV pp65 peptide-pulsed T2 cells did result in an increased NK cell degranulation and activation compared to the co-culture with survivin peptide-pulsed control T2 cells, as seen by increased expression of CD107a, CD69, CD137, IFNγ and TNFα.

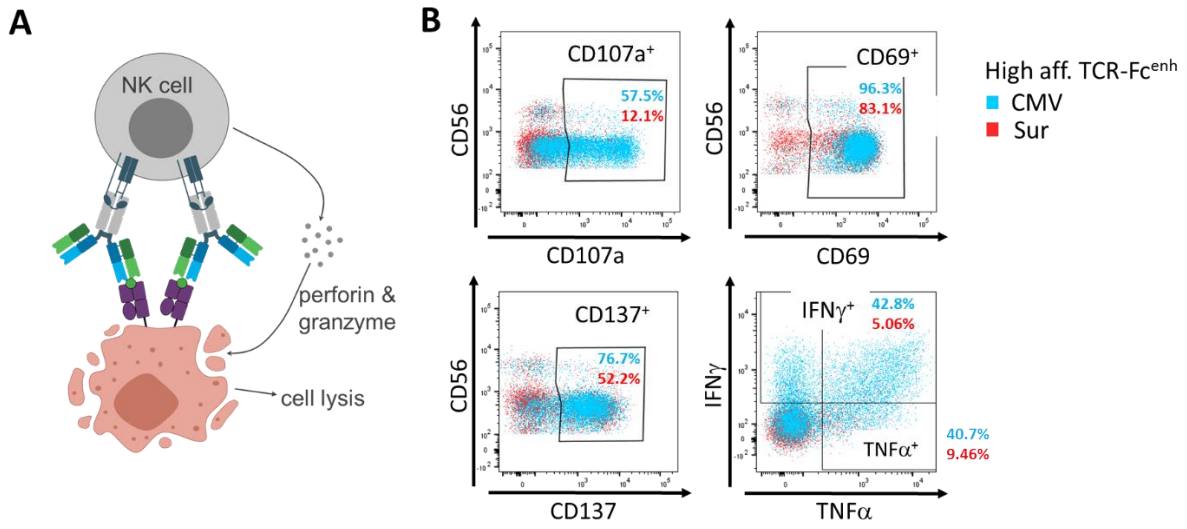

Figure 11: NK cell activation upon co-culture with peptide pulsed T2 cells in presence of the CMV pp65-specific TCR-Fc^{enh} fusion protein
A) NK cell redirection of the TCR-Fc^{enh} construct was evaluated using a co-culture of NK cells with 100 µM peptide-pulsed HLA-A*02:01$^+$ T2 cells in presence of 6 nM CMV pp65-specific TCR-Fc^{enh}. B) NK cell degranulation and activation were analyzed using flow cytometry by staining for CD107a, CD69, CD137, and intracellular IFNγ and TNFα. Expression of CD69 and CD137 was analyzed following 24 h co-culture. CD107a, IFNγ and TNFα were analyzed after 4 h co-culture in presence of Golgi transport inhibitors. Co-culture with CMV pp65 (CMV) peptide-pulsed T2 cells is shown in blue and with survivin (Sur) peptide-pulsed T2 cells is shown in red.

To analyze the importance of TCR affinity and antigen density for an efficient NK cell redirection and NK cell-mediated cytotoxicity induced by the TCR-Fc^{enh} fusion protein, the concentrations of TCR high/low-affinity constructs (Figure 12) and CMV pp65 peptide (Figure 13) were titrated. Survivin peptide-pulsed T2 cells and the TCR-Fc^{aglyc} constructs were included as a negative control. In both setups, the CMV pp65-specific TCR-Fc^{enh} constructs did result in increased NK cell-mediated target cell lysis, NK cell degranulation (CD107a) and NK cell activation (CD69, CD137, IFNγ and TNFα) upon co-culture with the CMV pp65 peptide-pulsed T2 cells in comparison to a co-culture without any TCR construct. This effect was likewise dependent on TCR concentration, TCR affinity and peptide concentration. In the TCR titration, saturation was reached around 6 nM for the low- and high-affinity variant and this concentration therefore was used for the following experiments. In case of the high-affinity TCR construct the

EC_{50} values ranged from 2-8 pM and were around 10-50 times lower than that of the low-affinity variant. A similar difference was observed in the peptide titration. In both experiments, no dose-dependent increase was observed for the co-culture of survivin peptide-pulsed T2 cells in presence of TCR-Fc^{enh} as well as the co-culture of CMV pp65 peptide-pulsed T2 cells in the presence of TCR-Fc^{aglyc}, demonstrating that the effects were target-specific and NK cell-dependent. Since NK cells showed a strong baseline expression of CD69 in co-cultures without TCR constructs (Figure 11, Figure 12), the following experiments only show the median fluorescence intensity (MFI) for better visualization. The ADCC-mediating monoclonal antibody Rituximab binding to CD20 molecules that are abundantly expressed on T2 cells was used for comparison. Rituximab is a chimeric human IgG1 antibody.

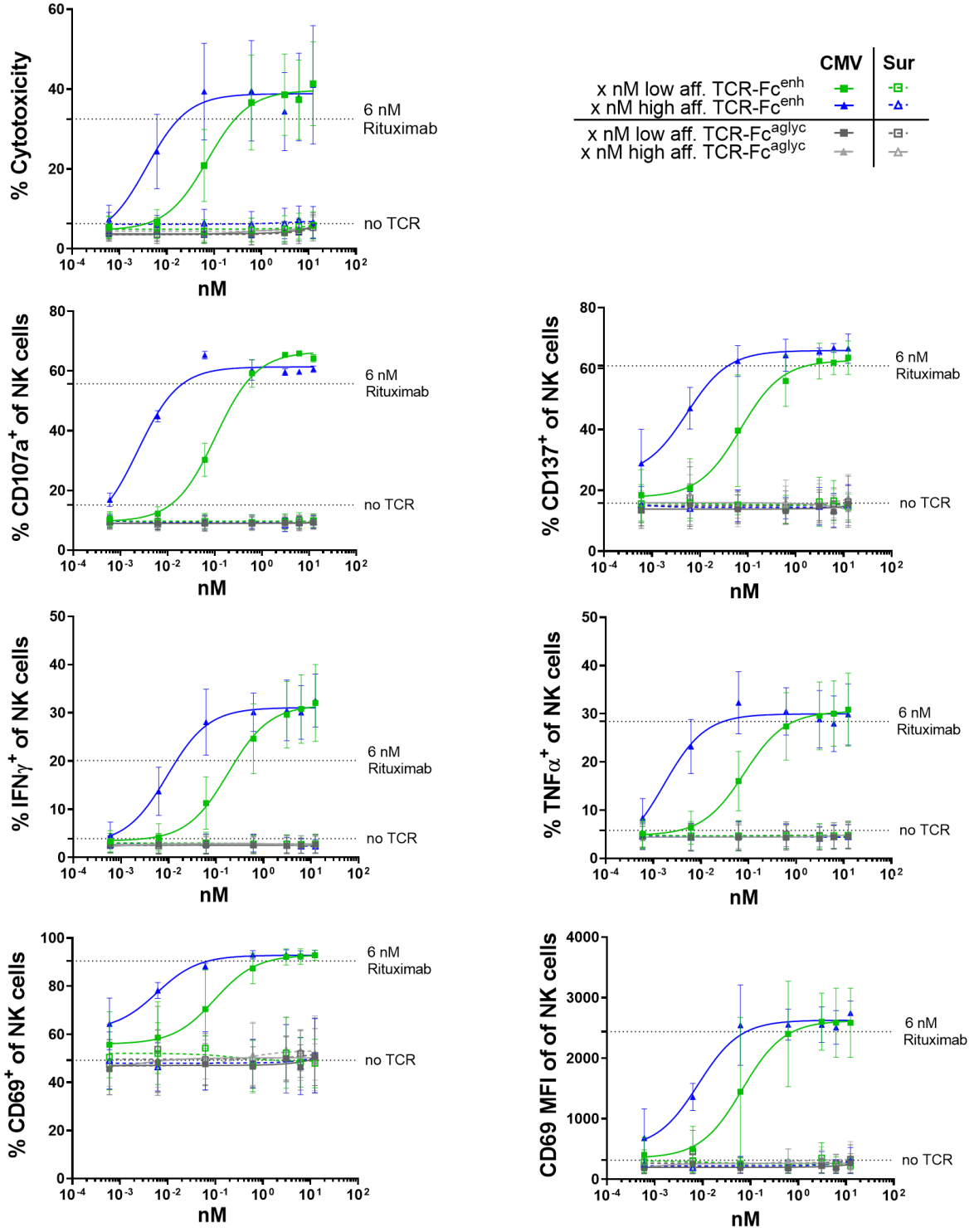

EC_{50} (nM)	Cytotoxicity	CD107a	CD137	IFNγ	TNFα	CD69 (%)	CD69 (MFI)
Low aff. TCR-Fc^{enh}	0.072	0.104	0.071	0.181	0.081	0.098	0.067
High aff. TCR-Fc^{enh}	0.004	0.002	0.005	0.009	0.002	0.006	0.008

Figure 12: Titration of the CMV pp65-specific TCR-Fc constructs in co-cultures of NK cells with peptide-pulsed T2 cells
100 µM CMV pp65 (CMV – solid line)/ survivin (Sur – dashed line) peptide-pulsed HLA-A*02:01$^+$ T2 cells were co-cultured with NK cells in presence of CMV pp65-specific TCR-Fc fusion proteins including proteins bearing an Fc part with enhanced FcγRIII binding (Fc^{enh}) and control constructs bearing an aglycan Fc (Fc^{aglyc}) incapable of FcγR binding. Concentration of the TCR-Fc proteins was titrated. 6 nM

Rituximab or a co-culture without TCR were included for comparison and are indicated with a dotted line. Cytotoxicity was evaluated following 4 h co-culture using an LDH release assay. NK cell degranulation and activation were analyzed using flow cytometry by staining for CD107a, CD69, CD137, and intracellular IFNγ or TNFα. Expression of CD69 and CD137 was analyzed following 24 h co-culture. CD107a, IFNγ and TNFα was analyzed after 4 h co-culture in presence of Golgi transport inhibitors. Cytotoxicity, CD107, IFNγ, TNFα, n=3. CD69, CD137, n=2. Mean values ± s.e.m. are shown. Computed EC_{50} values for the co-culture with CMV pp65 peptide-pulsed T2 cells are given in the table below.

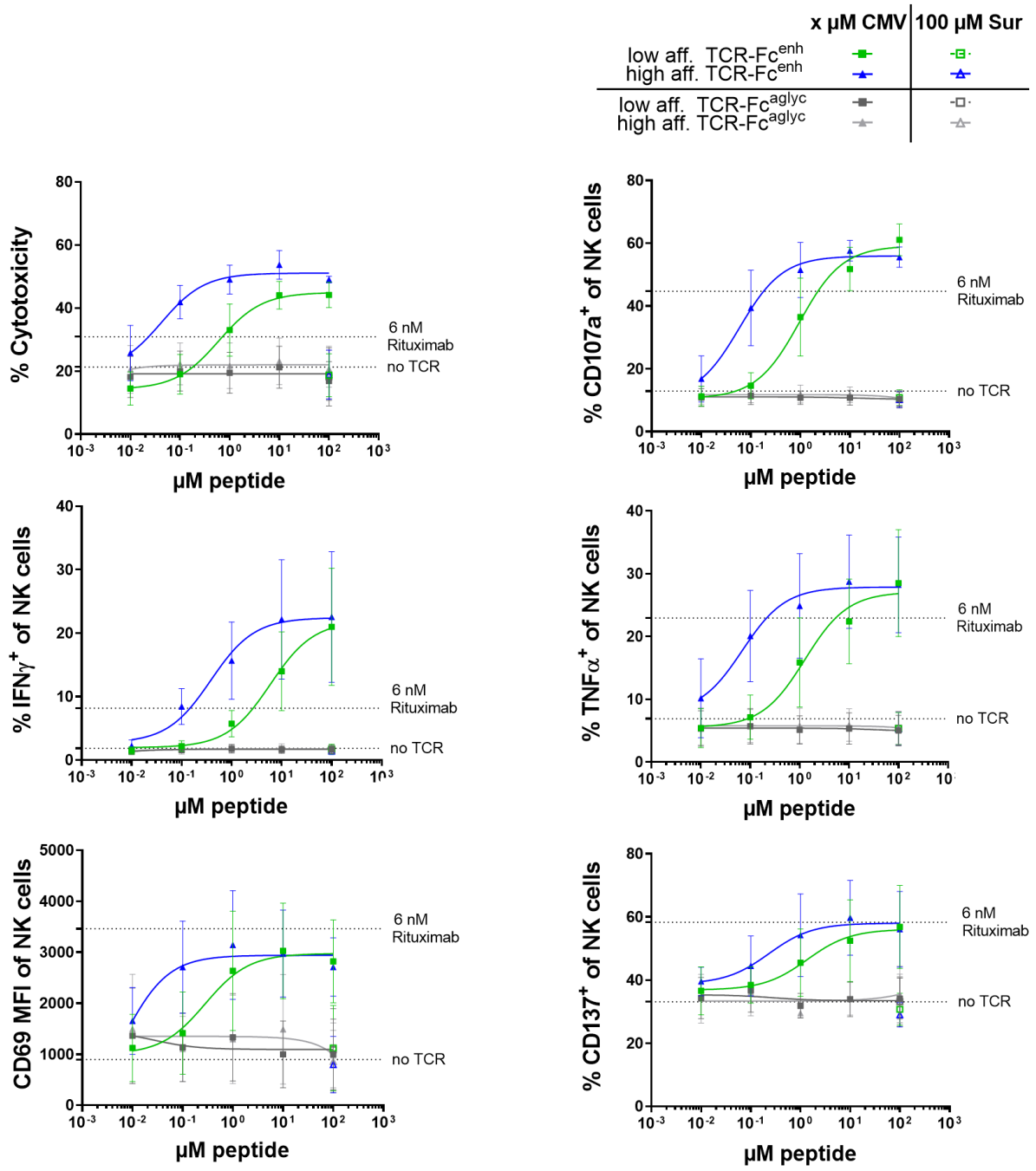

EC_{50} (µM)	Cytotoxicity	CD107a	CD137	IFNγ	TNFα	CD69
Low aff. TCR-Fc^{enh}	0.604	0.957	1.362	5.929	1.269	0.280
High aff. TCR-Fc^{enh}	0.042	0.059	0.232	0.382	0.069	0.007

Figure 13: Titration of peptide concentration in co-cultures of peptide-pulsed T2 cells with NK cells in presence of CMV pp65-specific TCR-Fc constructs

CMV pp65 (CMV)/ survivin (Sur) peptide-pulsed HLA-A*02:01$^+$ T2 cells were co-cultured with NK cells in presence of 6 nM TCR-Fc fusion proteins including those bearing an Fc part with enhanced FcγRIII binding (Fc^{enh}) and the control constructs bearing an aglycan Fc (Fc^{aglyc}) incapable of FcγR binding. The peptide concentration was titrated. The dotted lines indicate co-culture with 6 nM Rituximab or without TCR. Target cell lysis was analyzed using an LDH release assay following 4 h co-culture. NK cell degranulation and activation were analyzed using flow cytometry by staining for CD107a, CD69, CD137, and intracellular IFNγ or TNFα. CD107a, IFNγ and TNFα were analyzed after 4 h co-culture in presence of Golgi transport inhibitors. CD69 and CD137 were stained following 24 h co-culture and CD69 expression is shown in percentage and median fluorescence intensity (MFI), mean values ± s.e.m. from n=3 independent experiments. The computed EC_{50} values for the co-culture with CMV pp65 peptide-pulsed T2 cells are given in the table below.

Following the preliminary evaluation using peptide-pulsed TAP-deficient HLA-A*02:01$^+$ T2 cells, a co-culture was setup with T2 cells in comparison to the TAP$^+$ HLA-A*02:01 breast cancer cell line MCF-7 as a more relevant target cell (Figure 14). Upon peptide pulse, MCF-7 showed a strongly reduced peptide presentation compared to the TAP-deficient T2 cells as demonstrated using flow cytometry by staining with the soluble high-affinity CMV pp65-specific TCR-Fc fusion protein and a fluorophore-conjugated secondary human Fc-specific antibody (Figure 14A). Notably, MCF-7 are characterized by a lower HLA-A2 expression as evaluated using a fluorophore-conjugated HLA-A2 specific antibody (BB7.2) (Figure 14B). To compare NK cell redirection using peptide-pulsed MCF-7 and T2 cells a co-culture was set up (Figure 14C). The high-affinity CMV pp65-specific TCR-Fc^{enh} construct resulted in comparable NK cell-mediated cytotoxicity, NK cell degranulation (CD107a) and NK cell activation (IFNγ, TNFα, CD69, CD137) for T2 cells and MCF-7. The low-affinity variant however induced only little response to peptide-pulsed MCF-7 in contrast to peptide-pulsed T2 cells, for which the response was similar for the high- and low-affinity constructs, further indicating that TCR affinity is an important factor for soluble TCR-based NK cell redirection when using tumor targets with low antigen density. The weak staining of MCF-7 cells with the high-affinity TCR-Fc^{enh} construct also suggests that exogenous peptide exchange is less efficient in these TAP/tapasin proficient cells. Even though T2 and MCF-7 cells might also express different levels of activating and inhibitory NK cell ligands, which could have contributed to the difference.

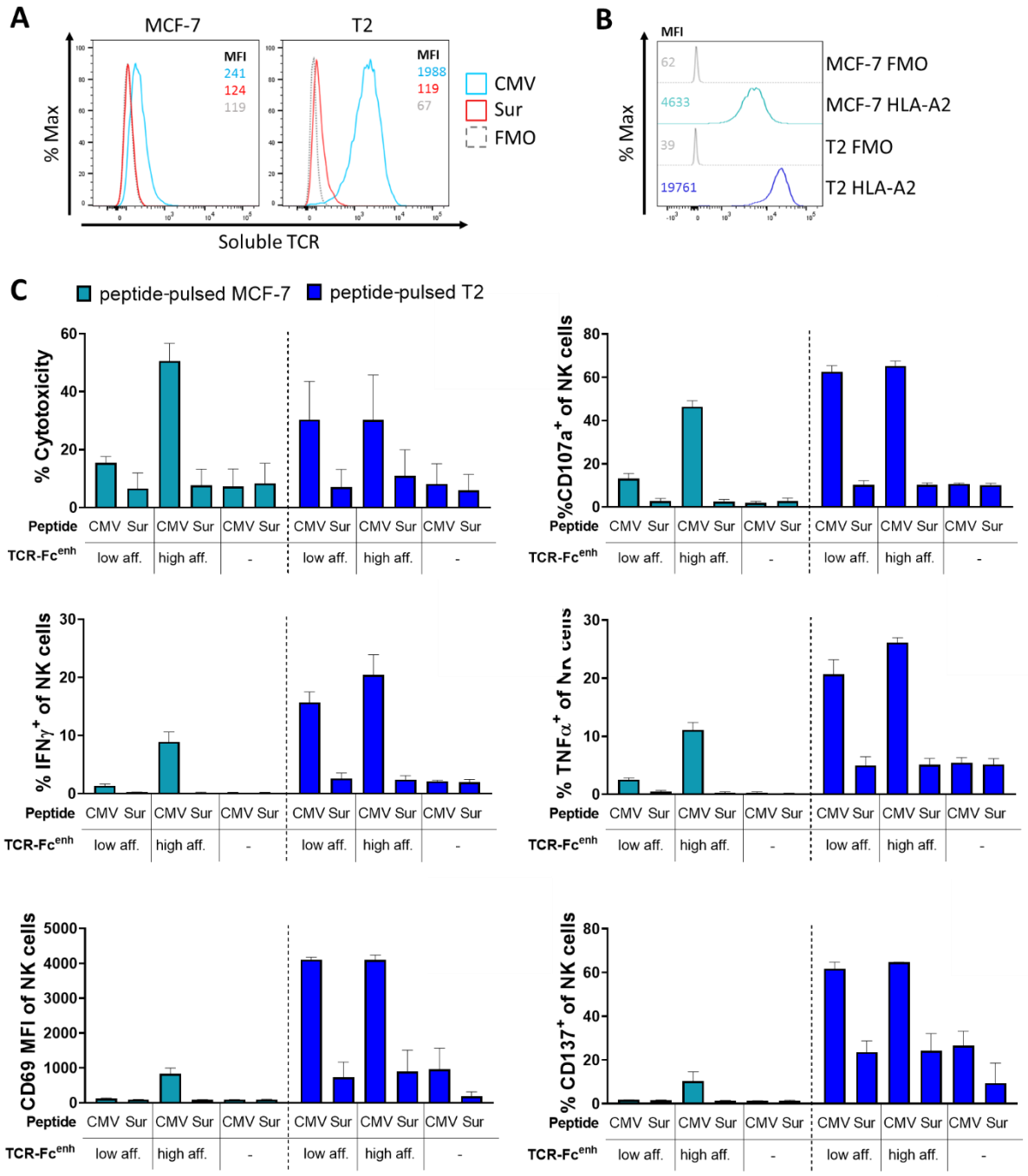

Figure 14: Comparison of peptide-pulsed T2 cells and MCF-7 as target cells for co-culture with NK cells in presence of the CMV-specific TCR-Fc^{enh} construct

A) Peptide presentation following peptide pulse of T2 and MCF-7 cells [100 µM] was analyzed using flow cytometry by staining with the CMV pp65-specific high-affinity TCR-Fc construct and a secondary fluorophore-conjugated human Fc-specific antibody for detection. B) Expression of HLA-A2 was analyzed by flow cytometry using the fluorophore-conjugated antibody BB7.2. C) Co-culture of 100 µM CMV pp65 (CMV) / survivin (Sur) peptide pulsed HLA-A*02:01$^+$ MCF-7 and T2 with NK cells in presence of the TCR-Fc constructs bearing an Fc part with enhanced FcγRIII binding (Fc^{enh}). An LDH release assay was performed to evaluate target-directed cytotoxicity following 4 h co-culture. NK cell degranulation and activation were analyzed using flow cytometry by staining for CD107a, CD69, CD137, intracellular IFNγ and TNFα. CD107a, IFNγ and TNFα were analyzed after 4 h co-culture in presence of golgi transport inhibitors. CD69 and CD137 were analyzed following 24 h co-culture. Mean values ± s.e.m. from n=3 (cytotoxicity) or n=2 (CD107, CD69, CD137, IFNγ, TNFα) are shown.

To evaluate the different NK cell-targeting TCR-scFv-Fc constructs in comparison to the TCR-Fc format, NK cell binding was analyzed by staining of NK cells using the soluble high-affinity TCR constructs and a fluorophore-conjugated CMV pp65 peptide-tethered MHC multimer for detection (Figure 15A, 2.2.4). These streptavidin-based multimers are generated using biotinylated pMHC-SCT monomers, which can be released from the previously used pMHC-Fc fusion proteins using a thrombin site between HLA allele and Fc part (2.2.1.2). TCR-Fc^{aglyc} was included as a negative control and expression of CD16 and NKp46 was confirmed using commercial fluorophore-conjugated antibodies. Strongest NK cell binding was detected for the TCR-Fc^{enh} and TCR-scFv-Fc^{enh} constructs rather independent of any included scFvs. The TCR-scFv-Fc^{aglyc} were characterized by a lower binding. To evaluate the different formats considering NK cell redirection, a co-culture with peptide-pulsed MCF-7 was set up (Figure 15B) because they offer a higher resolution between weaker and stronger TCR constructs compared to peptide-pulsed T2 cells as shown above for the low and high-affinity TCR-Fc^{enh} constructs (Figure 14C). The strongest response considering NK cell-mediated target cell lysis, NK cell degranulation (CD107a) and NK cell activation (IFNγ, TNFα, CD69) was observed for the high-affinity TCR-scFv-Fc^{enh} fusion proteins, which in contrast to the NK cell binding, was even increased compared to the high-affinity TCR-Fc^{enh} format and greater than that of the monoclonal antibody targeting EGFR (cetuximab). EGFR is strongly expressed on MCF-7 cells (Warwas et al., 2021). In accordance with the NK cell binding data, the high-affinity TCR-scFv-Fc^{aglyc} constructs induced little to no response compared to the co-culture without TCR. Except for TCRβ-αCD16-Fc^{enh}, no response was observed towards survivin peptide-pulsed MCF-7, demonstrating that the mediated response remained largely CMV/A*02:01 target-specific. TCRβ-αCD16-Fc^{enh} induced a moderate and significant increase in NK cell degranulation and activation but not in target cell lysis upon co-culture with survivin peptide-pulsed MCF-7.

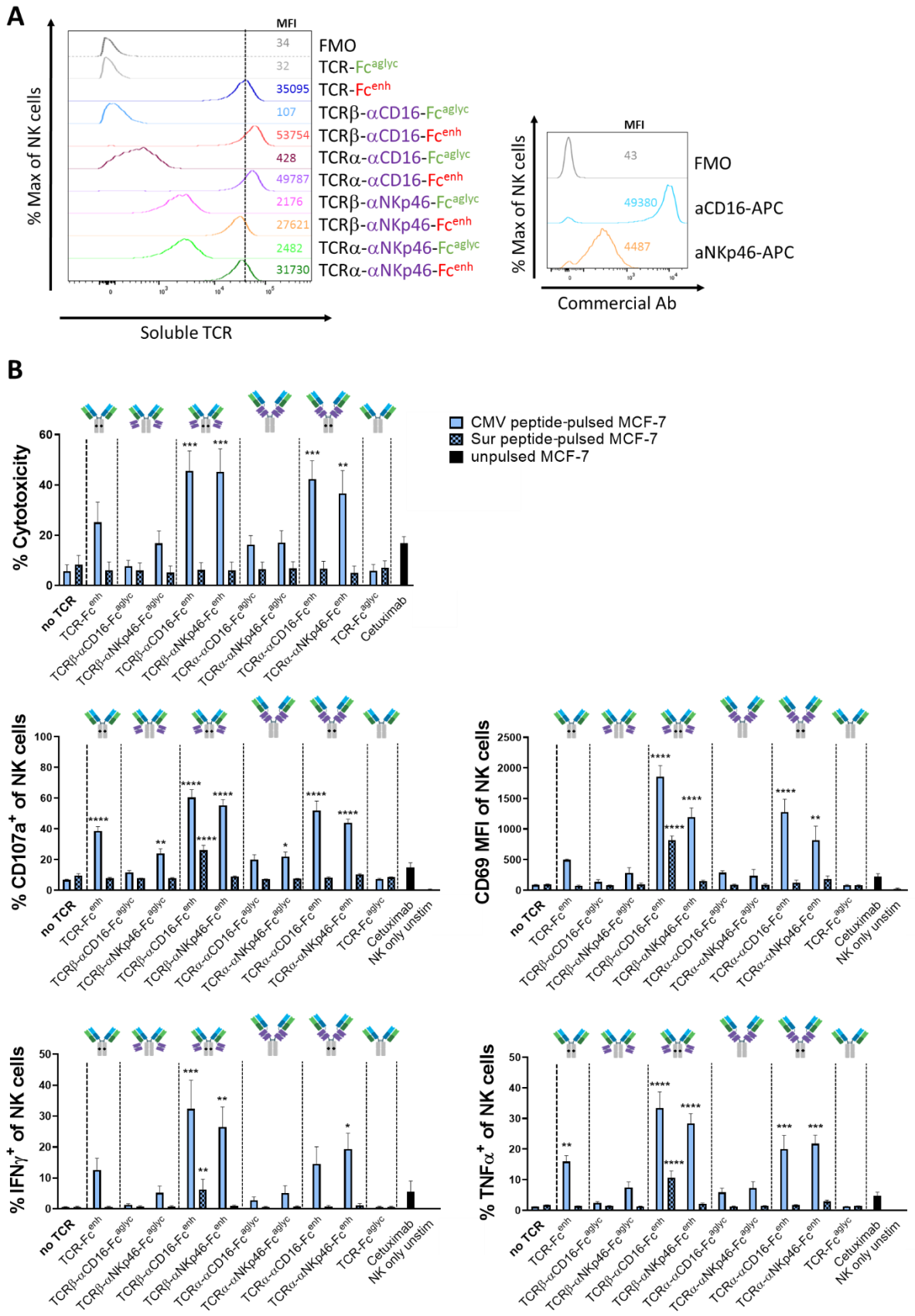

Figure 15: Comparison of different CMV pp65-specific high-affinity TCR-Fc and TCR-scFv-Fc constructs for NK cell redirection

A) NK cell binding was analyzed by flow cytometry using 30 nM TCR-Fc/ TCR-scFv-Fc (left). Expression of CD16 and NKp46 was confirmed using commercial fluorochrome-labeled antibodies (right). B) 100

µM CMV pp65 (CMV)/ survivin (Sur) peptide-pulsed HLA-A*02:01$^+$ MCF-7 were co-cultured with NK cells in presence of 6 nM high-affinity TCR-Fc and TCR-scFv-Fc fusion proteins bearing an Fc part with enhanced FcγRIII binding (Fc^{enh}) or bearing an aglycan Fc (Fc^{aglyc}) incapable of FcγR binding. 6 nM Cetuximab was applied for comparison of NK cell-mediated ADCC. Cytotoxicity was analyzed using an LDH release assay following 4 h co-culture. NK cell degranulation and activation were analyzed using flow cytometry by staining for CD107a, CD69, intracellular IFNγ and TNFα. CD107a, IFNγ and TNFα were evaluated following 4 h co-culture in presence of Golgi transport inhibitors. CD69 was analyzed following 24 h co-culture without further supplements. Mean values ± s.e.m. are shown. Significance compared to "no TCR" was evaluated using OneWay ANOVA for the CMV pp65 and survivin peptide-pulsed data groups separately followed by Dunnett's multiple comparison test. Cytotoxicity n=3; CD107, CD69, IFNγ, TNFα, n=3 independent experiments.

To evaluate the sensitivity of the different TCR-scFv-Fc^{enh} and the TCR-Fc^{enh} constructs in more detail, a co-culture with CMV pp65 peptide-pulsed MCF-7 was set up in which the concentration of TCR construct (Figure 16) or peptide used for the peptide pulse (Figure 17) were titrated. Upon TCR construct titration (Figure 16), the highest sensitivity considering NK cell-mediated cytotoxicity, NK cell degranulation (CD107a) and NK cell activation (IFNγ, TNFα, CD69) was observed for the two TCR-αNKp46-Fc^{enh} constructs. Thus, the EC_{50} values ranged from 9-23 pM and were about 10-60 times lower than those of the TCR-Fc^{enh} construct without an additional scFv. The induced response using 6 nM compound was comparable to that induced by equimolar concentrations of monoclonal antibody trastuzumab targeting HER2, which is strongly expressed in MCF-7, and no or only very little response was observed towards survivin peptide-pulsed MCF-7. As reported above (Fig. 15), TCRβ-αCD16-Fc^{enh} resulted in unspecific NK cell activation and degranulation without inducing unspecific target cell lysis. Upon peptide titration (Figure 17), fewer differences were observed between the constructs, with TCR-Fc^{enh} and TCRβ-αNKp46-Fc^{enh} showing slightly lower target cell lysis compared to the other TCR-scFv-Fc^{enh} constructs as also indicated by higher EC_{50} values. NK cell activation and degranulation was rather equal among TCRα-αCD16-Fc^{enh}, TCRα-αNKp46-Fc^{enh}, and TCRβ-αNKp46-Fc^{enh}. Consistent with previous results, TCRβ-αCD16-Fc^{enh} induced a quite strong NK cell activation and NK cell degranulation upon co-culture with survivin peptide-pulsed MCF-7 and also when decreasing the CMV pp65 peptide-concentration to very low concentrations (10^{-2} µM) not mediating any response using other TCR constructs.

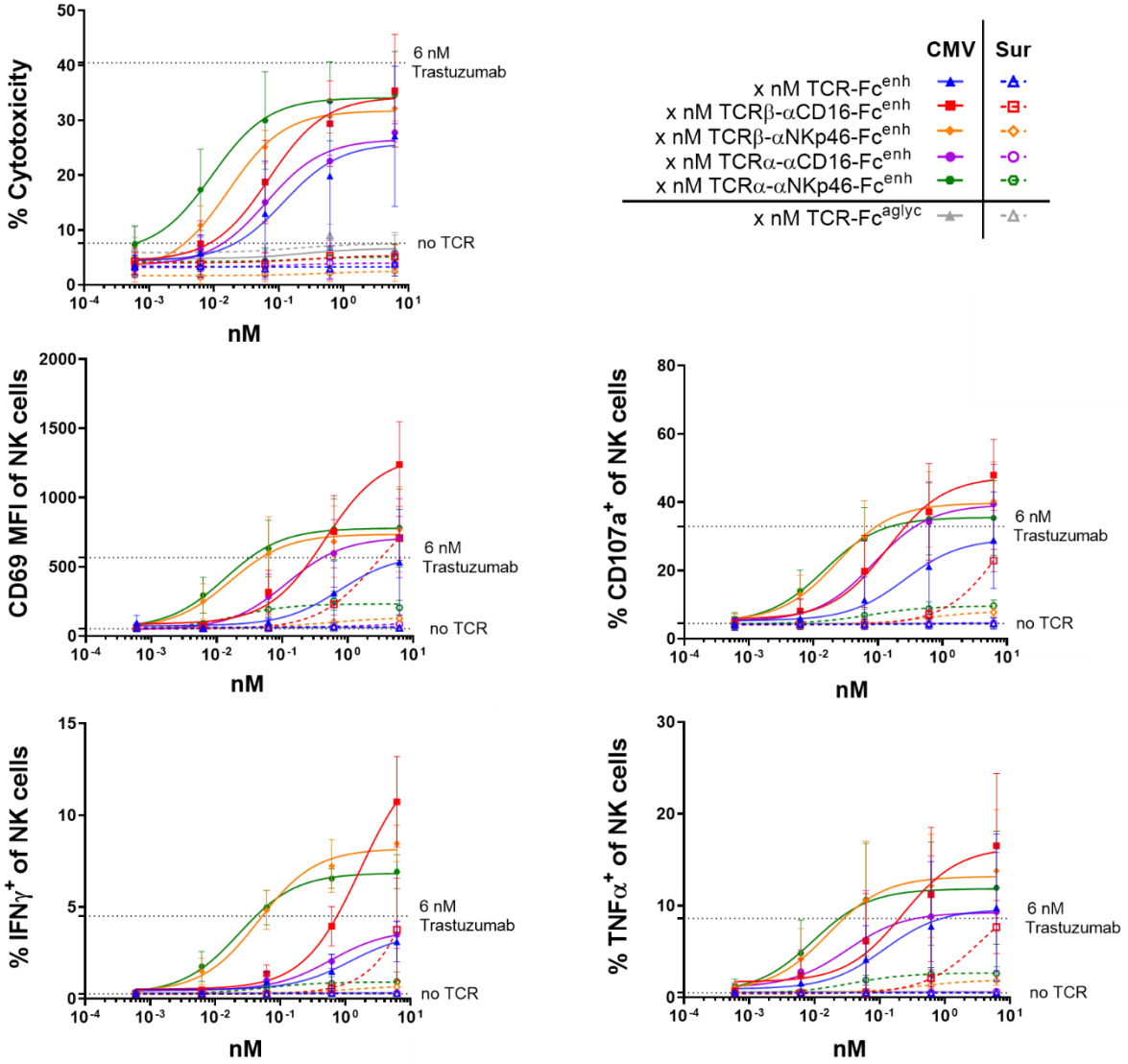

EC_{50} (nM)	Cytotoxicity	CD107a	IFNγ	TNFα	CD69
TCR-Fc^{enh}	0.119	0.258	1.188	0.119	0.750
TCRβ-αCD16-Fc^{enh}	0.071	0.143	1.673	0.224	0.452
TCRβ-αNKp46-Fc^{enh}	0.017	0.023	0.047	0.016	0.016
TCRα-αCD16-Fc^{enh}	0.064	0.086	0.597	0.032	0.116
TCRα-αNKp46-Fc^{enh}	0.009	0.015	0.023	0.010	0.013

Figure 16: Titration of the high-affinity CMV pp65-specific TCR-scFv-Fc^{enh} and TCR-Fc^{enh} constructs upon co-culture with peptide-pulsed MCF-7 and NK cells
100 µM CMV pp65 (CMV – solid line)/ survivin (Sur – dashed line) peptide-pulsed HLA-A*02:01$^+$ MCF-7 were co-cultured with NK cells in presence of high-affinity TCR-Fc^{enh} and different TCR-scFv-Fc^{enh} constructs. The high-affinity CMV pp65-specific TCR-Fc^{aglyc} was included as a negative control incapable of NK cell binding. The concentrations of the soluble TCR constructs were titrated. 6 nM Trastuzumab was applied for comparison. An LDH release assay was performed to analyze cytotoxicity following 4 h co-culture. NK cell degranulation and activation were analyzed using flow cytometry by staining for CD107a, CD69, intracellular IFNγ and TNFα. CD107a, IFNγ and TNFα were evaluated after 4 h co-culture in presence of Golgi transport inhibitors. CD69 was stained following 24 h co-culture. Mean values ± s.e.m. from n=3 independent experiments are shown. EC_{50} values for the co-culture with CMV pp65 peptide-pulsed MCF-7 are listed in the table below.

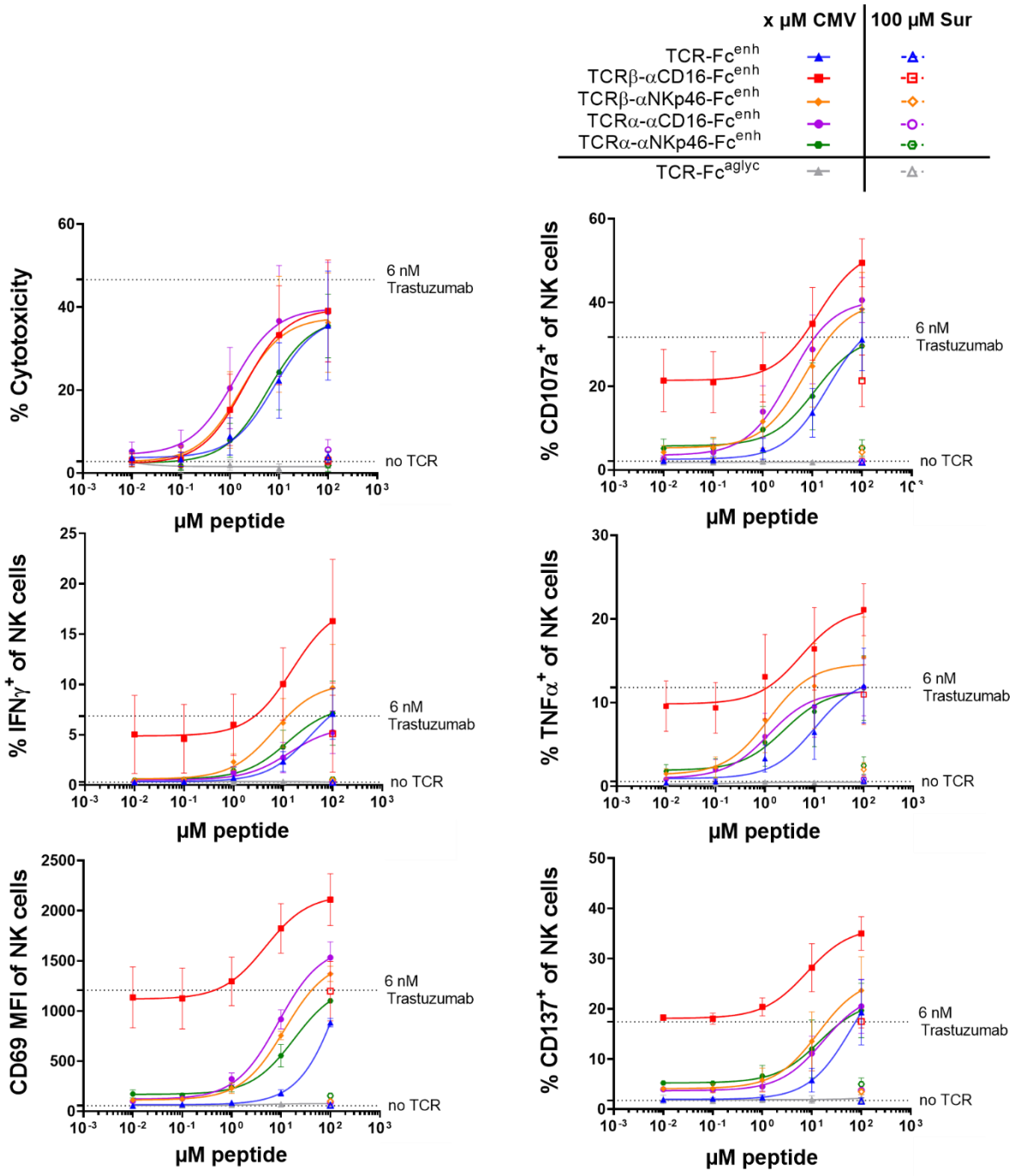

EC_{50} (µM)	Cytotoxicity	CD107a	IFNγ	TNFα	CD69	CD137
TCR-Fc^{enh}	7.880	20.43	35.50	10.25	199.3	64.40
TCRβ-αCD16-Fc^{enh}	1.953	13.03	15.15	5.379	4.824	7.846
TCRβ-αNKp46-Fc^{enh}	1.699	7.118	6.537	1.194	11.76	13.39
TCRα-αCD16-Fc^{enh}	1.189	3.552	13.19	1.190	8.765	16.74
TCRα-αNKp46-Fc^{enh}	5.879	11.27	12.32	2.437	18.36	14.20

Figure 17: Titration of peptide concentration upon co-culture of NK cells with peptide-pulsed MCF-7 in presence of the high-affinity CMV pp65-specific TCR-Fc^{enh} and TCR-scFv-Fc^{enh} constructs

CMV pp65 (CMV)/ survivin (Sur) peptide pulsed HLA-A*02:01^{+} MCF-7 were co-cultured with NK cells in presence of different TCR-Fc and TCR-scFv-Fc constructs bearing an Fc part with enhanced FcγRIII binding (Fc^{enh}) and the negative control construct bearing an aglycan Fc (Fc^{aglyc}) incapable of FcγR binding. CMV pp65 peptide concentration was titrated. 100 µM Survivin peptide were included as a

control. 6 nM Trastuzumab was applied for comparison. An LDH release assay was performed to evaluate target cell lysis following 4 h co-culture. NK cell degranulation and activation were analyzed using flow cytometry by staining for CD107a, CD69, CD137, intracellular IFNγ and TNFα. CD107a, IFNγ and TNFα were evaluated following 4 h co-culture in presence of golgi transport inhibitors. CD69 was analyzed after 24 h co-culture. Mean values from 3 independent experiments ± s.e.m. are shown.

To analyze the NK cell-targeting constructs under conditions approaching the *in vivo* situation, a tumor spheroid model was used as this mimics a solid tumor more closely than a two-dimensional monolayer. However, the peptide-pulse was not applicable to the three-dimensional culture model. To this end, an MCF-7 cell line was stably transfected with a transmembrane CMV pp65 or survivin peptide-tethered MHC single chain trimer (mSCT/ pMHC-mSCT) (Figure 18) (2.2.6.1). This construct comprises the peptide MHC-ligand linked to the β2-microglobulin followed by an AviTag for site-specific biotinylation and a HLA-A*02:01 allele including the transmembrane domain (Figure 18A). To strengthen peptide binding in the MHC-I peptide binding groove a so-called disulfide trap was included, which generates a disulfide bridge between an artificially introduced cysteine (Y84C) in the HLA allele and a cysteine included in the serine glycine linker C-terminal of the peptide (2nd aa, 2.2.6.1). To ensure mSCT biotinylation an ER-retained, KDEL-tagged BirA ligase was included in the same open reading frame connected via a T2A sequence, which induces ribosomal skipping upon translation as used for the soluble TCR constructs. The cells were furthermore previously stably transfected with CD80 to gain better co-stimulation especially for later experiments using T cells. To select for the clones that stably integrated the transfected DNA, the cells were cultured under antibiotic selection pressure for two weeks. Required antibiotic concentration was determined using untransfected cells beforehand. CD80 and mSCT expression was confirmed by staining with a commercial fluorophore-conjugated CD80 antibody and a fluorophore-conjugated streptavidin, which binds to the biotinylated mSCTs (Figure 18B). Unfortunately, no co-expression was observed and only single positive cells were generated. Furthermore, the stably transfected cell line also contained a CD80$^-$mSCT$^-$ double negative population. The peptide presentation of the CMV pp65 peptide-tethered mSCT$^+$ MCF-7 was then compared to that of CMV pp65 peptide-pulsed MCF-7 by staining with the soluble high-affinity CMV pp65-specific TCR-Fc construct and a secondary fluorophore-conjugated human Fc-specific antibody, demonstrating that the mSCT$^+$ expressing cells seem to result in a stronger peptide presentation (Figure 18C). However this was not the case for all cells as a negative population was observed, which is in agreement with the previously analyzed mSCT expression. Upon a direct comparison of peptide-pulsed and pMHC-transfected cells in the co-culture with NK cells (Figure 18D), the low- and high-affinity TCR-Fc^{enh} construct could induce comparable cytotoxicity, NK cell degranulation (CD107a) and NK cell activation (IFNγ, TNFα, CD69, CD137), while the low-affinity TCR-Fc^{enh} construct induced only little response towards peptide-pulsed MCF-7 as observed before (Figure 14).

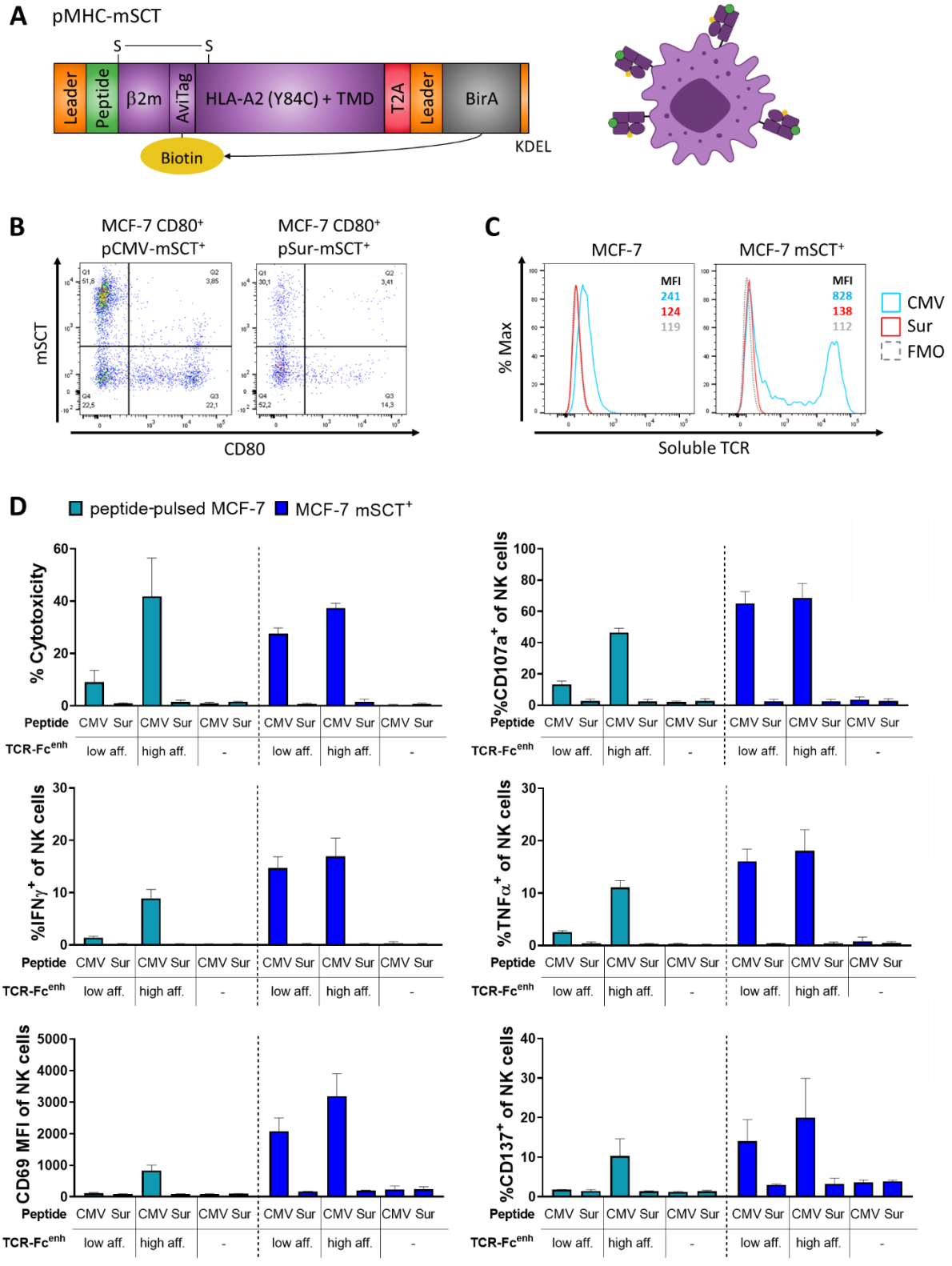

Figure 18: Comparison of stably pMHC-SCT transfected and peptide-pulsed MCF-7 as target cells for co-culture with NK cells in the presence of the CMV pp65-specific TCR-Fc^{enh} constructs
A) Molecular design of biotinylated transmembrane peptide-tethered MHC single chain trimers. B) Staining of MCF-7 stably transfected with CD80 and CMV pp65 (CMV) /survivin (Sur) peptide-tethered MHC-SCT with an fluorophore-conjugated αCD80 antibody and fluorophore-conjugated Streptavidin C) Evaluation of peptide presentation by staining with the high-affinity CMV pp65-specific TCR-Fc and a fluorophore-conjugated secondary human Fc-specific antibody for detection. D) Co-culture of CMV pp65/ survivin peptide-pulsed [100 µM] and pMHC-SCT transfected HLA-A*02:01+ MCF-7 with NK cells

in presence of the low- and high-affinity CMV pp65-specific TCR-Fc bearing an Fc part with enhanced FcγRIII binding (Fc^{enh}). Target cell lysis was evaluated following 4 h co-culture using an LDH release assay. NK cell degranulation and activation were analyzed using flow cytometry by staining for CD107a, CD69, CD137, intracellular IFNg and TNFa. Expression of CD69 and CD137 was analyzed following 24 h co-culture. CD107a, IFNg and TNFa was analyzed after 4 h co-culture in presence of Golgi transport inhibitors. Mean values ± s.e.m. are shown. Cytotoxicity n=3; CD107, CD69, CD137, IFNγ, TNFα, n=2

Since the pMHC-mSCT transfected MCF-7 were proven to be suitable as target cells for CMV pp65-specific TCR-Fc fusion proteins, they were finally used to generate tumor spheroids (2.2.7.5). For the co-culture with tumor spheroids the incubation time was extended to 24 h since no effect was observed following 4 h co-culture as done for the two-dimensional co-culture (data not shown). Upon co-culture of tumor spheroids with NK cells, the CMV pp65-specific TCR-Fc^{enh}, TCRα-αNKp46-Fc^{enh} and TCRβ-αNKp46-Fc^{enh} fusion proteins induced significant levels of target-specific NK cell-mediated target cell lysis, NK cell degranulation and NK cell activation (Figure 19). Interestingly, in contrast to the two-dimensional co-culture experiments, only little response was observed with regard to IFNγ production. Also the cytotoxicity measured was lower than observed in the two-dimensional co-culture, indicating a slightly weaker NK cell activation in the 3D co-culture model.

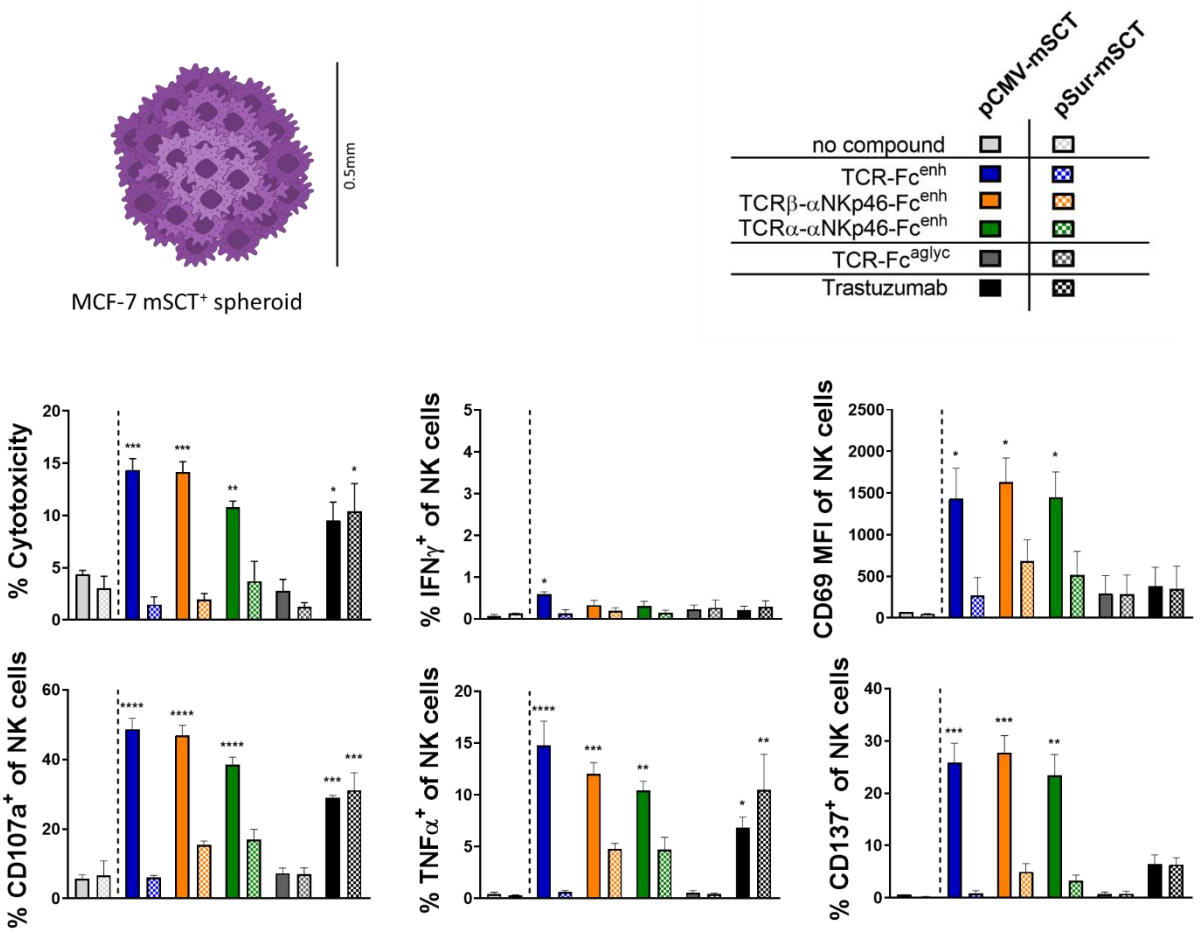

Figure 19: NK co-culture with pMHC-mSCT transfected MCF-7 spheroids in the presence of CMV pp65-specific TCR-Fc^{enh} and TCR-scFv-Fc^{enh} constructs
NK cells were co-cultured for 24 h with tumor cell spheroids generated from MCF-7 stably transfected with CMV pp65 (CMV)/ survivin (Sur) pMHC-mSCT in presence of different TCR-Fc^{enh} and TCR-scFv-Fc^{enh} constructs (6 nM). TCR-Fc^{aglyc} was included as a negative control incapable of FcγR binding and trastuzumab were applied for comparison of ADCC. Target cell lysis was evaluated following 24 h co-culture using an LDH release assay. NK cell degranulation and activation were analyzed after 24 h using flow cytometry by staining for CD107a, CD69, CD137, and intracellular IFNγ or TNFα. CD107a, IFNγ and TNFα were analyzed following co-culture in presence of Golgi transport inhibitors. Significance compared to the co-culture without TCR was analyzed by OneWay ANOVA tests for the CMV and survivin groups separately followed by Dunnet's multiple comparison test. Mean values ± s.e.m. from 3 independent experiments are shown.

3.2.3 T cell redirection

To evaluate the different T cell-targeting constructs, T cell binding was analyzed (Figure 20) (2.2.4). To this end, purified CD3$^+$ T cells were stained with the soluble TCR-αCD3-Fc fusion proteins and a secondary fluorophore-conjugated human Fc-specific antibody. The TCR-Fc^{aglyc} was included as a negative control and CD3 expression was confirmed using a commercial fluorophore-conjugated αCD3 antibody (clone HIT3a). The strongest binding of CD4$^+$ and CD8$^+$ T cells was observed for TCRα-αCD3(OKT3$_{HGL}$)-Fc^{aglyc}. Since NK cell redirection of the NK cell-targeting constructs was also shown to correlate with NK cell binding (Figure 15), this construct was chosen for further evaluation considering T cell redirection.

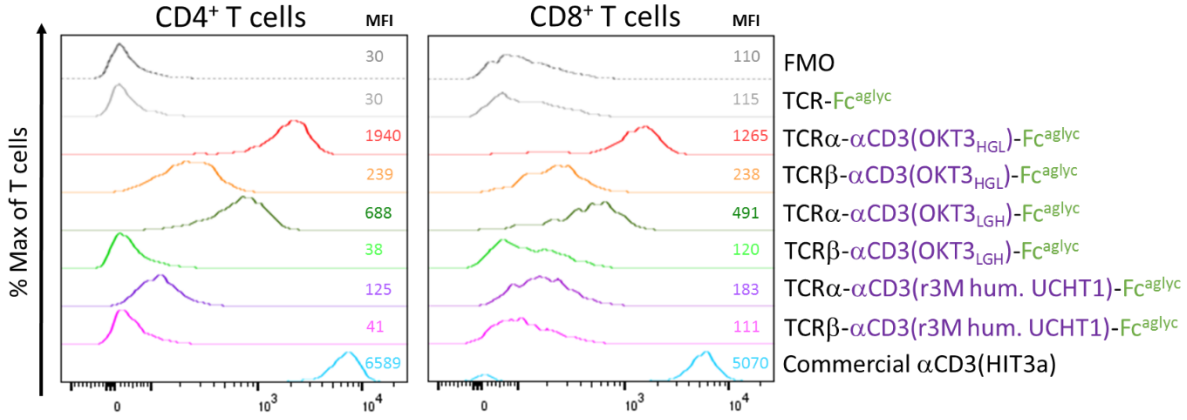

Figure 20: T cell binding of different TCR-αCD3-Fc^{aglyc} constructs
T cell binding of different TCR-αCD3-Fc^{aglyc} constructs was evaluated by staining with the 6 nM soluble TCR construct and a fluorophore-conjugated secondary human Fc-specific antibody. TCR-Fc^{aglyc} was included as a negative control and a commercial fluorophore-conjugated αCD3 (clone HIT3a) antibody as a positive control.

To evaluate the T cell redirection mediated by TCRα-αCD3(OKT3$_{HGL}$)-Fc^{aglyc}, a co-culture of peptide-pulsed TAP-deficient HLA-A*02:01$^+$ T2 cells with T cells was set up (Figure 21). After 24 h of co-culture, target cell lysis, T cell degranulation and T cell activation were analyzed (2.2.7). Target cell lysis was again evaluated using an LDH release assay and T cell degranulation using flow cytometry by staining for the degranulation marker CD107a following

co-culture in presence of Golgi transport inhibitors. T cell activation was assessed by the detection of intracellular IFNγ and TNFα following co-culture in presence of Golgi transport inhibitors and also by cell surface staining of CD25, CD69, CD134 (OX40) and CD137 (4-1BB) activation markers. Additionally, T cell proliferation was evaluated after 5 days of co-culture using CTV (CellTrace Violet)-labeled T cells. In contrast to 100 µM survivin peptide-pulsed T2 cells, the co-culture of 100 µM CMV pp65 peptide-pulsed T2 cells was characterized by increased T cell degranulation, T cell proliferation as observed by diluting CTV signals and increased T cell activation in presence of the high-affinity TCRα-αCD3($OKT3_{HGL}$)-Fc^{aglyc}. This was observed for $CD4^+$ and $CD8^+$ T cells rather equally. However, CD134 was more prominent for $CD4^+$ T cells, which is why following data only show CD134 results obtained for $CD4^+$ T cells but not for $CD8^+$ T cells. The same accounts for CD137, CD107a and IFNγ, which were more prominent in $CD8^+$ T cells and are thus not shown for the $CD4^+$ T cells in the following experiments.

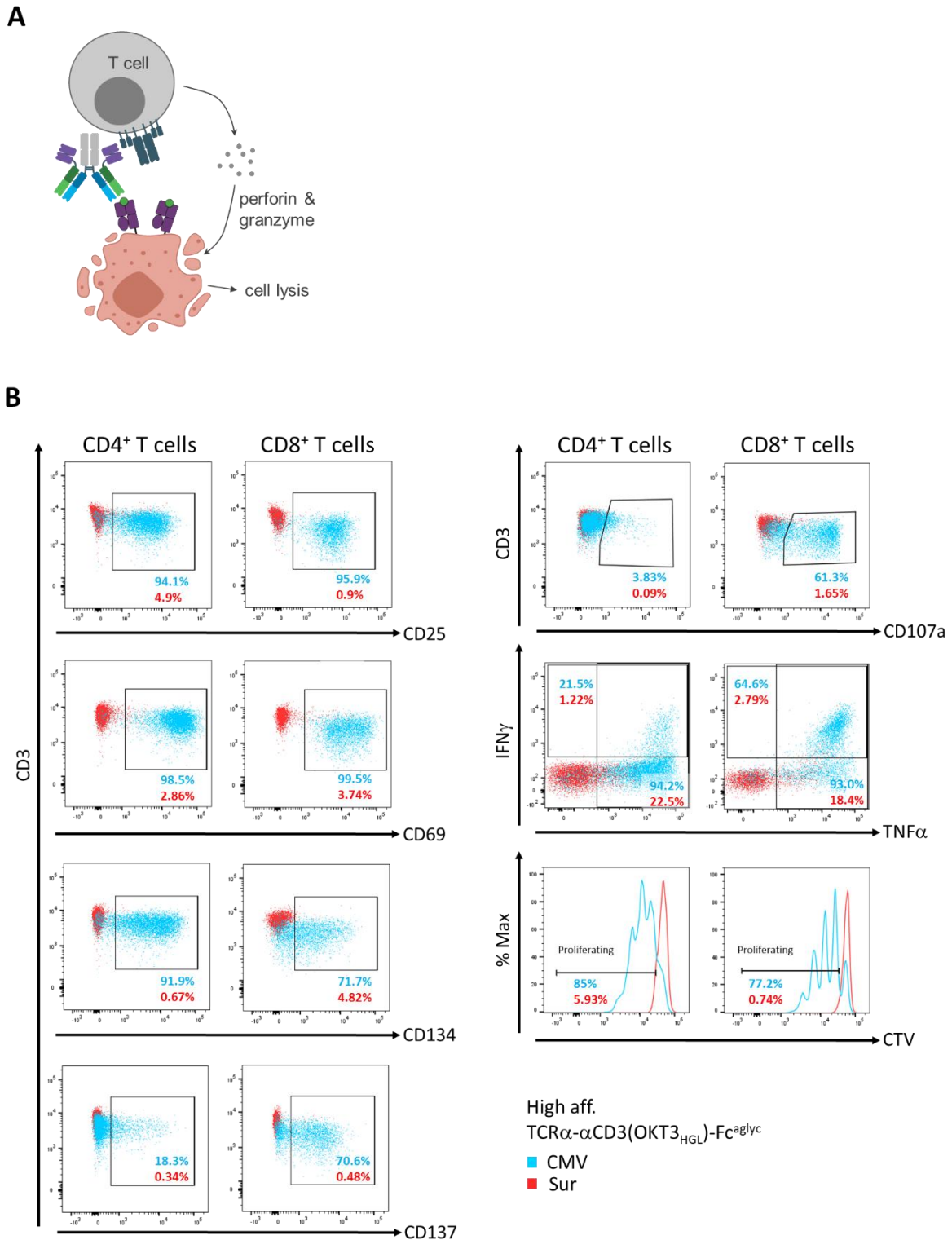

Figure 21: T cell activation upon co-culture with peptide-pulsed T2 cells in the presence of TCRα-αCD3(OKT3$_{HGL}$)-Fc^{aglyc}

A) To evaluate T cell redirection of TCRα-αCD3(OKT3$_{HGL}$)-Fc^{aglyc}. B) T cell degranulation and activation were analyzed using flow cytometry following 24 h co-culture with 100 µM CMV pp65 (CMV)/ survivin (Sur) pulsed T2 cells by staining for CD107a, CD25, CD69, CD134, CD137, intracellular IFNγ and TNFα. CD107a, IFNγ and TNFα were analyzed after co-culture in presence of golgi transport inhibitors. T cell proliferation was analyzed using CTV-labeled T cells following 5 days of co-culture.

To evaluate the influence of TCR affinity and antigen density for the redirection of T cells and target-directed cytotoxicity, the concentration of TCR construct (Figure 22) and CMV pp65 peptide (Figure 23) used for the peptide pulse were titrated. 100 µM survivin peptide-pulsed T2 cells and TCR-Fc^{aglyc} were included as negative controls. Since CD3-specific BiMabs are regularly used for T cell redirection, an αCD19-Fc^{KO}-αCD3 BiMab was used for comparison. Upon titration of the compound (Figure 22), the CMV pp65-specific TCRα-αCD3($OKT3_{HGL}$)-Fc^{aglyc} did result in increased target cell lysis, T cell degranulation, T cell activation and T cell proliferation compared to a co-culture without compound. No increase was observed using the TCR-Fc^{aglyc} control, demonstrating that the observed effect was T cell-dependent. As for the NK cell-targeting constructs, the response was dependent on TCRα-αCD3($OKT3_{HGL}$)-Fc^{aglyc} concentration and TCR affinity. Thus, the EC_{50} value of the high-affinity variant were around 4-10 times lower than that of the low-affinity TCR and ranged between 1-8 pM upon TCR titration. Interestingly, the observed response of the low and the high-affinity construct was overall higher than that induced by equimolar concentrations of the αCD19-Fc^{KO}-αCD3 BiMab. Using concentrations higher than 0.06 nM the low-affinity and more prominently also the high-affinity TCRα-αCD3($OKT3_{HGL}$)-Fc^{aglyc} induced increasing unspecific T cell activation and proliferation and to a lower degree also unspecific target cell lysis upon co-culture with the survivin peptide-pulsed T2 cells. Thus following experiments using peptide-pulsed T2 cells were carried out with the saturating but still specific concentration of 0.06 nM for TCRα-αCD3($OKT3_{HGL}$)-Fc^{aglyc} and 0.6 nM αCD19-Fc^{KO}-αCD3 BiMab, since lower concentrations of the BiMab were not saturated and insufficient to induce target cell lysis. Upon titration of the peptide concentration used for the peptide pulse (Figure 23), the low-affinity TCRα-αCD3($OKT3_{HGL}$)-Fc^{aglyc} was characterized by a lower sensitivity as it induced a weaker response upon lower peptide concentrations compared to the high-affinity variant. Thus, the EC_{50} values of the high-affinity TCR constructs were around 150 times lower, further demonstrating that T cell redirection and target cell lysis are dependent on TCR affinity. Furthermore, the observed effect of the low and high-affinity construct was dependent on peptide concentration and thus on antigen density on the target cell.

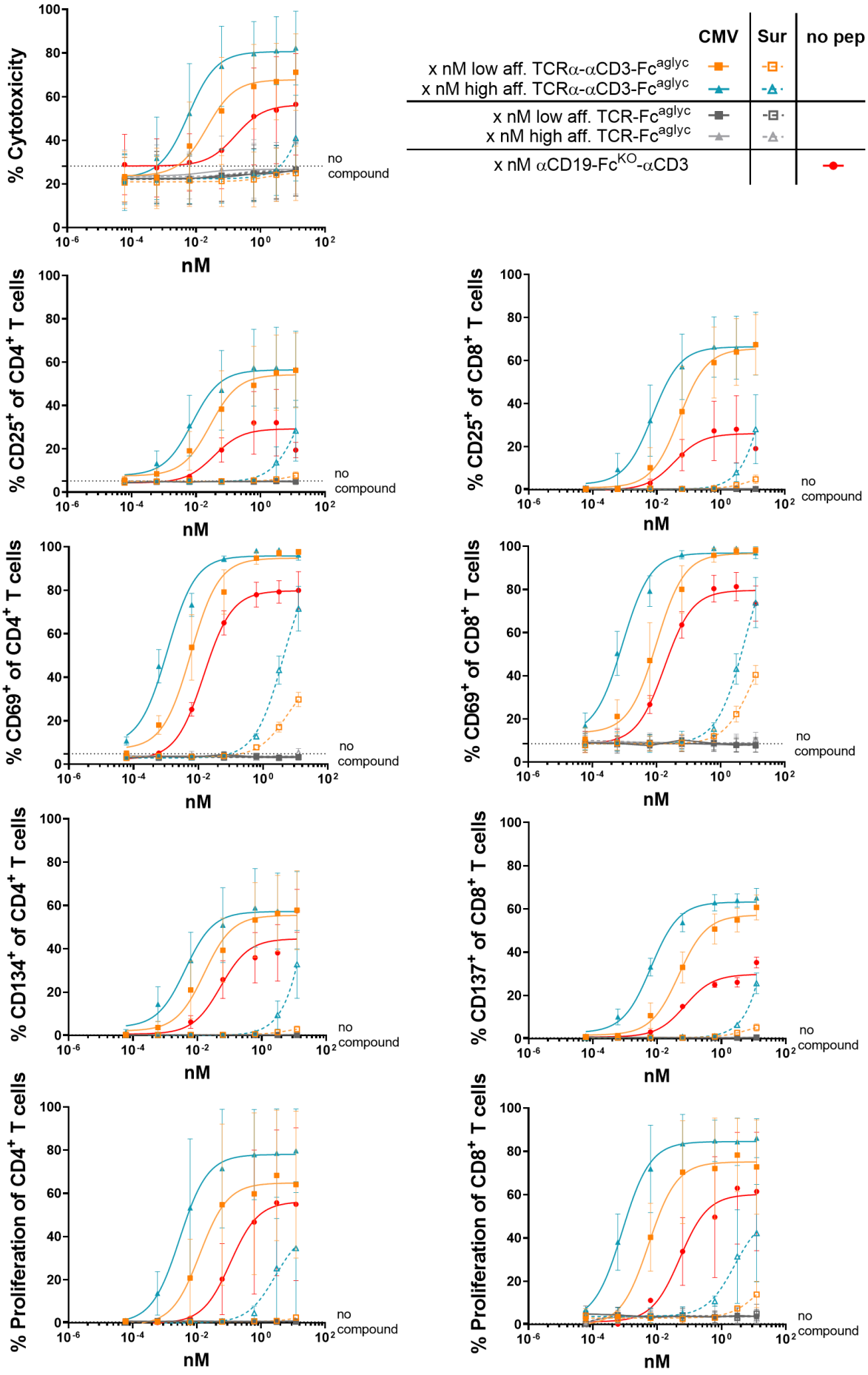
CMV
Sur
no pep
x nM low aff. TCRα-αCD3-Fc^aglyc
x nM high aff. TCRα-αCD3-Fc^aglyc
x nM low aff. TCR-Fc^aglyc
x nM high aff. TCR-Fc^aglyc
x nM αCD19-Fc^KO-αCD3
% Cytotoxicity
% CD25+ of CD4+ T cells
% CD25+ of CD8+ T cells
% CD69+ of CD4+ T cells
% CD69+ of CD8+ T cells
% CD134+ of CD4+ T cells
% CD137+ of CD8+ T cells
% Proliferation of CD4+ T cells
% Proliferation of CD8+ T cells
nM
no compound

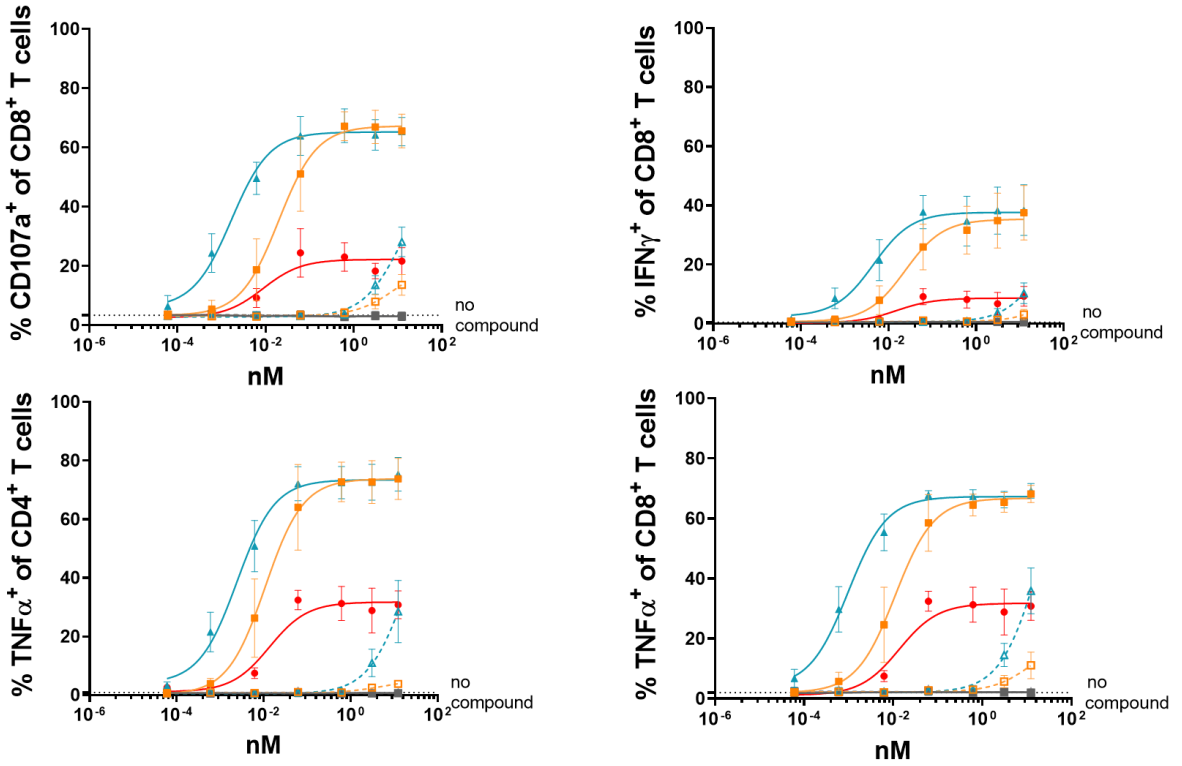

EC_{50} (nM)	Cyto-toxicity	CD4/ CD8	CD25	CD69	CD134	CD137	Prolifer -ation	CD107a	IFNγ	TNFα
Low aff. TCRα-αCD3-Fc^{aglyc}	0.021	CD4	0.027	0.006	0.016	-	0.012	-	-	0.011
		CD8	0.05	0.01	-	0.047	0.005	0.02	0.024	0.011
High aff. TCRα-αCD3-Fc^{aglyc}	0.006	CD4	0.008	0.001	0.004	-	0.003	-	-	0.002
		CD8	0.007	0.001	-	0.006	0.001	0.002	0.005	0.001
αCD19-Fc^{KO}-αCD3	0.168	CD4	0.036	0.015	0.053	-	0.112	-	-	0.014
		CD8	0.036	0.018	-	0.073	0.051	0.009	0.015	0.014

Figure 22: Titration of TCRα-αCD3($OKT3_{HGL}$)-Fc^{aglyc} upon co-culture of T cells with peptide-pulsed T2 cells
100 µM CMV pp65 (CMV – solid line)/ survivin (Sur – dashed line) pulsed T2 cells were co-cultured with T cells in presence of TCRα-αCD3($OKT3_{HGL}$)-Fc^{aglyc}. The negative control TCR-Fc^{aglyc} and an αCD19-Fc^{KO}-αCD3 BiMab were included for comparison. Compound concentration was titrated. Cytotoxicity was analyzed following 24 h co-culture using an LDH release assay. T cell degranulation and activation were analyzed using flow cytometry following 24 h co-culture by staining for CD107a, CD25, CD69, CD134, CD137, and intracellular IFNγ or TNFα. CD107a, IFNγ and TNFα were evaluated after co-culture in presence of Golgi transport inhibitors. T cell proliferation was assessed using CTV-labeled T cells following 5 days co-culture. Mean values ± s.e.m. from 3 independent experiments are shown. EC_{50} values is shown for the αCD19-Fc^{KO}-αCD3 BiMab and for the TCRs constructs upon co-culture with CMV pp65 peptide-pulsed T2 cells are shown in the table below.

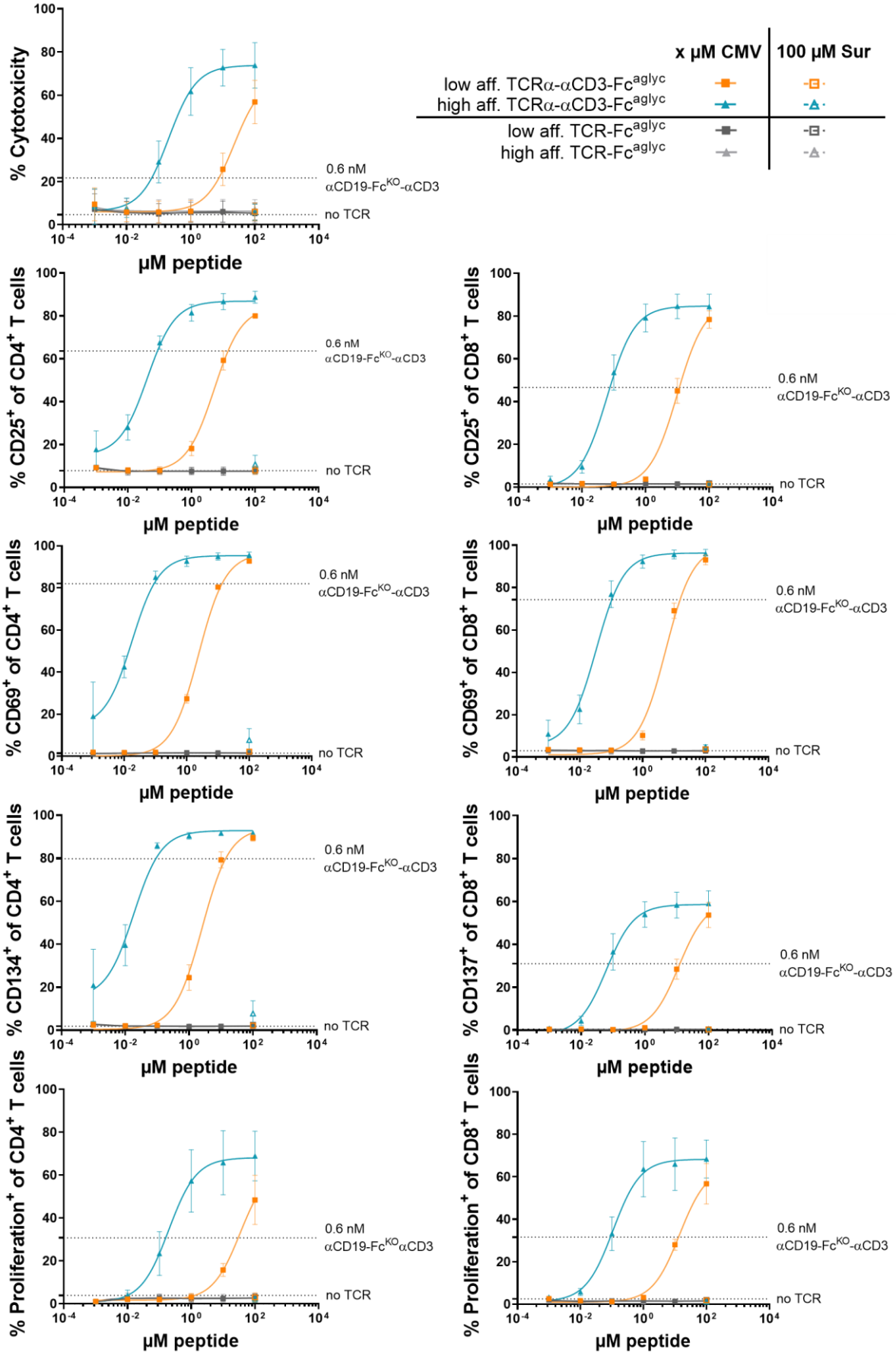
x µM CMV
100 µM Sur
low aff. TCRα-αCD3-Fc^aglyc
high aff. TCRα-αCD3-Fc^aglyc
low aff. TCR-Fc^aglyc
high aff. TCR-Fc^aglyc
% Cytotoxicity
% CD25+ of CD4+ T cells
% CD25+ of CD8+ T cells
% CD69+ of CD4+ T cells
% CD69+ of CD8+ T cells
% CD134+ of CD4+ T cells
% CD137+ of CD8+ T cells
% Proliferation+ of CD4+ T cells
% Proliferation+ of CD8+ T cells
µM peptide
0.6 nM αCD19-Fc^KO-αCD3
no TCR

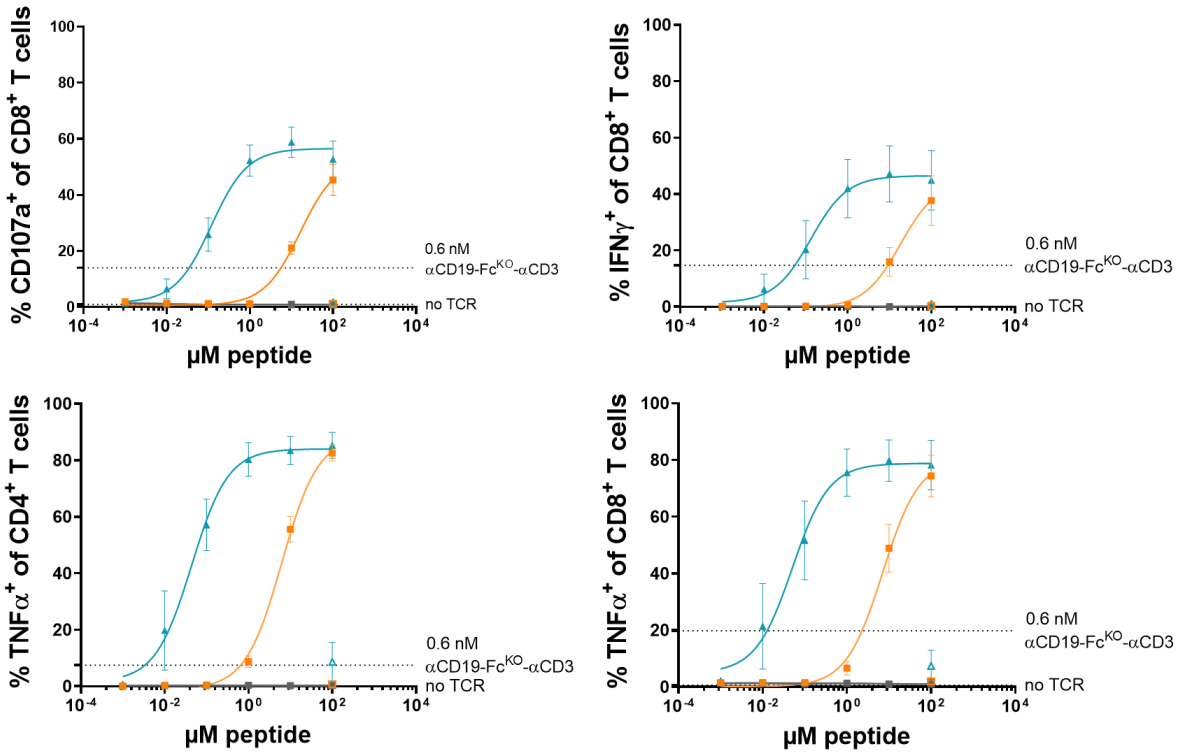

EC_{50} (µM)	Cyto-toxicity	CD4/ CD8	CD25	CD69	CD134	CD137	Prolifer -ation	CD107a	IFNγ	TNFα
Low aff. TCRα-αCD3-Fc^{aglyc}	22.5	CD4	5.143	0.018	2.521	-	34.70	22.35	63.16	6.231
		CD8	9.913	5.421	-	11.65	14.06	16.27	18.15	7.027
High aff. TCRα-αCD3-Fc^{aglyc}	0.205	CD4	0.04	0.005	0.018	-	0.196	0.172	0.371	0.044
		CD8	0.061	0.033	-	0.062	0.108	0.118	0.131	0.05

Figure 23: Titration of peptide concentration upon co-culture of T cells and peptide-pulsed T2 cells in presence of TCRα-αCD3(OKT3$_{HGL}$)-Fc^{aglyc}
CMV pp65 (CMV)/ survivin (Sur) pulsed T2 cells were co-cultured with T cells in presence of 0.06 nM TCRα-αCD3-$Fc^{aglyc.}$ 0.06 nM TCR-Fc^{aglyc} and 0.6 nM of a αCD19-Fc^{KO}-αCD3 BiMab were included for comparison. Peptide concentration was titrated. Target-directed cytotoxicity was assessed following 24 h co-culture using an LDH release assay. T cell degranulation and activation were analyzed using flow cytometry following 24 h co-culture by staining for CD107a, CD25, CD69, CD134, CD137, and intracellular IFNγ or TNFα. CD107a, IFNγ and TNFα were assesed using a co-culture in presence of Golgi transport inhibitors. T cell proliferation was evaluated using CTV-labeled T cells following 5 days co-culture. Mean values ± s.e.m. from 3 independent experiments are shown. EC_{50} values are indicated for the co-culture with CMV pp65 peptide-pulsed T2 cells in the table below.

Similar to NK cells, T cell redirection was also assessed for the more relevant peptide-pulsed and pMHC-mSCT transfected MCF-7. However, when using the same concentration of 0.06 nM, there was no or barely any effect with and without co-stimulation delivered by 1 nM αEpCAM-Fc^{KO}-αCD28 BiMab (data not shown). Thus, the titration was repeated with and without co-stimulation for the peptide-pulsed (Figure 24) and pMHC-mSCT transfected cells (Figure 25). This titration gained overall higher EC_{50} values and saturation was reached using a 10-fold higher concentration of 0.6 nM. However, still no cytotoxicity and little T cell activation

was observed using the low-affinity TCRα-αCD3(OKT3$_{HGL}$)-Fc^{aglyc} upon co-culture of peptide-pulsed MCF-7 without co-stimulation. When adding the co-stimulatory αEpCAM-Fc^{KO}-αCD28 BiMab still no cytotoxicity was induced by the low-affinity TCR construct while T cell activation was strongly increased. As before, the response mediated by TCRα-αCD3(OKT3$_{HGL}$)-Fc^{aglyc} was stronger than equimolar concentrations of an αEpCAM-Fc^{KO}-αCD3 BiMab, which did not reach saturation considering cytotoxicity within the tested concentration range. However, upon co-culture with peptide-pulsed MCF-7 (Figure 24) there was still only little cytotoxicity using the high-affinity TCRα-αCD3(OKT3$_{HGL}$)-Fc^{aglyc} and no cytotoxicity using the low-affinity variant. Administration of the co-stimulatory αEpCAM-Fc^{KO}-αCD28 BiMab, led to a slight increase in cytotoxicity induced by the high-affinity TCR construct and a stronger increase of T cell activation especially for the low-affinity variant. However, using concentrations higher than 0.6 nM unspecific T cell activation was observed upon co-culture with survivin peptide-pulsed MCF-7, which was most prominent with co-stimulation. Upon co-culture with the pMHC-mSCT transfected MCF-7 (Figure 25), there was only little improvement obtained when adding co-stimulation, probably due to the presence of CD80^{+} MCF-7 or the higher degree of peptide presentation (Figure 18). As for the peptide-pulsed MCF-7, unspecific T cell activation was observed using concentrations higher than 0.6 nM. Similar to the NK cell-targeting constructs, the overall response considering target cell lysis, effector cell degranulation and activation was higher towards pMHC-mSCT transfected MCF-7 than to the peptide-pulsed MCF-7.

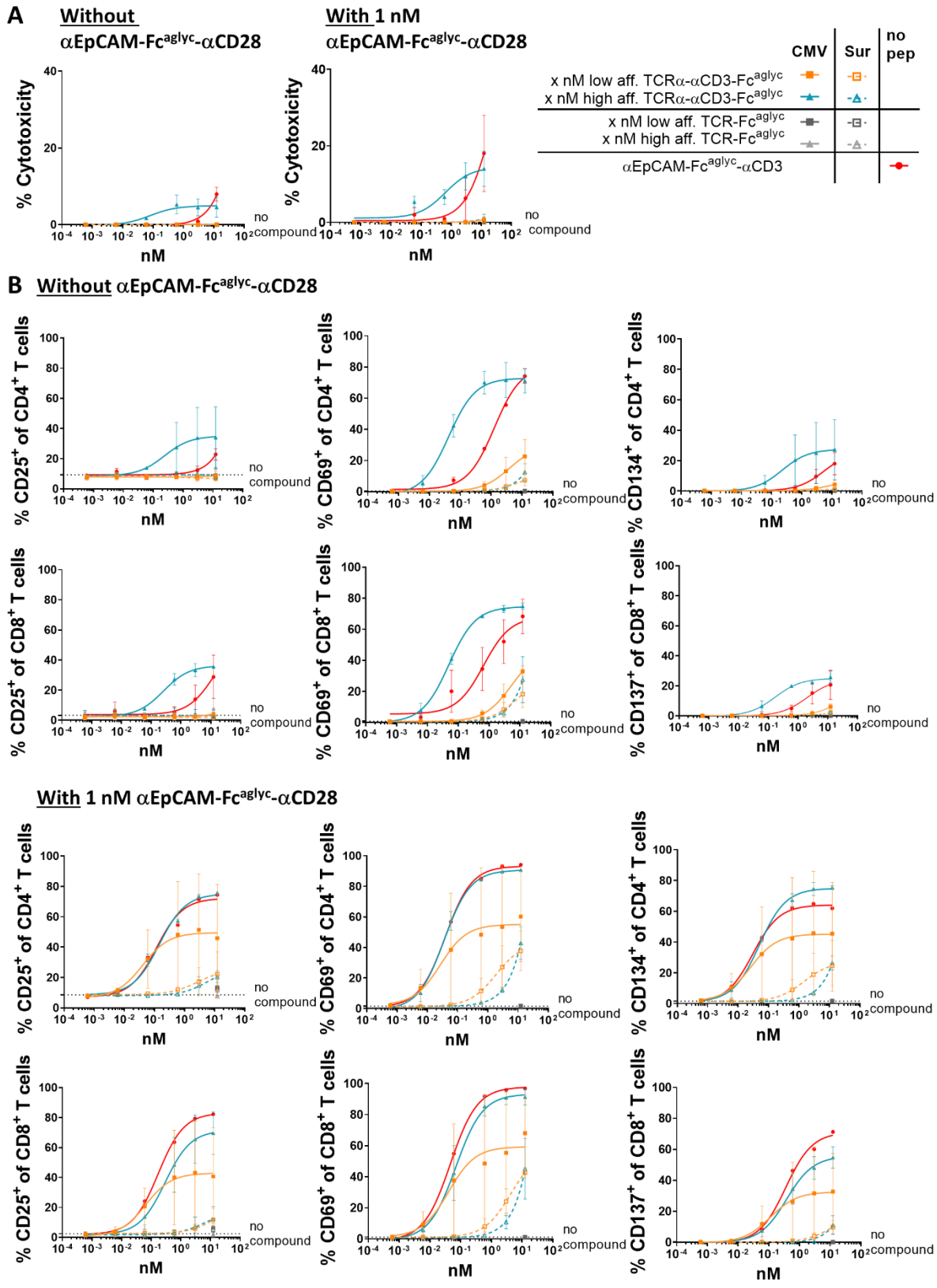
A
Without
αEpCAM-Fc^aglyc-αCD28
With 1 nM
αEpCAM-Fc^aglyc-αCD28
% Cytotoxicity
nM
no compound
CMV
Sur
no pep
x nM low aff. TCRα-αCD3-Fc^aglyc
x nM high aff. TCRα-αCD3-Fc^aglyc
x nM low aff. TCR-Fc^aglyc
x nM high aff. TCR-Fc^aglyc
αEpCAM-Fc^aglyc-αCD3
B
Without αEpCAM-Fc^aglyc-αCD28
% CD25+ of CD4+ T cells
% CD69+ of CD4+ T cells
% CD134+ of CD4+ T cells
% CD25+ of CD8+ T cells
% CD69+ of CD8+ T cells
% CD137+ of CD8+ T cells
With 1 nM αEpCAM-Fc^aglyc-αCD28

C

EC_{50} (nM)	Cyto-toxicity	CD4/ CD8	CD25	CD69	CD134	CD137
Without co-stimulation						
Low aff. TCRα-αCD3-Fc^{aglyc}	ND	CD4	ND	3.844	11.83	-
		CD8	ND	5.243	-	47.28
High aff. TCRα-αCD3-Fc^{aglyc}	0.081	CD4	0.236	0.042	0.224	-
		CD8	0.256	0.05	-	0.169
αEpCAM-Fc^{KO}-αCD3	ND	CD4	ND	1.269	5.47	-
		CD8	12.57	0.663	-	2.008
With co-stimulation						
Low aff. TCRα-αCD3-Fc^{aglyc}	ND	CD4	0.041	0.027	0.025	-
		CD8	0.065	0.04	-	0.113
High aff. TCRα-αCD3-Fc^{aglyc}	0.642	CD4	0.146	0.036	0.05	-
		CD8	0.293	0.07	-	0.381
αEpCAM-Fc^{KO}-αCD3	25.50	CD4	0.118	0.04	0.031	-
		CD8	0.172	0.047	-	0.357

Figure 24: Titration of TCRα-αCD3($OKT3_{HGL}$)-Fc^{aglyc} in co-cultures of T cells with peptide-pulsed MCF-7 cells

CMV pp65 (CMV – solid line)/ survivin (Sur – dashed line) pulsed MCF-7 cells were co-cultured with T cells in presence of following compounds: TCRα-αCD3($OKT3_{HGL}$)-Fc^{aglyc}, TCR-Fc^{aglyc} and αEpCAM-Fc^{KO}-αCD3 BiMab. Compound concentration was titrated. Co-culture was set up with 1 nM a co-stimulatory αEpCAM-Fc^{KO}-αCD28 BiMab or without. A) Cytotoxicity was analyzed following 24 h co-culture using an LDH release assay. B) T cell activation was analyzed using flow cytometry following 24 h co-culture by staining for CD25, CD69, CD134, CD137. C) EC_{50} values were calculates for the TCR constructs upon co-culture with CMV pp65 peptide-pulsed MCF-7 cells and for the co-culture with αEpCAM-Fc^{KO}-αCD3. ND = not detected. n=2

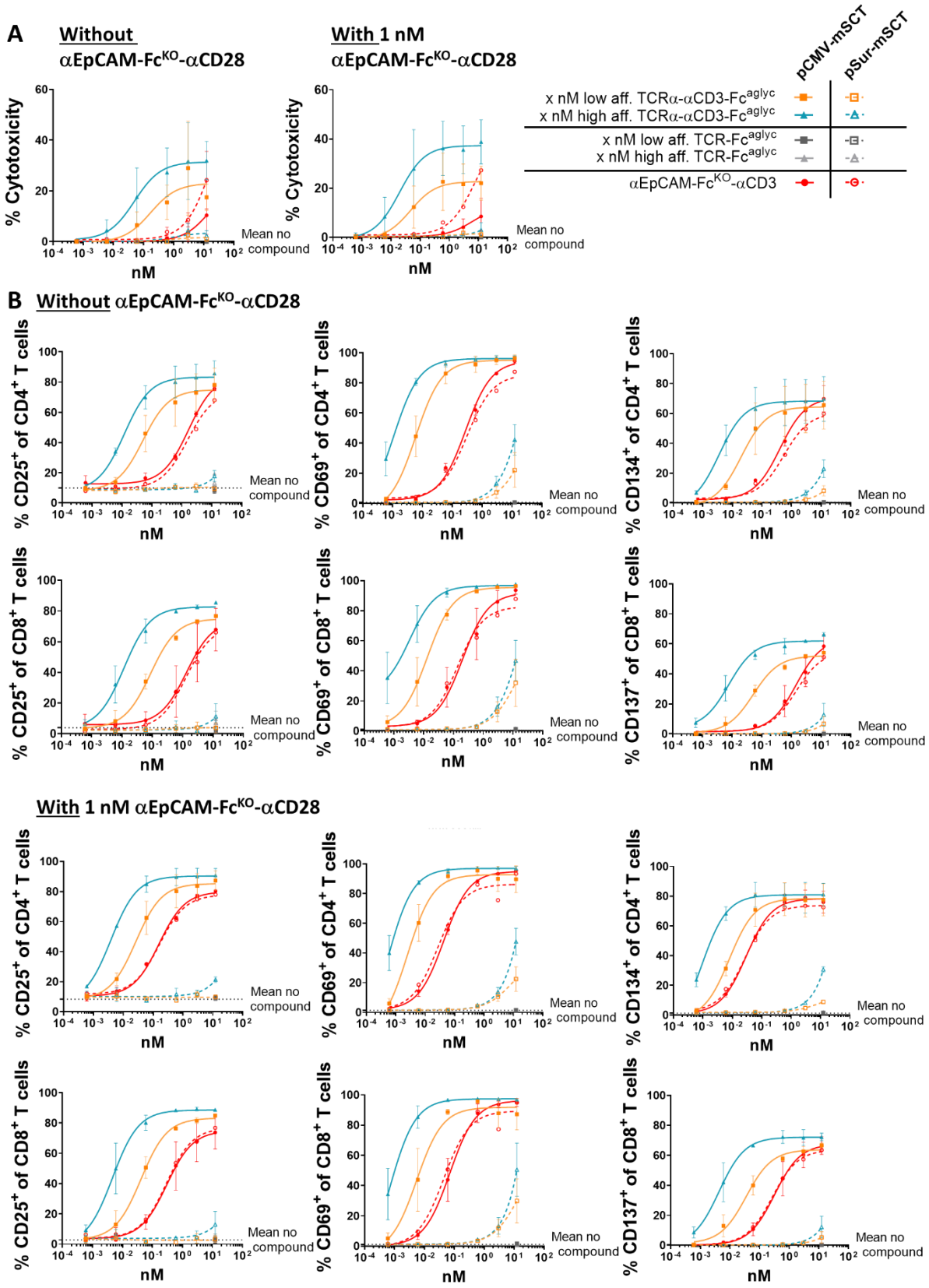
A
Without αEpCAM-Fc^KO-αCD28
With 1 nM αEpCAM-Fc^KO-αCD28
% Cytotoxicity
nM
Mean no compound
pCMV-mSCT
pSur-mSCT
x nM low aff. TCRα-αCD3-Fc^aglyc
x nM high aff. TCRα-αCD3-Fc^aglyc
x nM low aff. TCR-Fc^aglyc
x nM high aff. TCR-Fc^aglyc
αEpCAM-Fc^KO-αCD3
B
Without αEpCAM-Fc^KO-αCD28
% CD25+ of CD4+ T cells
% CD69+ of CD4+ T cells
% CD134+ of CD4+ T cells
% CD25+ of CD8+ T cells
% CD69+ of CD8+ T cells
% CD137+ of CD8+ T cells
With 1 nM αEpCAM-Fc^KO-αCD28

C

EC_{50} (nM)	Cyto-toxicity	CD4/ CD8	CD25	CD69	CD134	CD137
Without co-stimulation						
Low aff. TCRα-αCD3-Fc^{aglyc}	0.170	CD4	0.05	0.006	0.02	-
		CD8	0.088	0.013	-	0.052
High aff. TCRα-αCD3-Fc^{aglyc}	0.051	CD4	0.012	0.001	0.003	-
		CD8	0.011	0.003	-	0.008
αEpCAM-Fc^{KO}-αCD3 (CMV/ Sur)	16.34	CD4	1.682/ 1.551	0.279/ 0.307	0.409/ 0551	-
		CD8	1.340/ 1.288	0.2/0137	-	1.429/ 1.426
With co-stimulation						
Low aff. TCRα-αCD3-Fc^{aglyc}	0.047	CD4	0.026	0.003	0.008	-
		CD8	0.042	0.005	-	0.035
High aff. TCRα-αCD3-Fc^{aglyc}	0.02	CD4	0.004	0.001	0.001	-
		CD8	0.005	0.001	-	0.004
αEpCAM-Fc^{KO}-αCD3 (CMV/ Sur)	6.056	CD4	0.158/ 0.163	0.043/ 0.027	0.03/ 0.026	-
		CD8	0.301/ 0.297	0.07/ 0.044	-	0.322/ 0.266

Figure 25: Titration of TCRα-αCD3($OKT3_{HGL}$)-Fc^{aglyc} in co-cultures of T cells with pMHC-mSCT transfected MCF-7
CMV pp65 (CMV – solid line)/ survivin (Sur – dashed line) pMHC-mSCT transfected MCF-7 cells were co-cultured with T cells in presence of TCRα-αCD3($OKT3_{HGL}$)-Fc^{aglyc}, TCR-Fc^{aglyc} and αEpCAM-Fc^{aglyc}-αCD3 BiMab. The administered concentration was titrated. Co-culture was setup once with or without the co-stimulatory αEpCAM-Fc^{aglyc}-αCD28 BiMab (1 nM). A) Cytotoxicity was evaluated following 24 h co-culture using an LDH release assay. B) T cell activation was analyzed using flow cytometry by staining for CD25, CD69, CD134, CD137 following 24 h co-culture. C) EC_{50} values were calculates for the TCR constructs upon co-culture with CMV pp65 pMHC-mSCT transfected cells and for αEpCAM-Fc^{aglyc}-αCD3 upon co-culture with CMV pp65 and Sur pMHC-mSCT transfected cells. ND = not detected. n=2

As for the NK cell-targeting constructs, the T cell redirection mediated by TCRα-αCD3($OKT3_{HGL}$)-Fc^{aglyc} was analyzed in the 3D co-culture model. To this end, tumor spheroids were generated from the pMHC-mSCT transfected MCF-7 (2.2.7.5), which were proven to be a suitable target for the CMV pp65-specific TCR constructs, and co-cultured with T cells with and without co-stimulation delivered by the αEpCAM-Fc^{aglyc}-αCD28 BiMab. TCR-Fc^{aglyc} was included as a negative control and 0.6 nM αEpCAM-Fc^{aglyc}-αCD3 BiMab for comparison. Upon co-culture with CMV pp65 pMHC-mSCT transfected cells, the TCRα-αCD3($OKT3_{HGL}$)-Fc^{aglyc} induced target cell lysis, T cell degranulation, T cell activation and T cell proliferation in contrast to the co-culture with survivin pMHC-mSCT transfected cells, demonstrating a target-specific T cell redirection (Figure 26, Figure 27). Using equimolar concentrations, no cytotoxicity was observed for the αEpCAM-Fc^{KO}-αCD3 BiMab upon co-culture without co-stimulation, and little when adding co-stimulation. Also upon administration of the CMV pp65 peptide-specific TCRα-αCD3($OKT3_{HGL}$)-Fc^{KO} co-stimulation slightly increased the target-specific response without changing the response to pSur-$mSCT^{+}$ transfected cells or that of the aglycan TCR-Fc control construct.

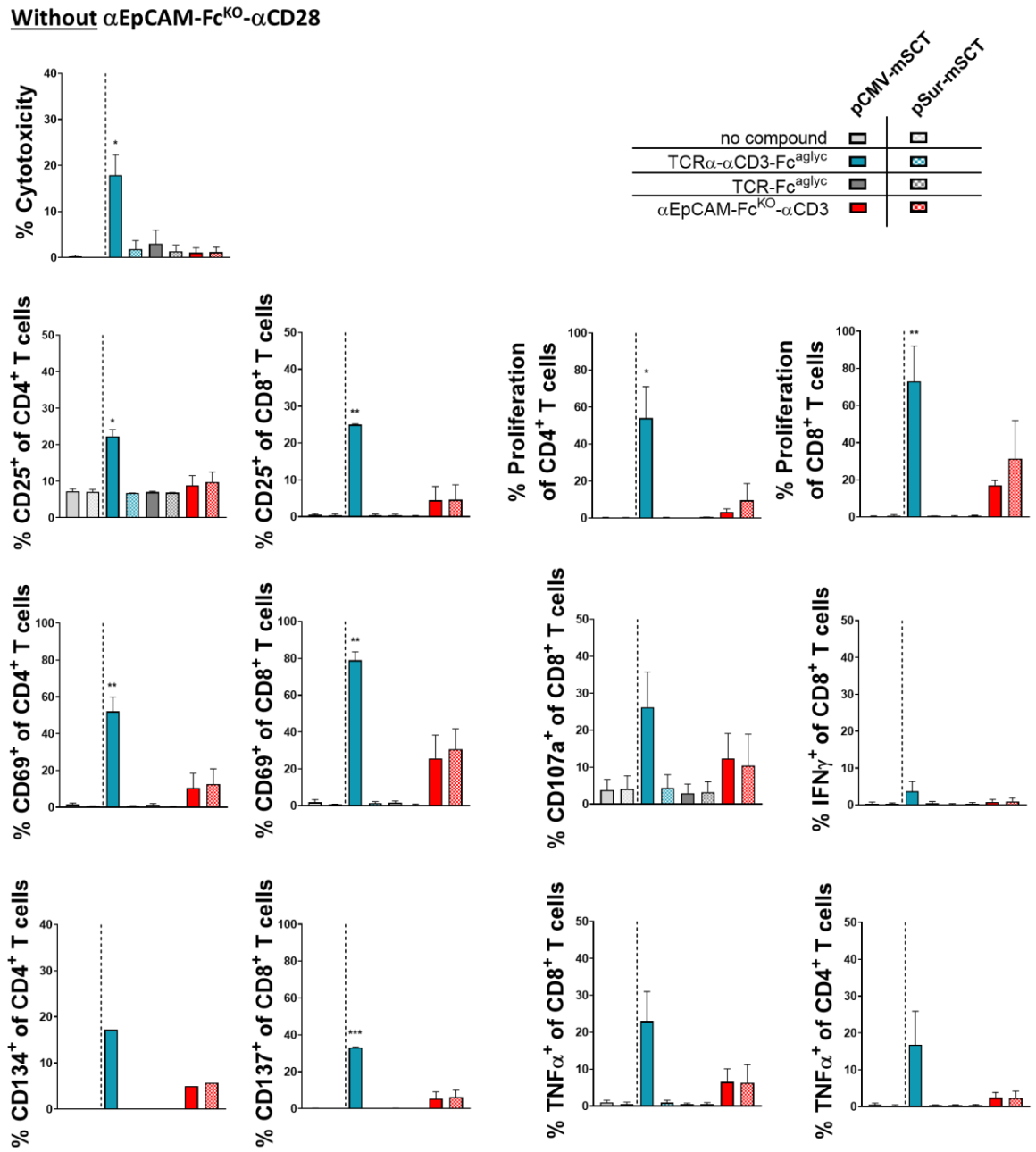

Figure 26: Co-culture of pMHC-mSCT transfected MCF-7 spheroids with T cells in presence of TCRα-αCD3-Fc^{aglyc} without co-stimulation

T cells were co-cultured for 24 h with tumor cell spheroids generated of the stably CMV pp65 (CMV)/ survivin (Sur) mSCT transfected MCF-7 in presence of 0.6nM TCRα-αCD3-Fc^{aglyc}. 0.6 nM TCR-Fc^{aglyc} and αEpCAM-Fc^{KO}-αCD3 were applied for comparison. Target cell lysis was analyzed following 24 h co-culture using an LDH release assay. T cell degranulation and activation were analyzed using flow cytometry following 24 h co-culture by staining for CD107a, CD25, CD69, CD134, CD137, and intracellular IFNγ or TNFα. CD107a, IFNγ and TNFα were assesed using a co-culture supplemented with Golgi transport inhibitors. T cell proliferation was analyzed using CTV-labeled T cells following 5 days of co-culture. Significance compared to “no compound” was analyzed by OneWay ANOVA test for the CMV pp65 and survivin group separately followed by Dunnett’s multiple comparison test. Mean values ± s.e.m. are shown. Cytotoxicity, CD25, CD69, CD134, CD137, IFNγ, TNFα, n=2; CD134, n=1

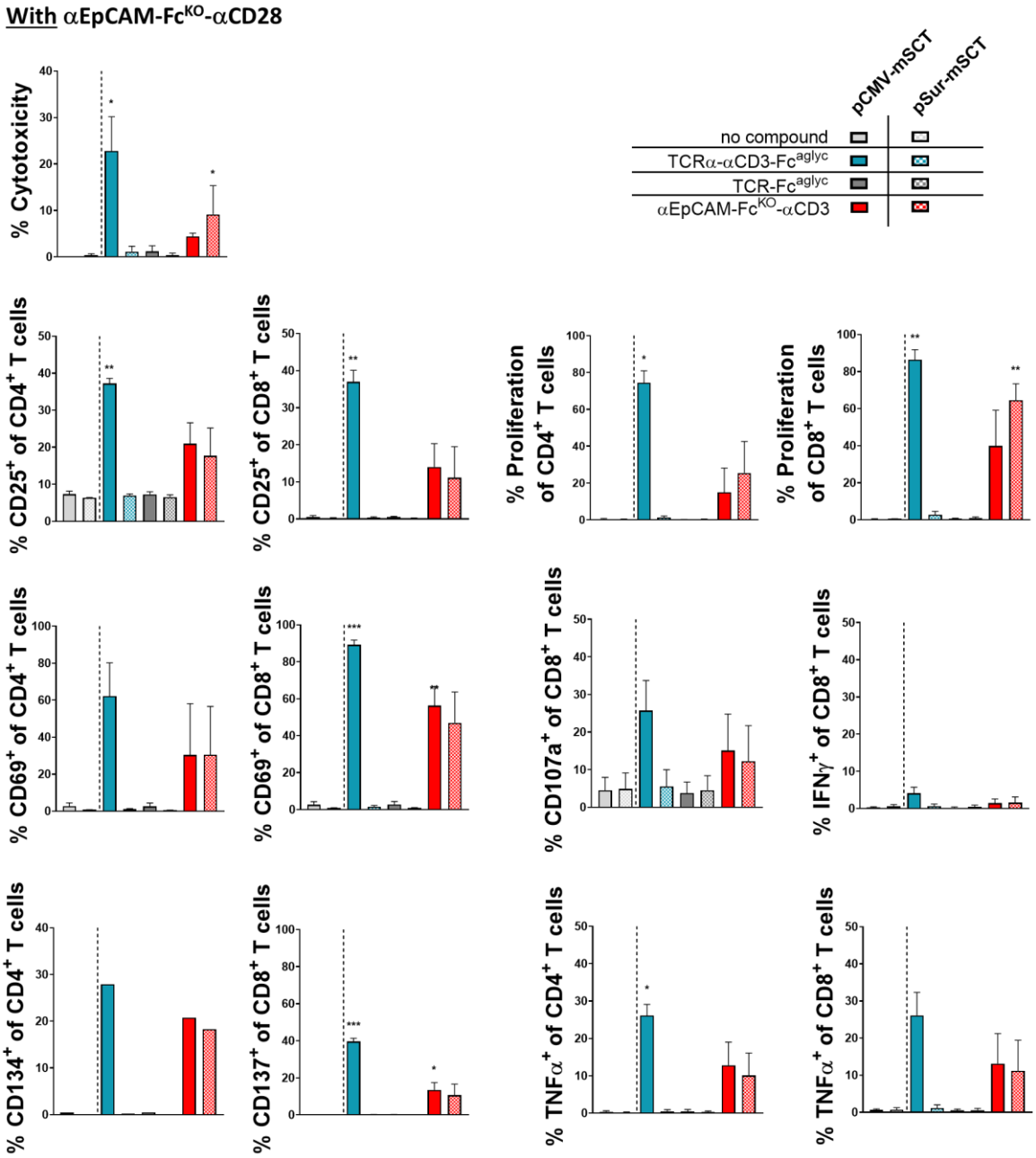

Figure 27: Co-culture of pMHC-mSCT transfected MCF-7 spheroids with T cells in presence of TCRα-αCD3-Fc^{aglyc} and co-stimulation

Tumor spheroids were generated cells were of the stably CMV pp65 (CMV)/ survivin (Sur) mSCT transfected MCF-7 and co-cultured with T cells for 24 h in presence of 0.6 nM TCRα-αCD3-Fc^{aglyc} and 0.6 nM TCR-Fc^{aglyc}. αEpCAM-Fc^{KO}-αCD3 BiMab was applied for comparison. The co-stimulatory αEpCAM-Fc^{KO}-αCD28 BiMab was added at 1 nM concentration. Cytotoxicity was analyzed using an LDH release assay following 24 h co-culture. T cell degranulation and activation were evaluated using flow cytometry by staining for CD107a, CD25, CD69, CD134, CD137, and intracellular IFNγ or TNFα following 24 h co-culture. CD107a, IFNγ and TNFα were analyzed using a co-culture supplemented with Golgi transport inhibitors. T cell proliferation was analyzed using CTV-labeled T cells following 5 days co-culture. Significance was analyzed by OneWay ANOVA test for the CMV pp65 and survivin group separately compared to the “no compound” control followed by Dunnett’s multiple comparison test. Mean values ± s.e.m. are shown. Cytotoxicity, CD25, CD69, CD134, CD137, IFNγ, TNFα n=2; CD134 n=1.

3.3 Evaluation of soluble TCR-Fc fusion proteins using different TAA-specific TCR clones

3.3.1 Target binding

Following initial evaluation using the CMV pp65-specific TCR clone as a model system, the soluble TCR-Fc fusion proteins were further evaluated using three different TCR clones directed against different tumor-associated antigens (TAA) (Figure 28). The TCRs investigated include published HLA-A*02:01-restricted TCR clones, which were previously also affinity maturated or mutated. Clone 1G4 is directed against NY-ESO-$1_{157-165}$ (Robbins et al., 2008), clone IMCgp100 against the $gp100_{280-288}$ peptide (Boudousquie et al., 2017; Li et al., 2005) and clone DMF5 against the MART-1_{26-35} peptide (Johnson et al., 2006; Robbins et al., 2008). The wildtype or lower affinity variant as well as the mutated or higher affinity variant were included for evaluation. For the wildtype and affinity-maturated gp100-specific TCR, K_D affinity constants of 26 µM and 30 pM, respectively, were measured (Liddy et al., 2012). In case of 1G4 the affinity maturation decreased the K_D from 9.3 µM to 730 nM. The K_D value of the wildtype DMF5 is relatively low with about 30 nM (Malecek et al., 2014; Sádio et al., 2020), the K_D of the mutated variant is unknown. All TAA-specific TCR clones were producible in the TCR-Fc format.

To confirm functionality in the recombinant TCR-Fc format, target binding was analyzed using ELISA and flow cytometry (Figure 28A). For analysis using ELISA, 5 µg/ml peptide-tethered HLA-A*02:01 SCT-Fc fusion proteins were coated and different concentrations of the TCR-Fc fusion protein were added. To improve peptide binding within the peptide-tethered HLA-A*02:01 SCT-Fc fusion proteins, an amino acid was exchanged within an anchor position that is not relevant for TCR recognition but important for peptide binding to the MHC. For the gp100 peptide-tethered MHC the amino acid Ala288 was exchanged with a valine, for MART-1 Ala27 was exchanged with a leucine, and for NY-ESO-1 Cys165 was exchanged with a valine. In case of NY-ESO-1 and MART-1, the same sequence was used for the synthetic soluble peptide used for the peptide pulse. Survivin peptide-tethered SCT-Fc fusion proteins were included as a negative control. For the evaluation using flow cytometry, TAP-deficient HLA-A*02:01$^+$ T2 cells were pulsed with the matching HLA-A*02:01-restricted peptides or survivin peptide for control and stained with the soluble TCR-Fc using the indicated concentrations and a secondary human Fc-specific fluorophore-conjugated antibody. All TAA-specific TCR constructs showed a concentration and target-specific binding and no unspecific binding was observed towards the survivin peptide-tethered SCTs or peptide-pulsed T2 cells. As expected, the mutated TCR variants were all characterized by a stronger target binding. Using ELISA, only the mutated gp100-specific TCR-Fc showed a binding affinity comparable to the high-affinity CMV pp65-specific TCR-Fc with an EC_{50} of 300 pM, which was included for

comparison. In the flow cytometry analysis, the mutated gp100-specific TCR-Fc as well as the mutated and wildtype NY-ESO-1 specific TCR-Fc showed binding that was comparable, or in case of the mutated variants even stronger than that of the high-affinity CMV pp65-specific TCR. For the high-affinity gp100-specific TCR this was about 20-fold lower with an EC_{50} of around 100 pM in contrast to 2 nM calculated for the high-affinity CMV pp65-specific TCR. The mutated MART-1 specific TCR showed binding comparable to the wildtype CMV pp65-specific in the ELISA and a slightly stronger binding in flow cytometry. Since all TCR constructs showed a functional and specific target binding towards peptide-pulsed T2 cells, binding was furthermore evaluated using tumor cell lines endogenously expressing the antigen of choice and HLA-A2. These included the melanoma cell line MeWo expressing MART-1 and gp100, the melanoma cell line SK-Mel-5 expressing gp100 and the melanoma cell lines SK-Mel-37 and A375 expressing NY-ESO-1. Peptide presentation was not confirmed in this study, however each of the cell lines had already been used for similar approaches such as validation of the gp100-specific ImmTAC TCR or evaluation of antigen-specific T cells in different studies (Chang et al., 2011; Ichikawa et al., 2020; Liddy et al., 2012; McCormack et al., 2013; Zhao et al., 2021). HLA-A2 expression was analyzed by flow cytometry using a fluorophore-conjugated HLA-A2 specific antibody (BB7.2) (Figure 28B). The lowest expression was observed for MeWo and A375, intermediate expression was observed for SK-Mel-5 and SK-Mel-37 and strongest expression for T2. TCR-Fc binding to the matching tumor cell line with endogenous antigen expression was evaluated using flow cytometry as before (Figure 28C). As a control, the tumor cell lines were further pulsed with 100 µM of the matching peptide or survivin peptide for control. The CMV pp65-specific TCR and CMV pp65 peptide-pulsed T2 cells were included for comparison. Unfortunately, when using 60 nM TCR-Fc for the staining no binding to the untreated matching tumor cell lines was detected. When adding 100 µM of the matching peptide, binding was detected for the high-affinity gp100- and NY-ESO-1-specific TCR constructs as well as for the CMV pp65-specific TCR-Fc included for comparison. However, no binding was observed for the low-affinity variants. In case of the MART-1-specific TCR-Fc, no binding was detected towards peptide-pulsed MeWo neither for the low- nor for the high-affinity variant, probably due to the rather weak HLA-A2 expression in combination with the weak TCR affinity observed. Furthermore, none of the TCRs showed binding towards survivin peptide-pulsed cells.

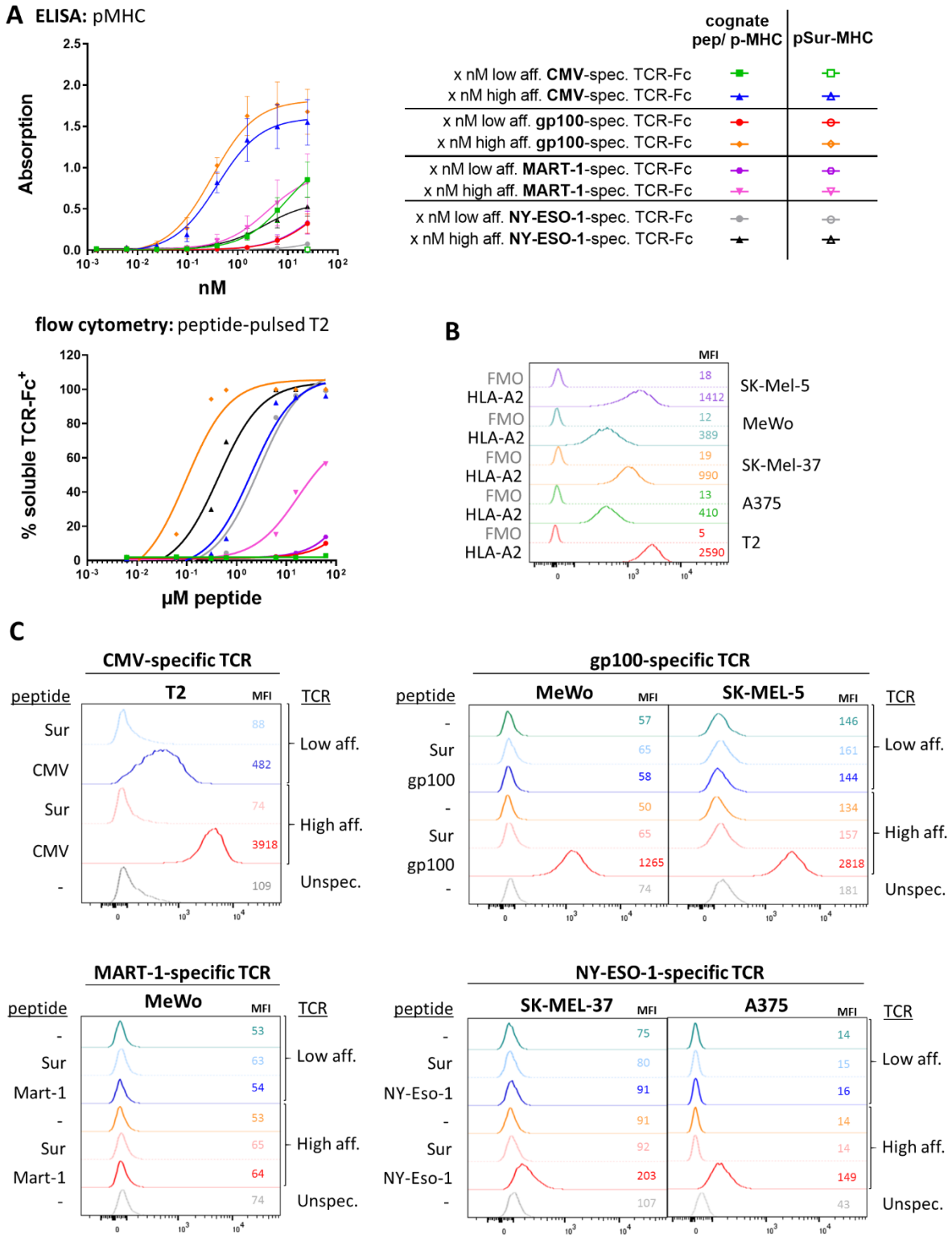

Figure 28: Target binding of different tumor-specific TCR-Fc constructs
A) Target binding of wildtype/ low-affinity TCR-Fc and mutated/ high-affinity TCR-Fc constructs specific for HLA-A*02:01 restricted CMV, gp100, MART-1, NY-ESO-1 was analyzed using ELISA (binding to peptide-tethered MHC-Fc fusion proteins) and using flow cytometry (binding to 100 µM peptide pulsed HLA-A*02:01$^+$ T2 cells). EC_{50} values are indicated in the matching color on the right of each graph. B) Evaluation of HLA-A2 expression of different tumor cell lines using flow cytometry. MFI values are indicated. C) Binding of the low- and high-affinity TCR-Fc constructs specific for the HLA-A*02:01-restricted peptides gp100[280-288], MART-1[26-35], NY-ESO-1[157-165] to tumor cells expressing the respective antigen was analyzed by flow cytometry. A 100 µM peptide pulse using the matching peptide

or survivin peptide was included for comparison. The CMV pp65-specific TCR-Fc and peptide-pulsed HLA-A*02:01$^+$ T2 cells were included as a control.

3.3.2 NK cell redirection

To evaluate if the TCR-Fc^{enh} and TCR-αNKp46-Fc^{enh} formats, which showed the strongest effect within the CMV model system, are also able to mediate NK cell redirection towards other targets, they were adapted for the TAA-specific TCR clones. Since none of the wildtype TCRs showed any binding towards the matching TAA-expressing tumor cells, also not when adding soluble peptide to increase antigen density on the cell surface, only the high-affinity variants were analyzed in the co-culture (Figure 29, Figure 30, Figure 31). To this end, the matching tumor cells were co-cultured with NK cells in presence of 6 nM of the respective high-affinity TAA-specific TCR constructs (2.2.7). As for the staining, this was set up with untreated tumor cells and with peptide-pulsed tumor cells. Besides the TAA-specific TCRs, the high-affinity CMV pp65-specific TCR constructs were included as a non-TAA-specific isotype control to control for target specificity. To evaluate the gp100-specific TCR constructs, the gp100-expressing tumor cells MeWo and SK-MEL-5 were used (Figure 29). Increased target cell lysis, NK cell degranulation and NK cell activation were observed upon co-culture with the gp100 peptide-pulsed tumor cells. However, no effect was observed towards the untreated tumor cells compared to the co-culture without TCR. The MART-1 NK-redirecting constructs were evaluated using the MART-1-expressing tumor cells MeWo as well as MART-1 peptide-pulsed T2 cells as a control, since the high-affinity MART-1-specific TCR construct showed no binding to MART-1 peptide-pulsed MeWo cells. As expected from the absent binding (Figure 28C), the MART-1-specific TCR constructs did not induce any NK cell activation towards untreated or MART-1 peptide-pulsed MeWo cells (Figure 30). However, increased cytotoxicity, NK cell degranulation and NK cell activation were observed in the co-culture of MART-1 peptide-pulsed T2 cells in comparison to the co-culture with survivin peptide-pulsed T2 cells or to the co-culture without TCR constructs, demonstrating that the MART-1-specific TCR constructs per se are functional. NY-ESO-1 was evaluated using the NY-ESO-1-expressing tumor cells SK-MEL-37 and A375 (Figure 31). For both cell lines increased cytotoxicity, NK cell degranulation and NK cell activation was only observed using peptide-pulsed but not using untreated tumor cells compared to the co-culture without TCR construct. Overall, there were no significant unspecific effects induced by the CMV pp65-specific control TCRs in any co-culture (Figure 29, Figure 30, Figure 31). To ensure that the chosen concentration of the TCR constructs (6 nM) was not the reason for absent responses towards the untreated tumor cells, a co-culture using 30 nM was evaluated as well. However, there was no difference between 30 and 6 nM (data not shown). Interestingly, the inclusion of αNKp46 scFv in the NK-redirecting construct did not augment the reactivity of TCR-Fc^{enh}.

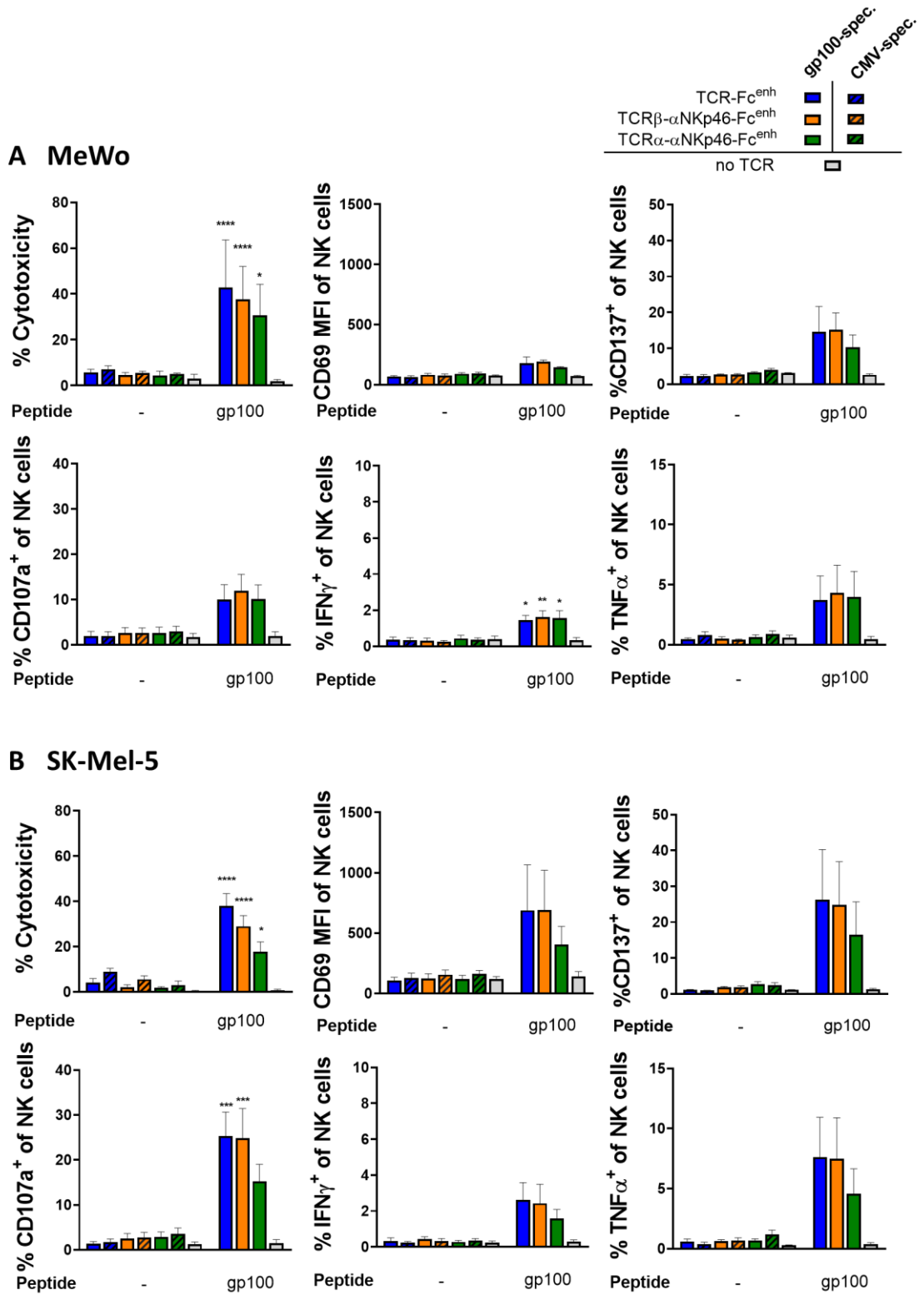

Figure 29: Co-culture of NK cells with gp100-expressing tumor cells in presence of the high-affinity gp100-specific TCR-Fc^{enh} and TCR-αNKp46-Fc^{enh} fusion proteins
A co-culture of NK cells with untreated and 100 µM gp100 peptide-pulsed MeWo or SK-Mel-5 was set up in the presence of the high-affinity gp100-specific TCR-Fc^{enh}, TCRα-αNKp46-Fc^{enh} and TCRβ-αNKp46-Fc^{enh}. The high-affinity CMV pp65-specific TCR-Fc^{enh} was included for control. Cytotoxicity was analyzed using an LDH release assay following 4 h co-culture. NK cell degranulation and activation were evaluated using flow cytometry by staining for CD107a, CD69, CD137, and intracellular IFNγ or TNFα. CD107a, IFNγ and TNFα were analyzed after 4 h co-culture in presence of Golgi transport

inhibitors. CD69 and CD137 were stained following 24 h co-culture. Significance compared to “no TCR” was analyzed using OneWay ANOVA for each cell line separately using Tukey’s test for multiple comparison. Mean values from 3 independent experiments ± s.e.m. are shown.

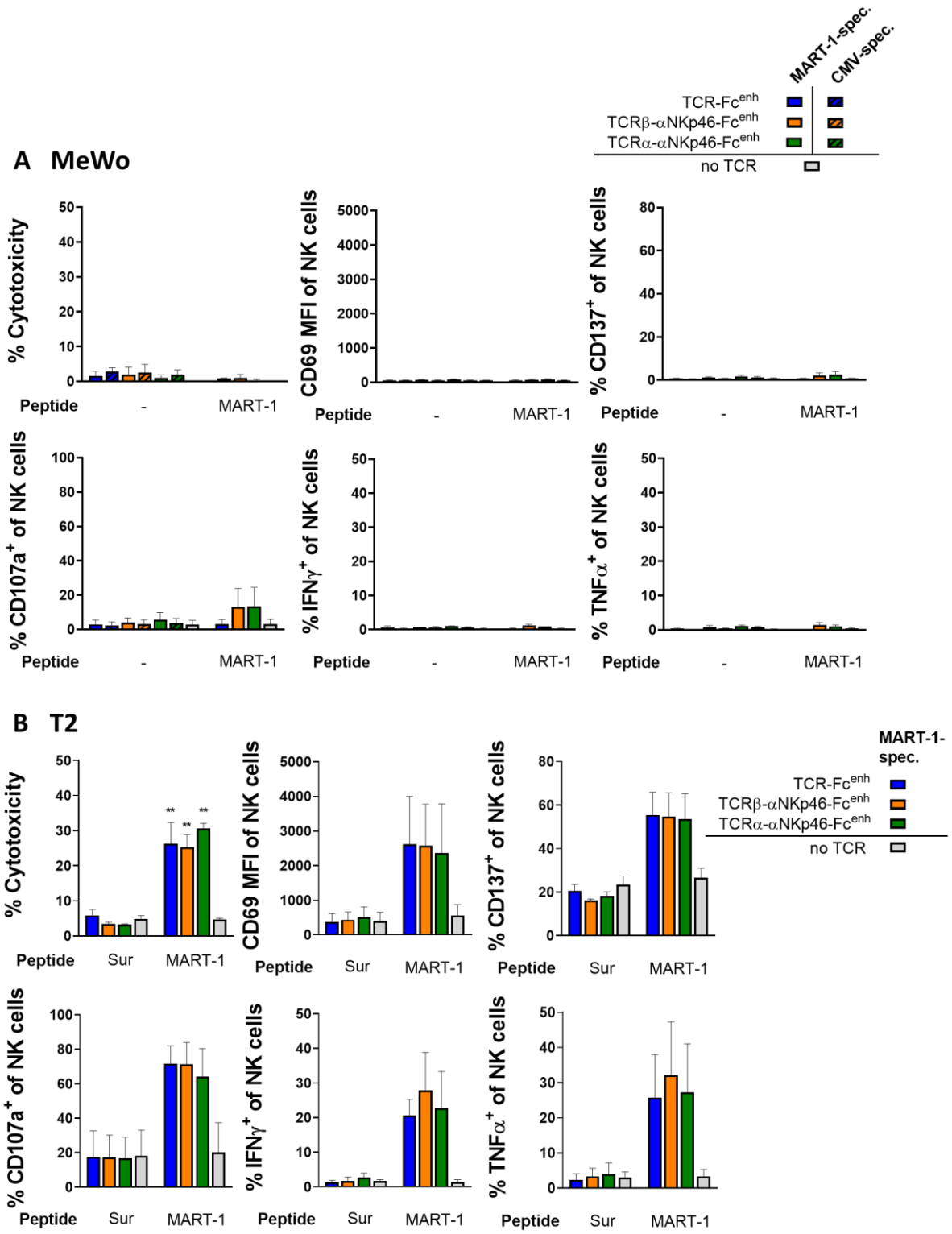

Figure 30: Co-culture of NK cells with MART-1 expressing MeWo and peptide-pulsed T2 cells in presence of high-affinity MART-1-specific TCR-Fc^{enh} and TCR-αNKp46-Fc^{enh} fusion proteins
Untreated and 100 µM MART-1 peptide-pulsed MeWo (A) or T2 (B) cells were co-cultured with NK cells in the presence of the high-affinity MART-1-specific TCR-Fc^{enh}, TCRα-αNKp46-Fc^{enh} and TCRβ-

αNKp46-Fc^{enh} fusion proteins. For control the high-affinity CMV pp65-specific TCR-Fc^{enh} constructs were included. Cytotoxicity was evaluated using an LDH release assay following 4 h co-culture. NK cell degranulation and activation were assessed using flow cytometry by staining for CD107a, CD69, CD137, and intracellular IFNγ or TNFα. CD107a, IFNγ and TNFα were analyzed after 4 h co-culture in presence of Golgi transport inhibitors. CD69 and CD137 were stained following 24 h co-culture. Significance compared to “no TCR” was analyzed using OneWay ANOVA for each cell line separately followed by Tukey’s test for multiple comparison. Mean values from 2 independent experiments ± s.e.m. are shown.

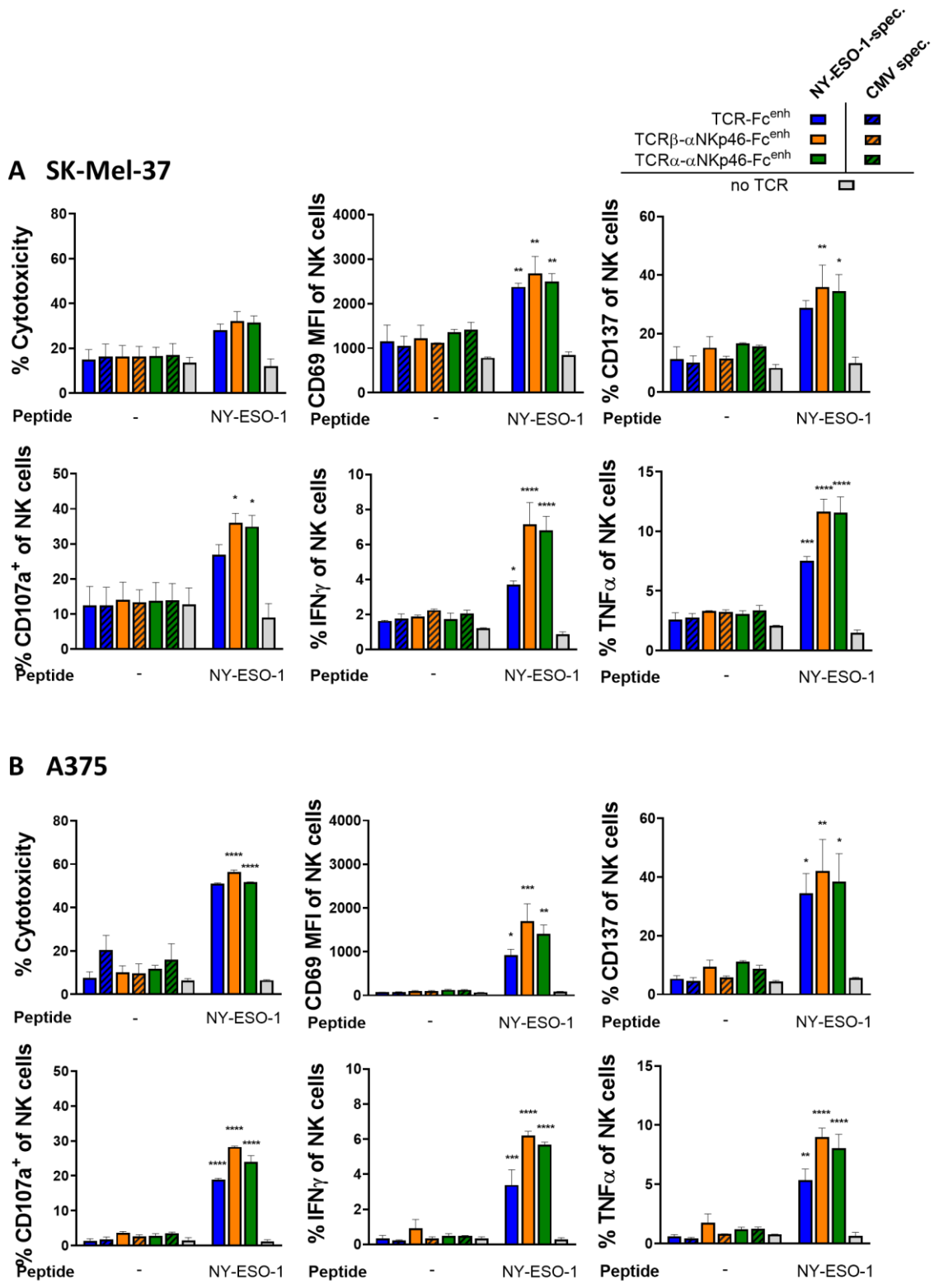

Figure 31: Co-culture of NK cells with NY-ESO-1 expressing tumor cells in presence of the high-affinity NY-ESO-1 specific TCR-Fc^{enh} and TCR-αNKp46-Fc^{enh}
Untreated and 100 µM NY-ESO-1 peptide-pulsed A375 and SK-Mel-37 were co-cultured with NK cells in the presence of the high-affinity NY-ESO-1-specific TCR-Fc^{enh}, TCRα-αNKp46-Fc^{enh} and TCRβ-αNKp46-Fc^{enh}. The high-affinity CMV pp65-specific TCR-Fc^{enh} constructs were included as specificity controls. Target cell lysis was assessed following 4 h co-culture using an LDH release assay. NK cell degranulation and activation were analyzed using flow cytometry by staining for CD107a, CD69, CD137, and intracellular IFNγ or TNFα. CD107a, IFNγ and TNFα were evaluated after 4 h co-culture in presence

of golgi transport inhibitors. CD69 and CD137 were stained following 24 h co-culture without supplements. Significance compared to “no TCR” was analyzed using OneWay ANOVA for each cell line separately followed (?) by Tukey’s test for multiple comparison. Mean values from 2 independent experiments ± s.e.m. are shown.

4 Discussion

MHC-I-restricted antigens are a highly attractive target for tumor immunotherapy as they offer the access to the universe of intracellular antigens that are usually inaccessible using classical antibody-based therapies. In contrast to the cell surface and endosomes (ca. 27%), the intracellular space contains a much greater number of proteins (ca. 73%) (Chandran & Klebanoff, 2019), and most oncogenic driver mutations only affect intracellular proteins. Thus, many different TCR- and T cell-based therapies have been investigated to take advantage of this opportunity. However, not all of them are easily applicable and yet not all patients can benefit from them. One strategy that could be used as an easily applicable off-the-shelf approach is the use of soluble TCR-based therapies. The development of such therapies was hampered for a long time due to inadequate ways of production and TCR affinity maturation. However, meanwhile different protocols and strategies have been adapted to overcome these limitations. Most soluble TCR-based therapies that are currently under investigation are based on a bispecific format linking the TCR-dependent MHC-I recognition site to an αCD3 scFv for T cell redirection and promising results were obtained. Only few studies also demonstrated the possibility to induce ADCC using TCR-Fc fusion constructs (Mosquera et al., 2005; Zheng et al., 2013). This study aimed to further develop such soluble bispecific TCRs for the redirection of NK cells as well as for the redirection of T cells using a new construct format. In contrast to the commonly targeted T cells, targeting of NK cells is thought to offer a faster response with a lower risk of a cytokine release syndrome due to the almost 10 times lower frequency and slightly different cytokine production profile (Demaria et al., 2021; Lian et al., 2021). In general, both cell types are able to migrate and extravasate along chemokine axes guiding them to the tumor site and tumor infiltration was likewise observed for both cells, even though most tumors are characterized by lower NK cell numbers (Cózar et al., 2021; Melero et al., 2014; Ran et al., 2022). In the tumor microenvironment different immunosuppressive mechanisms can decrease their activation and cytotoxic properties. Thus, immunotherapy, such as the TCR-based agents in this thesis, can be further important to counteract this inhibition promoting an effective anti-tumor immune response (Ben-Shmuel et al., 2020; Zhang et al., 2020).

4.1 The therapeutic effect of soluble TCR-Fc fusion proteins depends on TCR affinity and antigen density

To generate soluble bispecific TCRs, a bivalent IgG-like format was adapted that was previously investigated by Wagner and colleagues (Wagner et al., 2019) (Figure 9). Thus, two double disulfide-bridged TCR monomers were fused to the hinge and Fc part of an human IgG1. This design should increase avidity compared to a TCR monomer and might thus help to increase the potency especially for TCRs of lower affinity. Using this bivalent TCR-Fc design

Wagner et al. measured an affinity of 3 µM for the wildtype CMV pp65-specific TCR, while 6 µM were reported for the monovalent form (Wagner et al., 2019). Similar effects were observed in other studies showing that target binding can be increased using TCR constructs of higher valency such as TCR dimers, tetramers or dextramers compared to a monovalent format or compared to TCR constructs of lower valency (Bethune et al., 2017; Low et al., 2012; Mosquera et al., 2005). Furthermore, as mentioned in the introduction, the fusion to an Fc part can increase protein half-life and induce antibody-dependent cellular cytotoxicity (1.2.1). For NK and T cell redirection, different modifications were included in this work such as a mutated glycosylated Fc that is characterized by increased FcγRIIIa binding, which is the ADCC-inducing receptor expressed on NK cells; and the use of scFvs directed against FcγRIIIa or NKp46 for NK cell targeting or against CD3 (clones r3M, $OKT3_{HGL}$, $OKT3_{LGH}$) for T cell targeting. The scFvs were incorporated at two different positions within the bivalent IgG-like format: either C-terminally of TCRβ or C-terminally of TCRα followed by the hinge region. For T cell redirection an aglycan (N297Q) Fc part was used to avoid FcR binding and unspecific T cell activation as observed for the bispecific antibody catumaxomab targeting CD3 and EpCAM (Borlak et al., 2016). This full-length antibody incorporated a functional FcR-binding Fc, which led to fatal hepatotoxicity upon intravenous administration due to cross-linking of T cells with FcR^+ Kupffer cells in the liver also in absence of the target EpCAM. The scFv-containing NK cell-targeting constructs on the other hand incorporated either the aglycan non-FcR-binding Fc to analyze the effect of the scFv alone or the engineered FcR-binding Fc to further boost NK cell activation by engaging more activating NK cell receptors as already observed for an αNKp46-Fc^{enh}-αCD20 NK cell engager (Gauthier et al., 2019).

To analyze the different TCR formats considering their ability to induce NK and T cell redirection, the published cytomegalovirus (CMV) tegument $pp65_{495-503}$ peptide-specific TCR clone was used as a model system. This clone was previously affinity-maturated (Wagner et al., 2019) and available in the natural low-affinity variant of 3 µM and a high-affinity variant of 50 nM (measured in the bivalent TCR-Fc format by surface plasmon resonance). To assess the importance of TCR affinity for a soluble TCR-based therapy, both variants were analyzed in parallel. Initial investigations could demonstrate that the produced bivalent IgG-like TCRs showed a target-specific binding dependent on concentration and TCR affinity (Figure 10) confirming the results obtained by Wagner et al., 2019, which is in agreement with other studies demonstrating stronger target binding following affinity maturation (Li et al., 2005; Zhao et al., 2021). As expected, a similar correlation was observed for NK and T cell redirection upon co-culture with CMV pp65 peptide-pulsed target cells in the presence of the low and high-affinity TCR constructs – as analyzed using the NK cell-redirecting TCR-Fc^{enh} and the T cell-redirecting TCRα-αCD3($OKT3_{HGL}$)-Fc^{aglyc} format (Figure 12-14, Figure 22-25). Thus, the induced response considering target cell lysis, NK and T cell degranulation, NK and T cell

activation and T cell proliferation was likewise dependent on compound concentration and TCR affinity, which matches the results obtained in other studies comparing soluble T cell-targeting TCRs of different affinity (Zhao et al., 2021; Liddy et al., 2012). Additionally, as reported by Liddy et al. analyzing the sensitivity of differently affine, soluble gp100-specific TCR constructs (Liddy et al., 2012), the response was dependent on peptide concentration and thus antigen density, whereas the low-affinity variant was characterized by a strongly decreased sensitivity upon lower peptide concentration compared to the high-affinity construct (Figure 13, Figure 23). The same accounts for the co-culture using peptide-pulsed MCF-7 in comparison to peptide-pulsed T2 cells (Figure 14), as MCF-7 were characterized by a lower rate of peptide presentation. This lower peptide presentation is probably due to a lower HLA-A2 expression and expression of the TAP peptide transporter necessary for translocation of cytosolic peptides into the ER. Thus, this transporter enables MHC-I loading with endogenous high-affinity peptides making MCF-7 slightly less susceptible for a peptide pulse compared to T2 cells lacking TAP. Nevertheless, both the NK and T cell targeting constructs, were functional not only using peptide-pulsed T2 cells optimized for peptide-presentation but also using the physiologically more relevant breast cancer cell line MCF-7 thus demonstrating a broad clinical potential. However, as the effect was TCR affinity-dependent and a higher sensitivity was observed for the high-affinity variant, a high TCR affinity seems to be important for soluble TCR-based therapies especially for tumor cells with lower degrees of peptide presentation.

4.2 A potent NK cell redirection is gained using a combination of different NK cell binding moieties

Following detailed investigation of the different NK cell targeting constructs, a correlation was observed between NK cell binding and response in the co-culture (Figure 15). Thus, little to no effect was observed in the co-culture for the constructs that bound the NK cells only via the scFv, which were characterized by a strongly decreased NK cell binding compared to the constructs bearing the engineered glycosylated Fc part. Furthermore, the combination of two different NK cell binding moieties, the glycosylated “enhanced” Fc part and a scFv targeting FcγRIIIa or NKp46, did indeed further improve the response in the co-culture considering target cell lysis, NK cell degranulation and activation compared to the TCR-Fc^{enh} construct. This additive effect probably results from increased NK cell receptor engagement and clustering as expected from results obtained in the study evaluating an αNKp46-Fc^{enh}-αCD20 NK cell engager bearing an Fc part with enhanced FcγRIIIa binding, which showed stronger tumor cell lysis compared to a variant with an aglycan Fc part incapable of FcγRIIIa binding or compared to a CD20-specific monoclonal antibody without additional scFv (Gauthier et al., 2019). However, in case of the TCRβ-αCD16-Fc^{enh}, this increased response was accompanied by an

unspecific NK cell activation and NK cell degranulation that was not observed for the sibling constructs that used αNKp46 instead of αCD16 in the same position or that incorporated the αCD16 scFv at the C-terminus of TCRα (TCRα-αCD16-Fc^{enh}). Thus, scFv positioning and the targeted receptors both seem to be important factors for fine-tuning NK cell activation and redirection and TCRβ-αCD16-Fc^{enh} probably induced a too strong receptor clustering or possibly cross-linked two NK cells via both scFvs, thereby triggering NK cell activation without target engagement. The risk that bivalent immune cell engagers can induce unspecific effector cell activation is well known and was already observed for some bivalent αCD3 formats (Dickopf et al., 2020; Moore et al., 2015; Wu & Cheung, 2018). However, this is not always the case and seems to be format-dependent. In another study analyzing different bispecific IgG-scFv formats by fusing an scFv C- or N-terminal of an IgG's light or heavy chain, they also found that ADCC activity was dependent on scFv positioning and fusion of the scFv C-terminal of the C_H3 led to loss of this function probably due to steric hindrance, further demonstrating the influence of scFv positioning (Croasdale et al., 2012; Schanzer et al., 2014). Nevertheless, upon TCR titration in the co-culture, the highest sensitivity was observed for TCRα-αNKp46-Fc^{enh} and TCRβ-αNKp46-Fc^{enh}, which induced a strong and target-specific response (Figure 16). Additionally, this response was comparable or even stronger compared to the response induced by commonly used monoclonal antibodies, demonstrating the great potential of soluble TCR constructs. Thus, the response was greater than that induced by the ADCC-mediating mAb cetuximab, which targets EGFR that is expressed in low levels by MCF-7, and comparable to that induced by the ADCC$^+$ mAb trastuzumab targeting HER2, which is strongly expressed by MCF-7.

4.3 TCRα-αCD3(OKT3$_{HGL}$)-Fc^{aglyc} enables potent T cell redirection

To choose the best TCR construct for T cell redirection, they were analyzed for T cell binding by flow cytometry. Within the six formats that incorporated one of the three different αCD3 scFv clones (r3M, OKT3$_{HGL}$, OKT3$_{LGH}$) at the C-terminus of TCRβ or TCRα, TCRα-αCD3(OKT3$_{HGL}$)-Fc^{aglyc} showed the strongest binding (Figure 20) and was thus chosen for further evaluation in the co-culture. As mentioned above, the response mediated by bispecific constructs considering target cell lysis, T cell activation, T cell degranulation and T cell proliferation was dependent on TCR affinity, construct concentration and antigen density. Using higher TCR concentrations the TCR constructs also induced some antigen-unspecific T cell degranulation, activation and proliferation and to a lower degree also unspecific target cell lysis (Figure 22, Figure 24, Figure 25). This might be due to the bivalent construct design. As mentioned before, some other bivalent CD3-specific agents were also reported to induce unspecific T cell activation (Dickopf et al., 2020; Moore et al., 2015; Z. Wu & Cheung, 2018).

However, this was not always the case and seemed to depend on the exact format and CD3 affinity. Interestingly, the observed unspecific response was often slightly higher for the high-affinity construct compared to the wildtype variant, indicating that affinity maturation might have reduced specificity and the unspecific effect was not only due to the construct format. However, this was in contrast to the analyzed TCR target binding, as no unspecific binding was observed towards survivin peptide-pulsed T2 cells or survivin peptide-tethered MHC-Fc fusion proteins (Figure 10). Therefore, it seems likely that unspecific T cell activation resulted from unspecific TCR binding as well as unspecific CD3ε crosslinking. The original mouse IgG2a antibody OKT3, that is the basis for the scFv incorporated in bispecific constructs used here, is readily able activate human T cells upon crosslinking and even induce activation-induced cell death (Abramowicz et al., 1989; Carpenter et al., 2000; Herold et al., 2003; Martin et al., 2013). Nevertheless, unspecific T cell activation can often be avoided using lower concentrations, which was the case for TCRα-αCD3($OKT3_{HGL}$)-Fc^{aglyc} as lower concentration (≤ 0.6 nM) remained antigen-specific and still induced a strong, almost saturated response. This response was furthermore stronger compared to equimolar concentrations of a commonly used bispecific T cell engager format targeting CD19 (αCD19-Fc^{aglyc}-αCD3) upon co-culture with T2 cells (Figure 22) or targeting EpCAM (αEpCAM-Fc^{aglyc}-αCD3) upon co-culture with MCF-7 (Figure 24, Figure 25), further demonstrating the potential of soluble TCR constructs.

When redirecting T cell using bispecific agents, co-stimulation might also play an important role depending on the co-stimulatory receptors expressed on the target cell (Hornig et al., 2013; Müller et al., 2008; Sapski et al., 2017; Warwas et al., 2021). Thus, when using untransfected peptide-pulsed MCF-7, addition of a co-stimulatory BiMab targeting EpCAM (αEpCAM-Fc^{aglyc}-αCD28) strongly improved the performance especially for the low-affinity TCR variant. In contrast to outdated co-stimulatory anti-CD28 antibodies that acted target cell-independent potentially leading to a cytokine storm, bispecific tumor-targeted co-stimulatory antibodies or TNF ligand fusion proteins were shown to be a potent and safe alternative avoiding severe toxicities (Dubrot et al., 2010; Hornig et al., 2013; Müller et al., 2008; Sapski et al., 2017; Suntharalingam et al., 2006; Warwas et al., 2021). Lesser effects of the co-stimulatory BiMAb were observed when using the CD80 and CMV pp65 peptide-tethered mSCT-transfected MCF-7 cells as targets, probably due to the presence of CD80 expressing cells. CD80 acts as a co-stimulatory ligand for CD28 expressed on T cells and was introduced to generate an optimal target cell for T cell redirection. Even though no co-expression of CD80 and pMHC-mSCT was observed following stable transfection, co-stimulation could also have been delivered by neighbouring cells. Another difference, that might have diminished the effect of co-stimulation for the mSCT transfectants might be the much higher levels of pMHC-I presentation as compared to peptide-pulsed MCF-7, making the TCR construct itself more potent. In conclusion, a combination therapy with co-stimulatatory BiMabs might be beneficial

or even required for soluble T cell-targeting TCR-based bispecific agents depending on the target cells.

When comparing the sensitivity of the high-affinity CMV pp65-specific TCRα-αCD3(OKT3$_{HGL}$)-Fc^{aglyc} with the FDA-approved monovalent gp100-specific ImmTAC TCR-αCD3 construct, it can be noted that the induced response in this study was reached at 1-10 µM in co-cultures with peptide-pulsed T2 cells as estimated by cytotoxicity, T cell degranulation, T cell activation and proliferation after 24 h (Figure 23). The ImmTAC construct on the other hand reached functional saturation using ~100 nM peptide-pulsed T2 cells as evaluated by IFNγ ELISpot after 24 h co-culture (Liddy et al., 2012). By contrast, the TCR affinity as measured by SPR of the gp100-specific TCR clone was with 30 pM around 1700 times higher than that of the CMV pp65-specific TCR clone with an apparent K_D value of 50 nM in the bivalent format (Liddy et al., 2012; Wagner et al., 2019). Another gp100-specific TCR clone variant with 43 nM affinity that was tested in parallel with the TCR of 30 pM also showed a lower sensitivity in terms of IFNγ ELISpot response with an estimated 1 µM saturation (Liddy et al., 2012). Hence, in functional read-out assays reflecting differences in avidity rather than affinity the bivalent CMV-specific TCRα-αCD3-Fc^{aglyc} construct evaluated in this study performed only 10-100fold less efficiently than the high-affinity gp100-specific ImmTAC fusion protein and similarly to the gp100-specific clone with 43 nM affinity.

When comparing EC_{50} values obtained from TCR construct titrations, TCRα-αCD3(OKT3$_{HGL}$)-Fc^{aglyc} achieved EC_{50} values of 2-8 pM in co-cultures with peptide-pulsed T2 cells (Figure 22) while the high-affinity gp100-specific ImmTAC gained values in the 40 pM range. However, the ImmTAC construct was evaluated by Liddy et al., 2012, using melanoma cells with an endogenous antigen expression of less than 70 epitopes, which is hardly comparable to peptide-pulsed T2 cells. In co-culture experiments with peptide pulsed MCF-7 cells, the EC_{50} values obtained for T cell activation mediated by the high-affinity Ra14 TCRα-αCD3(OKT3$_{HGL}$)-Fc^{aglyc} construct were also considerably higher ranging between 40-230 pM (Figure 24), suggesting that the number of cognate pMHC-I complexes is critical for functional efficacy. Thus, to enable a better comparison and evaluation of the overall potencies of bispecific CMV and gp100-specific TCR constructs further experiments will be required for example by using exactly the same construct design as in the gp100-TCR x anti-CD3ε scFv ImmTACgp100 construct and the use of the same target cells for peptide and TCR titration experiments.

4.4 Soluble NK and T cell-redirecting TCR-Fc fusion proteins mediate tumor cell lysis in a 3D culture model

In co-cultures with CMV pp65 peptide-tethered mSCT transfected MCF-7 cells the low- and high-affinity, both NK and T cell-targeting constructs induced an efficient response. Also when using MCF-7/mSCT cells to set up a 3-dimensional co-culture with tumor spheroids for more *in vivo*-like conditions (Jeppesen et al., 2017; Weeber et al., 2017), the different high-affinity NK (TCR-Fc^{enh}, TCRα-αNKp46-Fc^{enh}, TCRβ-αNKp46-Fc^{enh}) and T cell-targeting (TCRα-αCD3(OKT3$_{HGL}$)-Fc^{aglyc}) constructs also induced target cell lysis, NK and T cell degranulation and activation, and T cell proliferation even though the overall response appeared slightly lower compared to the experiments before using the conventional 2-dimensional monolayer, indicating that the spheroid architecture dampens the immune response because initially only tumor cells at the outside of spheroids can be attacked by NK or T cells, respectively. Similar to the 2-dimensional cultures with MCF-7/mSCT cells, addition of the αEpCAM-Fc^{aglyc}-αCD28 co-stimulatory BiMab only had a moderate effect on T cell activation and killing. Nevertheless, the results indicate a high potential for further development.

4.5 TAA-specific NK cell-targeting TCR-Fc fusion proteins are incapable to induce a response towards tumor cells with endogenous TAA expression levels

As the results obtained from the CMV model system strongly indicated a dependence on TCR affinity and antigen density on target cells, the results of this work have been verified using different tumor associated antigens and tumor cells with endogenous antigen expression levels. Hence, three different TCR clones were chosen, that were previously also affinity-maturated or mutated: the gp100-specific ImmTAC TCR clone IMCgp100 targeting the HLA-A*02:01-bound gp100$_{280-288}$ peptide (Boudousquie et al., 2017; Li et al., 2005), clone 1G4 directed against the HLA-A*02:01-bound NY-ESO-1$_{157-165}$ peptide (Robbins et al., 2008) and clone DMF5 targeting HLA-A*02:01-bound Mart-1$_{26-35}$ (Johnson et al., 2006; Robbins et al., 2008). These TCR clones were then transferred to the TCR-Fc^{enh} format and evaluated for target binding towards tumor cells endogenously expressing the matching HLA allele and TAA. Peptide presentation was not verified in this study as the chosen tumor cell lines were already used in previous studies in a similar TCR-based context (Chang et al., 2011; Ichikawa et al., 2020; Liddy et al., 2012; McCormack et al., 2013; Zhao et al., 2021). Even though the TAA-specific TCR-Fc clones were all functional as they showed a target-specific binding in ELISA towards peptide-tethered MHC-Fc fusion proteins and towards peptide-pulsed T2 cells (Figure 28), however, none of the TCR clones, neither the wildtype variants nor the affinity-maturated

variants, did mediate detectable binding towards the matching untreated tumor cell line. Binding was only observed upon a peptide pulse for the maturated gp100- and NY-ESO-1-specific TCR clones, but not for the wildtype variants and not for the wildtype nor maturated MART-1-specific TCR clone using the chosen cell lines. However, it cannot be excluded that the chosen cell lines are characterized by a particularly low peptide presentation, which could abrogate the benefit of a stronger target binding mediated by the bivalent TCR-Fc design as a bivalent binding requires two antigens in rather close proximity. Interestingly, when looking at the results obtained from ELISA and flow cytometry in more detail, it can be noticed that the relative target binding compared to the high-affinity CMV pp65-specific TCR clone did not exactly match the published K_D values. For the wildtype MART-1-specific TCR clone DMF5 for example an affinity constant of about 30 nM was measured in previous studies by ELISA and flow cytometry, however, the DMF5 TCR-Fc construct of this study showed a weaker binding with an approximately 10 times higher EC_{50} value compared to the high-affinity CMV pp65-specific TCR clone Ra14 which was actually characterized by a rather similar affinity constant of 50 nM in the bivalent format (Malecek et al., 2014; Sádio et al., 2020). On the other hand, the high-affinity gp100-specific TCR clone showed a comparable binding in ELISA and an around 20-fold stronger binding in flow cytometry as estimated comparing the EC_{50} values, which is in contrast to the published 1700-fold lower K_D value of 30 pM (Liddy et al., 2012). In case of the affinity-maturated NY-ESO-1-specific TCR clone 1G4, the EC_{50} value were 10 times higher in ELISA, indicating a lower affinity, but 4.6 fold lower by flow cytometry, which would indicate a higher affinity, compared to the high-affinity CMV pp65-specific TCR. The published K_D value of affinity-maturated TCR 1G4 was reported to be about 10-fold higher with a K_D of 750 nM, which is similar to the difference observed in ELISA in this study (Robbins et al., 2008). In this case it is possible that the soluble pMHC molecule used in the ELISA assay not precisely matched the conformation of peptide-loaded HLA-A*02:01 molecules presented on the cell surface of T2 cells. Furthermore, it seems possible, that the chosen format or production system might not be optimal for every TCR clone potentially resulting in improper folding and loss of affinity. One study for example observed that TCR glycosylation had an influence on TCR affinity (Rollins et al., 2022). In this study however, the *N*-glycosylation sites within the TCR constant domains were mutated, since TCR *N*-glycosylation of the soluble CMV pp65-specific TCR-Fc construct had no obvious impact on TCR affinity but on the other hand increased production yields (Wagner et al., 2019). The ImmTAC TCR construct for example does not contain these aglycan mutations (sequence in patent US 2020/0040055 A1), but was produced in *E. coli* which usually also does not mediate *N*-glycosylation (Liddy et al., 2012).

Nevertheless, as expected from the non-detectable binding of untreated melanoma cell lines, no response was induced upon co-culture of NK cells with the matching tumor cells in the presence of the NK cell-targeting high-affinity TAA-specific TCR-Fc^{enh}, TCRα-αNKp46-Fc^{enh} or

TCRβ-αNKp46-Fc^{enh} constructs when no peptide was added (Figure 29, Figure 30, Figure 31). A response was detected for the gp100- and NY-ESO-specific TCR when the melanoma cells were pulsed with the matching peptide. In case of MART-1, no response was detected towards MART-1 peptide-pulsed MeWo, however towards MART-1 peptide-pulsed T2 cells. Thus, all TAA-specific NK cell-targeting constructs are functional and all cell lines are in general susceptible towards NK cell-mediated ADCC, but the antigen density of the chosen cells seems too low and in case of MART-1 the unexpected weak target binding is probably negatively contributing as well. To assess if the optimized NK cell-targeting TCR constructs can be used for other tumor cells with higher antigen density, further evaluation would be required.

These negative results obtained from tumor cell binding and NK cell redirection are especially unexpected in case of the ImmTAC-derived high-affinity gp100-specific TCR clone as this clone was shown to be highly potent in the T cell-targeting ImmTAC TCR format using the same cell lines for evaluation (Liddy et al., 2012). Even when increasing the concentration to 30 nM TCR construct no effect was observed, while 1 nM were found to be saturated for the ImmTAC construct (Liddy et al., 2012). Thus, the TCR clone and the cell lines itself should be sufficient and the negative response might be due to other problems, concerning the produced TCR as mentioned above, the TCR-Fc format or the NK cell redirection in contrast to T cell redirection. In the CMV model used in this work, NK cell redirection also required higher concentrations of TCR construct than T cell redirection, indicating that NK cell-mediated effects might be less sensitive. Compound concentrations greater than 30 nM however, are not feasible in this setting, as this would quickly exceed the production capacities. Nevertheless, a co-culture with a T cell-targeting TAA-specific TCRα-αCD3(OKT3$_{HGL}$)-Fc^{aglyc} construct could help to answer the question of higher T cell sensitivity as compared with NK cells. Furthermore, a gp100-specific monovalent TCR-αCD3 format similar to that of the ImmTAC design could help to assess if the produced TCR is as potent as the FDA-approved ImmTAC TCR and would thus answer the question if there are potential problems with the produced TCR itself, such as slightly different protein folding resulting from mutation of the *N*-glycosylation sites, resulting from the second disulfide bridge, or resulting from the chosen production system, that would also explain the lower target binding observed. In this case a more detailed trouble-shooting would be required.

Considering the construct format there are two other studies which evaluated different TCR-Fc formats. One study analyzed the ImmTAC-derived NY-ESO-1-specific TCR clone within a monovalent T cell-targeting TCR-Fc-αCD3 fusion protein and found this to be less potent than the smaller Fc-less TCR-αCD3 ImmTAC construct as it required at least 10 µg/ml (about 60 nM) to be saturated after 48 h co-culture with NY-ESO-1 expressing A375 (Zhao et al., 2021).

Thus, the authors reasoned that the bigger molecular size resulting from the Fc fusion might have dampened the T cell-activating effect. Similar effects were observed in the second study that evaluated different NY-ESO-1-specific TCR-based T cell engager formats (McCormack et al., 2013). The authors reported that a monovalent TCR-IgG format in which one arm was directed against CD3 and the other Fab arm was replaced with the TCR was less potent or even completely ineffective considering T cell redirection compared to smaller monovalent Fc-less constructs including an ImmTAC-like TCR-scFv design and a TCR-Fab. Thus, it was likewise concluded that the bigger size and the more rigid structure of the IgG-like design are suboptimal to fit in the immunological synapse (McCormack et al., 2013).The influence of construct size for example was already shown to be an important factor for different bispecific T cell engagers, as a smaller more compact molecule might more easily penetrate the immunological synapse (Chen et al., 2021; Dickopf et al., 2019, 2020). Using fluorescence microscopy, it was shown that dextrans smaller than 4 nm could rather freely diffuse into the immune synapse of NK and T cells while 10 to 13 nm dextrans were already retained by up to 50 % (Cartwright et al., 2014). Likewise, smaller antibody fragments penetrated the IS more easily than full-length antibodies. Thus, these studies indicate that the relatively large TCR-Fc constructs might as well be suboptimal for NK and T cell redirection and a smaller format design could potentially improve the potency especially for the TAA-specific NK cell-targeting constructs. To maintain the additive effect observed for simultaneous targeting of FcγRIII and NKp46, a potential format that could be investigated is a single TCR or a TCR F(ab')$_2$ fused to αCD16 (αFcγRIII) *and* αNKp46 scFvs. In general, another possibility that could improve the potency of soluble TCR constructs could be the generation of TCR multimers of even higher valency as already used for staining purposes (Bethune et al., 2017; Low et al., 2012). This could be done using a dextramer backbone that typically contains multiple binding sites and thus could be loaded with TCR monomers and αNKp46 and αCD16, or αCD3 scFvs. The ratio between TCR monomer and effector cell binding moiety could be adapted as required to avoid extensive effector cell crosslinking resulting in unspecific activation. In the course of this work a pentamerization domain was investigated (Özbek S, Engel J, Stetefeld J. EMBO J. 21:5960-5968, 2002) to assemble five TCR–scFv monomers into a pentamer. Pentamers were difficult to express and did not yield an improved binding to CMV-A2 SCTs in ELISA (data not shown). Nevertheless, in future experiments other ways to increase the avidity of TCR binding will be evaluated by using the molecular framework of IgM molecules in order to assemble five TCRα/β-IgM-Fc to a pentameric decavalent complex. An NK/T cell-activating scFv will be fused with the J chain that usually assembles in a 1:1 ratio with a pentameric IgM molecule.

Taken together, TCR-based bispecific agents seem to offer a great potential for T and NK cell redirection leading to target cell lysis, NK and T cell degranulation, NK and T cell activation and T cell proliferation. This study is the first on this scale to demonstrate this for NK cell

redirection as well. The observed immune responses were verified using different antigens and target cells. However, as the obtained results were only observed using peptide-pulsed cells and not towards tumor cells endogenously expressing the target antigen, further investigations are necessary to verify that the produced TAA-specific TCRs are completely functional and to evaluate different formats that could potentially improve the overall response.

5 References

Abel, A. M., Yang, C., Thakar, M. S., & Malarkannan, S. (2018). Natural killer cells: Development, maturation, and clinical utilization. *Frontiers in Immunology*, *9*(AUG), 1869. https://doi.org/10.3389/FIMMU.2018.01869/BIBTEX

Abramowicz, D., Schandene, L., Goldman, M., Crusiaux, A., Vereerstraeten, P., de Pauw, L., Wybran, J., Kinnaert, P., Dupont, E., & Toussaint, C. (1989). Release of tumor necrosis factor, interleukin-2, and gamma-interferon in serum after injection of OKT3 monoclonal antibody in kidney transplant recipients. *Transplantation*, *47*(4), 606–608. https://doi.org/10.1097/00007890-198904000-00008

Ataie, N., Xiang, J., Cheng, N., Brea, E. J., Lu, W., Scheinberg, D. A., Liu, C., & Ng, H. L. (2016). Structure of a TCR-Mimic Antibody with Target Predicts Pharmacogenetics. *Journal of Molecular Biology*, *428*(1), 194–205. https://doi.org/10.1016/J.JMB.2015.12.002

Barrow, A. D., Martin, C. J., & Colonna, M. (2019). The natural cytotoxicity receptors in health and disease. *Frontiers in Immunology*, *10*(MAY), 909. https://doi.org/10.3389/FIMMU.2019.00909/BIBTEX

Bassan, D., Gozlan, Y. M., Sharbi-Yunger, A., Tzehoval, E., & Eisenbach, L. (2019). Optimizing T-cell receptor avidity with somatic hypermutation. *International Journal of Cancer*, *145*(10), 2816–2826. https://doi.org/10.1002/IJC.32612

Ben-Shmuel, A., Biber, G., & Barda-Saad, M. (2020). Unleashing Natural Killer Cells in the Tumor Microenvironment–The Next Generation of Immunotherapy? *Frontiers in Immunology*, *11*, 275. https://doi.org/10.3389/FIMMU.2020.00275/BIBTEX

Bethune, M. T., Comin-Anduix, B., Fu, Y. H. H., Ribas, A., & Baltimore, D. (2017). Preparation of peptide–MHC and t-cell receptor dextramers by biotinylated dextran doping. *BioTechniques*, *62*(3), 123–130. https://doi.org/10.2144/000114525/ASSET/IMAGES/LARGE/FIGURE4.JPEG

Blunt, M. D., & Khakoo, S. I. (2020). Activating killer cell immunoglobulin-like receptors: Detection, function and therapeutic use. *International Journal of Immunogenetics*, *47*(1), 1–12. https://doi.org/10.1111/IJI.12461

Boesch, A. W., Miles, A. R., Chan, Y. N., Osei-Owusu, N. Y., & Ackerman, M. E. (2017). IgG Fc variant cross-reactivity between human and rhesus macaque FcγRs. *MAbs*, *9*(3), 455. https://doi.org/10.1080/19420862.2016.1274845

Borlak, J., Länger, F., Spanel, R., Schöndorfer, G., & Dittrich, C. (2016). Immune-mediated

liver injury of the cancer therapeutic antibody catumaxomab targeting EpCAM, CD3 and Fcγ receptors. *Oncotarget*, *7*(19), 28059. https://doi.org/10.18632/ONCOTARGET.8574

Borst, J., Ahrends, T., Bąbała, N., Melief, C. J. M., & Kastenmüller, W. (2018). CD4+ T cell help in cancer immunology and immunotherapy. *Nature Reviews Immunology*, *18*(10), 635–647. https://doi.org/10.1038/S41577-018-0044-0

Boudousquie, C., Bossi, G., Hurst, J. M., Rygiel, K. A., Jakobsen, B. K., & Hassan, N. J. (2017). Polyfunctional response by ImmTAC (IMCgp100) redirected CD8+ and CD4+ T cells. *Immunology*, *152*(3), 425–438. https://doi.org/10.1111/IMM.12779

Boulter, J. M., Glick, M., Todorov, P. T., Baston, E., Sami, M., Rizkallah, P., & Jakobsen, B. K. (2003). Stable, soluble T-cell receptor molecules for crystallization and therapeutics. *Protein Engineering*, *16*(9), 707–711. https://doi.org/10.1093/PROTEIN/GZG087

Bray, F., Laversanne, M., Weiderpass, E., & Soerjomataram, I. (2021). The ever-increasing importance of cancer as a leading cause of premature death worldwide. *Cancer*, *127*(16), 3029–3030. https://doi.org/10.1002/CNCR.33587

Brinkhaus, M., Douwes, R. G. J., Bentlage, A. E. H., Temming, A. R., de Taeye, S. W., Tammes Buirs, M., Gerritsen, J., Mok, J. Y., Brasser, G., Ligthart, P. C., van Esch, W. J. E., Verheesen, P., de Haard, H., Rispens, T., & Vidarsson, G. (2020). Glycine 236 in the Lower Hinge Region of Human IgG1 Differentiates FcγR from Complement Effector Function. *Journal of Immunology (Baltimore, Md.: 1950)*, *205*(12), 3456–3467. https://doi.org/10.4049/JIMMUNOL.2000961

Brown, P. (2018). Blinatumomab for MRD+ B-ALL: the evidence strengthens. *Blood*, *131*(14), 1497–1498. https://doi.org/10.1182/BLOOD-2018-02-830364

Cameron, B. J., Gerry, A. B., Dukes, J., Harper, J. V., Kannan, V., Bianchi, F. C., Grand, F., Brewer, J. E., Gupta, M., Plesa, G., Bossi, G., Vuidepot, A., Powlesland, A. S., Legg, A., Adams, K. J., Bennett, A. D., Pumphrey, N. J., Williams, D. D., Binder-Scholl, G., … Jakobsen, B. K. (2013). Identification of a Titin-derived HLA-A1-presented peptide as a cross-reactive target for engineered MAGE A3-directed T cells. *Science Translational Medicine*, *5*(197). https://doi.org/10.1126/SCITRANSLMED.3006034

Campillo-Davo, D., Flumens, D., & Lion, E. (2020). The Quest for the Best: How TCR Affinity, Avidity, and Functional Avidity Affect TCR-Engineered T-Cell Antitumor Responses. *Cells*, *9*(7). https://doi.org/10.3390/CELLS9071720

Carpenter, P. A., Pavlovic, S., Tso, J. Y., Press, O. W., Gooley, T., Yu, X.-Z., & Anasetti, C. (2000). Non-Fc receptor-binding humanized anti-CD3 antibodies induce apoptosis of activated human T cells. *Journal of Immunology (Baltimore, Md. : 1950)*, *165*(11), 6205–

6213. https://doi.org/10.4049/JIMMUNOL.165.11.6205

Cartwright, A. N. R., Griggs, J., & Davis, D. M. (2014). The immune synapse clears and excludes molecules above a size threshold. *Nature Communications 2014 5:1*, *5*(1), 1–13. https://doi.org/10.1038/ncomms6479

Cassioli, C., & Baldari, C. T. (2019). A Ciliary View of the Immunological Synapse. *Cells 2019, Vol. 8, Page 789*, *8*(8), 789. https://doi.org/10.3390/CELLS8080789

Chandran, S. S., & Klebanoff, C. A. (2019). T cell receptor-based cancer immunotherapy: Emerging efficacy and pathways of resistance. In *Immunological Reviews*. https://doi.org/10.1111/imr.12772

Chang, G. Y., Kohrt, H. E., Stuge, T. B., Schwartz, E. J., Weber, J. S., & Lee, P. P. (2011). Cytotoxic T lymphocyte responses against melanocytes and melanoma. *Journal of Translational Medicine*, *9*(1), 122. https://doi.org/10.1186/1479-5876-9-122

Chang, H. C., Bao, Z. Z., Yao, Y., Tse, A. G. D., Goyarts, E. C., Madsen, M., Kawasaki, E., Brauer, P. P., Sacchettini, J. C., Nathenson, S. G., & Reinherz, E. L. (1994). A general method for facilitating heterodimeric pairing between two proteins: application to expression of alpha and beta T-cell receptor extracellular segments. *Proceedings of the National Academy of Sciences of the United States of America*, *91*(24), 11408–11412. https://doi.org/10.1073/PNAS.91.24.11408

Chen, L., & Flies, D. B. (2013). Two-signal model Molecular mechanisms of T cell co-stimulation and co-inhibition. *NATURE REVIEWS | IMMUNOLOGY*, *13*. https://doi.org/10.1038/nri3405

Chen, W., Yang, F., Wang, C., Narula, J., Pascua, E., Ni, I., Ding, S., Deng, X., Chu, M. L. H., Pham, A., Jiang, X., Lindquist, K. C., Doonan, P. J., Van Blarcom, T., Yeung, Y. A., & Chaparro-Riggers, J. (2021). One size does not fit all: navigating the multi-dimensional space to optimize T-cell engaging protein therapeutics. *MAbs*, *13*(1). https://doi.org/10.1080/19420862.2020.1871171/SUPPL_FILE/KMAB_A_1871171_SM6911.ZIP

Chester, C., Fritsch, K., & Kohrt, H. E. (2015). Natural Killer Cell Immunomodulation: Targeting Activating, Inhibitory, and Co-stimulatory Receptor Signaling for Cancer Immunotherapy. *Frontiers in Immunology*, *6*(DEC), 601. https://doi.org/10.3389/FIMMU.2015.00601

Chiu, M. L., Goulet, D. R., Teplyakov, A., & Gilliland, G. L. (2019). Antibody Structure and Function: The Basis for Engineering Therapeutics. *Antibodies (Basel, Switzerland)*, *8*(4), 55. https://doi.org/10.3390/ANTIB8040055

Cichocki, F., Grzywacz, B., & Miller, J. S. (2019). Human NK cell development: One road or many? *Frontiers in Immunology*, *10*(AUG), 2078. https://doi.org/10.3389/FIMMU.2019.02078/BIBTEX

Coënon, L., & Villalba, M. (2022). From CD16a Biology to Antibody-Dependent Cell-Mediated Cytotoxicity Improvement. *Frontiers in Immunology*, *0*, 2731. https://doi.org/10.3389/FIMMU.2022.913215

Connerotte, T., Van Pel, A., Godelaine, D., Tartour, E., Schuler-Thurner, B., Lucas, S., Thielemans, K., Schuler, G., & Coulie, P. G. (2008). Functions of Anti-MAGE T-cells induced in melanoma patients under different vaccination modalities. *Cancer Research*, *68*(10), 3931–3940. https://doi.org/10.1158/0008-5472.CAN-07-5898

Cooper, M. A., Fehniger, T. A., & Caligiuri, M. A. (2001). The biology of human natural killer-cell subsets. *Trends in Immunology*, *22*(11), 633–640. https://doi.org/10.1016/S1471-4906(01)02060-9

Cox, M. A., Harrington, L. E., & Zajac, A. J. (2011). Cytokines and the inception of CD8 T cell responses. *Trends in Immunology*, *32*(4), 180–186. https://doi.org/10.1016/J.IT.2011.01.004

Cózar, B., Greppi, M., Carpentier, S., Narni-Mancinelli, E., Chiossone, L., & Vivier, E. (2021). Tumor-infiltrating natural killer cells. *Cancer Discovery*, *11*(1), 34. https://doi.org/10.1158/2159-8290.CD-20-0655

Croasdale, R., Wartha, K., Schanzer, J. M., Kuenkele, K. P., Ries, C., Mayer, K., Gassner, C., Wagner, M., Dimoudis, N., Herter, S., Jaeger, C., Ferrara, C., Hoffmann, E., Kling, L., Lau, W., Staack, R. F., Heinrich, J., Scheuer, W., Stracke, J., … Klein, C. (2012). Development of tetravalent IgG1 dual targeting IGF-1R–EGFR antibodies with potent tumor inhibition. *Archives of Biochemistry and Biophysics*, *526*(2), 206–218. https://doi.org/10.1016/J.ABB.2012.03.016

Cui, W., & Kaech, S. M. (2010). Generation of effector CD8+ T cells and their conversion to memory T cells. *Immunological Reviews*, *236*(1), 151. https://doi.org/10.1111/J.1600-065X.2010.00926.X

Curtsinger, J. M., & Mescher, M. F. (2010). *Inflammatory Cytokines as a Third Signal for T Cell Activation*. https://doi.org/10.1016/j.coi.2010.02.013

Dahan, R., & Reiter, Y. (2012). T-cell-receptor-like antibodies - Generation, function and applications. *Expert Reviews in Molecular Medicine*, *14*(February), 1–17. https://doi.org/10.1017/erm.2012.2

Davila, M. L., Riviere, I., Wang, X., Bartido, S., Park, J., Curran, K., Chung, S. S., Stefanski, J., Borquez-Ojeda, O., Olszewska, M., Qu, J., Wasielewska, T., He, Q., Fink, M., Shinglot, H., Youssif, M., Satter, M., Wang, Y., Hosey, J., … Brentjens, R. (2014). Efficacy and Toxicity Management of 19-28z CAR T Cell Therapy in B Cell Acute Lymphoblastic Leukemia. *Science Translational Medicine*, *6*(224), 224ra25. https://doi.org/10.1126/SCITRANSLMED.3008226

De La Roche, M., Asano, Y., & Griffiths, G. M. (2016). Origins of the cytolytic synapse. *Nature Reviews Immunology 2016 16:7*, *16*(7), 421–432. https://doi.org/10.1038/nri.2016.54

De Sousa Linhares, A., Leitner, J., Grabmeier-Pfistershammer, K., & Steinberger, P. (2018). Not All Immune Checkpoints Are Created Equal. *Frontiers in Immunology*, *9*, 1909. https://doi.org/10.3389/FIMMU.2018.01909/BIBTEX

De Villartay, J.-P., Fischer, A., Durandy, A., & Hypermutation, S. (2003). *THE MECHANISMS OF IMMUNE DIVERSIFICATION AND THEIR DISORDERS*. *3*. https://doi.org/10.1038/nri1247

Demaria, O., Gauthier, L., Debroas, G., & Vivier, E. (2021). Natural killer cell engagers in cancer immunotherapy: Next generation of immuno-oncology treatments. *European Journal of Immunology*, *51*(8), 1934–1942. https://doi.org/10.1002/EJI.202048953

Di Vito, C., Mikulak, J., & Mavilio, D. (2019). On the Way to Become a Natural Killer Cell. *Frontiers in Immunology*, *10*, 1812. https://doi.org/10.3389/FIMMU.2019.01812

Dickopf, S., Georges, G. J., & Brinkmann, U. (2020). Format and geometries matter: Structure-based design defines the functionality of bispecific antibodies. *Computational and Structural Biotechnology Journal*, *18*, 1221–1227. https://doi.org/10.1016/J.CSBJ.2020.05.006

Dickopf, S., Lauer, M. E., Ringler, P., Spick, C., Kern, P., & Brinkmann, U. (2019). Highly flexible, IgG-shaped, trivalent antibodies effectively target tumor cells and induce T cell-mediated killing. *Biological Chemistry*, *400*(3). https://doi.org/10.1515/HSZ-2018-0338

Dilchert, J., Hofmann, M., Unverdorben, F., Kontermann, R., & Bunk, S. (2022). Mammalian Display Platform for the Maturation of Bispecific TCR-Based Molecules. *Antibodies (Basel, Switzerland)*, *11*(2). https://doi.org/10.3390/ANTIB11020034

Dolgin, E. (2022). First soluble TCR therapy opens ‘new universe’ of cancer targets. *Nature Biotechnology*, *40*(4), 441–444. https://doi.org/10.1038/S41587-022-01282-6

Dong, D., Zheng, L., Lin, J., Zhang, B., Zhu, Y., Li, N., Xie, S., Wang, Y., Gao, N., & Huang, Z. (2019). Structural basis of assembly of the human T cell receptor–CD3 complex. *Nature*,

573(7775), 546–552. https://doi.org/10.1038/s41586-019-1537-0

Dubrot, J., Milheiro, F., Alfaro, C., Palazón, A., Martinez-Forero, I., Perez-Gracia, J. L., Morales-Kastresana, A., Romero-Trevejo, J. L., Ochoa, M. C., Hervás-Stubbs, S., Prieto, J., Jure-Kunkel, M., Chen, L., & Melero, I. (2010). Treatment with anti-CD137 mAbs causes intense accumulations of liver T cells without selective antitumor immunotherapeutic effects in this organ. *Cancer Immunology, Immunotherapy : CII*, *59*(8), 1223–1233. https://doi.org/10.1007/S00262-010-0846-9

Dumet, C., Pottier, J., Gouilleux-Gruart, V., & Watier, H. (2019). Insights into the IgG heavy chain engineering patent landscape as applied to IgG4 antibody development. *Https://Doi.Org/10.1080/19420862.2019.1664365*, *11*(8), 1341–1350. https://doi.org/10.1080/19420862.2019.1664365

Dustin, M. L., & Long, E. O. (2010). Cytotoxic immunological synapses. *Immunological Reviews*, *235*(1), 24. https://doi.org/10.1111/J.0105-2896.2010.00904.X

Farkona, S., Diamandis, E. P., & Blasutig, I. M. (2016). Cancer immunotherapy: The beginning of the end of cancer? *BMC Medicine*, *14*(1), 1–18. https://doi.org/10.1186/S12916-016-0623-5/TABLES/3

Fooksman, D. R., Vardhana, S., Vasiliver-Shamis, G., Liese, J., Blair, D. A., Waite, J., Sacristán, C., Victora, G. D., Zanin-Zhorov, A., & Dustin, M. L. (2010). Functional Anatomy of T Cell Activation and Synapse Formation. *Http://Dx.Doi.Org/10.1146/Annurev-Immunol-030409-101308*, *28*, 79–105. https://doi.org/10.1146/ANNUREV-IMMUNOL-030409-101308

Froning, K. J., Sereno, A., Huang, F., Demarest, S. J., & Biotechnology Center, L. (2022). Generalizable design parameters for soluble T cell receptor-based T cell engagers. *J Immunother Cancer*, *10*, 4281. https://doi.org/10.1136/jitc-2021-004281

Fucà, G., Spagnoletti, A., Ambrosini, M., de Braud, F., & Di Nicola, M. (2021). Immune cell engagers in solid tumors: promises and challenges of the next generation immunotherapy. *ESMO Open*, *6*(1). https://doi.org/10.1016/J.ESMOOP.2020.100046

Gang, M., Wong, P., Berrien-Elliott, M. M., & Fehniger, T. A. (2020). Memory-like natural killer cells for cancer immunotherapy. *Seminars in Hematology*, *57*(4), 185. https://doi.org/10.1053/J.SEMINHEMATOL.2020.11.003

Gauthier, L., Morel, A., Anceriz, N., Rossi, B., Blanchard-Alvarez, A., Grondin, G., Trichard, S., Cesari, C., Sapet, M., Bosco, F., Rispaud-Blanc, H., Guillot, F., Cornen, S., Roussel, A., Amigues, B., Habif, G., Caraguel, F., Arrufat, S., Remark, R., … Vivier, E. (2019). Multifunctional Natural Killer Cell Engagers Targeting NKp46 Trigger Protective Tumor

Immunity. *Cell*, *177*(7), 1701-1713.e16. https://doi.org/10.1016/J.CELL.2019.04.041/ATTACHMENT/6E06D828-7EEF-4D04-AF75-0407BC5F398E/MMC1.PDF

Gonzalez, H., Hagerling, C., & Werb, Z. (2018). Roles of the immune system in cancer: from tumor initiation to metastatic progression. *Genes & Development*, *32*(19–20), 1267–1284. https://doi.org/10.1101/GAD.314617.118

Graziano, R. F., & Engelhardt, J. J. (2019). Role of FcγRs in Antibody-Based Cancer Therapy. *Current Topics in Microbiology and Immunology*, *423*, 13–34. https://doi.org/10.1007/82_2019_150/FIGURES/1

Greten, T. F., Korangy, F., Neumann, G., Wedemeyer, H., Schlote, K., Heller, A., Scheffer, S., Pardoll, D. M., Garbe, A. I., Schneck, J. P., & Manns, M. P. (2002). Peptide–$β$2-microglobulin–MHC fusion molecules bind antigen-specific T cells and can be used for multivalent MHC–Ig complexes. *Journal of Immunological Methods*, *271*(1–2), 125–135. https://doi.org/10.1016/S0022-1759(02)00346-0

Gunnarsen, K. S., Høydahl, L. S., Neumann, R. S., Bjerregaard-Andersen, K., Nilssen, N. R., Sollid, L. M., Sandlie, I., & Løset, G. Å. (2018). Soluble T-cell receptor design influences functional yield in an E. coli chaperone-assisted expression system. *PLoS ONE*, *13*(4). https://doi.org/10.1371/JOURNAL.PONE.0195868

Halle, S., Halle, O., & Förster, R. (2017). Mechanisms and Dynamics of T Cell-Mediated Cytotoxicity In Vivo. *Trends in Immunology*, *38*(6), 432–443. https://doi.org/10.1016/J.IT.2017.04.002

Harper, J., Adams, K. J., Bossi, G., Wright, D. E., Stacey, A. R., Bedke, N., Martinez-Hague, R., Blat, D., Humbert, L., Buchanan, H., Le Provost, G. S., Donnellan, Z., Carreira Id, R. J., Paston, S. J., Weigand, L. U., Canestraro, M., Sanderson, J. P., Botta, S., Id, G.-S., … Dukes, J. (2018). *An approved in vitro approach to preclinical safety and efficacy evaluation of engineered T cell receptor anti-CD3 bispecific (ImmTAC) molecules*. https://doi.org/10.1371/journal.pone.0205491

He, Q., Liu, Z., Liu, Z., Lai, Y., Zhou, X., & Weng, J. (2019). TCR-like antibodies in cancer immunotherapy. In *Journal of Hematology and Oncology*. https://doi.org/10.1186/s13045-019-0788-4

Heckel, F., Turaj, A. H., Fisher, H., Chan, H. T. C., Marshall, M. J. E., Dadas, O., Penfold, C. A., Inzhelevskaya, T., Mockridge, C. I., Alvarado, D., Tews, I., Keler, T., Beers, S. A., Cragg, M. S., & Lim, S. H. (2022). Agonistic CD27 antibody potency is determined by epitope-dependent receptor clustering augmented through Fc-engineering.

Communications Biology 2022 5:1, *5*(1), 1–15. https://doi.org/10.1038/s42003-022-03182-6

Herold, K. C., Burton, J. B., Francois, F., Poumian-Ruiz, E., Glandt, M., & Bluestone, J. A. (2003). Activation of human T cells by FcR nonbinding anti-CD3 mAb, hOKT3gamma1(Ala-Ala). *The Journal of Clinical Investigation*, *111*(3), 409–418. https://doi.org/10.1172/JCI16090

Holland, C. J., Crean, R. M., Pentier, J. M., de Wet, B., Lloyd, A., Srikannathasan, V., Lissin, N., Lloyd, K. A., Blicher, T. H., Conroy, P. J., Hock, M., Pengelly, R. J., Spinner, T. E., Cameron, B., Potter, E. A., Jeyanthan, A., Molloy, P. E., Sami, M., Aleksic, M., … Cole, D. K. (2020). Specificity of bispecific T cell receptors and antibodies targeting peptide-HLA. *The Journal of Clinical Investigation*, *130*(5), 2673. https://doi.org/10.1172/JCI130562

Hornig, N., Reinhardt, K., Kermer, V., Kontermann, R. E., & Müller, D. (2013). Evaluating combinations of costimulatory antibody-ligand fusion proteins for targeted cancer immunotherapy. *Cancer Immunology, Immunotherapy : CII*, *62*(8), 1369–1380. https://doi.org/10.1007/S00262-013-1441-7

Hülsmeyer, M., Chames, P., Hillig, R. C., Stanfield, R. L., Held, G., Coulie, P. G., Alings, C., Wille, G., Saenger, W., Uchanska-Ziegler, B., Hoogenboom, H. R., & Ziegler, A. (2005). A Major Histocompatibility Complex·Peptide-restricted Antibody and T Cell Receptor Molecules Recognize Their Target by Distinct Binding Modes: CRYSTAL STRUCTURE OF HUMAN LEUKOCYTE ANTIGEN (HLA)-A1·MAGE-A1 IN COMPLEX WITH FAB-HYB3. *Journal of Biological Chemistry*, *280*(4), 2972–2980. https://doi.org/10.1074/JBC.M411323200

Ichikawa, J., Yoshida, T., Isser, A., Laino, A. S., Vassallo, M., Woods, D., Kim, S., Oelke, M., Jones, K., Schneck, J. P., & Weber, J. S. (2020). Rapid Expansion of Highly Functional Antigen-Specific T Cells from Patients with Melanoma by Nanoscale Artificial Antigen-Presenting Cells. *Clinical Cancer Research : An Official Journal of the American Association for Cancer Research*, *26*(13), 3384–3396. https://doi.org/10.1158/1078-0432.CCR-19-3487

Jeppesen, M., Hagel, G., Glenthoj, A., Vainer, B., Ibsen, P., Harling, H., Thastrup, O., Jørgensen, L. N., & Thastrup, J. (2017). Short-term spheroid culture of primary colorectal cancer cells as an in vitro model for personalizing cancer medicine. *PLoS ONE*, *12*(9). https://doi.org/10.1371/JOURNAL.PONE.0183074

Jin, S., Sun, Y., Liang, X., Gu, X., Ning, J., Xu, Y., Chen, S., & Pan, L. (2022). Emerging new therapeutic antibody derivatives for cancer treatment. *Signal Transduction and Targeted*

Therapy 2022 7:1, *7*(1), 1–28. https://doi.org/10.1038/s41392-021-00868-x

Joffre, O. P., Segura, E., Savina, A., & Amigorena, S. (2012). Cross-presentation by dendritic cells. *Nature Reviews. Immunology*, *12*(8), 557–569. https://doi.org/10.1038/NRI3254

Johnson, L. A., Heemskerk, B., Powell, D. J., Jr., Cohen, C. J., Morgan, R. A., Dudley, M. E., Robbins, P. F., & Rosenberg, S. A. (2006). Gene Transfer of Tumor-Reactive TCR Confers Both High Avidity and Tumor Reactivity to Nonreactive Peripheral Blood Mononuclear Cells and Tumor-Infiltrating Lymphocytes. *Journal of Immunology (Baltimore, Md. : 1950)*, *177*(9), 6548. https://doi.org/10.4049/JIMMUNOL.177.9.6548

Jones, H. F., Molvi, Z., Klatt, M. G., Dao, T., & Scheinberg, D. A. (2021). Empirical and Rational Design of T Cell Receptor-Based Immunotherapies. *Frontiers in Immunology*, *11*, 3545. https://doi.org/10.3389/FIMMU.2020.585385/BIBTEX

Joshi, N. S., & Kaech, S. M. (2008). Effector CD8 T Cell Development: A Balancing Act between Memory Cell Potential and Terminal Differentiation. *The Journal of Immunology*, *180*(3), 1309–1315. https://doi.org/10.4049/JIMMUNOL.180.3.1309

Kedzierska, K., & Koutsakos, M. (2020). The ABC of Major Histocompatibility Complexes and T Cell Receptors in Health and Disease. *Viral Immunology*, *33*(3), 160. https://doi.org/10.1089/VIM.2019.0184

Krogsgaard, M., & Davis, M. M. (2005). How T cells “see” antigen. *NATURE IMMUNOLOGY*, *6*. https://doi.org/10.1038/ni1173

Labrijn, A. F., Janmaat, M. L., Reichert, J. M., & Parren, P. W. H. I. (2019). Bispecific antibodies: a mechanistic review of the pipeline. *Nature Reviews Drug Discovery 2019 18:8*, *18*(8), 585–608. https://doi.org/10.1038/s41573-019-0028-1

Lazar, G. A., Dang, W., Karki, S., Vafa, O., Peng, J. S., Hyun, L., Chan, C., Chung, H. S., Eivazi, A., Yoder, S. C., Vielmetter, J., Carmichael, D. F., Hayes, R. J., & Dahiyat, B. I. (2006a). Engineered antibody Fc variants with enhanced effector function. *Proceedings of the National Academy of Sciences of the United States of America*. https://doi.org/10.1073/pnas.0508123103

Lazar, G. A., Dang, W., Karki, S., Vafa, O., Peng, J. S., Hyun, L., Chan, C., Chung, H. S., Eivazi, A., Yoder, S. C., Vielmetter, J., Carmichael, D. F., Hayes, R. J., & Dahiyat, B. I. (2006b). Engineered antibody Fc variants with enhanced effector function. *Proceedings of the National Academy of Sciences*, *103*(11), 4005–4010. https://doi.org/10.1073/PNAS.0508123103

Leone, P., Shin, E. C., Perosa, F., Vacca, A., Dammacco, F., & Racanelli, V. (2013). MHC

Class I Antigen Processing and Presenting Machinery: Organization, Function, and Defects in Tumor Cells. *JNCI: Journal of the National Cancer Institute*, *105*(16), 1172–1187. https://doi.org/10.1093/JNCI/DJT184

Li, Y., Moysey, R., Molloy, P. E., Vuidepot, A. L., Mahon, T., Baston, E., Dunn, S., Liddy, N., Jacob, J., Jakobsen, B. K., & Boulter, J. M. (2005). Directed evolution of human T-cell receptors with picomolar affinities by phage display. *Nature Biotechnology 2005 23:3*, *23*(3), 349–354. https://doi.org/10.1038/nbt1070

Lian, G. Y., Mak, T. S. K., Yu, X. Q., & Lan, H. Y. (2021). Challenges and Recent Advances in NK Cell-Targeted Immunotherapies in Solid Tumors. *International Journal of Molecular Sciences*, *23*(1). https://doi.org/10.3390/IJMS23010164

Liddy, N., Bossi, G., Adams, K. J., Lissina, A., Mahon, T. M., Hassan, N. J., Gavarret, J., Bianchi, F. C., Pumphrey, N. J., Ladell, K., Gostick, E., Sewell, A. K., Lissin, N. M., Harwood, N. E., Molloy, P. E., Li, Y., Cameron, B. J., Sami, M., Baston, E. E., … Jakobsen, B. K. (2012). Monoclonal TCR-redirected tumor cell killing. *Nature Medicine*, *18*(6), 980–987. https://doi.org/10.1038/NM.2764

Linette, G. P., Stadtmauer, E. A., Maus, M. V., Rapoport, A. P., Levine, B. L., Emery, L., Litzky, L., Bagg, A., Carreno, B. M., Cimino, P. J., Binder-Scholl, G. K., Smethurst, D. P., Gerry, A. B., Pumphrey, N. J., Bennett, A. D., Brewer, J. E., Dukes, J., Harper, J., Tayton-Martin, H. K., … June, C. H. (2013). Cardiovascular toxicity and titin cross-reactivity of affinity-enhanced T cells in myeloma and melanoma. *Blood*. https://doi.org/10.1182/blood-2013-03-490565

Liu, W., Scott, J. M., Langguth, E., Chang, H., Park, P. H., & Kim, S. (2020). FcRγ Gene Editing Reprograms Conventional NK Cells to Display Key Features of Adaptive Human NK Cells. *IScience*, *23*(11). https://doi.org/10.1016/J.ISCI.2020.101709

Liu, Y., & Zeng, G. (2012). Cancer and Innate Immune System Interactions: Translational Potentials for Cancer Immunotherapy. *Journal of Immunotherapy (Hagerstown, Md.: 1997)*, *35*(4), 299. https://doi.org/10.1097/CJI.0B013E3182518E83

Liu, Z., Chen, O., Wall, J. B. J., Zheng, M., Zhou, Y., Wang, L., Ruth Vaseghi, H., Qian, L., & Liu, J. (2017). Systematic comparison of 2A peptides for cloning multi-genes in a polycistronic vector. *Scientific Reports 2017 7:1*, *7*(1), 1–9. https://doi.org/10.1038/s41598-017-02460-2

Low, J. L., Naidoo, A., Yeo, G., Gehring, A. J., Ho, Z. Z., Yau, Y. H., Shochat, S. G., Kranz, D. M., Bertoletti, A., & Grotenbreg, G. M. (2012). Binding of TCR Multimers and a TCR-Like Antibody with Distinct Fine-Specificities Is Dependent on the Surface Density of HLA

Complexes. *PLoS ONE*. https://doi.org/10.1371/journal.pone.0051397

Lowe, K. L., Cole, D., Kenefeck, R., OKelly, I., Lepore, M., & Jakobsen, B. K. (2019). Novel TCR-based biologics: mobilising T cells to warm 'cold' tumours. In *Cancer Treatment Reviews*. https://doi.org/10.1016/j.ctrv.2019.06.001

Luckheeram, R. V., Zhou, R., Verma, A. D., & Xia, B. (2012). CD4 + T Cells: Differentiation and Functions. *Clinical and Developmental Immunology*, *2012*, 12. https://doi.org/10.1155/2012/925135

Ma, J., Mo, Y., Tang, M., Shen, J., Qi, Y., Zhao, W., Huang, Y., Xu, Y., & Qian, C. (2021). Bispecific Antibodies: From Research to Clinical Application. *Frontiers in Immunology*, *12*. https://doi.org/10.3389/FIMMU.2021.626616

Malecek, K., Grigoryan, A., Zhong, S., Gu, W. J., Johnson, L. A., Rosenberg, S. A., Cardozo, T., & Krogsgaard, M. (2014). Specific increase in potency via structure-based design of a T cell receptor. *Journal of Immunology (Baltimore, Md.: 1950)*, *193*(5), 2587. https://doi.org/10.4049/JIMMUNOL.1302344

Malissen, B., & Bongrand, P. (2015). Early T Cell Activation: Integrating Biochemical, Structural, and Biophysical Cues. *Http://Dx.Doi.Org/10.1146/Annurev-Immunol-032414-112158*, *33*, 539–561. https://doi.org/10.1146/ANNUREV-IMMUNOL-032414-112158

Mariuzza, R. A., Agnihotri, P., & Orban, J. (2020). The structural basis of T-cell receptor (TCR) activation: An enduring enigma. *The Journal of Biological Chemistry*, *295*(4), 914. https://doi.org/10.1074/JBC.REV119.009411

Market, E., & Papavasiliou, F. N. (2003). V(D)J Recombination and the Evolution of the Adaptive Immune System. *PLoS Biology*, *1*(1). https://doi.org/10.1371/JOURNAL.PBIO.0000016

Martin, A., Tisch, R. M., & Getts, D. R. (2013). Manipulating T cell-mediated pathology: Targets and functions of monoclonal antibody immunotherapy. *Clinical Immunology*, *148*(1), 136–147. https://doi.org/10.1016/J.CLIM.2013.04.011

Mascarelli, D. E., Rosa, R. S. M., Toscaro, J. M., Semionatto, I. F., Ruas, L. P., Fogagnolo, C. T., Lima, G. C., & Bajgelman, M. C. (2021). Boosting Antitumor Response by Costimulatory Strategies Driven to 4-1BB and OX40 T-cell Receptors. *Frontiers in Cell and Developmental Biology*, *9*, 1611. https://doi.org/10.3389/FCELL.2021.692982/BIBTEX

Maude, S. L., Frey, N., Shaw, P. A., Aplenc, R., Barrett, D. M., Bunin, N. J., Chew, A., Gonzalez, V. E., Zheng, Z., Lacey, S. F., Mahnke, Y. D., Melenhorst, J. J., Rheingold, S.

R., Shen, A., Teachey, D. T., Levine, B. L., June, C. H., Porter, D. L., & Grupp, S. A. (2014). Chimeric antigen receptor T cells for sustained remissions in leukemia. *The New England Journal of Medicine*, *371*(16), 1507–1517. https://doi.org/10.1056/NEJMOA1407222

McCormack, E., Adams, K. J., Hassan, N. J., Kotian, A., Lissin, N. M., Sami, M., Mujić, M., Osdal, T., Gjertsen, B. T., Baker, D., Powlesland, A. S., Aleksic, M., Vuidepot, A., Morteau, O., Sutton, D. H., June, C. H., Kalos, M., Ashfield, R., & Jakobsen, B. K. (2013). Bi-specific TCR-anti CD3 redirected T-cell targeting of NY-ESO-1- and LAGE-1-positive tumors. *Cancer Immunology, Immunotherapy*. https://doi.org/10.1007/s00262-012-1384-4

McDaid, W. J., Lissin, N., Pollheimer, E., Greene, M., Leach, A., Smyth, P., Bossi, G., Longley, D., Cole, D. K., & Scott, C. J. (2021). Enhanced target-specific delivery of docetaxel-loaded nanoparticles using engineered T cell receptors. *Nanoscale*, *13*(35), 15010–15020. https://doi.org/10.1039/D1NR04001D

Melero, I., Rouzaut, A., Motz, G. T., & Coukos, G. (2014). T-cell and NK-cell infiltration into solid tumors: A key limiting factor for efficacious cancer immunotherapy. *Cancer Discovery*, *4*(5), 522–526. https://doi.org/10.1158/2159-8290.CD-13-0985

Mellor, J. D., Brown, M. P., Irving, H. R., Zalcberg, J. R., & Dobrovic, A. (2013). A critical review of the role of Fc gamma receptor polymorphisms in the response to monoclonal antibodies in cancer. *Journal of Hematology and Oncology*, *6*(1), 1–10. https://doi.org/10.1186/1756-8722-6-1/TABLES/2

Michalk, I., Feldmann, A., Koristka, S., Arndt, C., Cartellieri, M., Ehninger, A., Ehninger, G., & Bachmann, M. P. (2014). Characterization of a Novel Single-Chain Bispecific Antibody for Retargeting of T Cells to Tumor Cells via the TCR Co-Receptor CD8. *PLOS ONE*, *9*(4), e95517. https://doi.org/10.1371/JOURNAL.PONE.0095517

Monks, C. R. F., Freiberg, B. A., Kupfer, H., Sciaky, N., & Kupfer, A. (1998). Three-dimensional segregation of supramolecular activation clusters in T cells. *Nature 1998 395:6697*, *395*(6697), 82–86. https://doi.org/10.1038/25764

Moon, D., Tae, N., Park, Y., Lee, S. W., & Kim, D. H. (2022). Development of Bispecific Antibody for Cancer Immunotherapy: Focus on T Cell Engaging Antibody. *Immune Network*, *22*(1). https://doi.org/10.4110/IN.2022.22.E4

Moore, G. L., Lee, S.-H., Schubbert, S., Miranda, Y., Rashid, R., Pong, E., Phung, S., Chan, E. W., Chen, H., Endo, N., Ardila, M. C., Bernett, M. J., Chu, S., Leung, I. W. L., Muchhal, U., Bonzon, C., Szymkowski, D. E., & Desjarlais, J. (2015). Tuning T Cell Affinity Improves

Efficacy and Safety of Anti-CD38 × Anti-CD3 Bispecific Antibodies in Monkeys - a Potential Therapy for Multiple Myeloma. *Blood*, *126*(23), 1798–1798. https://doi.org/10.1182/BLOOD.V126.23.1798.1798

Mørch, A. M., Bálint, Š., Santos, A. M., Davis, S. J., & Dustin, M. L. (2020). Coreceptors and TCR Signaling – the Strong and the Weak of It. *Frontiers in Cell and Developmental Biology*, *8*, 1147. https://doi.org/10.3389/FCELL.2020.597627/BIBTEX

Morotti, M., Albukhari, A., Alsaadi, A., Artibani, M., Brenton, J. D., Curbishley, S. M., Dong, T., Dustin, M. L., Hu, Z., McGranahan, N., Miller, M. L., Santana-Gonzalez, L., Seymour, L. W., Shi, T., Van Loo, P., Yau, C., White, H., Wietek, N., Church, D. N., … Ahmed, A. A. (2021). Promises and challenges of adoptive T-cell therapies for solid tumours. *British Journal of Cancer 2021 124:11*, *124*(11), 1759–1776. https://doi.org/10.1038/s41416-021-01353-6

Morton, L. T., Wachsmann, T. L. A., Meeuwsen, M. H., Wouters, A. K., Remst, D. F. G., Van Loenen, M. M., Falkenburg, J. H. F., & Heemskerk, M. H. M. (2022). T cell receptor engineering of primary NK cells to therapeutically target tumors and tumor immune evasion. *Journal for ImmunoTherapy of Cancer*, *10*(3), e003715. https://doi.org/10.1136/JITC-2021-003715

Mosquera, L. A., Card, K. F., Price-Schiavi, S. A., Belmont, H. J., Liu, B., Builes, J., Zhu, X., Chavaillaz, P.-A., Lee, H., Jiao, J., Francis, J. L., Amirkhosravi, A., Wong, R. L., & Wong, H. C. (2005). In Vitro and In Vivo Characterization of a Novel Antibody-Like Single-Chain TCR Human IgG1 Fusion Protein. *The Journal of Immunology*, *174*(7), 4381–4388. https://doi.org/10.4049/JIMMUNOL.174.7.4381

Mujal, A. M., Delconte, R. B., & Sun, J. C. (2021). Natural Killer Cells: From Innate to Adaptive Features. *Https://Doi.Org/10.1146/Annurev-Immunol-101819-074948*, *39*, 417–447. https://doi.org/10.1146/ANNUREV-IMMUNOL-101819-074948

Müller, D., Frey, K., & Kontermann, R. E. (2008). A novel antibody-4-1BBL fusion protein for targeted costimulation in cancer immunotherapy. *Journal of Immunotherapy (Hagerstown, Md. : 1997)*, *31*(8), 714–722. https://doi.org/10.1097/CJI.0B013E31818353E9

Myers, J. A., & Miller, J. S. (2021). Exploring the NK cell platform for cancer immunotherapy. *Nature Reviews. Clinical Oncology*, *18*(2), 85–100. https://doi.org/10.1038/S41571-020-0426-7

Naimi, A., Mohammed, R. N., Raji, A., Chupradit, S., Yumashev, A. V., Suksatan, W., Shalaby, M. N., Thangavelu, L., Kamrava, S., Shomali, N., Sohrabi, A. D., Adili, A., Noroozi-

Aghideh, A., & Razeghian, E. (2022). Tumor immunotherapies by immune checkpoint inhibitors (ICIs); the pros and cons. *Cell Communication and Signaling*, *20*(1), 1–31. https://doi.org/10.1186/S12964-022-00854-Y/TABLES/6

Novotny, J., Ganju, R. K., Smiley, S. T., Hussey, R. E., Luther, M. A., Recny, M. A., Siliciano, R. F., & Reinherz, E. L. (1991). A soluble, single-chain T-cell receptor fragment endowed with antigen-combining properties. *Proceedings of the National Academy of Sciences of the United States of America*, *88*(19), 8646–8650. https://doi.org/10.1073/PNAS.88.19.8646

Oates, J., Hassan, N. J., & Jakobsen, B. K. (2015). ImmTACs for targeted cancer therapy: Why, what, how, and which. *Molecular Immunology*, *67*(2 Pt A), 67–74. https://doi.org/10.1016/J.MOLIMM.2015.01.024

Orbelyan, G. A., Tang, F., Sally, B., Solus, J., Meresse, B., Ciszewski, C., Grenier, J.-C., Barreiro, L. B., Lanier, L. L., & Jabri, B. (2014). Human NKG2E is expressed and forms an intracytoplasmic complex with CD94 and DAP12. *Journal of Immunology (Baltimore, Md. : 1950)*, *193*(2), 610. https://doi.org/10.4049/JIMMUNOL.1400556

Pandya, P. H., Murray, M. E., Pollok, K. E., & Renbarger, J. L. (2016). The Immune System in Cancer Pathogenesis: Potential Therapeutic Approaches. *Journal of Immunology Research*, *2016*. https://doi.org/10.1155/2016/4273943

Paul, S., & Lal, G. (2017). The molecular mechanism of natural killer cells function and its importance in cancer immunotherapy. *Frontiers in Immunology*, *8*(SEP), 1124. https://doi.org/10.3389/FIMMU.2017.01124/BIBTEX

Pegram, H. J., Andrews, D. M., Smyth, M. J., Darcy, P. K., & Kershaw, M. H. (2011). Activating and inhibitory receptors of natural killer cells. *Immunology and Cell Biology*, *89*(2), 216–224. https://doi.org/10.1038/ICB.2010.78

Pellicci, D. G., Koay, H. F., & Berzins, S. P. (2020). Thymic development of unconventional T cells: how NKT cells, MAIT cells and γδ T cells emerge. *Nature Reviews Immunology 2020 20:12*, *20*(12), 756–770. https://doi.org/10.1038/s41577-020-0345-y

Pende, D., Falco, M., Vitale, M., Cantoni, C., Vitale, C., Munari, E., Bertaina, A., Moretta, F., Del Zotto, G., Pietra, G., Mingari, M. C., Locatelli, F., & Moretta, L. (2019). Killer Ig-like receptors (KIRs): Their role in NK cell modulation and developments leading to their clinical exploitation. *Frontiers in Immunology*, *10*(MAY), 1179. https://doi.org/10.3389/FIMMU.2019.01179/BIBTEX

Pierce, S., Geanes, E. S., & Bradley, T. (2020). Targeting Natural Killer Cells for Improved Immunity and Control of the Adaptive Immune Response. *Frontiers in Cellular and*

Infection Microbiology, *10*, 231. https://doi.org/10.3389/FCIMB.2020.00231/BIBTEX

Pishesha, N., Harmand, T. J., & Ploegh, H. L. (2022). A guide to antigen processing and presentation. *Nature Reviews Immunology 2022*, 1–14. https://doi.org/10.1038/s41577-022-00707-2

Rajendra, Y., Kiseljak, D., Baldi, L., Hacker, D. L., & Wurm, F. M. (2011a). A simple high-yielding process for transient gene expression in CHO cells. *Journal of Biotechnology*, *153*(1–2), 22–26. https://doi.org/10.1016/J.JBIOTEC.2011.03.001

Rajendra, Y., Kiseljak, D., Baldi, L., Hacker, D. L., & Wurm, F. M. (2011b). Reduced glutamine concentration improves protein production in growth-arrested CHO-DG44 and HEK-293E cells. *Undefined*, *34*(4), 619–626. https://doi.org/10.1007/S10529-011-0809-Z

Ran, G. he, Lin, Y. qing, Tian, L., Zhang, T., Yan, D. mei, Yu, J. hua, & Deng, Y. cai. (2022). Natural killer cell homing and trafficking in tissues and tumors: from biology to application. *Signal Transduction and Targeted Therapy*, *7*(1). https://doi.org/10.1038/s41392-022-01058-z

Rapoport, A. P., Stadtmauer, E. A., Binder-Scholl, G. K., Goloubeva, O., Vogl, D. T., Lacey, S. F., Badros, A. Z., Garfall, A., Weiss, B., Finklestein, J., Kulikovskaya, I., Sinha, S. K., Kronsberg, S., Gupta, M., Bond, S., Melchiori, L., Brewer, J. E., Bennett, A. D., Gerry, A. B., … June, C. H. (2015). NY-ESO-1 specific TCR engineered T-cells mediate sustained antigen-specific antitumor effects in myeloma. *Nature Medicine*, *21*(8), 914. https://doi.org/10.1038/NM.3910

Robbins, P. F., Li, Y. F., El-Gamil, M., Zhao, Y., Wargo, J. A., Zheng, Z., Xu, H., Morgan, R. A., Feldman, S. A., Johnson, L. A., Bennett, A. D., Dunn, S. M., Mahon, T. M., Jakobsen, B. K., & Rosenberg, S. A. (2008). Single and Dual Amino Acid Substitutions in TCR CDRs Can Enhance Antigen-Specific T Cell Functions. *The Journal of Immunology*, *180*(9), 6116–6131. https://doi.org/10.4049/JIMMUNOL.180.9.6116

Robinson, R. A., McMurran, C., McCully, M. L., & Cole, D. K. (2021). Engineering soluble T-cell receptors for therapy. *The FEBS Journal*, *288*(21), 6159–6173. https://doi.org/10.1111/FEBS.15780

Rölle, A., Jäger, D., & Momburg, F. (2018). HLA-E Peptide Repertoire and Dimorphism—Centerpieces in the Adaptive NK Cell Puzzle? *Frontiers in Immunology*, *9*(OCT), 2410. https://doi.org/10.3389/FIMMU.2018.02410

Rollins, Z., Harris, B., George, S., & Faller, R. (2022). A molecular dynamics investigation of N-glycosylation effects on T-cell receptor kinetics. *Journal of Biomolecular Structure & Dynamics*, 1–10. https://doi.org/10.1080/07391102.2022.2091660

Rosenberg, S. A., Yang, J. C., Sherry, R. M., Kammula, U. S., Hughes, M. S., Phan, G. Q., Citrin, D. E., Restifo, N. P., Robbins, P. F., Wunderlich, J. R., Morton, K. E., Laurencot, C. M., Steinberg, S. M., White, D. E., & Dudley, M. E. (2011). Durable complete responses in heavily pretreated patients with metastatic melanoma using T-cell transfer immunotherapy. *Clinical Cancer Research : An Official Journal of the American Association for Cancer Research*, *17*(13), 4550–4557. https://doi.org/10.1158/1078-0432.CCR-11-0116

Rosenberg, S. A., Yannelli, J. R., Yang, J. C., Topalian, S. L., Schwartzentruber, D. J., Weber, J. S., Parkinson, D. R., Seipp, C. A., Einhorn, J. H., & White, D. E. (1994). Treatment of Patients With Metastatic Melanoma With Autologous Tumor-Infiltrating Lymphocytes and Interleukin 2. *JNCI: Journal of the National Cancer Institute*, *86*(15), 1159–1166. https://doi.org/10.1093/JNCI/86.15.1159

Rossjohn, J., Gras, S., Miles, J. J., Turner, S. J., Godfrey, D. I., & McCluskey, J. (2015). T cell antigen receptor recognition of antigen-presenting molecules. *Annual Review of Immunology*. https://doi.org/10.1146/annurev-immunol-032414-112334

Runbeck, E., Crescioli, S., Karagiannis, S. N., & Papa, S. (2021). Utilizing Immunocytokines for Cancer Therapy. *Antibodies*, *10*(1), 1–23. https://doi.org/10.3390/ANTIB10010010

Sádio, F., Stadlmayr, G., Stadlbauer, K., Gräf, M., Scharrer, A., Rüker, F., & Wozniak-Knopp, G. (2020). Stabilization of soluble high-affinity T-cell receptor with de novo disulfide bonds. *FEBS Letters*, *594*(3), 477–490. https://doi.org/10.1002/1873-3468.13616

Sahin, U., Derhovanessian, E., Miller, M., Kloke, B. P., Simon, P., Löwer, M., Bukur, V., Tadmor, A. D., Luxemburger, U., Schrörs, B., Omokoko, T., Vormehr, M., Albrecht, C., Paruzynski, A., Kuhn, A. N., Buck, J., Heesch, S., Schreeb, K. H., Müller, F., … Türeci, Ö. (2017). Personalized RNA mutanome vaccines mobilize poly-specific therapeutic immunity against cancer. *Nature*, *547*(7662), 222–226. https://doi.org/10.1038/NATURE23003

Sapski, S., Beha, N., Kontermann, R., & Müller, D. (2017). Tumor-targeted costimulation with antibody-fusion proteins improves bispecific antibody-mediated immune response in presence of immunosuppressive factors. *Oncoimmunology*, *6*(12). https://doi.org/10.1080/2162402X.2017.1361594

Sato, T., Nathan, P. D., Hernandez-Aya, L., Sacco, J. J., Orloff, M. M., Visich, J., Little, N., Hulstine, A.-M., Coughlin, C. M., & Carvajal, R. D. (2018). Redirected T cell lysis in patients with metastatic uveal melanoma with gp100-directed TCR IMCgp100: Overall survival findings. *Https://Doi.Org/10.1200/JCO.2018.36.15_suppl.9521*, *36*(15_suppl), 9521–9521. https://doi.org/10.1200/JCO.2018.36.15_SUPPL.9521

Saxena, M., van der Burg, S. H., Melief, C. J. M., & Bhardwaj, N. (2021). Therapeutic cancer vaccines. *Nature Reviews Cancer 2021 21:6*, *21*(6), 360–378. https://doi.org/10.1038/s41568-021-00346-0

Schanzer, J. M., Wartha, K., Croasdale, R., Moser, S., Künkele, K. P., Ries, C., Scheuer, W., Duerr, H., Pompiati, S., Pollman, J., Stracke, J., Lau, W., Ries, S., Brinkmann, U., Klein, C., & Umana, P. (2014). A Novel Glycoengineered Bispecific Antibody Format for Targeted Inhibition of Epidermal Growth Factor Receptor (EGFR) and Insulin-like Growth Factor Receptor Type I (IGF-1R) Demonstrating Unique Molecular Properties. *Journal of Biological Chemistry*, *289*(27), 18693–18706. https://doi.org/10.1074/JBC.M113.528109

Schlothauer, T., Herter, S., Koller, C. F., Grau-Richards, S., Steinhart, V., Spick, C., Kubbies, M., Klein, C., Umaña, P., & Mössner, E. (2016). Novel human IgG1 and IgG4 Fc-engineered antibodies with completely abolished immune effector functions. *Protein Engineering, Design and Selection*, *29*(10), 457–466. https://doi.org/10.1093/PROTEIN/GZW040

Schwartz, R. H. (2003). T Cell Anergy*. *Https://Doi.Org/10.1146/Annurev.Immunol.21.120601.141110*, *21*, 305–334. https://doi.org/10.1146/ANNUREV.IMMUNOL.21.120601.141110

Seidel, U. J. E., Schlegel, P., & Lang, P. (2013). Natural killer cell mediated antibody-dependent cellular cytotoxicity in tumor immunotherapy with therapeutic antibodies. *Frontiers in Immunology*, *4*(MAR), 76. https://doi.org/10.3389/FIMMU.2013.00076/BIBTEX

Shah, A., Rauth, S., Aithal, A., Kaur, S., Ganguly, K., Orzechowski, C., Varshney, G. C., Jain, M., & Batra, S. K. (2021). The Current Landscape of Antibody-based Therapies in Solid Malignancies. *Theranostics*, *11*(3), 1493. https://doi.org/10.7150/THNO.52614

Shields, R. L., Namenuk, A. K., Hong, K., Meng, Y. G., Rae, J., Briggs, J., Xie, D., Lai, J., Stadlen, A., Li, B., Fox, J. A., & Presta, L. G. (2001). High Resolution Mapping of the Binding Site on Human IgG1 for FcγRI, FcγRII, FcγRIII, and FcRn and Design of IgG1 Variants with Improved Binding to the FcγR. *Journal of Biological Chemistry*, *276*(9), 6591–6604. https://doi.org/10.1074/JBC.M009483200

Sidaway, P. (2022). LAG3 inhibition improves outcomes. *Nature Reviews Clinical Oncology 2022 19:3*, *19*(3), 149–149. https://doi.org/10.1038/s41571-022-00602-8

Hoo, W. F., Lacy, M. J., Denzin, L. K., Voss, E. W., Hardman, K. D., & Kranz, D. M. (1992). Characterization of a single-chain T-cell receptor expressed in Escherichia coli. *Proceedings of the National Academy of Sciences of the United States of America*,

89(10), 4759–4763. https://doi.org/10.1073/PNAS.89.10.4759

Strohl, W. R. (2009). Optimization of Fc-mediated effector functions of monoclonal antibodies. In *Current Opinion in Biotechnology*. https://doi.org/10.1016/j.copbio.2009.10.011

Sung, H., Ferlay, J., Siegel, R. L., Laversanne, M., Soerjomataram, I., Jemal, A., & Bray, F. (2021). Global Cancer Statistics 2020: GLOBOCAN Estimates of Incidence and Mortality Worldwide for 36 Cancers in 185 Countries. *CA: A Cancer Journal for Clinicians*, *71*(3), 209–249. https://doi.org/10.3322/CAAC.21660

Suntharalingam, G., Perry, M. R., Ward, S., Brett, S. J., Castello-Cortes, A., Brunner, M. D., & Panoskaltsis, N. (2006). Cytokine storm in a phase 1 trial of the anti-CD28 monoclonal antibody TGN1412. *The New England Journal of Medicine*, *355*(10), 1018–1028. https://doi.org/10.1056/NEJMOA063842

Suurs, F. V., Lub-de Hooge, M. N., de Vries, E. G. E., & de Groot, D. J. A. (2019). A review of bispecific antibodies and antibody constructs in oncology and clinical challenges. *Pharmacology & Therapeutics*, *201*, 103–119. https://doi.org/10.1016/J.PHARMTHERA.2019.04.006

Szeto, C., Lobos, C. A., Nguyen, A. T., & Gras, S. (2021). TCR Recognition of Peptide–MHC-I: Rule Makers and Breakers. *International Journal of Molecular Sciences*, *22*(1), 1–26. https://doi.org/10.3390/IJMS22010068

Tai, Y., Wang, Q., Korner, H., Zhang, L., & Wei, W. (2018). Molecular mechanisms of T cells activation by dendritic cells in autoimmune diseases. *Frontiers in Pharmacology*, *9*(JUN), 642. https://doi.org/10.3389/FPHAR.2018.00642/BIBTEX

Tan, S., Li, D., & Zhu, X. (2020). Cancer immunotherapy: Pros, cons and beyond. *Biomedicine & Pharmacotherapy*, *124*, 109821. https://doi.org/10.1016/J.BIOPHA.2020.109821

Tao, M. H., & Morrison, S. L. (1989). *Studies of aglycosylated chimeric mouse-human IgG. Role of carbohydrate in the structure and effector functions mediated by the human IgG constant region.* http://www.jimmunol.org/content/143/8/2595

Trapani, J. A., & Smyth, M. J. (2002). Functional significance of the perforin/granzyme cell death pathway. *Nature Reviews Immunology 2002 2:10*, *2*(10), 735–747. https://doi.org/10.1038/nri911

Truscott, S. M., Wang, X., Lybarger, L., Biddison, W. E., McBerry, C., Martinko, J. M., Connolly, J. M., Linette, G. P., Fremont, D. H., Hansen, T. H., & Carreno, B. M. (2008). Human Major Histocompatibility Complex (MHC) Class I Molecules with Disulfide Traps Secure Disease-related Antigenic Peptides and Exclude Competitor Peptides *. *Journal of*

Biological Chemistry, *283*(12), 7480–7490. https://doi.org/10.1074/JBC.M709935200

Tsimberidou, A. M., Van Morris, K., Vo, H. H., Eck, S., Lin, Y. F., Rivas, J. M., & Andersson, B. S. (2021). T-cell receptor-based therapy: an innovative therapeutic approach for solid tumors. *Journal of Hematology & Oncology 2021 14:1*, *14*(1), 1–22. https://doi.org/10.1186/S13045-021-01115-0

Turtle, C. J., Hanafi, L. A., Berger, C., Gooley, T. A., Cherian, S., Hudecek, M., Sommermeyer, D., Melville, K., Pender, B., Budiarto, T. M., Robinson, E., Steevens, N. N., Chaney, C., Soma, L., Chen, X., Yeung, C., Wood, B., Li, D., Cao, J., … Maloney, D. G. (2016). CD19 CAR–T cells of defined CD4+:CD8+ composition in adult B cell ALL patients. *The Journal of Clinical Investigation*, *126*(6), 2123. https://doi.org/10.1172/JCI85309

Vallera, D. A., Felices, M., McElmurry, R., McCullar, V., Zhou, X., Schmohl, J. U., Zhang, B., Lenvik, A. J., Panoskaltsis-Mortari, A., Verneris, M. R., Tolar, J., Cooley, S., Weisdorf, D. J., Blazar, B. R., & Miller, J. S. (2016). IL15 Trispecific Killer Engagers (TriKE) Make Natural Killer Cells Specific to CD33+ Targets While Also Inducing Persistence, In Vivo Expansion, and Enhanced Function. *Clinical Cancer Research : An Official Journal of the American Association for Cancer Research*, *22*(14), 3440–3450. https://doi.org/10.1158/1078-0432.CCR-15-2710

van Boxel, G. I., Stewart-Jones, G., Holmes, S., Sainsbury, S., Shepherd, D., Gillespie, G. M. A., Harlos, K., Stuart, D. I., Owens, R., & Jones, E. Y. (2009). Some lessons from the systematic production and structural analysis of soluble (alpha)(beta) T-cell receptors. *Journal of Immunological Methods*, *350*(1–2), 14–21. https://doi.org/10.1016/J.JIM.2009.08.008

van der Horst, H. J., Nijhof, I. S., Mutis, T., & Chamuleau, M. E. D. (2020). Fc-Engineered Antibodies with Enhanced Fc-Effector Function for the Treatment of B-Cell Malignancies. *Cancers*, *12*(10), 1–24. https://doi.org/10.3390/CANCERS12103041

Van Erp, E. A., Luytjes, W., Ferwerda, G., & Van Kasteren, P. B. (2019). Fc-mediated antibody effector functions during respiratory syncytial virus infection and disease. *Frontiers in Immunology*, *10*(MAR), 548. https://doi.org/10.3389/FIMMU.2019.00548/BIBTEX

Vesely, M. D., Kershaw, M. H., Schreiber, R. D., & Smyth, M. J. (2011). Natural Innate and Adaptive Immunity to Cancer. *Http://Dx.Doi.Org/10.1146/Annurev-Immunol-031210-101324*, *29*, 235–271. https://doi.org/10.1146/ANNUREV-IMMUNOL-031210-101324

Voskoboinik, I., Whisstock, J. C., & Trapani, J. A. (2015). Perforin and granzymes: function, dysfunction and human pathology. *Nature Reviews Immunology 2015 15:6*, *15*(6), 388–400. https://doi.org/10.1038/nri3839

Wagner, E. K., Qerqez, A. N., Stevens, C. A., Nguyen, A. W., Delidakis, G., & Maynard, J. A. (2019). Human cytomegalovirus-specific T-cell receptor engineered for high affinity and soluble expression using mammalian cell display. *Journal of Biological Chemistry*, *294*(15), 5790–5804. https://doi.org/10.1074/jbc.RA118.007187

Wang, X., Mathieu, M., & Brezski, R. J. (2018). IgG Fc engineering to modulate antibody effector functions. In *Protein and Cell*. https://doi.org/10.1007/s13238-017-0473-8

Warwas, K. M., Meyer, M., Gonçalves, M., Moldenhauer, G., Bulbuc, N., Knabe, S., Luckner-Minden, C., Ziegelmeier, C., Heussel, C. P., Zörnig, I., Jäger, D., & Momburg, F. (2021). Co-Stimulatory Bispecific Antibodies Induce Enhanced T Cell Activation and Tumor Cell Killing in Breast Cancer Models. *Frontiers in Immunology*, *12*. https://doi.org/10.3389/FIMMU.2021.719116

Weeber, F., Ooft, S. N., Dijkstra, K. K., & Voest, E. E. (2017). Tumor Organoids as a Pre-clinical Cancer Model for Drug Discovery. *Cell Chemical Biology*, *24*(9), 1092–1100. https://doi.org/10.1016/J.CHEMBIOL.2017.06.012

Wei, F., Cheng, X. X., Xue, J. Z., & Xue, S. A. (2022). Emerging Strategies in TCR-Engineered T Cells. *Frontiers in Immunology*, *13*, 1279. https://doi.org/10.3389/FIMMU.2022.850358/BIBTEX

Wieczorek, M., Abualrous, E. T., Sticht, J., Álvaro-Benito, M., Stolzenberg, S., Noé, F., & Freund, C. (2017). Major histocompatibility complex (MHC) class I and MHC class II proteins: Conformational plasticity in antigen presentation. *Frontiers in Immunology*, *8*(MAR), 292. https://doi.org/10.3389/FIMMU.2017.00292/BIBTEX

Willcoj, B. E., Gao, G. F., Wyer, J. R., O'callaghan, C. A., Jakobsen, B. K., Boulter, J. M., Bell, J. I., Jones, E. Y., & Van Der Merwe, P. A. (1999). Production of soluble alphabeta T-cell receptor heterodimers suitable for biophysical analysis of ligand binding. *Protein Science : A Publication of the Protein Society*, *8*(11), 2418–2423. https://doi.org/10.1110/PS.8.11.2418

Wu, J., Fu, J., Zhang, M., & Liu, D. (2015). AFM13: A first-in-class tetravalent bispecific anti-CD30/CD16A antibody for NK cell-mediated immunotherapy. *Journal of Hematology and Oncology*, *8*(1), 1–4. https://doi.org/10.1186/S13045-015-0188-3/FIGURES/3

Wu, Z., & Cheung, N. V. (2018). T cell engaging bispecific antibody (T-BsAb): from technology to therapeutics. *Pharmacology & Therapeutics*, *182*, 161. https://doi.org/10.1016/J.PHARMTHERA.2017.08.005

Wulhfard, S., Baldi, L., Hacker, D. L., & Wurm, F. (2010). Valproic acid enhances recombinant mRNA and protein levels in transiently transfected Chinese hamster ovary cells. *Journal*

of Biotechnology, *148*(2–3), 128–132. https://doi.org/10.1016/J.JBIOTEC.2010.05.003

Wulhfard, S., Tissot, S., Bouchet, S., Cevey, J., De Jesus, M., Hacker, D. L., & Wurm, F. M. (2008). Mild hypothermia improves transient gene expression yields several fold in Chinese hamster ovary cells. *Biotechnology Progress*, *24*(2), 458–465. https://doi.org/10.1021/BP070286C

Xu, D., Alegre, M. L., Varga, S. S., Rothermel, A. L., Collins, A. M., Pulito, V. L., Hanna, L. S., Dolan, K. P., Parren, P. W. H. I., Bluestone, J. A., Jolliffe, L. K., & Zivin, R. A. (2000). In Vitro Characterization of Five Humanized OKT3 Effector Function Variant Antibodies. *Cellular Immunology*, *200*(1), 16–26. https://doi.org/10.1006/CIMM.2000.1617

Xuan, X. Y., Zhang, J. F., Hu, G. M., Li, Q. R., Liu, P. P., & Du, Y. (2015). Upregulated expression of NKG2D and its ligands give potential therapeutic targets for patients with thymoma. *Cancer Gene Therapy 2015 22:7*, *22*(7), 368–374. https://doi.org/10.1038/cgt.2015.29

Zahavi, D., & Weiner, L. (2020). Monoclonal Antibodies in Cancer Therapy. *Antibodies (Basel, Switzerland)*, *9*(3), 34. https://doi.org/10.3390/ANTIB9030034

Zhang, N., & Bevan, M. J. (2011). CD8+ T Cells: Foot Soldiers of the Immune System. *Immunity*, *35*(2), 161–168. https://doi.org/10.1016/J.IMMUNI.2011.07.010

Zhang, T., Scott, J. M., Hwang, I., & Kim, S. (2013). Antibody-dependent memory-like NK cells distinguished by FcRγ-deficiency. *Journal of Immunology (Baltimore, Md. : 1950)*, *190*(4), 1402. https://doi.org/10.4049/JIMMUNOL.1203034

Zhang, Z., Liu, S., Zhang, B., Qiao, L., Zhang, Y., & Zhang, Y. (2020). T Cell Dysfunction and Exhaustion in Cancer. *Frontiers in Cell and Developmental Biology*, *8*, 17. https://doi.org/10.3389/FCELL.2020.00017/BIBTEX

Zhao, W. Bin, Shen, Y., Liu, W. H., Li, Y. M., Jin, S. J., Xu, Y. C., Pan, L. Q., Zhou, Z., & Chen, S. Q. (2021). Soluble Expression of Fc-Fused T Cell Receptors Allows Yielding Novel Bispecific T Cell Engagers. *Biomedicines*, *9*(7). https://doi.org/10.3390/BIOMEDICINES9070790

Zheng, J., Guo, Y., Ji, X., Cui, L., & He, W. (2013). A novel antibody-like TCRγδ-Ig fusion protein exhibits antitumor activity against human ovarian carcinoma. *Cancer Letters*, *341*(2), 150–158. https://doi.org/10.1016/J.CANLET.2013.07.036

Zhu, J., & Paul, W. E. (2008). CD4 T cells: Fates, functions, and faults. *Blood*, *112*(5), 1557–1569. https://doi.org/10.1182/blood-2008-05-078154

Zikherman, J., & Weiss, A. (2009). Antigen receptor signaling in the rheumatic diseases.

Arthritis Research & Therapy 2009 11:1, *11*(1), 1–9. https://doi.org/10.1186/AR2528

6 Appendix

6.1 Sequences used for the different TCR formats

The following section lists the sequences of all different TCR formats incorporating the CMV pp65-specific TCR as example. The ER leader peptides are marked in grey and the T2A is marked in purple. The glycine-serine linkers are marked in light grey and the antigen binding domains from the scFv are marked in turquoise. Affinity-enhancing mutations within the TCR are shown in red and the original amino acids within the wildtype TCRs are shown in green and. The Strep Tag is shown in bold black letters.

TCR-Fc^{enh}

MEKNPLAAPLLILWFHLDC*VSS*ILNVEQSPQSLHVQEGDSTNFTCSFPSSNFYALHWYRWETAKSPEALFVMTLN
GDEKKKGRISATLNTKEGYSYLYIKGSQPEDSATYLCARN**Y**GN**H**FYFGTGTSLTVIPNIQNPDPAVYQLRDSKSS
DKSVCLFTDFDSQTQVSQSKDSDVYITDKCVLDMRSMDFKSNSAVAWSQKSDFACANAFQNSIIPEDTFFPSPES
SCDVKL*AS*EPKS***S***DKTHTCPPCPAPELLGGP***D***VFLFPPKPKDTLMISRTPEVTCVVVDVSHEDPEVKFNWYVDGV
EVHNAKTKPREEQYNSTYRVVSVLTVLHQDWLNGKEYKCKVSNKALP***L***P***E***EKTISKAKGQPREPQVYTLPPSRDE
LTKNQVSLTCLVKGFYPSDIAVEWESNGQPENNYKTTPPVLDSDGSFFLYSKLTVDKSRWQQGNVFSCSVMHEAL
HNHYTQKSLSLSPGK*DPG***WSHPQFEK***SS*RRKRGSGEGR*GSL*LTCGDVEENPGPMYRMQLLSCIALSLALV*TNS*GV
TQTPKFQVLKTGQSMTLQCAQDMNHEYMSWYRQDPGMGLRLIHYSVGAGITDQGEVPNGYNVSRSTTEDFPLRLL
SAAPSQTSVYFCASS**L**VTGG**V**Y**L**YTFGSGTRLTVVEDLKNVFPPKVAVFEPSEAEISHTQKATLVCLATGFYPDH
VELSWWVNGKEVHSGVCTDPQPLKEQPALQDSRYSLSSRLRVSATFWQNPRNHFRCQVQFYGLSENDEWTQDRAK
PVTQIVSAEAWGRADC*

TCR-Fc^{aglyc}

MEKNPLAAPLLILWFHLDC*VSS*ILNVEQSPQSLHVQEGDSTNFTCSFPSSNFYALHWYRWETAKSPEALFVMTLN
GDEKKKGRISATLNTKEGYSYLYIKGSQPEDSATYLCARN**Y**GN**H**FYFGTGTSLTVIPNIQNPDPAVYQLRDSKSS
DKSVCLFTDFDSQTQVSQSKDSDVYITDKCVLDMRSMDFKSNSAVAWSQKSDFACANAFQNSIIPEDTFFPSPES
SCDVKL*AS*EPKS***S***DK*TRQL*HHHHHHHHQLGLNDIFEAQKIEWHELVPRGSLVPRGS*TS*HTCPPCPAPELLGGPSV
FLFPPKPKDTLMISRTPEVTCVVVDVSHEDPEVKFNWYVDGVEVHNAKTKPREEQY***Q***STYRVVSVLTVLHQDWLN
GKEYKCKVSNKALPAPIEKTISKAKGQPREPQVYTLPPSRDELTKNQVSLTCLVKGFYPSDIAVEWESNGQPENN
YKTTPPVLDSDGSFFLYSKLTVDKSRWQQGNVFSCSVMHEALHNHYTQKSLSLSPGK*DPG***WSHPQFEK***SS*RRKRG
SGEGR*GSL*LTCGDVEENPGPMYRMQLLSCIALSLALV*TNS*GVTQTPKFQVLKTGQSMTLQCAQDMNHEYMSWYRQ
DPGMGLRLIHYSVGAGITDQGEVPNGYNVSRSTTEDFPLRLLSAAPSQTSVYFCASS**L**VTGG**V**Y**L**YTFGSGTRLT
VVEDLKNVFPPKVAVFEPSEAEISHTQKATLVCLATGFYPDHVELSWWVNGKEVHSGVCTDPQPLKEQPALQDSR
YSLSSRLRVSATFWQNPRNHFRCQVQFYGLSENDEWTQDRAKPVTQIVSAEAWGRADC*

TCRα-αCD16-Fc^{aglyc}

MEKNPLAAPLLILWFHLDC*VSS*ILNVEQSPQSLHVQEGDSTNFTCSFPSSNFYALHWYRWETAKSPEALFVMTLN
GDEKKKGRISATLNTKEGYSYLYIKGSQPEDSATYLCARN**Y**GN**H**FYFGTGTSLTVIPNIQN*PDP*AVYQLRDSKSS
DKSVCLFTDFDSQTQVSQSKDSDVYITDKCVLDMRSMDFKSNSAVAWSQKSDFACANAFQNSIIPEDTFFPSPES
SCDVKL*AS*GGGSEVQLVQSGAEVKKPGESLKVSCKASGYTFTSYYMHWVRQAPGQGLEWMGIINPSGGSTSYAQK

FQGRVTMTRDTSTSTVYMELSSLRSEDTAVYYCARGSAYYYDFADYWGQGTLVTVSSGSASAPTLKLEEGEFSEA
RVQPVLTQPSSVSVAPGQTATISCGGHNIGSKNVHWYQQRPGQSPVLVIYQDNKRPSGIPERFSGSNSGNTATLT
ISGTQAMDEADYYCQVWDNYSVLFGGGTKLTVL*AS*EPKSSDKTS*QL***HHHHHHHH***QL***GLNDIFEAQKIEWHE**LVPR
GSLVPRGS*TS*HTCPPCPAPELLGGPSVFLFPPKPKDTLMISRTPEVTCVVVDVSHEDPEVKFNWYVDGVEVHNAK
TKPREEQY***Q***STYRVVSVLTVLHQDWLNGKEYKCKVSNKALPAPIEKTISKAKGQPREPQVYTLPPSRDELTKNQV
SLTCLVKGFYPSDIAVEWESNGQPENNYKTTPPVLDSDGSFFLYSKLTVDKSRWQQGNVFSCSVMHEALHNHYTQ
KSLSLSPGK*DPG***WSHPQFEK***SS*RRKRGSGEGR*GSL*LTCGDVEENPGPMYRMQLLSCIALSLALV*TNS*GVTQTPKF
QVLKTGQSMTLQCAQDMNHEYMSWYRQDPGMGLRLIHYSVGAGITDQGEVPNGYNVSRSTTEDFPLRLLSAAPSQ
TSVYFCASS**L**VTGG**V**Y**L**YTFGSGTRLTVVEDLKNVFPPKVAVFEPSEAEISHTQKATLVCLATGFYPDHVELSWW
VNGKEVHSGVCTDPQPLKEQPALQDSRYSLSSRLRVSATFWQNPRNHFRCQVQFYGLSENDEWTQDRAKPVTQIV
SAEAWGRADC*

TCRβ-αCD16-Fc^{aglyc}

MEKNPLAAPLLILWFHLDC*VSS*ILNVEQSPQSLHVQEGDSTNFTCSFPSSNFYALHWYRWETAKSPEALFVMTLN
GDEKKKGRISATLNTKEGYSYLYIKGSQPEDSATYLCARN**Y**GN**H**FYFGTGTSLTVIPNIQNPDPAVYQLRDSKSS
DKSVCLFTDFDSQTQVSQSKDSDVYITDKCVLDMRSMDFKSNSAVAWSQKSDFACANAFQNSIIPEDTFFPSPES
SCDVKL*AS*EPKS***S***DK*TRQL*HHHHHHHHHQLGLNDIFEAQKIEWHELVPRGSLVPRGS*TS*HTCPPCPAPELLGGPSV
FLFPPKPKDTLMISRTPEVTCVVVDVSHEDPEVKFNWYVDGVEVHNAKTKPREEQY***Q***STYRVVSVLTVLHQDWLN
GKEYKCKVSNKALPAPIEKTISKAKGQPREPQVYTLPPSRDELTKNQVSLTCLVKGFYPSDIAVEWESNGQPENN
YKTTPPVLDSDGSFFLYSKLTVDKSRWQQGNVFSCSVMHEALHNHYTQKSLSLSPGK*DPG***WSHPQFEK***SS*RRKRG
SGEGR*GSL*LTCGDVEENPGPMYRMQLLSCIALSLALV*TNS*GVTQTPKFQVLKTGQSMTLQCAQDMNHEYMSWYRQ
DPGMGLRLIHYSVGAGITDQGEVPNGYNVSRSTTEDFPLRLLSAAPSQTSVYFCASS**L**VTGG**V**Y**L**YTFGSGTRLT
VVEDLKNVFPPKVAVFEPSEAEISHTQKATLVCLATGFYPDHVELSWWVNGKEVHSGVCTDPQPLKEQPALQDSR
YSLSSRLRVSATFWQNPRNHFRCQVQFYGLSENDEWTQDRAKPVTQIVSAEAWGRADCGF*TS*GGGSEVQLVQSGA
EVKKPGESLKVSCKASGYTFTSYYMHWVRQAPGQGLEWMGIINPSGGSTSYAQKFQGRVTMTRDTSTSTVYMELS
SLRSEDTAVYYCARGSAYYYDFADYWGQGTLVTVSSGSASAPTLKLEEGEFSEARVQPVLTQPSSVSVAPGQTAT
ISCGGHNIGSKNVHWYQQRPGQSPVLVIYQDNKRPSGIPERFSGSNSGNTATLTISGTQAMDEADYYCQVWDNYS
VLFGGGTKLTVL*AS*GGGS*QLGNSAS**

TCRα-αCD16-Fc^{enh}

MEKNPLAAPLLILWFHLDC*VSS*ILNVEQSPQSLHVQEGDSTNFTCSFPSSNFYALHWYRWETAKSPEALFVMTLN
GDEKKKGRISATLNTKEGYSYLYIKGSQPEDSATYLCARN**Y**GN**H**FYFGTGTSLTVIPNIQN*PDP*AVYQLRDSKSS
DKSVCLFTDFDSQTQVSQSKDSDVYITDKCVLDMRSMDFKSNSAVAWSQKSDFACANAFQNSIIPEDTFFPSPES
SCDVKL*AS*GGGSEVQLVQSGAEVKKPGESLKVSCKASGYTFTSYYMHWVRQAPGQGLEWMGIINPSGGSTSYAQK
FQGRVTMTRDTSTSTVYMELSSLRSEDTAVYYCARGSAYYYDFADYWGQGTLVTVSSGSASAPTLKLEEGEFSEA
RVQPVLTQPSSVSVAPGQTATISCGGHNIGSKNVHWYQQRPGQSPVLVIYQDNKRPSGIPERFSGSNSGNTATLT
ISGTQAMDEADYYCQVWDNYSVLFGGGTKLTVL*AS*EPKS***S***DKTHTCPPCPAPELLGGP***D***VFLFPPKPKDTLMISR
TPEVTCVVVDVSHEDPEVKFNWYVDGVEVHNAKTKPREEQYNSTYRVVSVLTVLHQDWLNGKEYKCKVSNKALP***L***
P***E***EKTISKAKGQPREPQVYTLPPSRDELTKNQVSLTCLVKGFYPSDIAVEWESNGQPENNYKTTPPVLDSDGSFF
LYSKLTVDKSRWQQGNVFSCSVMHEALHNHYTQKSLSLSPGK*DPG***WSHPQFEK***SS*RRKRGSGEGR*GSL*LTCGDVE
ENPGPMYRMQLLSCIALSLALV*TNS*GVTQTPKFQVLKTGQSMTLQCAQDMNHEYMSWYRQDPGMGLRLIHYSVGA
GITDQGEVPNGYNVSRSTTEDFPLRLLSAAPSQTSVYFCASS**L**VTGG**V**Y**L**YTFGSGTRLTVVEDLKNVFPPKVAV

FEPSEAEISHTQKATLVCLATGFYPDHVELSWWVNGKEVHSGVCTDPQPLKEQPALQDSRYSLSSRLRVSATFWQ
NPRNHFRCQVQFYGLSENDEWTQDRAKPVTQIVSAEAWGRADC*

TCRβ-αCD16-Fc^{enh}

MEKNPLAAPLLILWFHLDC*VSS*ILNVEQSPQSLHVQEGDSTNFTCSFPSSNFYALHWYRWETAKSPEALFVMTLN
GDEKKKGRISATLNTKEGYSYLYIKGSQPEDSATYLCARN**Y**GN**H**FYFGTGTSLTVIPNIQNPDPAVYQLRDSKSS
DKSVCLFTDFDSQTQVSQSKDSDVYITDKCVLDMRSMDFKSNSAVAWSQKSDFACANAFQNSIIPEDTFFPSPES
SCDVKL*AS*EPKS***S***DKTHTCPPCPAPELLGGP***D***VFLFPPKPKDTLMISRTPEVTCVVVDVSHEDPEVKFNWYVDGV
EVHNAKTKPREEQYNSTYRVVSVLTVLHQDWLNGKEYKCKVSNKALP***L***P***E***EKTISKAKGQPREPQVYTLPPSRDE
LTKNQVSLTCLVKGFYPSDIAVEWESNGQPENNYKTTPPVLDSDGSFFLYSKLTVDKSRWQQGNVFSCSVMHEAL
HNHYTQKSLSLSPGK*DPG***WSHPQFEK***SS*RRKRGSGEGR*GSL*LTCGDVEENPGPMYRMQLLSCIALSLALV*TNS*GV
TQTPKFQVLKTGQSMTLQCAQDMNHEYMSWYRQDPGMGLRLIHYSVGAGITDQGEVPNGYNVSRSTTEDFPLRLL
SAAPSQTSVYFCASS**L**VTGG**V**Y**L**YTFGSGTRLTVVEDLKNVFPPKVAVFEPSEAEISHTQKATLVCLATGFYPDH
VELSWWVNGKEVHSGVCTDPQPLKEQPALQDSRYSLSSRLRVSATFWQNPRNHFRCQVQFYGLSENDEWTQDRAK
PVTQIVSAEAWGRADCGF*TS*GGGSEVQLVQSGAEVKKPGESLKVSCKASGYTFTSYYMHWVRQAPGQGLEWMGII
NPSGGSTSYAQKFQGRVTMTRDTSTSTVYMELSSLRSEDTAVYYCARGSAYYYDFADYWGQGTLVTVSSGSASAP
TLKLEEGEFSEARVQPVLTQPSSVSVAPGQTATISCGGHNIGSKNVHWYQQRPGQSPVLVIYQDNKRPSGIPERF
SGSNSGNTATLTISGTQAMDEADYYCQVWDNYSVLFGGGTKLTVL*AS*GGGS*QLGNSAS**

TCRα-αNKp46-Fc^{aglyc}

MEKNPLAAPLLILWFHLDC*VSS*ILNVEQSPQSLHVQEGDSTNFTCSFPSSNFYALHWYRWETAKSPEALFVMTLN
GDEKKKGRISATLNTKEGYSYLYIKGSQPEDSATYLCARN**Y**GN**H**FYFGTGTSLTVIPNIQN*PDP*AVYQLRDSKSS
DKSVCLFTDFDSQTQVSQSKDSDVYITDKCVLDMRSMDFKSNSAVAWSQKSDFACANAFQNSIIPEDTFFPSPES
SCDVKL*AS*GGGSQVQLVQSGAEVKKPGSSVKVSCKA*SG*YTFSDYVINWVRQAPGQGLEWMGEIYPGSGTNYYNEK
FKAKATITADKSTSTAYMELSSLRSEDTAVYYCARRGRYGLYAMDYWGQGTTVTVSSGGGGSGGGGSGGGGSDIQ
MTQSPSSLSASVGDRVTITCRASQDISNYLNWYQQKPGKAPKLLIYYTSRLHSGVPSRFSGSGSGTDFTFTISSL
QPEDIATYFCQQGNTRPWTFGGGTKVEIK*AS*EPKSSDKTS*QL*HHHHHHHH*QL*GLNDIFEAQKIEWHELVPRGSLV
PRGS*TS*HTCPPCPAPELLGGPSVFLFPPKPKDTLMISRTPEVTCVVVDVSHEDPEVKFNWYVDGVEVHNAKTKPR
EEQY***Q***STYRVVSVLTVLHQDWLNGKEYKCKVSNKALPAPIEKTISKAKGQPREPQVYTLPPSRDELTKNQVSLTC
LVKGFYPSDIAVEWESNGQPENNYKTTPPVLDSDGSFFLYSKLTVDKSRWQQGNVFSCSVMHEALHNHYTQKSLS
LSPGK*DPG***WSHPQFEK***SS*RRKRGSGEGR*GSL*LTCGDVEENPGPMYRMQLLSCIALSLALV*TNS*GVTQTPKFQVLK
TGQSMTLQCAQDMNHEYMSWYRQDPGMGLRLIHYSVGAGITDQGEVPNGYNVSRSTTEDFPLRLLSAAPSQTSVY
FCASS**L**VTGG**V**Y**L**YTFGSGTRLTVVEDLKNVFPPKVAVFEPSEAEISHTQKATLVCLATGFYPDHVELSWWVNGK
EVHSGVCTDPQPLKEQPALQDSRYSLSSRLRVSATFWQNPRNHFRCQVQFYGLSENDEWTQDRAKPVTQIVSAEA
WGRADC*

TCRβ-αNKp46-Fc^{aglyc}

MEKNPLAAPLLILWFHLDC*VSS*ILNVEQSPQSLHVQEGDSTNFTCSFPSSNFYALHWYRWETAKSPEALFVMTLN
GDEKKKGRISATLNTKEGYSYLYIKGSQPEDSATYLCARN**Y**GN**H**FYFGTGTSLTVIPNIQNPDPAVYQLRDSKSS
DKSVCLFTDFDSQTQVSQSKDSDVYITDKCVLDMRSMDFKSNSAVAWSQKSDFACANAFQNSIIPEDTFFPSPES
SCDVKL*AS*EPKS***S***DK*TRQL*HHHHHHHHQLGLNDIFEAQKIEWHELVPRGSLVPRGS*TS*HTCPPCPAPELLGGPSV

FLFPPKPKDTLMISRTPEVTCVVVDVSHEDPEVKFNWYVDGVEVHNAKTKPREEQY***Q***STYRVVSVLTVLHQDWLN
GKEYKCKVSNKALPAPIEKTISKAKGQPREPQVYTLPPSRDELTKNQVSLTCLVKGFYPSDIAVEWESNGQPENN
YKTTPPVLDSDGSFFLYSKLTVDKSRWQQGNVFSCSVMHEALHNHYTQKSLSLSPGK*DPG***WSHPQFEK***SS***RRKRG
SGEGR*GSL*LTCGDVEENPGPMYRMQLLSCIALSLALV*TNS*GVTQTPKFQVLKTGQSMTLQCAQDMNHEYMSWYRQ
DPGMGLRLIHYSVGAGITDQGEVPNGYNVSRSTTEDFPLRLLSAAPSQTSVYFCASS**L**VTGG**V**Y**L**YTFGSGTRLT
VVEDLKNVFPPKVAVFEPSEAEISHTQKATLVCLATGFYPDHVELSWWVNGKEVHSGVCTDPQPLKEQPALQDSR
YSLSSRLRVSATFWQNPRNHFRCQVQFYGLSENDEWTQDRAKPVTQIVSAEAWGRADCGF*TS*GGGSQVQLVQSGA
EVKKPGSSVKVSCKA*SG*YTFSDYVINWVRQAPGQGLEWMGEIYPGSGTNYYNEKFKAKATITADKSTSTAYMELS
SLRSEDTAVYYCARRGRYGLYAMDYWGQGTTVTVSSGGGGSGGGGSGGGGSDIQMTQSPSSLSASVGDRVTITCR
ASQDISNYLNWYQQKPGKAPKLLIYYTSRLHSGVPSRFSGSGSGTDFTFTISSLQPEDIATYFCQQGNTRPWTFG
GGTKVEIK*AS*GGGS*QLGNSAS**

TCRα-αNKp46-Fc^{enh}

MEKNPLAAPLLILWFHLDC*VSS*ILNVEQSPQSLHVQEGDSTNFTCSFPSSNFYALHWYRWETAKSPEALFVMTLN
GDEKKKGRISATLNTKEGYSYLYIKGSQPEDSATYLCARN**Y**GN**H**FYFGTGTSLTVIPNIQN*PDP*AVYQLRDSKSS
DKSVCLFTDFDSQTQVSQSKDSDVYITDKCVLDMRSMDFKSNSAVAWSQKSDFACANAFQNSIIPEDTFFPSPES
SCDVKL*AS*GGGSQVQLVQSGAEVKKPGSSVKVSCKA*SG*YTFSDYVINWVRQAPGQGLEWMGEIYPGSGTNYYNEK
FKAKATITADKSTSTAYMELSSLRSEDTAVYYCARRGRYGLYAMDYWGQGTTVTVSSGGGGSGGGGSGGGGSDIQ
MTQSPSSLSASVGDRVTITCRASQDISNYLNWYQQKPGKAPKLLIYYTSRLHSGVPSRFSGSGSGTDFTFTISSL
QPEDIATYFCQQGNTRPWTFGGGTKVEIK*AS*EPKS***S***DKTHTCPPCPAPELLGGP***D***VFLFPPKPKDTLMISRTPEV
TCVVVDVSHEDPEVKFNWYVDGVEVHNAKTKPREEQYNSTYRVVSVLTVLHQDWLNGKEYKCKVSNKALP***L***P***E***EK
TISKAKGQPREPQVYTLPPSRDELTKNQVSLTCLVKGFYPSDIAVEWESNGQPENNYKTTPPVLDSDGSFFLYSK
LTVDKSRWQQGNVFSCSVMHEALHNHYTQKSLSLSPGK*DPG***WSHPQFEK***SS***RRKRGSGEGR*GSL*LTCGDVEENPG
PMYRMQLLSCIALSLALV*TNS*GVTQTPKFQVLKTGQSMTLQCAQDMNHEYMSWYRQDPGMGLRLIHYSVGAGITD
QGEVPNGYNVSRSTTEDFPLRLLSAAPSQTSVYFCASS**L**VTGG**V**Y**L**YTFGSGTRLTVVEDLKNVFPPKVAVFEPS
EAEISHTQKATLVCLATGFYPDHVELSWWVNGKEVHSGVCTDPQPLKEQPALQDSRYSLSSRLRVSATFWQNPRN
HFRCQVQFYGLSENDEWTQDRAKPVTQIVSAEAWGRADC*

TCRβ-αNKp46-Fc^{enh}

MEKNPLAAPLLILWFHLDC*VSS*ILNVEQSPQSLHVQEGDSTNFTCSFPSSNFYALHWYRWETAKSPEALFVMTLN
GDEKKKGRISATLNTKEGYSYLYIKGSQPEDSATYLCARN**Y**GN**H**FYFGTGTSLTVIPNIQNPDPAVYQLRDSKSS
DKSVCLFTDFDSQTQVSQSKDSDVYITDKCVLDMRSMDFKSNSAVAWSQKSDFACANAFQNSIIPEDTFFPSPES
SCDVKL*AS*EPKS***S***DKTHTCPPCPAPELLGGP***D***VFLFPPKPKDTLMISRTPEVTCVVVDVSHEDPEVKFNWYVDGV
EVHNAKTKPREEQYNSTYRVVSVLTVLHQDWLNGKEYKCKVSNKALP***L***P***E***EKTISKAKGQPREPQVYTLPPSRDE
LTKNQVSLTCLVKGFYPSDIAVEWESNGQPENNYKTTPPVLDSDGSFFLYSKLTVDKSRWQQGNVFSCSVMHEAL
HNHYTQKSLSLSPGK*DPG***WSHPQFEK***SS***RRKRGSGEGR*GSL*LTCGDVEENPGPMYRMQLLSCIALSLALV*TNS*GV
TQTPKFQVLKTGQSMTLQCAQDMNHEYMSWYRQDPGMGLRLIHYSVGAGITDQGEVPNGYNVSRSTTEDFPLRLL
SAAPSQTSVYFCASS**L**VTGG**V**Y**L**YTFGSGTRLTVVEDLKNVFPPKVAVFEPSEAEISHTQKATLVCLATGFYPDH
VELSWWVNGKEVHSGVCTDPQPLKEQPALQDSRYSLSSRLRVSATFWQNPRNHFRCQVQFYGLSENDEWTQDRAK
PVTQIVSAEAWGRADCGF*TS*GGGSQVQLVQSGAEVKKPGSSVKVSCKA*SG*YTFSDYVINWVRQAPGQGLEWMGEI
YPGSGTNYYNEKFKAKATITADKSTSTAYMELSSLRSEDTAVYYCARRGRYGLYAMDYWGQGTTVTVSSGGGGSG

GGGSGGGGSDIQMTQSPSSLSASVGDRVTITCRASQDISNYLNWYQQKPGKAPKLLIYYTSRLHSGVPSRFSGSG
SGTDFTFTISSLQPEDIATYFCQQGNTRPWTFGGGTKVEIK*AS*GGGS*QLGNSAS**

TCRα-αCD3(OKT3$_{LGH}$)-Fc^{aglyc}

MEKNPLAAPLLILWFHLDC*VSS*ILNVEQSPQSLHVQEGDSTNFTCSFPSSNFYALHWYRWETAKSPEALFVMTLN
GDEKKKGRISATLNTKEGYSYLYIKGSQPEDSATYLCARN**T**GN**Q**FYFGTGTSLTVIPNIQNPDPAVYQLRDSKSS
DKSVCLFTDFDSQTQVSQSKDSDVYITDKCVLDMRSMDFKSNSAVAWSQKSDFACANAFQNSIIPEDTFFPSPES
SCDVKL*AR*SGGGGSQIVLTQSPAIMSASPGEKVTMTCSASSSVSYMNWYQQKSGTSPKRWIYDTSKLASGVPAHF
RGSGSGTSYSLTISGMEAEDAATYYCQQWSSNPFTFGSGTKLEINGGGGSGGGGSGGGGSQVQLQQSGAELARPG
ASVKMSCKASGYTFTRYTMHWVKQRPGQGLEWIGYINPSRGYTNYNQKFKDKATLTTDKSSSTAYMQLSSLTSED
SAVYYCARYYDDHYCLDYWGQGTTLTVSS*AS*EPKS***S***DK*TRQL*HHHHHHHHQLGLNDIFEAQKIEWHELVPRGSLV
PRGS*TS*HTCPPCPAPELLGGPSVFLFPPKPKDTLMISRTPEVTCVVVDVSHEDPEVKFNWYVDGVEVHNAKTKPR
EEQY***Q***STYRVVSVLTVLHQDWLNGKEYKCKVSNKALPAPIEKTISKAKGQPREPQVYTLPPSRDELTKNQVSLTC
LVKGFYPSDIAVEWESNGQPENNYKTTPPVLDSDGSFFLYSKLTVDKSRWQQGNVFSCSVMHEALHNHYTQKSLS
LSPG*DPG***WSHPQFEK***SS*RRKRGSGEGR*GSL*LTCGDVEENPGPMYRMQLLSCIALSLALV*TNS*GVTQTPKFQVLKT
GQSMTLQCAQDMNHEYMSWYRQDPGMGLRLIHYSVGAGITDQGEVPNGYNVSRSTTEDFPLRLLSAAPSQTSVYF
CASS**P**VTGG**I**Y**G**YTFGSGTRLTVVEDLKNVFPPKVAVFEPSEAEISHTQKATLVCLATGFYPDHVELSWWVNGKE
VHSGVCTDPQPLKEQPALQDSRYSLSSRLRVSATFWQNPRNHFRCQVQFYGLSENDEWTQDRAKPVTQIVSAEAW
GRADC*

TCRβ-αCD3(OKT3$_{LGH}$)-Fc^{aglyc}

MEKNPLAAPLLILWFHLDC*VSS*ILNVEQSPQSLHVQEGDSTNFTCSFPSSNFYALHWYRWETAKSPEALFVMTLN
GDEKKKGRISATLNTKEGYSYLYIKGSQPEDSATYLCARN**T**GN**Q**FYFGTGTSLTVIPNIQNPDPAVYQLRDSKSS
DKSVCLFTDFDSQTQVSQSKDSDVYITDKCVLDMRSMDFKSNSAVAWSQKSDFACANAFQNSIIPEDTFFPSPES
SCDVKL*AS*EPKS***S***DKTHTCPPCPAPELLGGPSVFLFPPKPKDTLMISRTPEVTCVVVDVSHEDPEVKFNWYVDGV
EVHNAKTKPREEQY***Q***STYRVVSVLTVLHQDWLNGKEYKCKVSNKALPAPIEKTISKAKGQPREPQVYTLPPSRDE
LTKNQVSLTCLVKGFYPSDIAVEWESNGQPENNYKTTPPVLDSDGSFFLYSKLTVDKSRWQQGNVFSCSVMHEAL
HNHYTQKSLSLSPG*DPG***WSHPQFEK***SS*RRKRGSGEGR*GSL*LTCGDVEENPGPMYRMQLLSCIALSLALV*TNS*GVT
QTPKFQVLKTGQSMTLQCAQDMNHEYMSWYRQDPGMGLRLIHYSVGAGITDQGEVPNGYNVSRSTTEDFPLRLLS
AAPSQTSVYFCASS**P**VTGG**I**Y**G**YTFGSGTRLTVVEDLKNVFPPKVAVFEPSEAEISHTQKATLVCLATGFYPDHV
ELSWWVNGKEVHSGVCTDPQPLKEQPALQDSRYSLSSRLRVSATFWQNPRNHFRCQVQFYGLSENDEWTQDRAKP
VTQIVSAEAWGRADCGF*TS*SGGGGSQIVLTQSPAIMSASPGEKVTMTCSASSSVSYMNWYQQKSGTSPKRWIYDT
SKLASGVPAHFRGSGSGTSYSLTISGMEAEDAATYYCQQWSSNPFTFGSGTKLEINGGGGSGGGGSGGGGSQVQL
QQSGAELARPGASVKMSCKASGYTFTRYTMHWVKQRPGQGLEWIGYINPSRGYTNYNQKFKDKATLTTDKSSSTA
YMQLSSLTSEDSAVYYCARYYDDHYCLDYWGQGTTLTVSS*AS**

TCRα-αCD3(OKT3$_{HGL}$)-Fc^{aglyc}

MEKNPLAAPLLILWFHLDC*VSS*ILNVEQSPQSLHVQEGDSTNFTCSFPSSNFYALHWYRWETAKSPEALFVMTLN
GDEKKKGRISATLNTKEGYSYLYIKGSQPEDSATYLCARN**T**GN**Q**FYFGTGTSLTVIPNIQNPDPAVYQLRDSKSS
DKSVCLFTDFDSQTQVSQSKDSDVYITDKCVLDMRSMDFKSNSAVAWSQKSDFACANAFQNSIIPEDTFFPSPES
SCDVKL*AR*SGGGGSQVQLQQSGAELARPGASVKMSCKASGYTFTRYTMHWVKQRPGQGLEWIGYINPSRGYTNYN

QKFKDKATLTTDKSSSTAYMQLSSLTSEDSAVYYCARYYDDHYCLDYWGQGTTLTVSSVEGGSGGSGGSGGSGGV
DQIVLTQSPAIMSASPGEKVTMTCSASSSVSYMNWYQQKSGTSPKRWIYDTSKLASGVPAHFRGSGSGTSYSLTI
SGMEAEDAATYYCQQWSSNPFTFGSGTKLEIN*AS*EPKS***S***DK*TRQL*HHHHHHHHHQLGLNDIFEAQKIEWHELVPRG
SLVPRGS*TS*HTCPPCPAPELLGGPSVFLFPPKPKDTLMISRTPEVTCVVVDVSHEDPEVKFNWYVDGVEVHNAKT
KPREEQY***Q***STYRVVSVLTVLHQDWLNGKEYKCKVSNKALPAPIEKTISKAKGQPREPQVYTLPPSRDELTKNQVS
LTCLVKGFYPSDIAVEWESNGQPENNYKTTPPVLDSDGSFFLYSKLTVDKSRWQQGNVFSCSVMHEALHNHYTQK
SLSLSPG*DPG***WSHPQFEK***SS***RRKRGSGEGR*GSL*LTCGDVEENPGPMYRMQLLSCIALSLALV*TNS*GVTQTPKFQV
LKTGQSMTLQCAQDMNHEYMSWYRQDPGMGLRLIHYSVGAGITDQGEVPNGYNVSRSTTEDFPLRLLSAAPSQTS
VYFCASSPVTGGIYGYTFGSGTRLTVVEDLKNVFPPKVAVFEPSEAEISHTQKATLVCLATGFYPDHVELSWWVN
GKEVHSGVCTDPQPLKEQPALQDSRYSLSSRLRVSATFWQNPRNHFRCQVQFYGLSENDEWTQDRAKPVTQIVSA
EAWGRADC*

TCRβ-αCD3(OKT3$_{HGL}$)-Fc^{aglyc}

MEKNPLAAPLLILWFHLDC*VSS*ILNVEQSPQSLHVQEGDSTNFTCSFPSSNFYALHWYRWETAKSPEALFVMTLN
GDEKKKGRISATLNTKEGYSYLYIKGSQPEDSATYLCARNTGNQFYFGTGTSLTVIPNIQNPDPAVYQLRDSKSS
DKSVCLFTDFDSQTQVSQSKDSDVYITDKCVLDMRSMDFKSNSAVAWSQKSDFACANAFQNSIIPEDTFFPSPES
SCDVKL*AS*EPKS***S***DKTHTCPPCPAPELLGGPSVFLFPPKPKDTLMISRTPEVTCVVVDVSHEDPEVKFNWYVDGV
EVHNAKTKPREEQY***Q***STYRVVSVLTVLHQDWLNGKEYKCKVSNKALPAPIEKTISKAKGQPREPQVYTLPPSRDE
LTKNQVSLTCLVKGFYPSDIAVEWESNGQPENNYKTTPPVLDSDGSFFLYSKLTVDKSRWQQGNVFSCSVMHEAL
HNHYTQKSLSLSPG*DPG***WSHPQFEK***SS***RRKRGSGEGR*GSL*LTCGDVEENPGPMYRMQLLSCIALSLALV*TNS*GVT
QTPKFQVLKTGQSMTLQCAQDMNHEYMSWYRQDPGMGLRLIHYSVGAGITDQGEVPNGYNVSRSTTEDFPLRLLS
AAPSQTSVYFCASSPVTGGIYGYTFGSGTRLTVVEDLKNVFPPKVAVFEPSEAEISHTQKATLVCLATGFYPDHV
ELSWWVNGKEVHSGVCTDPQPLKEQPALQDSRYSLSSRLRVSATFWQNPRNHFRCQVQFYGLSENDEWTQDRAKP
VTQIVSAEAWGRADCGF*TS*SGGGGSQVQLQQSGAELARPGASVKMSCKASGYTFTRYTMHWVKQRPGQGLEWIGY
INPSRGYTNYNQKFKDKATLTTDKSSSTAYMQLSSLTSEDSAVYYCARYYDDHYCLDYWGQGTTLTVSSVEGGSG
GSGGSGGSGGVDQIVLTQSPAIMSASPGEKVTMTCSASSSVSYMNWYQQKSGTSPKRWIYDTSKLASGVPAHFRG
SGSGTSYSLTISGMEAEDAATYYCQQWSSNPFTFGSGTKLEIN*AS**

TCRα-αCD3(r3M UCHT1)-Fc^{aglyc}

MEKNPLAAPLLILWFHLDC*VSS*ILNVEQSPQSLHVQEGDSTNFTCSFPSSNFYALHWYRWETAKSPEALFVMTLN
GDEKKKGRISATLNTKEGYSYLYIKGSQPEDSATYLCARNTGNQFYFGTGTSLTVIPNIQNPDPAVYQLRDSKSS
DKSVCLFTDFDSQTQVSQSKDSDVYITDKCVLDMRSMDFKSNSAVAWSQKSDFACANAFQNSIIPEDTFFPSPES
SCDVKL*AR*SGGGGSDIQMTQSPSSLSASVGDRVTITCRASQDIRNYLNWYQQKPGKAPKLLIYYTSRLESGVPSR
FSGSGSGTDYTLTISSLQPEDFATYYCQQGNTLPWTFGQGTKVEIKGGGGSGGGGSGGGGSEVQLVESGGGLVQP
GGSLRLSCAASGYSFTGYTMNWVRQAPGKGLEWVALINPYKGVSTYNQKFKDRFTISVDKSKNTAYLQMNSLRAE
DTAVYYCARSGYYGDSDWYFDVWGQGTLVTVSS*AS*EPKS***S***DK*TRQL*HHHHHHHHHQLGLNDIFEAQKIEWHELVPR
GSLVPRGS*TS*HTCPPCPAPELLGGPSVFLFPPKPKDTLMISRTPEVTCVVVDVSHEDPEVKFNWYVDGVEVHNAK
TKPREEQY***Q***STYRVVSVLTVLHQDWLNGKEYKCKVSNKALPAPIEKTISKAKGQPREPQVYTLPPSRDELTKNQV
SLTCLVKGFYPSDIAVEWESNGQPENNYKTTPPVLDSDGSFFLYSKLTVDKSRWQQGNVFSCSVMHEALHNHYTQ
KSLSLSPG*DPG***WSHPQFEK***SS***RRKRGSGEGR*GSL*LTCGDVEENPGPMYRMQLLSCIALSLALV*TNS*GVTQTPKFQ
VLKTGQSMTLQCAQDMNHEYMSWYRQDPGMGLRLIHYSVGAGITDQGEVPNGYNVSRSTTEDFPLRLLSAAPSQT
SVYFCASSPVTGGIYGYTFGSGTRLTVVEDLKNVFPPKVAVFEPSEAEISHTQKATLVCLATGFYPDHVELSWWV

NGKEVHSGVCTDPQPLKEQPALQDSRYSLSSRLRVSATFWQNPRNHFRCQVQFYGLSENDEWTQDRAKPVTQIVS
AEAWGRADC*

TCRβ-αCD3(r3M UCHT1)-Fc^{aglyc}

MEKNPLAAPLLILWFHLDC*VSS*ILNVEQSPQSLHVQEGDSTNFTCSFPSSNFYALHWYRWETAKSPEALFVMTLN
GDEKKKGRISATLNTKEGYSYLYIKGSQPEDSATYLCARN**T**GN**Q**FYFGTGTSLTVIPNIQNPDPAVYQLRDSKSS
DKSVCLFTDFDSQTQVSQSKDSDVYITDKCVLDMRSMDFKSNSAVAWSQKSDFACANAFQNSIIPEDTFFPSPES
SCDVKL*AS*EPKS***S***DKTHTCPPCPAPELLGGPSVFLFPPKPKDTLMISRTPEVTCVVVDVSHEDPEVKFNWYVDGV
EVHNAKTKPREEQY***Q***STYRVVSVLTVLHQDWLNGKEYKCKVSNKALPAPIEKTISKAKGQPREPQVYTLPPSRDE
LTKNQVSLTCLVKGFYPSDIAVEWESNGQPENNYKTTPPVLDSDGSFFLYSKLTVDKSRWQQGNVFSCSVMHEAL
HNHYTQKSLSLSPG*DPG***WSHPQFEK***SS*RRKRGSGEGR*GSL*LTCGDVEENPGPMYRMQLLSCIALSLALV*TNS*GVT
QTPKFQVLKTGQSMTLQCAQDMNHEYMSWYRQDPGMGLRLIHYSVGAGITDQGEVPNGYNVSRSTTEDFPLRLLS
AAPSQTSVYFCASS**P**VTGG**I**Y**G**YTFGSGTRLTVVEDLKNVFPPKVAVFEPSEAEISHTQKATLVCLATGFYPDHV
ELSWWVNGKEVHSGVCTDPQPLKEQPALQDSRYSLSSRLRVSATFWQNPRNHFRCQVQFYGLSENDEWTQDRAKP
VTQIVSAEAWGRADCGF*TS*SGGGGSDIQMTQSPSSLSASVGDRVTITCRASQDIRNYLNWYQQKPGKAPKLLIYY
TSRLESGVPSRFSGSGSGTDYTLTISSLQPEDFATYYCQQGNTLPWTFGQGTKVEIKGGGGSGGGGSGGGGSEVQ
LVESGGGLVQPGGSLRLSCAASGYSFTGYTMNWVRQAPGKGLEWVALINPYKGVSTYNQKFKDRFTISVDKSKNT
AYLQMNSLRAEDTAVYYCARSGYYGDSDWYFDVWGQGTLVTVSS*AS**

6.2 Sequences of the TCR clones used

This section lists the TCRα and TCRβ sequences of all different TCR clones used in this thesis. Affinity-enhancing mutations within the TCR are indicated in red and the original amino acids within the wildtype TCRs are indicated in green.

Wildtype/ low-affinity CMV pp65$_{495\text{-}503}$-specific TCR clone Ra14:

TCRα: ILNVEQSPQSLHVQEGDSTNFTCSFPSSNFYALHWYRWETAKSPEALFVMTLNGDEKKKGRISATLNTK
EGYSYLYIKGSQPEDSATYLCARN**T**GN**Q**FYFGTGTSLTVIPNIQNPDPAVYQLRDSKSSDKSVCLFTDFDSQTQV
SQSKDSDVYITDKCVLDMRSMDFKSNSAVAWSQKSDFACANAFQNSIIPEDTFFPSPESSCDVKL

TCRβ: GVTQTPKFQVLKTGQSMTLQCAQDMNHEYMSWYRQDPGMGLRLIHYSVGAGITDQGEVPNGYNVSRSTT
EDFPLRLLSAAPSQTSVYFCASS**P**VTGG**I**Y**G**YTFGSGTRLTVVED*LK*NVFPPKVAVFEPSEAEISHTQKATLV**C**L
ATGFYPDHVELSWWVNGKEVHSGV**C**TDPQPLKEQPALQDSRY**S**LSSRLRVSATFWQNPRNHFR**C**QVQFYGLSEND
EWTQDRAKPVTQIVSAEAWGRAD**C***

Mutated/ high-affinity CMV pp65$_{495\text{-}503}$-specific TCR clone Ra14:

TCRα: ILNVEQSPQSLHVQEGDSTNFTCSFPSSNFYALHWYRWETAKSPEALFVMTLNGDEKKKGRISATLNTK
EGYSYLYIKGSQPEDSATYLCARN**Y**GN**H**FYFGTGTSLTVIPNIQN*PDP*AVYQLRDSKSSDKSVCLFTDFDSQTQV
SQSKDSDVYITDKCVLDMRSMDFKSNSAVAWSQKSDFACANAFQNSIIPEDTFFPSPESSCDVKL

TCRβ: GVTQTPKFQVLKTGQSMTLQCAQDMNHEYMSWYRQDPGMGLRLIHYSVGAGITDQGEVPNGYNVSRSTT
EDFPLRLLSAAPSQTSVYFCASS**L**VTGG**V**Y**L**YTFGSGTRLTVVED*LK*NVFPPKVAVFEPSEAEISHTQKATLVCL
ATGFYPDHVELSWWVNGKEVHSGVCTDPQPLKEQPALQDSRYSLSSRLRVSATFWQNPRNHFRCQVQFYGLSEND
EWTQDRAKPVTQIVSAEAWGRADC*

Wildtype/ low-affinity gp100$_{280-288}$-specific TCR clone IMCgp100:

TCRα: QQGEEDPQALSIQEGENATMNCSYKTSINNLQWYRQNSGRGLVHLILIRSNEREKHSGRLRVTLDTSKK
SSSLLITASRAADTASYFCATDG**D**TP**LV**FGKGTRLSVIANIQK*PDP*AVYQLRDSKSSDKSVCLFTDFDSQTQVSQ
SKDSDVYITDKCVLDMRSMDFKSNSAVAWSQKSDFACANAFQNSIIPEDTFFPSPESSCDVKL

TCRβ: DGGITQSPKYLFRKEGQNVTLSCEQNLNHDAMYWYRQDPGQGLRLIYYSQIVNDFQKGDIAEGYSVSRE
KKESFPLTVTSAQKNPTAFYLCASS**I**G**G**PYEQYFGPGTRLTVTEDLKNVFPPKVAVFEPSEAEISHTQKATLVCL
ATGFYPDHVELSWWVNGKEVHSGVCTDPQPLKEQPALQDSRYSLSSRLRVSATFWQNPRNHFRCQVQFYGLSEND
EWTQDRAKPVTQIVSAEAWGRADC*

Mutated/ high-affinity gp100$_{280-288}$-specific TCR clone IMCgp100:

TCRα: QQGEEDPQALSIQEGENATMNCSYKTSINNLQWYRQNSGRGLVHLILIRSNEREKHSGRLRVTLDTSKK
SSSLLITASRAADTASYFCATDG**S**TP**MQ**FGKGTRLSVIANIQKPDPAVYQLRDSKSSDKSVCLFTDFDSQTQVSQ
SKDSDVYITDKCVLDMRSMDFKSNSAVAWSQKSDFACANAFQNSIIPEDTFFPSPESSCDVKL

TCRβ: DGGITQSPKYLFRKEGQNVTLSCEQNLNHDAMYWYRQDPGQGLRLIYYS**WAQG**DFQKGDIAEGYSVSRE
KKESFPLTVTSAQKNPTAFYLCASS**W**G**A**PYEQYFGPGTRLTVTED*LK*NVFPPKVAVFEPSEAEISHTQKATLVCL
ATGFYPDHVELSWWVNGKEVHSGVCTDPQPLKEQPALQDSRYSLSSRLRVSATFWQNPRNHFRCQVQFYGLSEND
EWTQDRAKPVTQIVSAEAWGRADC*

Wildtype/ low-affinity MART-1$_{26-35}$-specific TCR clone DMF5:

TCRα: QQKEVEQNSGPLSVPEGAIASLNCTYSDRGSQSFFWYRQYSGKSPELIMFIYSNGDKEDGRFTAQLNKA
SQYVSLLIRDSQPSDSATYLCAVNFGGGKLIFGQGTELSVKPNIQKPDPAVYQLRDSKSSDKSVCLFTDFDSQTQ
VSQSKDSDVYITDKCVLDMRSMDFKSNSAVAWSQKSDFACANAFQNSIIPEDTFFPSPESSCDVKL

TCRβ: GITQAPTSQILAAGRRMTLRCTQDMRHNAMYWYRQDLGLGLRLIHYSNTAG**T**TGKGEVPDGYSVSRANT
DDFPLTLASAVPSQTSVYFCASSLSFGTEAFFGQGTRLTVVEDLKNVFPPKVAVFEPSEAEISHTQKATLVCLAT
GFYPDHVELSWWVNGKEVHSGVCTDPQPLKEQPALQDSRYSLSSRLRVSATFWQNPRNHFRCQVQFYGLSENDEW
TQDRAKPVTQIVSAEAWGRADC*

Mutated/ high-affinity MART-1$_{26-35}$-specific TCR clone DMF5:

TCRα: QQKEVEQNSGPLRVPEGAIASLNCTYSDRGSQSFFWYRQYSGKSPELIMFIYSNGDKEDGRFTAQLNKA
SQYVSLLIRDSQPSDSATYLCAVNFGGGKLIFGQGTELSVKPNIQK*PDP*AVYQLRDSKSSDKSVCLFTDFDSQTQ
VSQSKDSDVYITDKCVLDMRSMDFKSNSAVAWSQKSDFACANAFQNSIIPEDTFFPSPESSCDVKL

TCRβ: GITQAPTSQILAAGRRMTLRCTQDMRHNAMYWYRQDLGLGLRLIHYSNTAG**A**TGKGEVPDGYSVSRANT
DDFPLTLASAVPSQTSVYFCASSLSFGTEAFFGQGTRLTVVED*LK*NVFPPKVAVFEPSEAEISHTQKATLVCLAT
GFYPDHVELSWWVNGKEVHSGVCTDPQPLKEQPALQDSRYSLSSRLRVSATFWQNPRNHFRCQVQFYGLSENDEW
TQDRAKPVTQIVSAEAWGRADC*

Wildtype/ low-affinity NY-ESO-$1_{157-165}$-specific TCR clone 1G4:

TCRα: KQEVTQIPAALSVPEGENLVLNCSFTDSAIYNLQWFRQDPGKGLTSLLLIQSSQREQTSGRLNASLDKS
SGRSTLYIAASQPGDSATYLCAVRP**TS**GGSYIPTFGRGTSLIVHPNIQNPDPAVYQLRDSKSSDKSVCLFTDFDS
QTQVSQSKDSDVYITDKCVLDMRSMDFKSNSAVAWSQKSDFACANAFQNSIIPEDTFFPSPESSCDVKL

TCRβ: GVTQTPKFQVLKTGQSMTLQCAQDMNHEYMSWYRQDPGMGLRLIHYSVGAGITDQGEVPNGYNVSRSTT
EDFPLRLLSAAPSQTSVYFCASSYVGNTGELFFGEGSRLTVLED*LK*NVFPPKVAVFEPSEAEISHTQKATLVCLA
TGFYPDHVELSWWVNGKEVHSGVCTDPQPLKEQPALQDSRYSLSSRLRVSATFWQNPRNHFRCQVQFYGLSENDE
WTQDRAKPVTQIVSAEAWGRADC*

Mutated/ high-affinity NY-ESO-$1_{157-165}$-specific TCR clone 1G4:

TCRα: KQEVTQIPAALSVPEGENLVLNCSFTDSAIYNLQWFRQDPGKGLTSLLLIQSSQREQTSGRLNASLDKS
SGRSTLYIAASQPGDSATYLCAVRP**LY**GGSYIPTFGRGTSLIVHPNIQNPDPAVYQLRDSKSSDKSVCLFTDFDS
QTQVSQSKDSDVYITDKCVLDMRSMDFKSNSAVAWSQKSDFACANAFQNSIIPEDTFFPSPESSCDVKL

TCRβ: GVTQTPKFQVLKTGQSMTLQCAQDMNHEYMSWYRQDPGMGLRLIHYSVGAGITDQGEVPNGYNVSRSTT
EDFPLRLLSAAPSQTSVYFCASSYVGNTGELFFGEGSRLTVLED*LK*NVFPPKVAVFEPSEAEISHTQKATLVCLA
TGFYPDHVELSWWVNGKEVHSGVCTDPQPLKEQPALQDSRYSLSSRLRVSATFWQNPRNHFRCQVQFYGLSENDE
WTQDRAKPVTQIVSAEAWGRADC*

6.3 SDS-PAGEs of produced TCR constructs

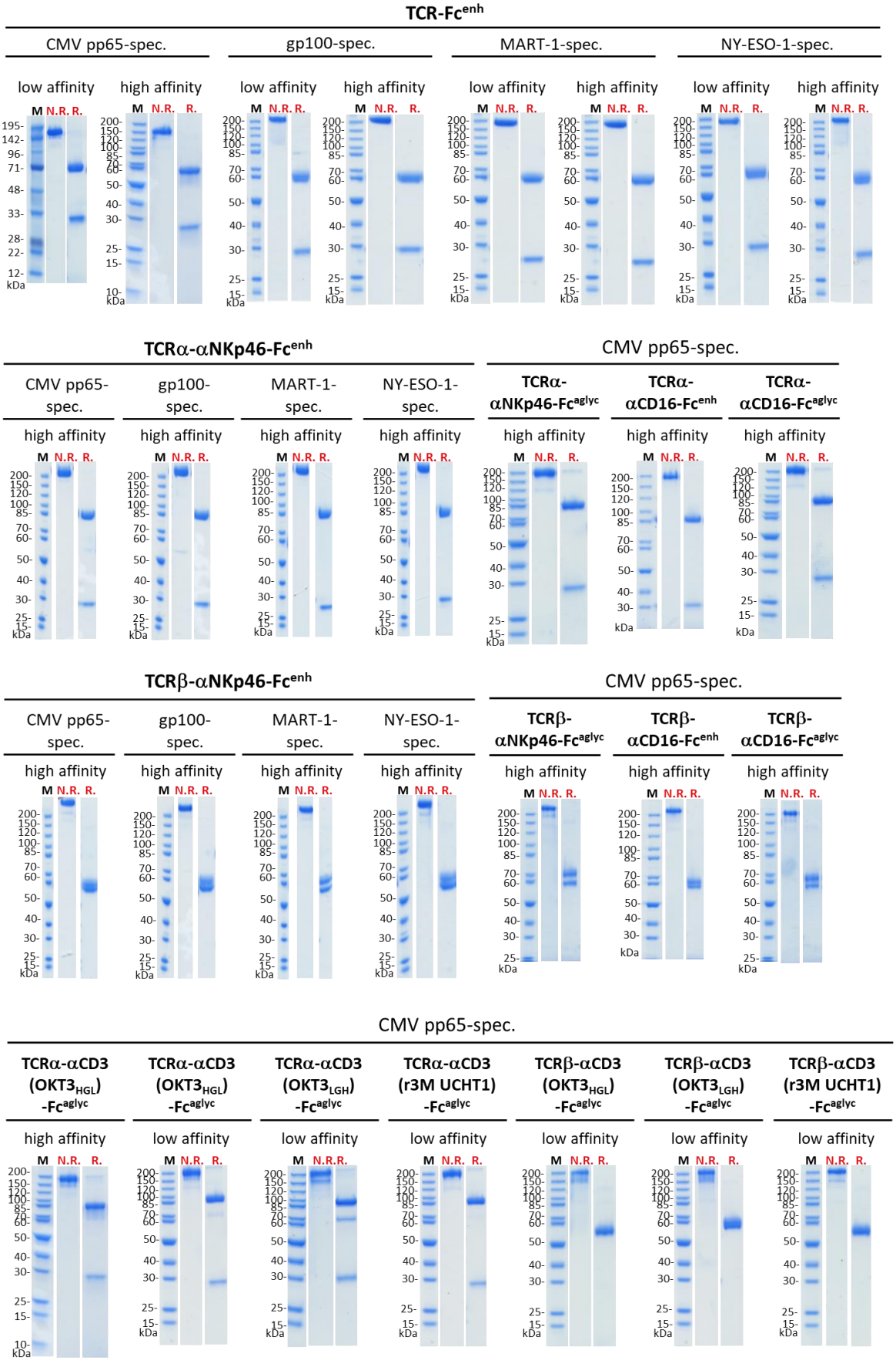

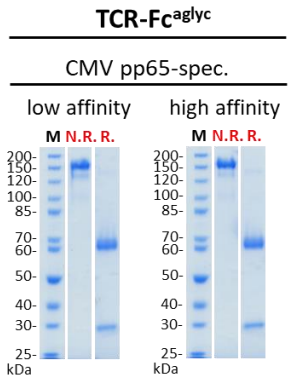

Figure 32: SDS-PAGE gel analysis of the TCR antibody fusion proteins used in this thesis
Shown are Coomassie-stained SDS-PAGE gels of the different TCR-Fc and TCR-scFv-Fc constructs under non reducing (N.R.) and reducing (R.) conditions. A protein marker is included as comparison (M). TCR specificity and construct format are indicated.

7 Acknowledgements

First of all, I would like to thank PD Dr. Frank Momburg for providing me with this interesting PhD project in his group “Antigen Presentation and T/NK Cell Activation” at the DKFZ (Deutsches Krebsforschungszentrum/ German Cancer Research Center) in Heidelberg, which is affiliated with the Clinical Cooperation Unit “Applied Tumor Immunity” led by Prof. Dr. Dirk Jäger. Furthermore, I am very thankful for his constant scientific support and for his time-consuming efforts to genetically engineer all the required TCR-Fc constructs and BiMabs. Likewise, I would like to thank Nadja Bulbuc, Selina Börsig, Dr. Marten Meyer and Susanne Knabe for taking care of the cloning and production process. Additionally, I want to thank my former student Nina Dehnert for her contribution to this project. Furthermore, I am very thankful for great and supporting, scientific and non-scientific conversations with my office mate Márcia Gonçalves and for her help with PBMC isolations. Likewise, I’m greatly thankful for my colleague Karsten Warwas for helping with PBMC isolations, for his great scientific support, his friendship and a lot of funny coffee breaks together. I am also very thankful for Selina’s friendship throughout the PhD.

I am furthermore very thankful that Prof. Dr. Oliver Fackler, Prof. Dr. Ilse Hofmann, Prof. Dr. Viktor Umansky and PD Dr. Frank Momburg agreed to be part of the defense examination committee.

Next, I would like to thank PD Dr. Frank Momburg, Prof Dr. Viktor Umansky, Dr. Inka Zörnig and Dr. Alexander Rölle for their time and feedback being part of the thesis advisory committee. Additionally, I would like to thank Dr. Alexander Rölle for introducing me in this lab.

Last but not least, I would like to thank my family, friends, brothers and sisters for their constant personal support and love throughout my way, especially my mother Susanne and my best friends Sebastian and Esraa.